

# **KTB REPORT 92-2**

## **KTB Hauptbohrung** Results of Geoscientific Investigation in the KTB Field Laboratory **0 – 6000 m**



Edited by  
the Project Management of the Continental  
Deep Drilling Programme of the Federal Republic of Germany  
in the Geological Survey of Lower Saxony

R. Emmermann, H.-G. Dietrich, J. Lauterjung, Th. Wöhrl

Editors: Prof. Dr. R. Emmermann, Dr. H.-G. Dietrich,  
Dr. J. Lauterjung and Dipl.-Geophys. Th. Wöhrl

Printed by: Wittmann & Wäsch, D-3007 Gehrden

Distribution: E. Schweitzerbart'sche Verlagsbuchhandlung

Orders: E. Schweitzerbart'sche Verlagsbuchhandlung  
Johannesstr. 3A  
D-7000 Stuttgart 1

Front cover: Principal of coring, using a 14 3/4" roller  
cone core bit (between 4149.0 and 6000 m in the  
KTB-Hauptbohrung) demonstrated with a core  
piece from the KTB pilot hole (Photo Dietrich/  
Neuber, 1991)

All projects reported hereafter are entirely funded by the  
Bundesministerium für Forschung und Technologie. The Editors  
cannot be held responsible for the opinions given and state-  
ments made in the articles published, the responsibility  
resting with the authors.

© Niedersächsisches Landesamt für Bodenforschung  
Hannover 1992

Reprinting, copying and translations, broadcasting, reproduc-  
tion by photomechanical or in other ways as well as storage  
in data banks - even in parts - are subject to prior permis-  
sion.

All rights are reserved.

Editors' address: Niedersächsisches Landesamt für Bodenfor-  
schung, POB 51 01 53, D-3000 Hannover 51.  
Phone: 0511/643-2675

ISSN 0939-8732  
ISBN 3-928559-05-2

## PREFACE

Establishment of a field laboratory at the drill site had a top priority since the very first discussions about a continental deep drilling program in Germany. Therefore, already in 1983 a working group headed by R. Emmermann was set up in order to define the tasks to be accomplished in the lab and to determine the equipment and personnel necessary. It was agreed that the main purpose of the field laboratory is to collect extensive geoscientific data on cores, cuttings, rock flour, drilling fluids and gases recovered from both the pilot hole (Vorbohrung) and the main borehole (Hauptbohrung).

In particular properties should be measured which :

- are necessary for quick operational decisions concerning drilling, sampling and testing
- have to be determined on a quasi-continuous scale as a function of depth
- are time-dependent and have to be recorded as soon as possible
- are necessary for correlation with data obtained by borehole measurements
- are needed for proper sample selection and serve as basic information for all individual research projects carried out at universities and other research institutions.

In order to meet these requirements a comprehensive scientific program is carried out on-site which includes :

- structural, petrographical and mineralogical investigations on cores and cuttings
- establishment of a "lithologic log" and a first interpretation of geological structures
- determination of major and trace elements on core material, cuttings, rock flour and drilling fluid
- on-line analysis of gases dissolved in the drilling fluid
- measurements of physical properties of cores, cuttings and rock flour.

Figure 1 summarizes the organizational structure and working scheme of the field laboratory. In addition to the specified investigations the field laboratory is responsible for distribution, management and archiving of samples, and for regular publication of all scientific results. Progress reports are published regularly and cover borehole sections of 500 m length (Emmermann et al. 1988, 1989, 1990, 1991).

Thus far, eleven KTB-reports containing all data corroborated in the field laboratory have been published and ten so-called "Sampling Parties" have been held where all scientists who are interested in obtaining material for their investigations are gathered during two days. In the meantime, over 2000 samples have been prepared and distributed by the field laboratory.

The staff currently includes 2 permanently employed assistants of the Project Management, 16 scientists from nine universities and 15 technicians who are mainly from the area around Windischeschenbach. These personnel are assigned to four working groups: Geology-Petrology, Geochemistry, Geophysics and Data Processing.

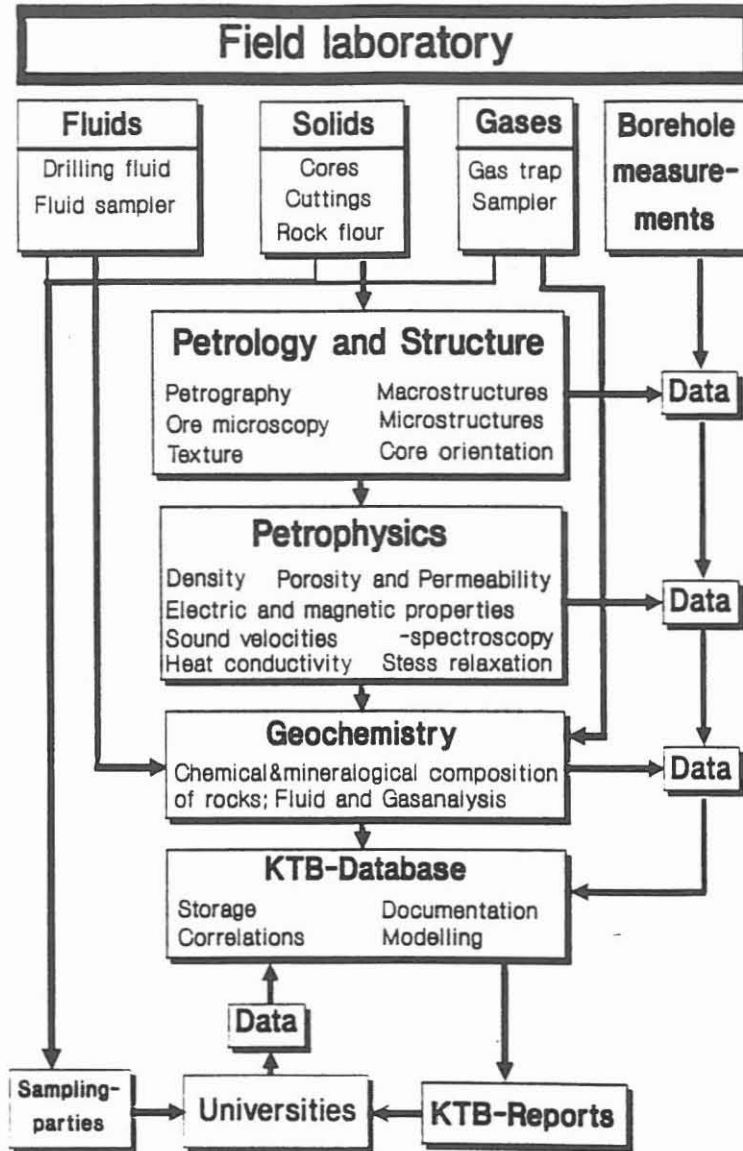


Fig. 1: Sampling and working scheme of the KTB field laboratory

The KTB project management is responsible for the operation of the field laboratory which belongs to the directorate for "Geosciences". The director on site is Dr. H. G. Dietrich and his deputy is T. Wöhr. Scientific and non-scientific personnel are financed by the DFG-project, "Staffing of the KTB Field Laboratory" and are employed through private contracts with R. Emmermann at the University of Giessen. Principle investigators of the DFG-project include Prof. Dr. R. Emmermann, Giessen, Prof. Dr. H. Berckhemer, Frankfurt, Prof. Dr. G. Friedrich, Aachen, Prof. Dr. K. von Gehlen, Frankfurt, Prof. Dr. O. Natau, Karlsruhe, Prof. Dr. H. Soffel, München, Prof. Dr. B. Stöckhert, Bochum, Prof. Dr. K. Weber and Prof. Dr. K. H. Wedepohl, Göttingen. These investigators are responsible for the scientific program carried out in the field laboratory and their institutes serve as so-called "parent institutes" for providing qualified personnel and maintaining the equipment.

These "Parent Institutes" are:

Institut für Geowissenschaften und Lithosphärenforschung der Universität Giessen

Institut für Meteorologie und Geophysik der Universität Frankfurt

Institut für Mineralogie und Lagerstättenlehre der RWTH Aachen

Institut für Geochemie, Petrologie und Lagerstättenkunde der Universität Frankfurt

Institut für Boden- und Felsmechanik der Universität Karlsruhe

Institut für Allgemeine und Angewandte Geophysik der Universität München

Institut für Geologie der Ruhr-Universität Bochum

Institut für Geologie und Dynamik der Lithosphäre der Universität Göttingen

Geochemisches Institut der Universität Göttingen

- Emmermann, R., Dietrich, H.-G., Heinisch, M. & Wöhr, Th. (eds., 1988), Tiefbohrung KTB Oberpfalz VB, Ergebnisse der geowissenschaftlichen Bohrungsbearbeitung im KTB-Feldlabor, Teufenbereich von 0 - 480 m. - KTB Report 88-1, Projektleitung Kontinentales Tiefbohrprogramm der Bundesrepublik Deutschland im Niedersächsischen Landesamt für Bodenforschung.
- Emmermann, R., Dietrich, H.-G., Heinisch, M. & Wöhr, Th. (eds., 1988), Tiefbohrung KTB Oberpfalz VB, Ergebnisse der geowissenschaftlichen Bohrungsbearbeitung im KTB-Feldlabor, Teufenbereich von 480 - 992 m. - KTB Report 88-2.
- Emmermann, R., Dietrich, H.-G., Heinisch, M. & Wöhr, Th. (eds., 1988), Tiefbohrung KTB Oberpfalz VB, Ergebnisse der geowissenschaftlichen Bohrungsbearbeitung im KTB-Feldlabor, Teufenbereich von 992 - 1530 m. - KTB Report 88-6.
- Emmermann, R., Dietrich, H.-G., Heinisch, M. & Wöhr, Th. (eds., 1988), Tiefbohrung KTB Oberpfalz VB, Ergebnisse der geowissenschaftlichen Bohrungsbearbeitung im KTB-Feldlabor, Teufenbereich von 1530 - 1998 m. - KTB Report 88-9.
- Emmermann, R., Dietrich, H.-G., Heinisch, M. & Wöhr, Th. (eds., 1989), Tiefbohrung KTB Oberpfalz VB, Ergebnisse der geowissenschaftlichen Bohrungsbearbeitung im KTB-Feldlabor, Teufenbereich von 1709 - 2500 m. - KTB Report 89-2.
- Emmermann, R., Dietrich, H.-G., Heinisch, M. & Wöhr, Th. (eds., 1989), Tiefbohrung KTB Oberpfalz VB, Ergebnisse der geowissenschaftlichen Bohrungsbearbeitung im KTB-Feldlabor, Teufenbereich von 2500 - 3009.7 m. - KTB Report 89-4.
- Emmermann, R., Dietrich, H.-G., Heinisch, M. & Wöhr, Th. (eds., 1989), Tiefbohrung KTB Oberpfalz VB, Ergebnisse der geowissenschaftlichen Bohrungsbearbeitung im KTB-Feldlabor, Teufenbereich von 3009.7 - 3500 m. - KTB Report 89-5.
- Emmermann, R., Dietrich, H.-G., Lauterjung, J. & Wöhr, Th. (eds., 1990), Tiefbohrung KTB Oberpfalz VB, Ergebnisse der geowissenschaftlichen Bohrungsbearbeitung im KTB-Feldlabor, Teufenbereich von 3500 - 4000.1 m (E.T.). - KTB Report 90-2.
- Emmermann, R., Dietrich, H.-G., Lauterjung, J. & Wöhr, Th. (eds., 1990), KTB Pilot Hole, Results of Geoscientific Investigation in the KTB Field Laboratory, 0 - 4000.1 m. - KTB-Report 90-8.
- Emmermann, R., Dietrich, H.-G., Lauterjung, J. & Wöhr, Th. (eds., 1991), Tiefbohrung KTB Oberpfalz HB, Ergebnisse der geowissenschaftlichen Bohrungsbearbeitung im KTB-Feldlabor, Teufenbereich 0 - 1720 m. - KTB-Report 91-3.



KTB Report 92-2  
KTB Hauptbohrung  
Results of Geoscientific Investigation  
in the KTB Field Laboratory

0 - 6000 m

CONTENT	PAGE
<b>A.</b>	<b>Introduction</b>
A.1	General introduction ..... A 2
A.2	Drilling technique ..... A 2
A.3	Sampling ..... A12
A.3.1	Sample types and extraction station ..... A12
A.3.2	Depth assignment of samples ..... A17
A.4	Sample notation and -requesting ..... A20
A.5	References ..... A26
<b>B.</b>	<b>Geology</b>
B.1	German Continental Deep Drilling Programme (KTB) - geological survey of the main hole 0 - 6000 m ..... B 1
B.1.1	Introduction ..... B 1
B.1.2	Methods ..... B 3
B.1.3	Geological Profile ..... B 4
B.1.4	Petrography ..... B 7
B.1.4.1	Paragneisses ..... B 7
B.1.4.1.1	Evolution of fabrics and metamorphism ..... B 7
B.1.4.2	Metabasic rocks ..... B12
B.1.4.2.1	Petrography ..... B12
B.1.4.2.2	Metamorphic evolution ..... B19
B.1.4.2.3	Deformation ..... B20
B.1.4.2.4	Chemical composition ..... B23
B.1.4.3	Late dykes ..... B25

B.1.4.3.1	Lamprophyres .....	B25
B.1.4.3.2	Aplites .....	B25
B.1.5	Ore Mineralization.....	B26
B.1.5.1	Sample routine .....	B26
B.1.5.2	Ore minerals.....	B26
B.1.5.3	Age relations and aspects of formation.....	B27
B.1.5.4	Qualitative and quantitative distribution of ferrimagnetic ore minerals. ....	B27
B.1.6	Open Porosity and its correlation with gas .....	B31
B.1.7	Structure.....	B34
B.1.8	Summary .....	B35
B.1.9	Acknowledgements .....	B37
B.1.10	References .....	B37
B.1.11	Appendix .....	B39
B.1.11.1	List of mineral abbreviations .....	B39
B.1.11.2	Description of the geological profile .....	B40
B.1.11.3	Short (preliminary) description of the cores in the KTB Hauptbohrung .....	B42
B.2	Drilling artifacts in cuttings samples .....	B43
B.3	The geological section of the KTB Hauptbohrung - Correlation with the KTB Vorbohrung and preliminary structural interpretation.....	B47
B.4	Cuttings profile 0 - 6000 m .....	B53
<b>C. Geochemistry/Mineralogy</b>		
	Summary.....	C03
C.1	Drill mud analysis.....	C04
C.1.1	Introduction .....	C04
C.1.2	Analytical methods .....	C04
C.1.3	KTB drill mud parameters and properties .....	C05
C.1.4	Results of "quasi-on-line analysis" .....	C07
C.1.5	Results of fluids collected by fluid samplers.....	C10
C.1.6	Conclusion .....	C11
C.2	Gas analysis .....	C12
C.2.1	Introduction .....	C12
C.2.2	Experimental methods.....	C12
C.2.3	Results .....	C13
C.2.3.1	Contamination of the drill mud and artificially generated gases .....	C13
C.2.3.2	Gas inflows.....	C17
C.2.3.3	Quantification of gases dissolved in drillmud .....	C23
C.2.4	Conclusions .....	C25



C.3	Geochemical investigations of solids .....	C26
C.3.1	Sample preparation .....	C26
C.3.2	Methods .....	C26
C.3.2.1	Mineralogical phase analysis.....	C26
C.3.3	Results .....	C27
C.4	Acknowledgements.....	C27
C.5	References .....	C28
C.6	Appendix .....	C29
C.6.1	Results of cation and anion analysis.....	C29
C.6.2	Results of solid analysis.....	C33
C.7	On-line determination of <sup>222</sup> Radon in the drilling fluid .....	C39

**D. Geophysics**

D.1	Introduction .....	D02
D.2	Density D .....	D03
D.3	Natural Gamma Ray Activity.....	D06
D.4	Magnetic Susceptibility.....	D14
D.5	Thermal Conductivity.....	D21
D.6	Electrical Resistivity .....	D26
D.7	Ultrasonic Seismics .....	D29
D.8	Depth Corrections Based On Petrophysical Data .....	D32
D.9	Summary and Discussion.....	D35
D.10	References .....	D41

**E. Rock Mechanics**

E.1	Introduction .....	E02
E.2	Test Results .....	E03
E.2.1	Uniaxial Compressive Tests .....	E03
E.2.2	Indirect Tensile Tests.....	E06

E.3 Reference ..... E07

**F. Core Reorientation by Comparison of Core Instabilities and Borehole Instabilities**

Abstract

F.1 Introduction ..... F 02

F.2 Core Disking ..... F 04

F.2.1 General ..... F 04

F.2.2 Shape of Core Disks..... F 05

F.3 Evaluation of the Orientation of Core Disking High Points..... F 06

F.3.1 In Situ Stress Indicators..... F 09

F.3.1.1 KTB Pilot Hole VB ..... F 13

F.3.1.2 "Practical use" ..... F 13

F.3.1.3 Core Orientation of the KTB Main Hole HB..... F 15

F.4 References ..... F 16

**G. Advanced Drilling Technology for the Continental Deep Drilling Program (KTB): Part of International Lithosphere Research**

Abstract

G.1 Introduction ..... G 02

G.2 The Pilot Hole ..... G 02

G.3 The Ultradeep Well ..... G 04

G.4 The Coring Concept..... G 05

G.5 The Vertical Drilling Strategy ..... G 05

G.6 New Heavy Deep Drilling Rig ..... G 06

G.7 State of Work in the Ultradeep Hole ..... G 07

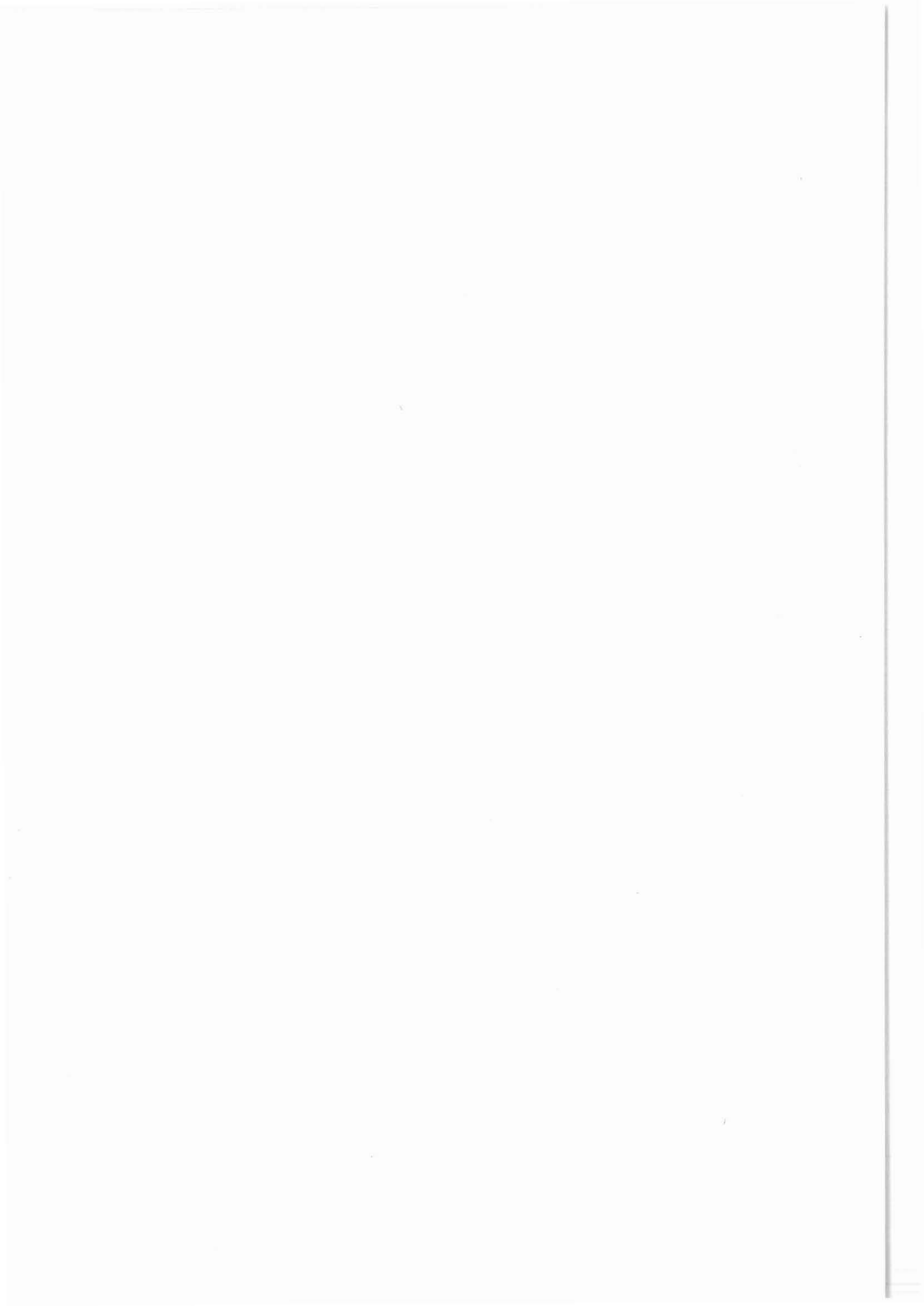
G.8 Conclusions ..... G 09

G.9 References ..... G 10

**APPENDIX: Compilation of geologically relevant data, 0 - 3000 m**

## A. Introduction

H.-G. Dietrich  
J. Lauterjung  
Th. Wöhrl



KTB-Report	92-2	A1-A26	34 Abb.	Hannover 1992
------------	------	--------	---------	---------------

## A. Introduction

<sup>1</sup>Dietrich, H.-G., J., <sup>2</sup>Lauterjung, J. & <sup>1</sup>Wöhrl, Th.

CONTENT	PAGE
A.1 General introduction	A2
A.2 Drilling technique	A2
A.3 Sampling	A12
A.3.1 Sample types and extraction station	A12
A.3.2 Depth assignment of samples	A17
A.4 Sample notation and -requesting	A20
A.5 References	A26

---

<sup>1</sup> KTB-Feldlabor, Postfach 67, W-8486 Windischeschenbach, FRG

<sup>2</sup> Institut für Geowissenschaften und Lithosphärenforschung der Justus-Liebig-Universität,  
Senckenbergstr. 3, W-6300 Gießen, FRG

## A. Introduction

### A.1 General Introduction

This second report on the KTB super deep borehole (KTB Oberpfalz HB) presents results obtained in the KTB field laboratory from the depth interval 0 - 6000 m. Together with the reports already published on the pilot hole (Vorbohrung) and main hole (Hauptbohrung), this is the eleventh report from the field laboratory (e.g. Emmermann et al. 1990, 1991).

The cuttings profile which is continuously up-dated provides an overview of selected geoscientific parameters (part B.4 of this report). The corresponding geological profile from the depth interval 0 - 3000 m, connecting results from the field laboratory and from logging (scale 1 : 400) is attached to this report (pages 1 - 12). The report is complemented by the following contributions:

- The Geological Section - Correlations with the Pilot Hole and preliminary Interpretation by G. Hirschmann (see part B.3).
- On-line determination of <sup>222</sup>Radon in Drilling Fluids of the KTB Hauptbohrung by J. Erzinger, J. Hansmann, H. Kamm & H.-J. Heinschild (see part C.7).
- Core Reorientation by Comparison of Core Instabilities and Borehole Instabilities by Th. Roeckel, O. Natau & H.-G. Dietrich (see part F.).

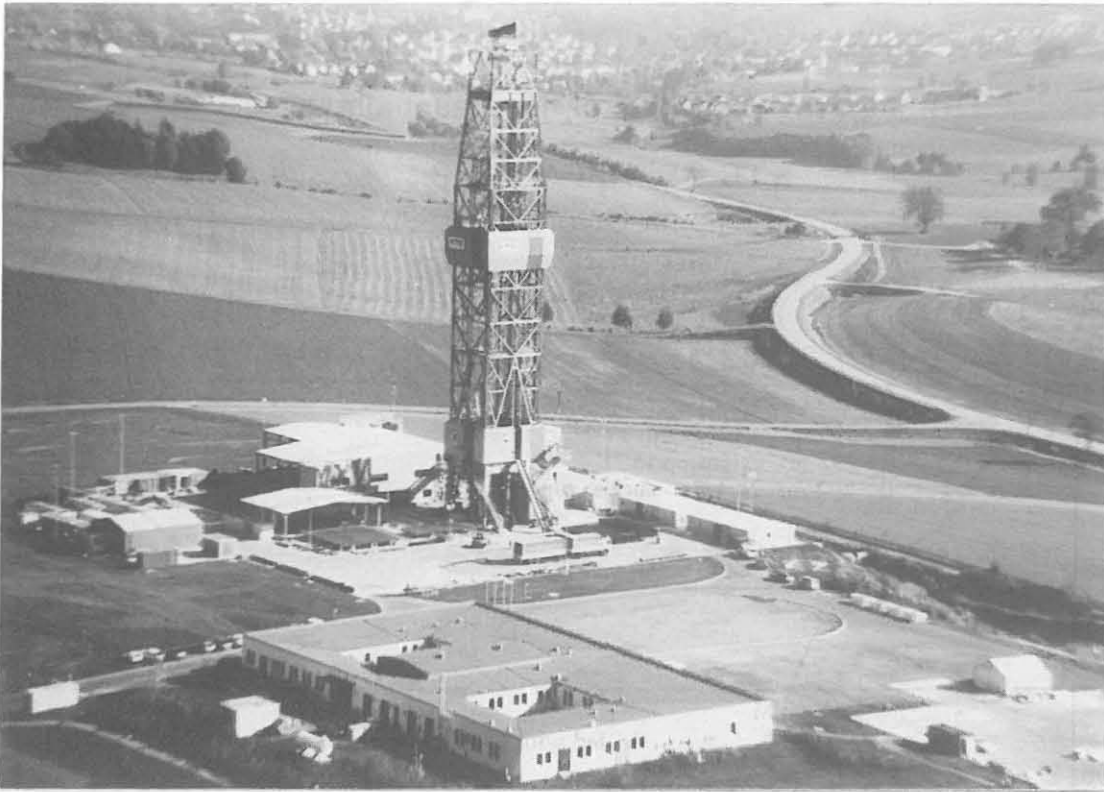
Both aerial photographs (Fig. A.1.1 and A.1.2) taken from the north-east and south-west respectively show the KTB Hauptbohrung to the east, the site of the pilot well to the west and the central building (field laboratory and administration) to the north. The distance between the main hole and the pilot hole is 200 m.

A short monthly report of the technical proceedings is regularly given in "Erdöl Erdgas Kohle", actual informations from the KTB field laboratory are published in "Die Geowissenschaften" (Dietrich 1992).

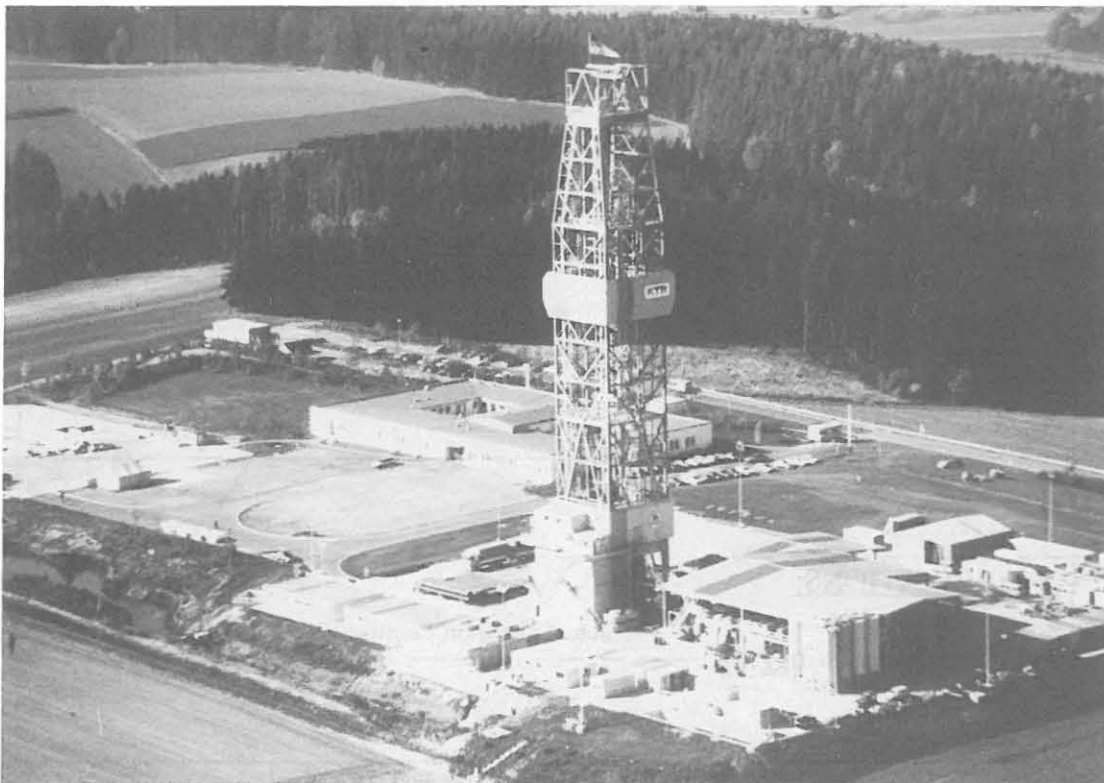
### A.2 Drilling technique

After the official inauguration ceremony of the main well (Hauptbohrung) of the KTB by the German Minister for Research and Technology, Dr. H. Riesenhuber on September 8, 1990, which included setting in operation of the drilling rig UTB-1 the largest on-shore rig of the world, actual drilling of the KTB HB began on October 6. The Hauptbohrung reached 4000.1 m the final depth of the pilot hole, at the end of August 1991. On November 21, 1991, after 13.5 months the 5000 m mark (the halfway mark of the planned final depth of 10000 m) was reached (Fig. A.2.1).

The upper 305 m were drilled with 17 1/2" insert bits and two active vertical drilling systems (ZBE 5000 and VDS-3) as well as a packed hole assembly (PHA) (Chur et al. 1990a, 1990b, Emmermann 1990, Emmermann and Rischmüller 1990, Rischmüller 1990, 1991). As a result of failure of one of the vertical drilling systems a deviation of 2° was built up between 270 m



**Fig. A.1.1:** Aerial view of the drilling rig UTB-1, especially built for the KTB-Hauptbohrung with the central building in the foreground and the village of Windischeschenbach in the background (Photo Hoffmannsbeck, October 1990).



**Fig. A.1.2:** Aerial view of the KTB location with the site of the pilot hole on the left hand side of the picture (Photo Hoffmannsbeck, October 1990).

### Drilling Progress Curve of the Hauptbohrung

KTB OBERPFALZ HB

Spud date on October 6, 1990

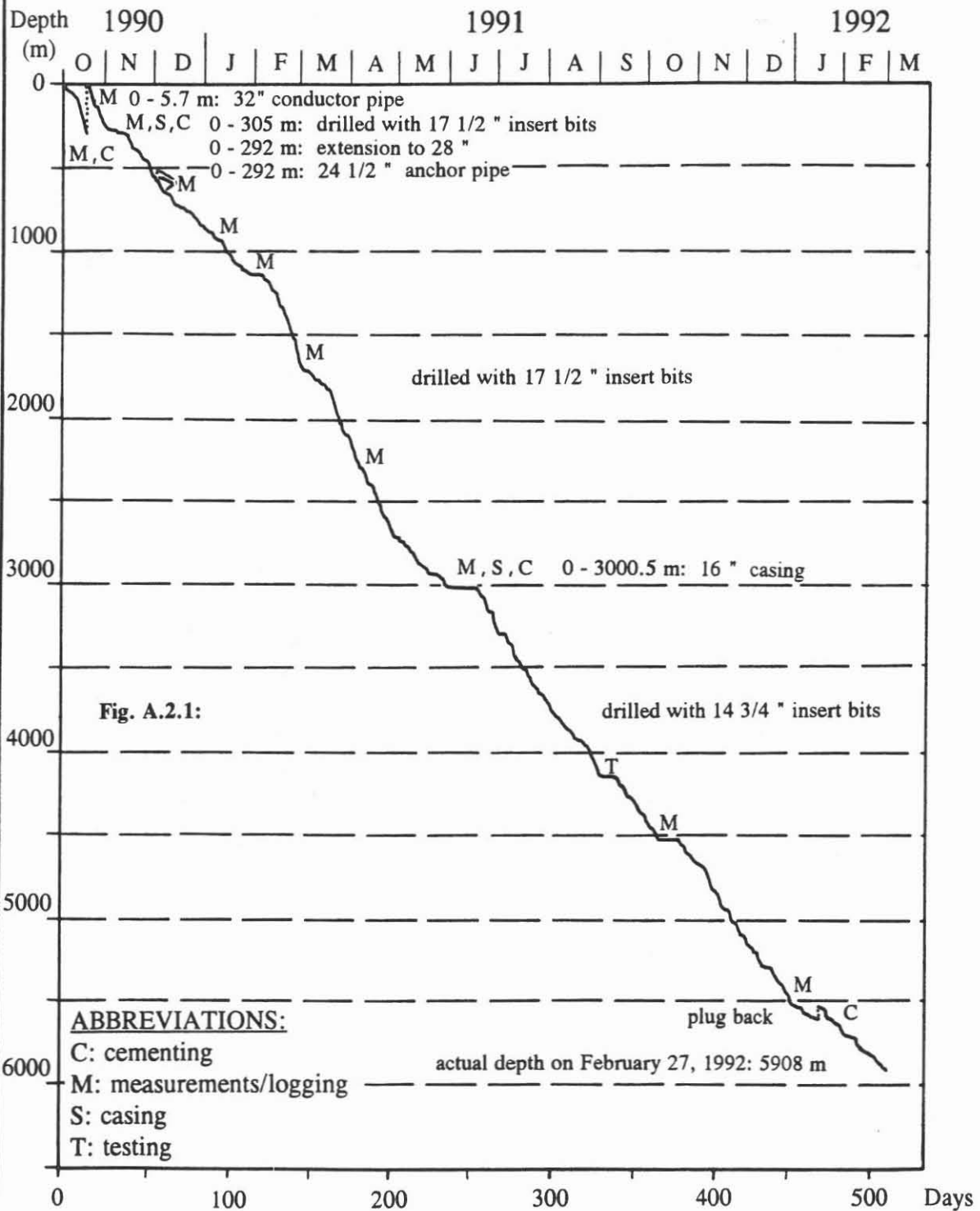


Fig. A.2.1:



and 305 m which called for the cementing of the borehole from 305 m back to 250 m. The borehole was then extended from 17 1/2" to 28" (Fig. A.2.2) and deepened to 292.0 m with a fully stabilized bottom hole assembly (PHA) and a 28" hole opener and a 28" milled tooth bit to allow to run the 24 1/2" anchor pipe.

After drilling of the casing shoe, the contaminated drilling mud was replaced by new Dehydril HT drilling fluid.

Down to 3003 m drilling continued with 17 1/2" insert bits in combination with the active vertical drilling systems (VDS-3 and ZBE 5000, Fig. A.2.4 - A.2.5). An overview of the different vertical and directional drilling systems and bottom hole assemblies is given in Chur et al. (1990).

On May 30, 1991, at a depth of 3003 m, the second casing depth was reached. A 16" casing was run and cemented from the casing shoe to the surface. After drilling the casing shoe, drilling continued on June 18, 1991 with 14 3/4" insert bits and two vertical drilling systems (VDS-3, VDS-4). The automatic directional drilling device ZBE 5000 was no longer used in the 14 3/4" borehole.

In order to improve the drilling progress a hydraulic thruster was tested to produce defined weight on the bits, making use of the drilling fluid pressure.

Junk baskets (as used in the pilot hole, Sigmund & Dietrich 1990, Emmermann et al. 1990) were used in order to obtain large rock fragments. After positive experiences, a prototype of an especially designed "cuttings sampler" has been used on a routine basis since December 1991 (Fig. A.2.6).

Cores were drilled with 14 3/4" roller cone bits (Fig. A.2.7 and A.2.8). To improve core recovery (see part B) and core quality several tests with a newly developed pilot hole coring system (core diameter 63 mm) were carried out. Within the framework of the borehole logging program (Bram et al. 1991) five larger measuring campaigns were carried out in addition to oriented caliper and deviation measurement:

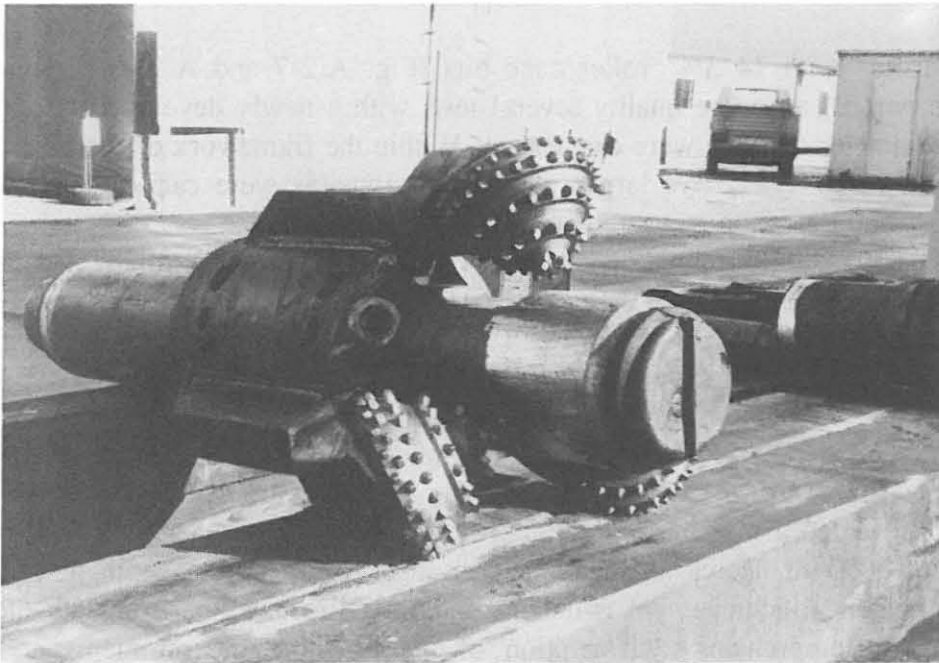
- at 305.0 m, borehole diameter 17 1/2", before extension to 28" and 24 1/2" casing
- at 762.5 m, borehole diameter 17 1/2"
- at 1720.0 m, borehole diameter 17 1/2"
- at 3003.0 m, borehole diameter 17 1/2", 16" casing
- at 4500.0 m, borehole diameter 14 3/4"

In addition to detailed geophysical data, in situ samples (solids and fluids) were recovered from the borehole (see Tab. A.3.1.1). Evaluation of the various deviation and azimuth measurements revealed a maximum horizontal borehole deviation of approx. 13 m NE in the depth range at 3000 m decreasing again to less than 10 m at the depth at 5800 m. This extraordinary technical achievement is demonstrated by direct comparison with the pilot hole (Fig. A.2.9). A comprehensive description of the borehole measurements and downhole sampling achieved so far is given by Bram et al. 1991 and Bram and Draxler 1992.

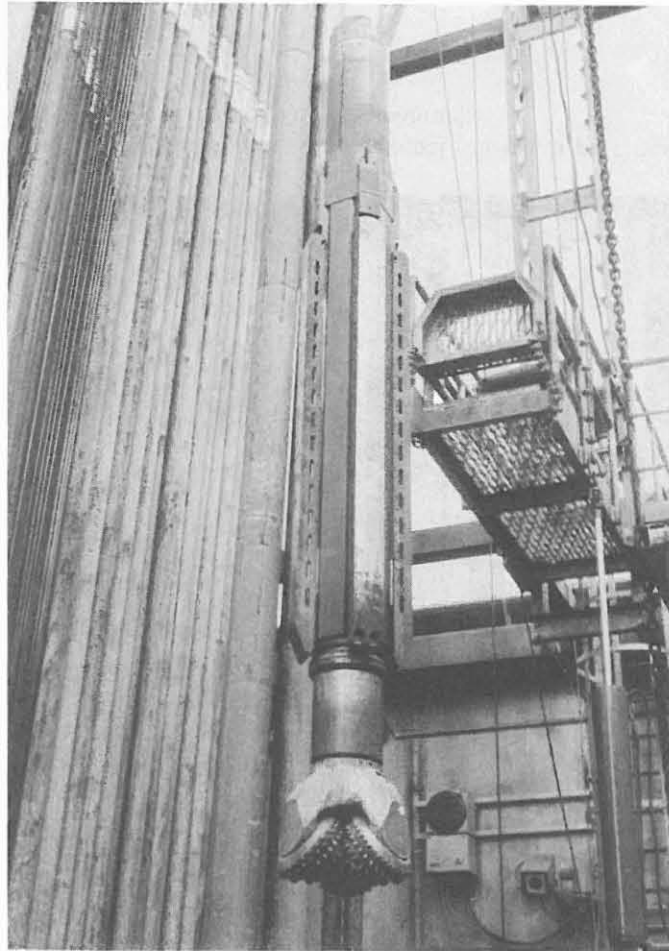
Fig. A.2.10 - A.2.11 presents an overview of the different drilling and casing intervals of the KTB HB.



**Fig. A.2.2:** 17 1/2" roller cone bits used in the Hauptbohrung down to 305 m and a 28" bit used for drilling a cement plug in the 28" borehole section.



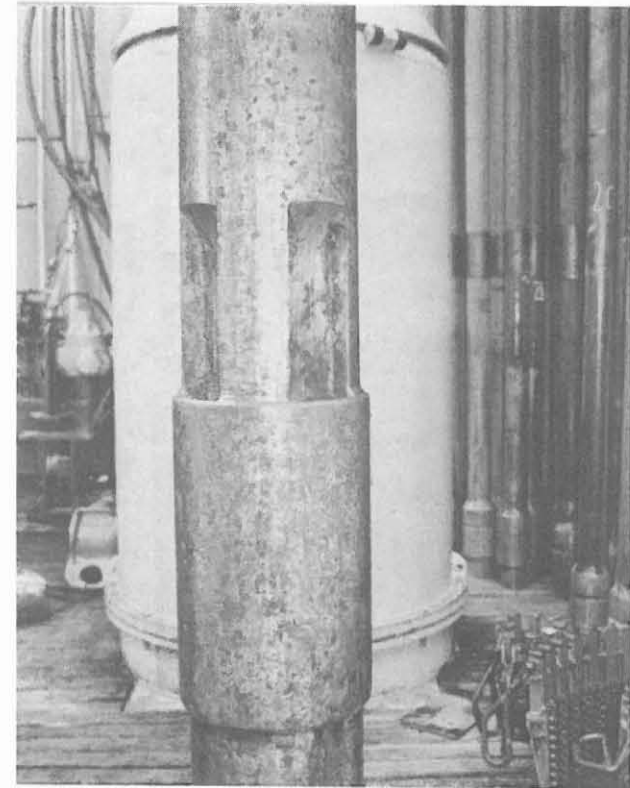
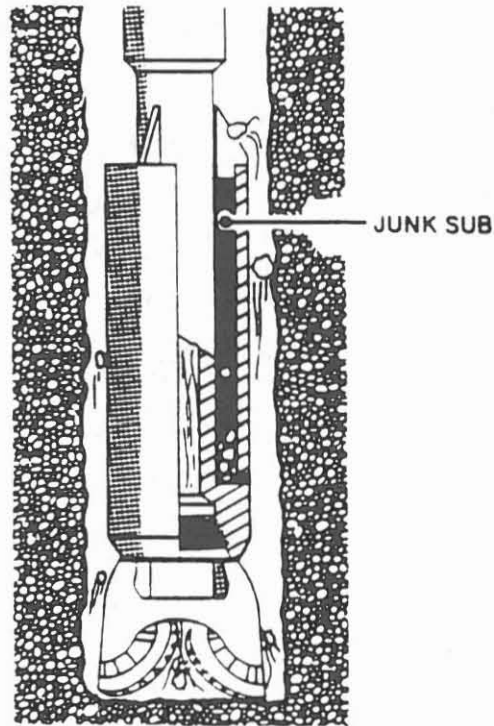
**Fig. A.2.3:** 28" hole opener used for the extension of the first 17 1/2" borehole section from 0 - 305 m.



**Fig. A.2.4:** The automatic directional drilling device ZBE 5000 combined with the 17 1/2" insert bit.



**Fig. A.2.5:** The active vertical drilling system VDS-3 combined with a 17 1/2" insert bit.



**Fig. A.2.6:** Junk basket (left) with an operational scheme, a prototype of a "cuttings sampler" for the 14 3/4" borehole section especially designed for use in the KTB Hauptbohrung.

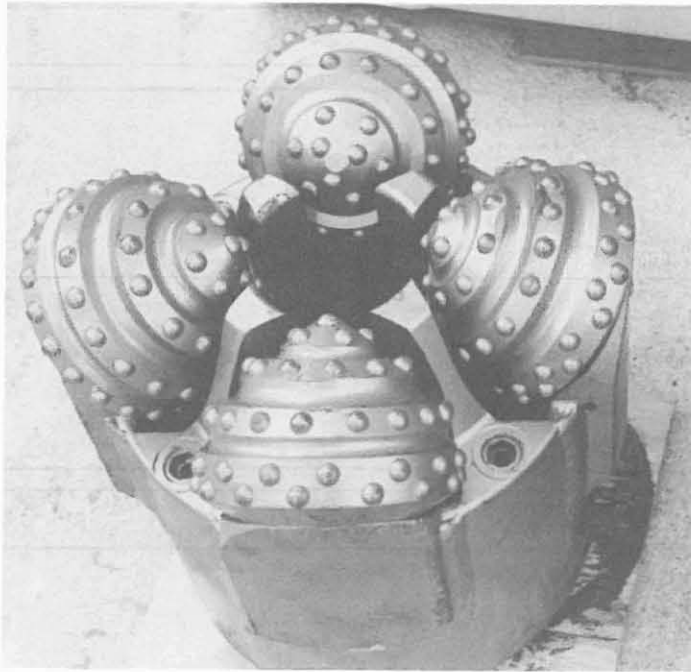


Fig. A.2.7: 14 3/4" roller cone core bits (new), yielding 4" cores.



Fig. A.2.8: 14 3/4" roller cone core bits (used), yielding 4" cores.

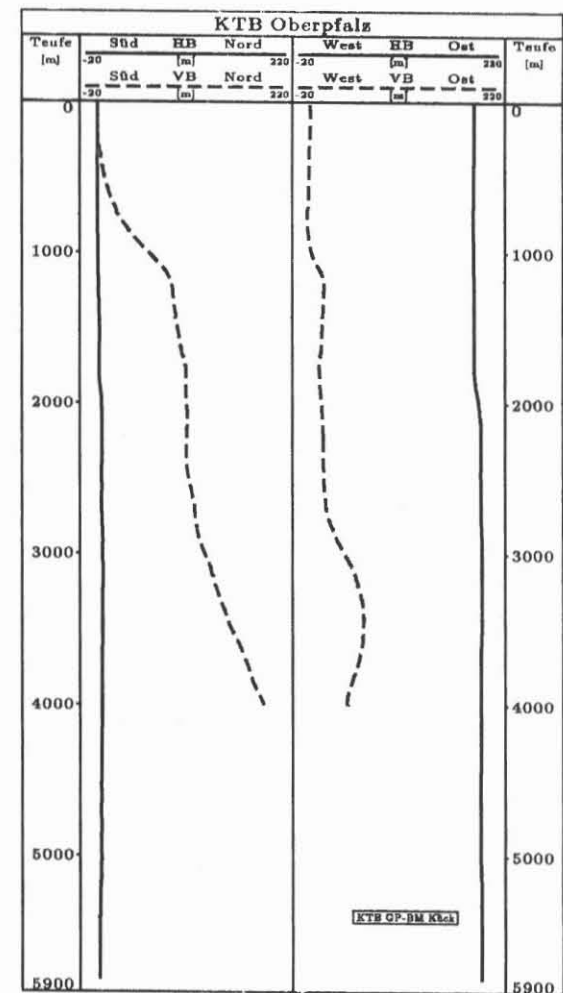
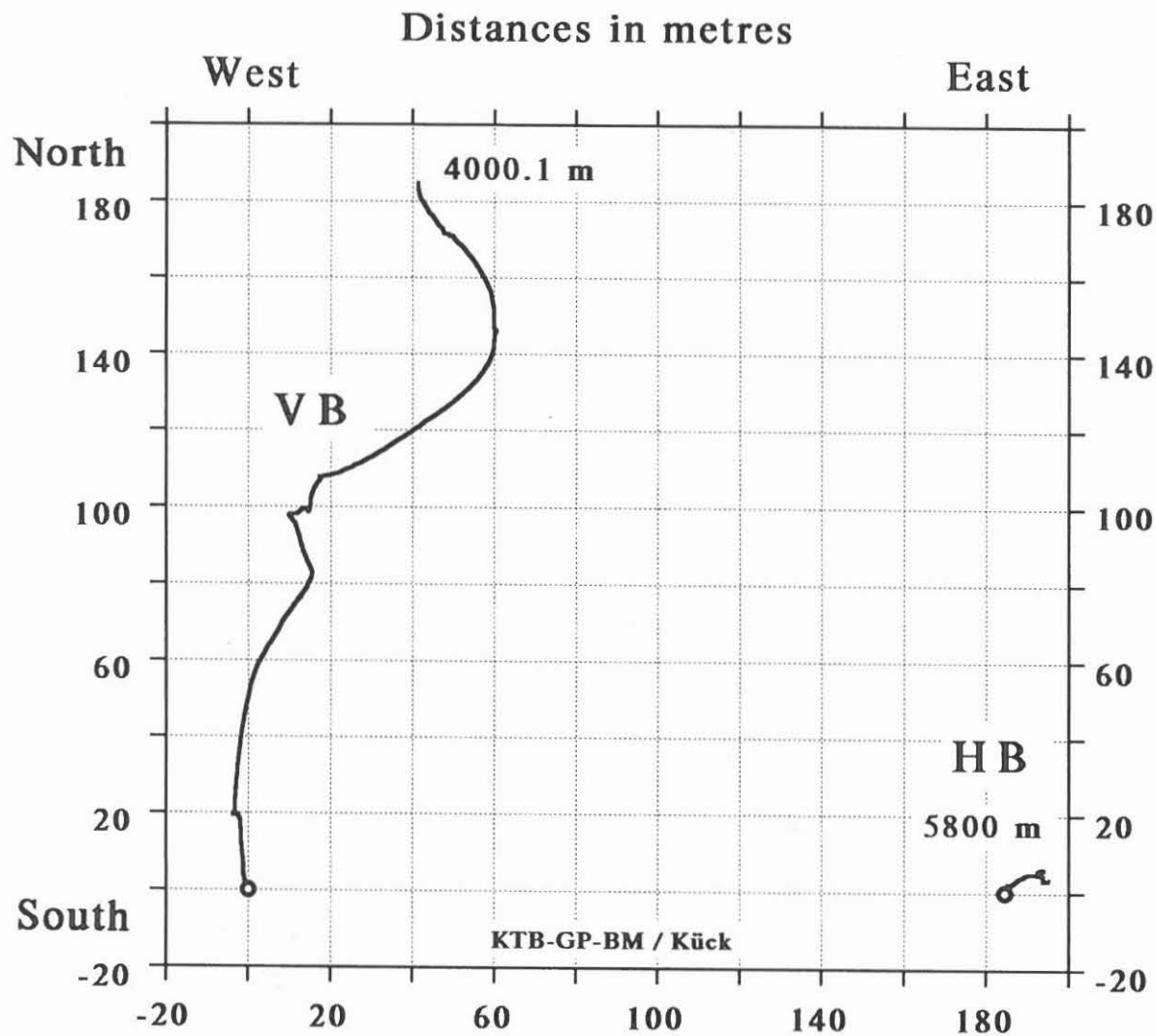
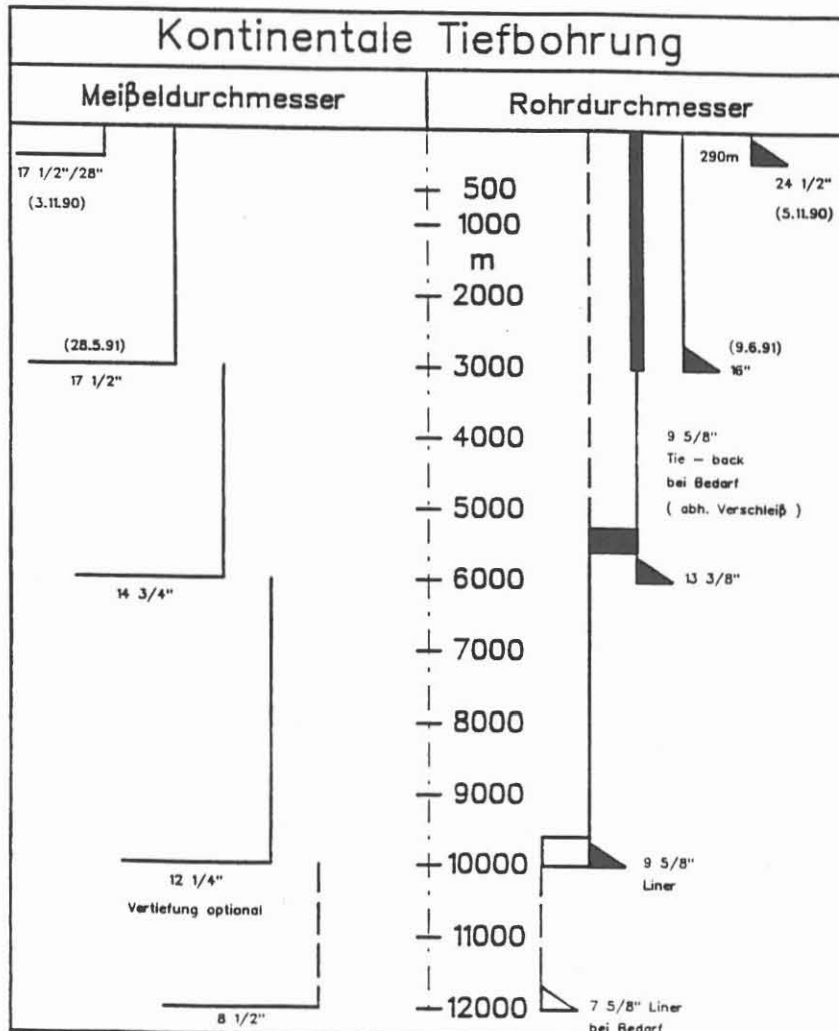


Fig. A.2.9: Horizontal and vertical projection of the KTB pilot hole (final depth 4000.1 m) and the KTB-Hauptbohrung (depth approx. 5820 m) at the end of February 1992.

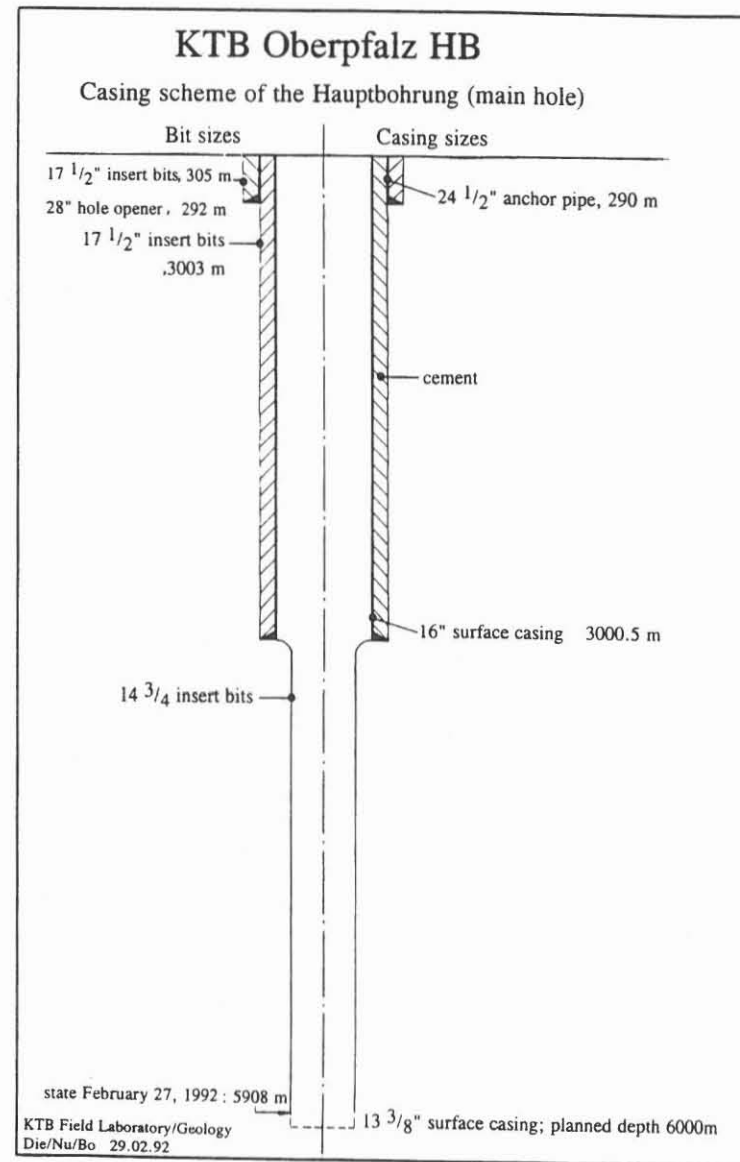


**KTB - Hauptbohrung**  
 - geplantes Bohr - u. Verrohrungsprogramm -

**KTB**

T 2297 / 12.91 / Sp      Niedersächsisches Landesamt für Bodenforschung

**Fig. A.2.10:** Drilling and casing scheme of the KTB Hauptbohrung.



**Fig. A.2.11:** Borehole view of the KTB Hauptbohrung to approx. 6000 m.

### A.3 Sampling

Since the pilot hole, situated about 200 m west of the KTB HB, was almost completely cored, no core material was taken from the upper 4000 m of the KTB HB. As a result of the change from wireline coring technique used in the pilot hole to the rotary technique used in the HB of which approx. only 15% is to be cored, for the depth interval down to 4000 m small rock particles, cuttings and rock flour are the only solid materials available for geoscientific investigations (Fig A.3.1). The first core from the Hauptbohrung was extracted in September 1991 at a depth of 4149.0 - 4156.8 m (Fig. A.3.2). Altogether 19 cores were taken up to February 1992 (see part B) whereby the last core was recovered between 5758.5 and 5782.5 m. On average 8 1/2 m were cored between 4149.0 and 5782.5 m at 100 m intervals, with an average core recovery of 3.4 m.

#### A.3.1 Sample Types and Extraction Station

For continuous scientific investigations the following sample types are available:

- solid samples (cores, cuttings, rock flour, side cores, core slices and rock fragments).
- fluid samples (drilling mud and fluids from the fluid samplers)
- gas samples (gases released from the drilling mud and fluid samplers).

Extraction stations for the various samples are shown in the flow chart (Fig. A.3.1.1):

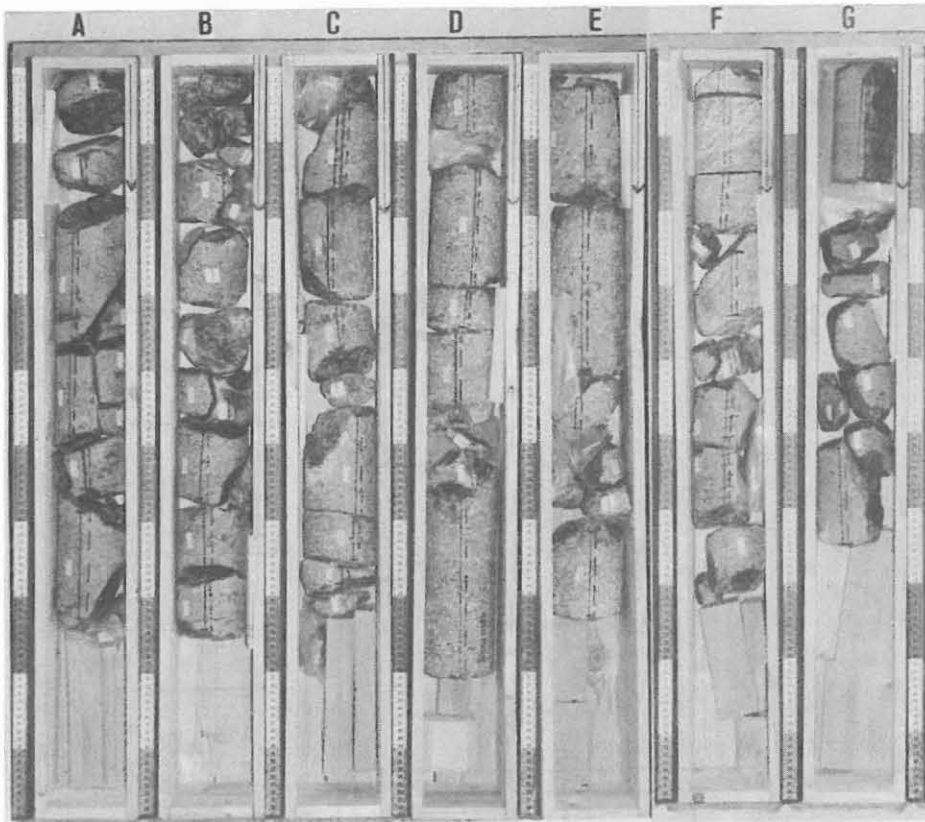
Cuttings are gathered routinely (Fig. A.3.1.2 - A.3.1.4) from the drilling mud 1) just before it enters the shakers (D), 2) from the shakers (C) and 3) from the centrifuge (E). Grain size decreases from sometimes many centimeter-large rock pieces over millimeter particles down to the so-called rock flour. Samples are generally collected at 1 m intervals. Samples were also taken during extension of the borehole from 17 1/2" to 28". Here, however, sampling intervals varied according to the known lithology between 1.0 and 4.0 m.

Drilling fluid samples taken behind the shakers (Fig. A.3.1.1) are collected at the same intervals as the solid samples.

For investigation and analysis of gases dissolved in the drilling mud, gas traps are installed just before the shakers (Fig. A.3.1.1) and connected to measuring instruments in the field laboratory by a heatable gas line. A gasmass-spectrometer, a gas chromatograph and a specially developed radon-measuring device are available at the field laboratory for the gas analysis (Fig. A.3.1.5). With the help of an automatic gas collector system, connected to the gas chromatograph, gas samples can at all times be automatically obtained (Fig. A.3.1.6).

In addition to the routine sample recovery, in-situ fluid samples (see Tab. A.3.1.1) were collected from the borehole using a Geocom Fluid Sampler before setting of the 16" casing at 3000.5 m within the framework of a test-measurement program executed at the end of May 1991. Based on the on-line gas and drilling mud analysis, fluid samplers were run at especially selected depths between 3000 - 6000 m. During the course of the borehole measuring programme seven core slices from the depth interval 306 - 4592 m were collected (Tab.

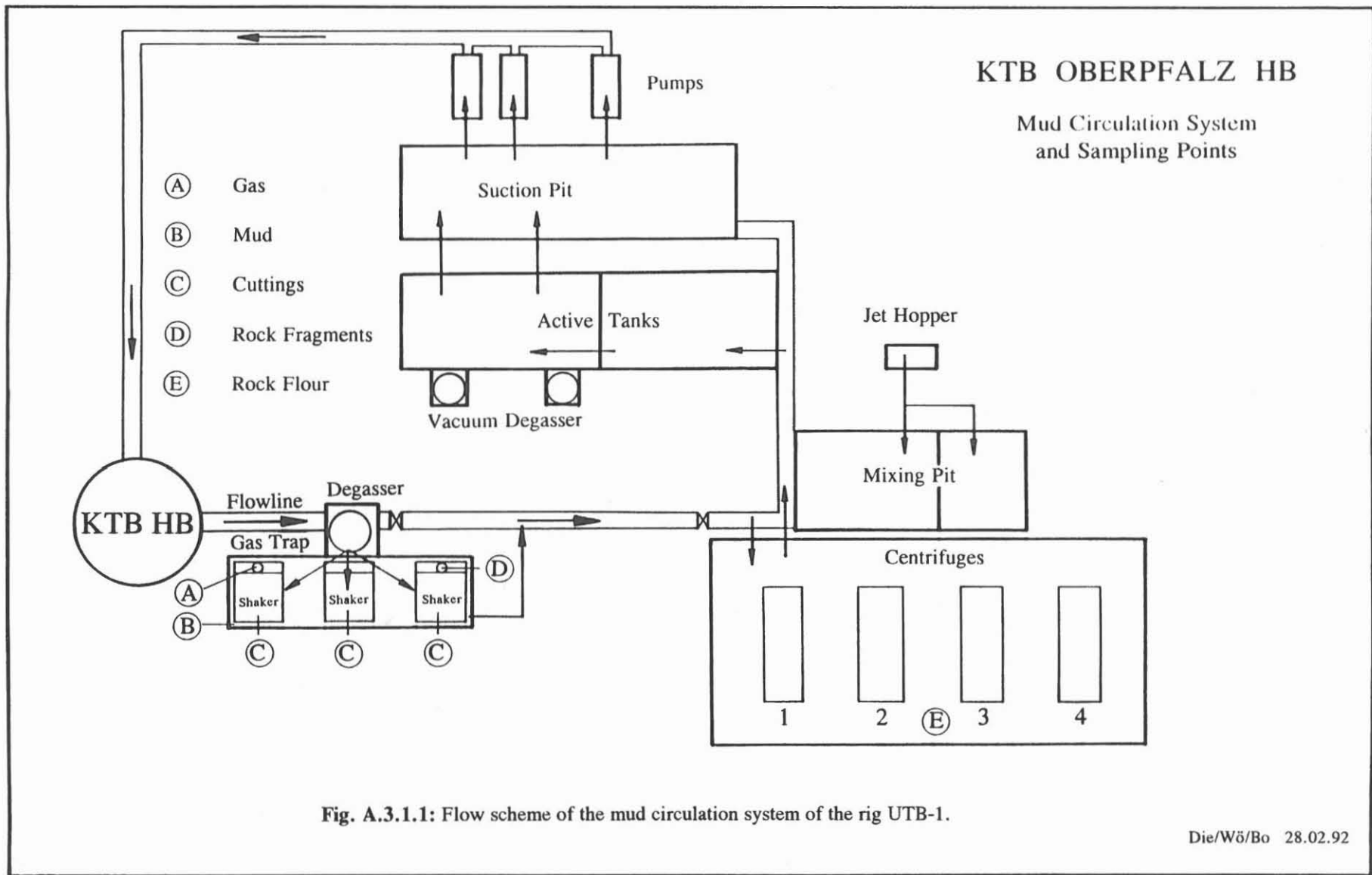


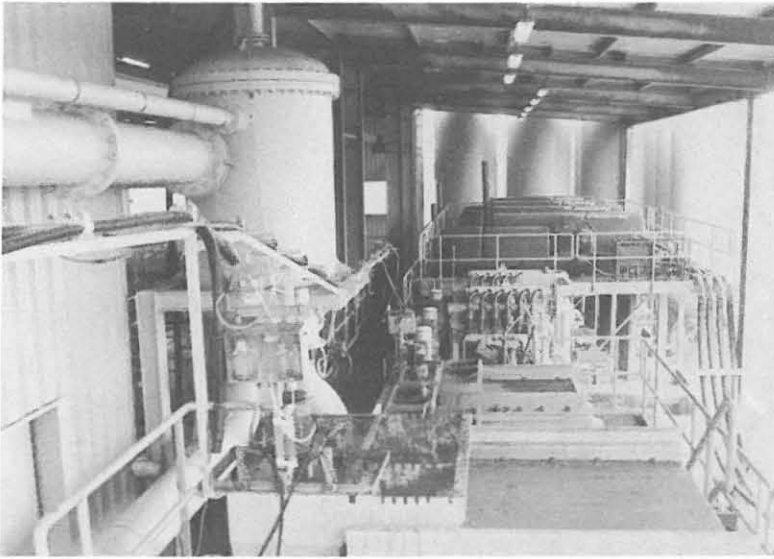


**Fig. A.3.1:** View of the first core recovered from the KTB Hauptbohrung (depth 4149.0 - 4156.8 m, core recovery 5.3 m)

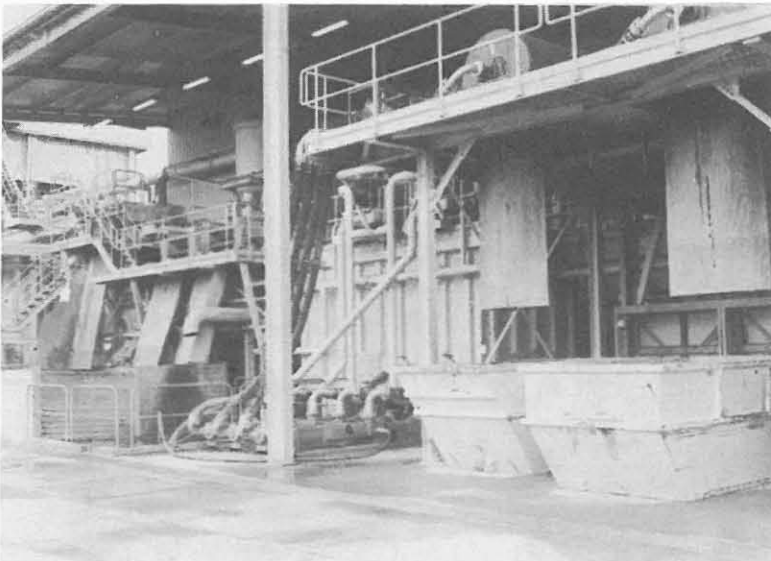


**Fig. A.3.2:** Example of washed, sieved and dried shaker samples (cuttings) from the uncored 4000 m of the KTB Hauptbohrung.





**Fig. A.3.1.2:** Shakers behind the gas separator.



**Fig. A.3.1.3:** View of flow line (left), shakers and centrifuges (right).



**Fig. A.3.1.4:** Recovery of large- sized cuttings from the possum belly in which a gas trap is installed.

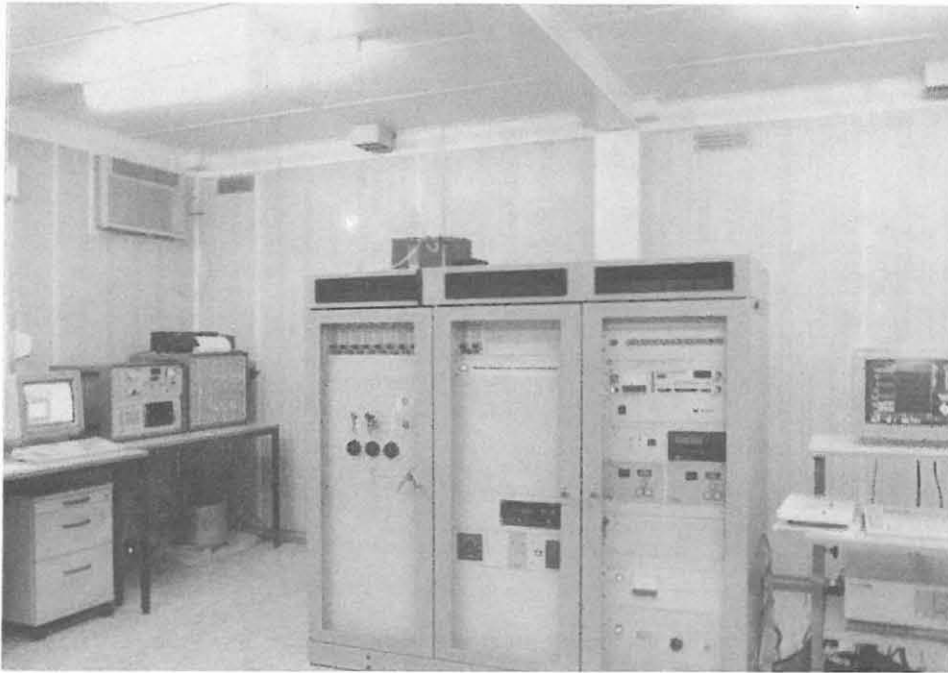


Fig. A.3.1.5: Process gas mass-spectrometer and FID chromatograph in the gas lab near the gas trap at the shakers.

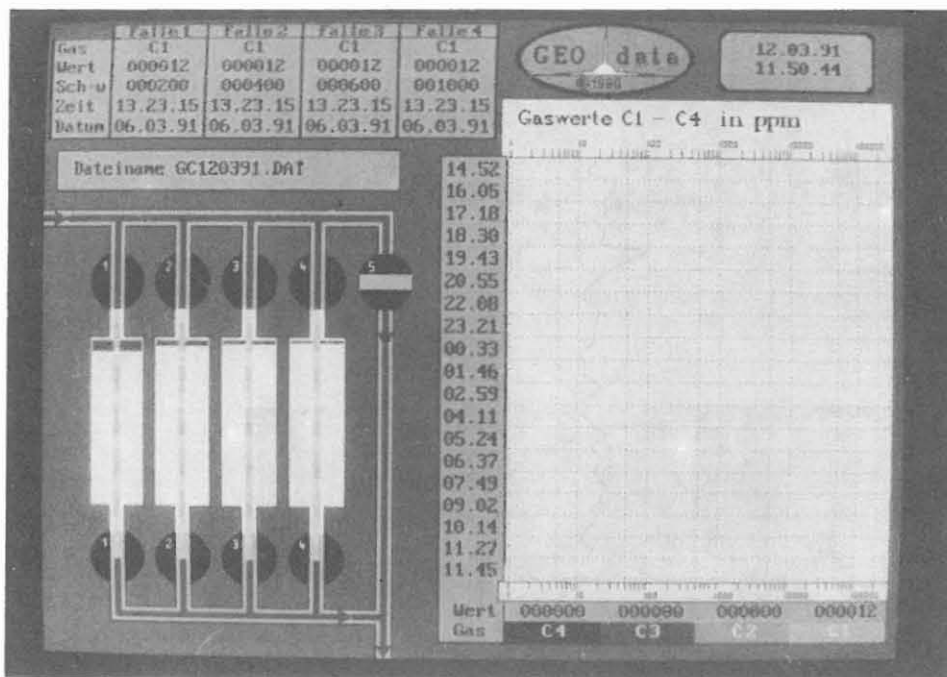


Fig. A.3.1.6: Monitor layout of the automatic gas collecting system connected to a gas chromatograph.

A.3.1.1). The sliced profile is triangle shaped (fig. A.3.1.7) with a side length of 1" and a slice length of maximum 36". Between 510 and 3961 m, 39 side cores (diameter 1" and av. length 2") were recovered (fig. A.3.1.8). Both sample types were taken using MSCT (mechanical side wall coring tool) and MCT (mechanical coring tool) tools respectively, developed by Schlumberger, whereby the core slicer was used for the first time in crystalline basement rocks. Both tools can only be employed in in-gauge hole sections.

A summary of the various "in situ samples" is given in Table A.3.1.1.

**Tab. A.3.1.1:** Overview of in situ sample collection from 0 - 6000 m in the KTB-HB at the end of February 1992:

sample type	date	depth (m)
fluid sampling	June 1-4, 1991	701, 1530, 1960, 2975, 3001
	Aug. 23, 1991	3950.5
	Oct. 15, 1991	4115
	Nov. 32, 1991	3184
	Jan. 4, 1992	5388
cores / core slicer	June 3, 1991	306, 1193, 2653, 2658
	Oct. 15, 1991	3196, 3725, 4295
side cores	June 4- 5, 1991	510, 861, 986, 972, 974, 1104, 1105, 1120, 1325, 1382, 1540, 1547.5, 1925, 1993.8, 2160, 2383.5, 2470, 2480, 2607.5, 2658.5, 2682, 2830, 2958, 3000.5, 3001,
	Oct. 16, 1991	3030, 3115, 3271, 3314, 3321, 3332, 3392, 3404, 3465, 3523, 3668, 3695, 3842, 3961.5

Junk basket and "cuttings sampler" were run about 20 times during 14 3/4" drilling with an average sample recovery of 15 kg. Between 5 - 10 kg of coarse fragments (> 2 cm) were recovered (figs. A.3.1.9 - A.3.1.10).

### A.3.2 Depth assignment of samples

The depth distribution of the recovered samples is of special importance for the interpretation of the samples obtained. To assure regularity of sampling, even in a monotonous interval, depth correction is continuously carried out by measuring lag time of the drilling mud from bottom hole to surface. A classification of the depth distribution of the recovered material, the dependance on borehole depth, the annulus between the drill string and borehole wall, drilling operation, composition of the drilling fluid and pompe rate would be practically impossible without depth correction (Dietrich et al., 1991).

Later, the depth classification of a sample, which was classified according to the actual drilling depth is performed using the results of borehole measurements, even in the case of the

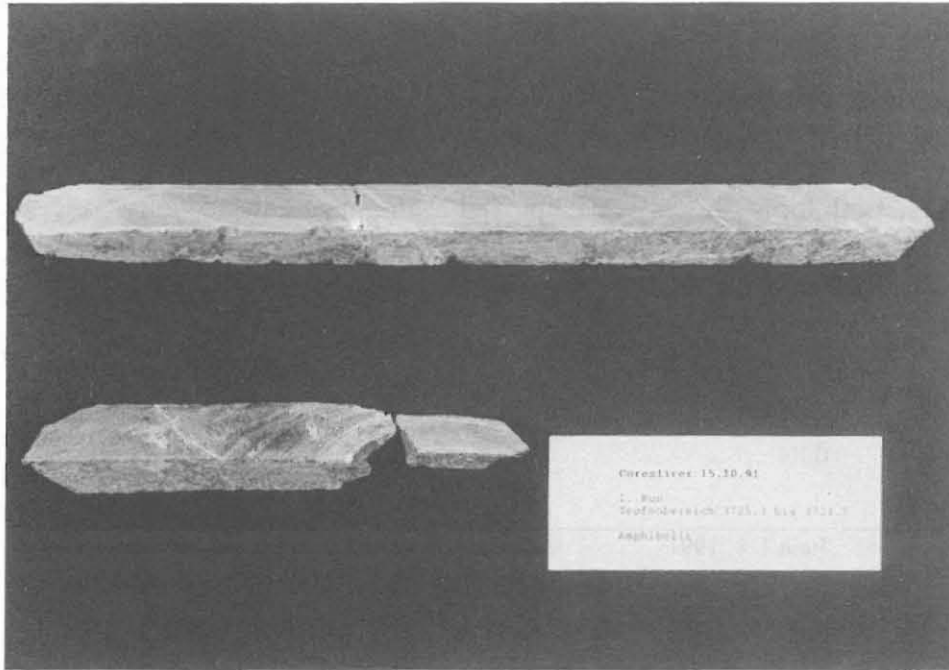


Fig. A.3.1.7: Core slices from the 14 3/4" hole section of the KTB Hauptbohrung.

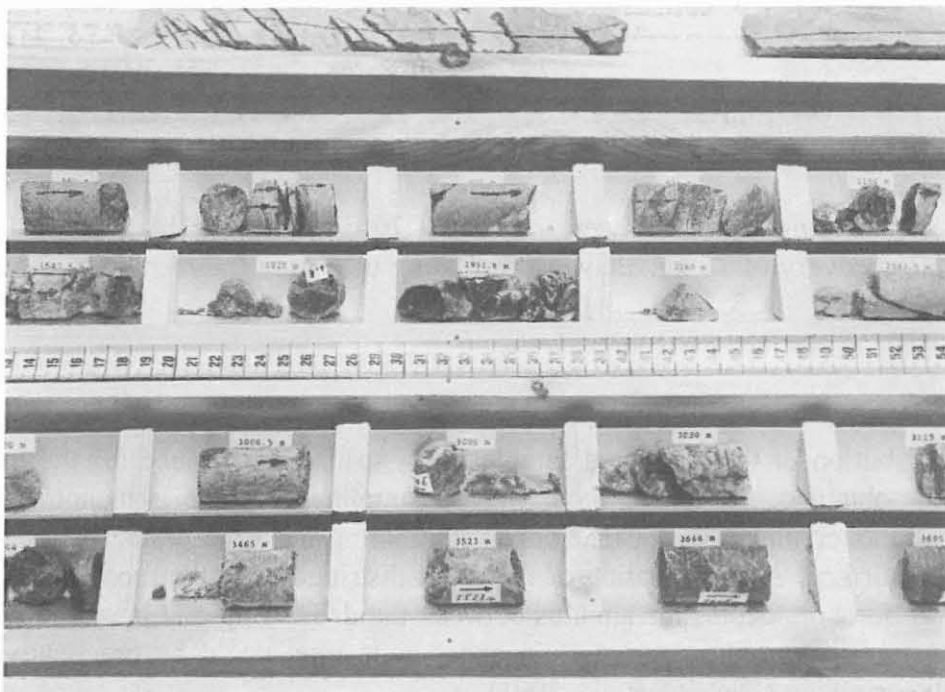


Fig. A.3.1.8: Side wall cores from 17 1/2" and 14 3/4" sections of the KTB Hauptbohrung.

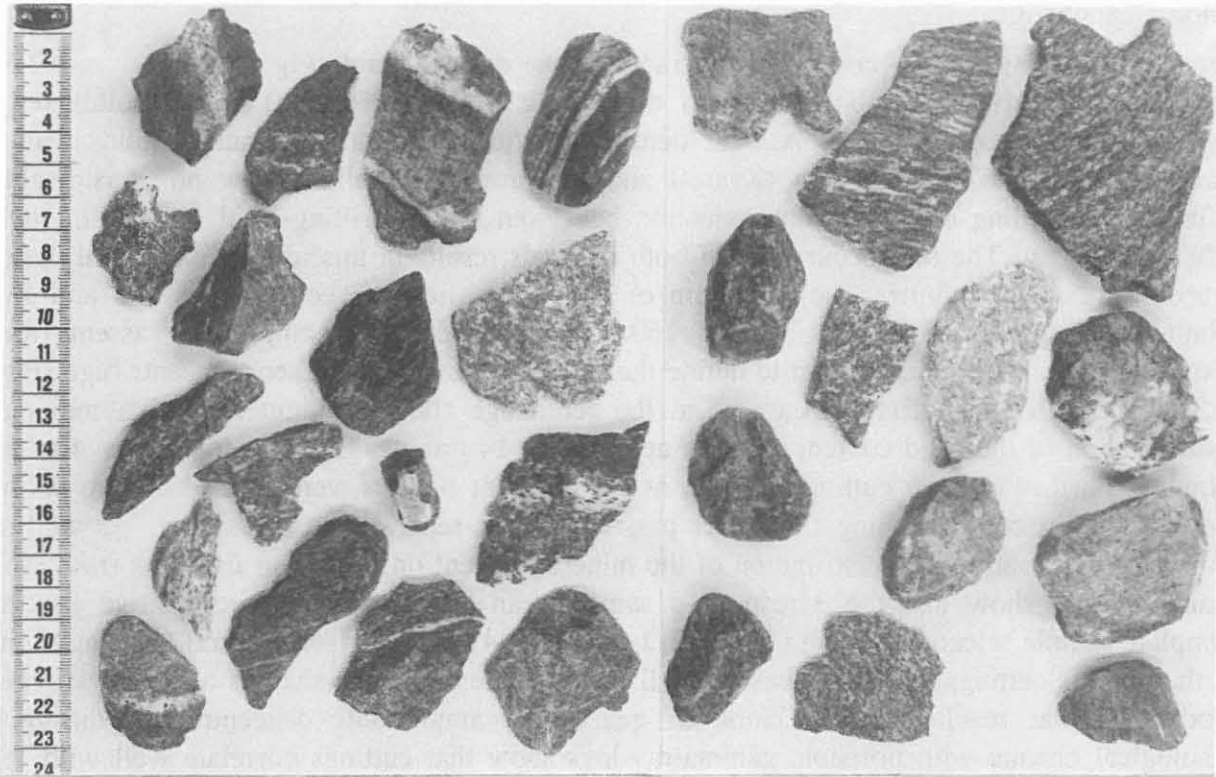


Fig. A.3.1.9: Larger sized rock fragments collected with the junk basket (depth interval 3923.4 - 3952.9 m).

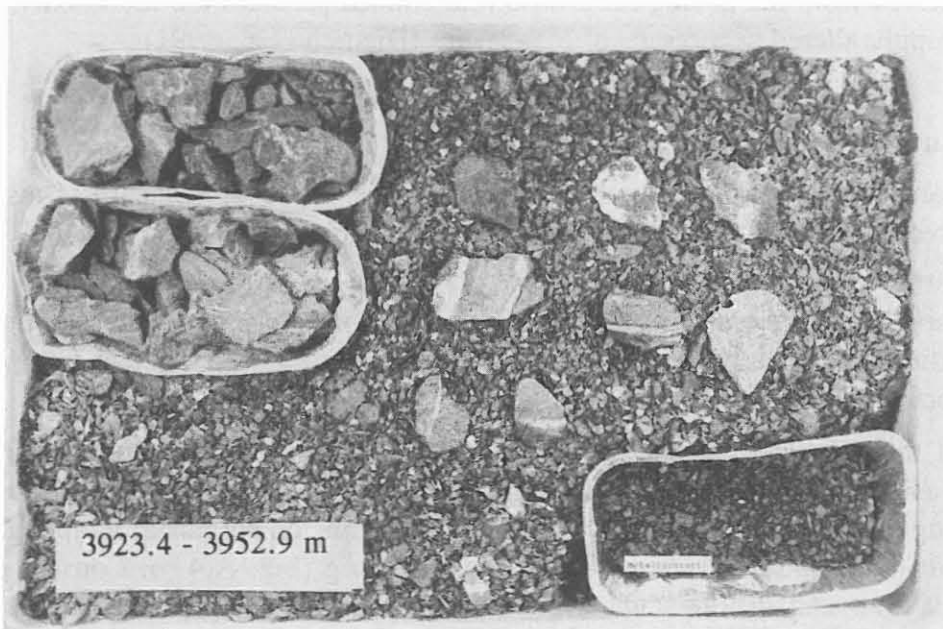


Fig. A.3.1.10: Overview of rock fragments collected with the junk basket

lithological change.

The calculated lag time is controlled by tracing the drilling fluid (Fig. A.3.2.1 - A.3.2.2) which is pumped into the borehole with different gases (e.g. Helium) and/or solids (e.g. Kyanite and Cristobalite). Fig. A.3.2.2 demonstrates that at least fine-grained solids with a maximum grain size of 175  $\mu\text{m}$  (Kyanit) and 128  $\mu\text{m}$  (cristabolite) show no considerable difference regarding dispersion and assention behaviour in the drilling fluid in spite of their differing density. The first occurrence of both minerals results in this test simultaneously after approx. 112 - 113 minutes, the maximum of both solids lies between approx. 120 and 140 minutes, the last proof follows approx. 160 - 170 minutes after commencing assent from bottom hole. A corresponding test to define the delay time between shaker and centrifuge (Fig. A.3.1.1) resulted in a first appearance at the centrifuge about 2 minutes later, a maximal concentration of the solid content between approx. 6 - 14 minutes an a last trace after 40 - 60 minutes. Further tests on cutting-selection at the different shakers were carried out, to define the distribution of the drilling fluid after passing the gas separator to the shaker. As well as grain size distribution, the distribution of the mineral content on two grain fractions from each shaker 1 - 3, show that the 3 respective samples can be judged as representative for the complete sample selection system (Fig. A.3.2.3 - A.3.2.4). Comparison mineral concentrations of the various cuttings prove that basically all solid samples from the shakers or the centrifuges produce similar results. A correlation of quarz- and amphibolite concentrations during a lithological change with borehole gamma-ray-logs show that cuttings correlate well with log results (Fig. A.3.2.5 - A.3.2.6).

Inspection of cuttings with a grain fraction of  $> 1 \text{ mm}$ ,  $< 1 \text{ mm}$  and  $> 63 \mu\text{m}$  and  $< 63 \mu\text{m}$  shows that as a rule approx. 60 - 80% of cutting material collected in the shakers are lager than 1 mm. As derived from the geological profile fine-grained particles are found only in intervals which are strongly altered as a results of cataclastics (Dietrich et al. 1991).

#### **A.4 Sample notation and -requesting**

To simplify and standardize the sample classification the following standard terms have been chosen for investigation, archiving and distribution of samples.

From the cutting samples listed under point 4 in Tab. A.4.1 approx. 1.5 to 2.0 kg of unchanged, non-analyzed, and wet samples are available in our archives. In addition prepared and dried cuttings and rock flour samples are also available, washed, sived and / or ground for field laboratory investigations (Fig. A.4.1 - A.4.2).

All results of the continuous investigations are directly stored in a database and are therefore immediately available for subsequent investigation. To assure the constant quality of sampling with increasing depth and thus reliabililty of scientific results, an automatic sampling system for cuttings and drilling fluid will be integrated into the drill rig (Fig. A.4.3). Constant amounts of cuttings, rock flour and drilling mud will be sampled from a by-pass flow regulated by the pumping rate and drilling progress (Heinisch 1991).



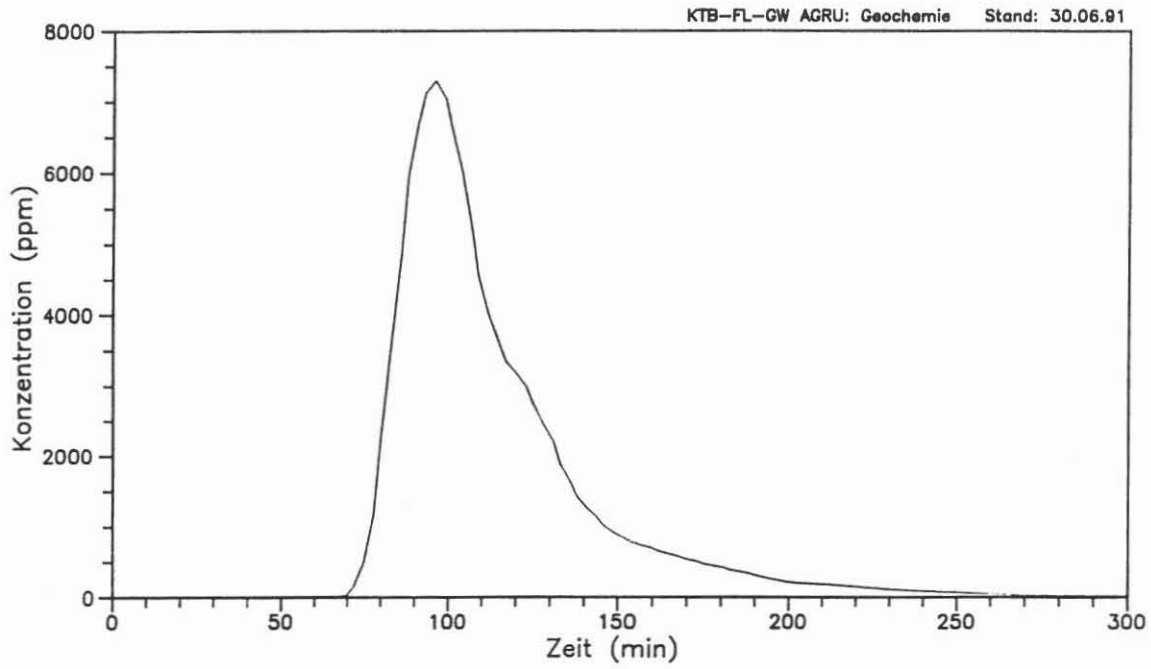


Fig. A.3.2.1: Helium tracer test March 16, 1991 (depth 1816.5 m).

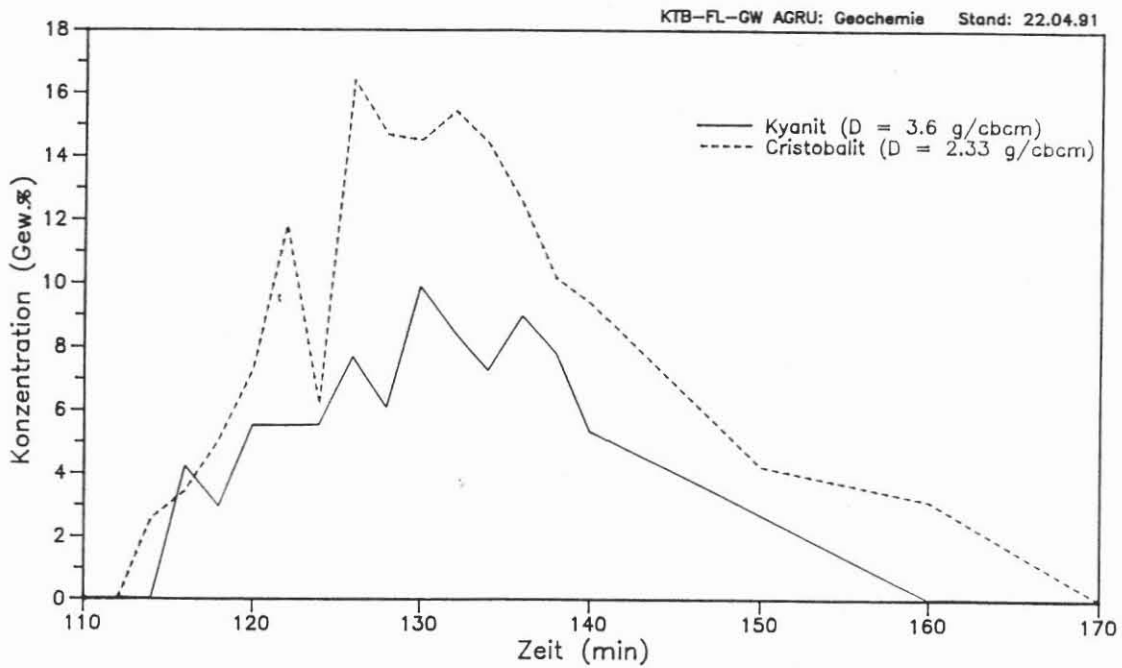


Fig. A.3.2.2: Cristobalite / Kyanite test April 18, 1991 (depth 2523 m).

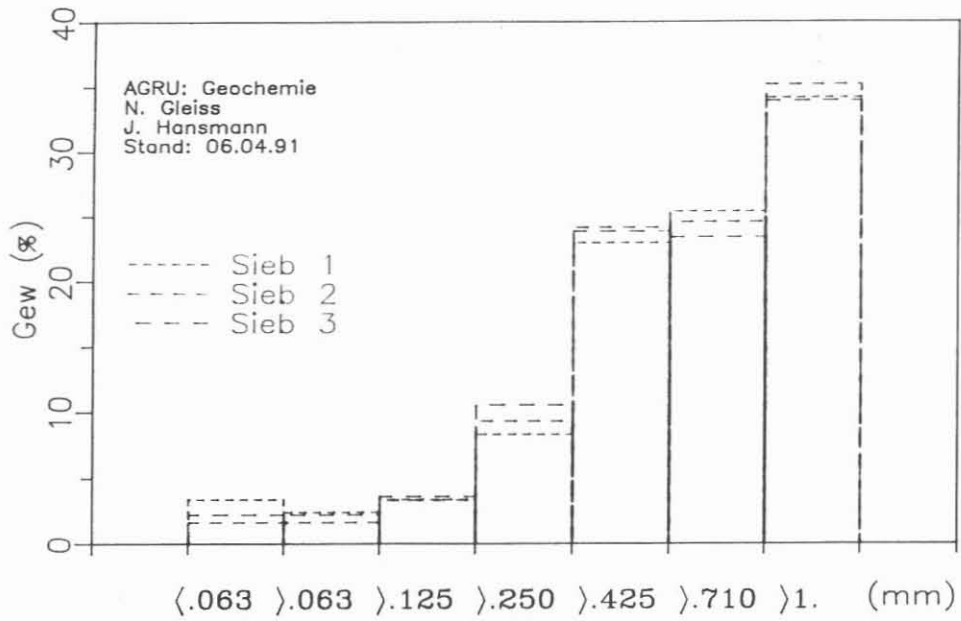


Fig. A.3.2.3: Grain size distributions of representative cutting samples from the three shakers (depth 2082 m).

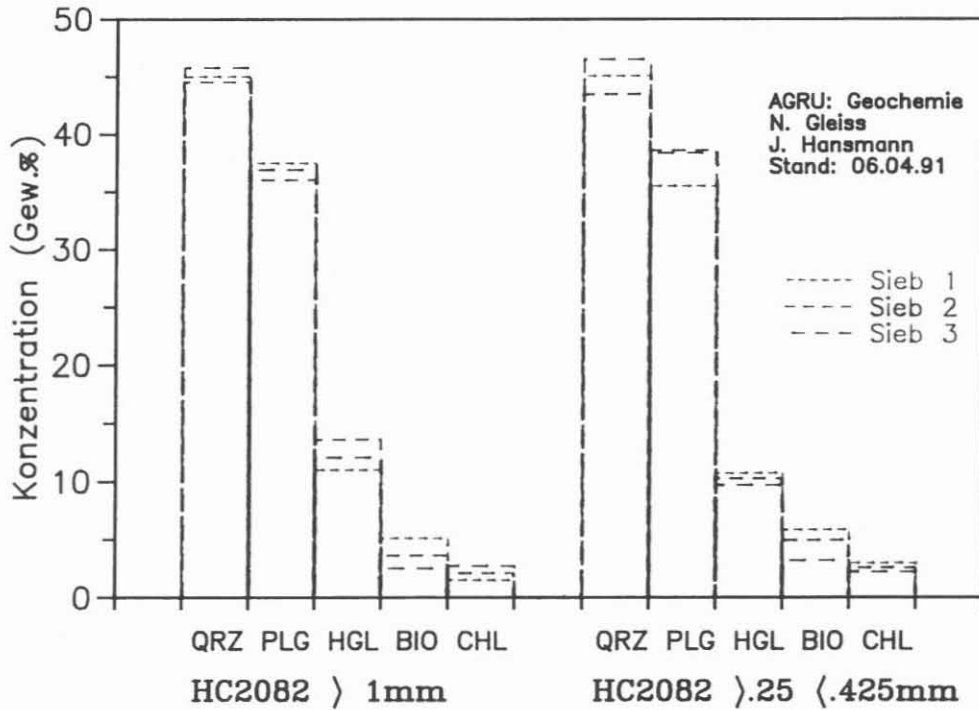


Fig. A.3.2.4: Distribution of the mineral content in grain size fraction > 1 mm respectively > 0.25 mm and < 0.425 mm in representative cutting samples at 2082 m.

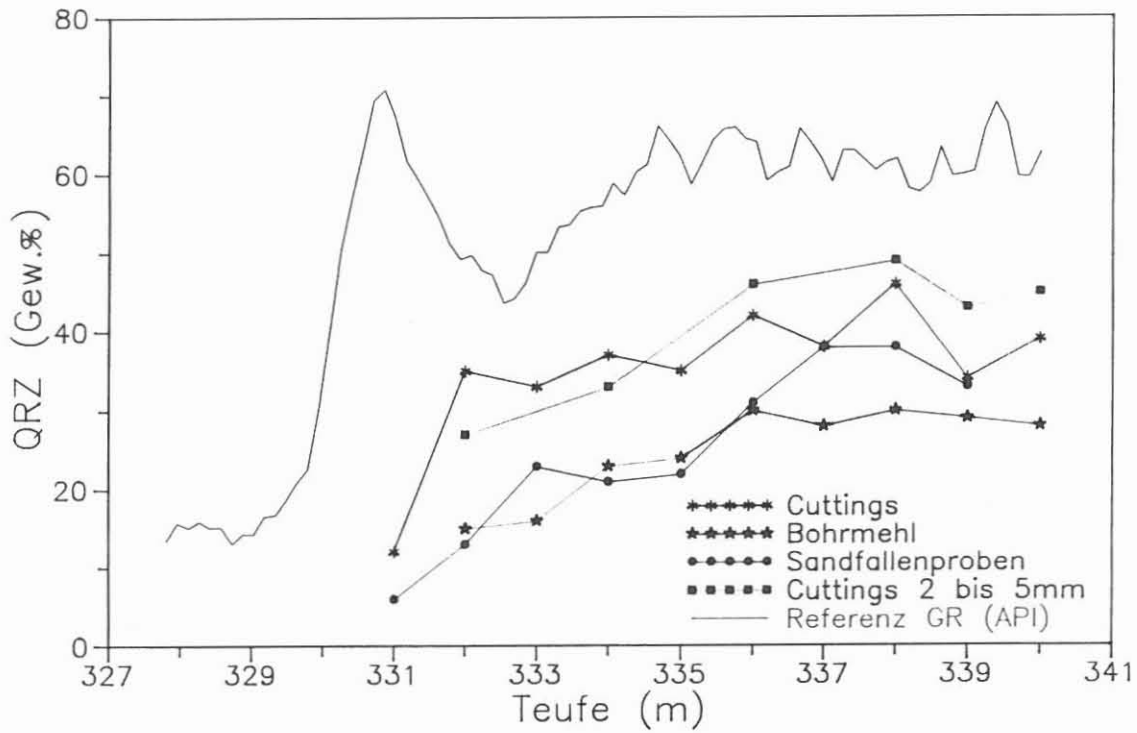


Fig. A.3.2.5: Change in quartz content marking a lithological change amphibolite to gneiss.

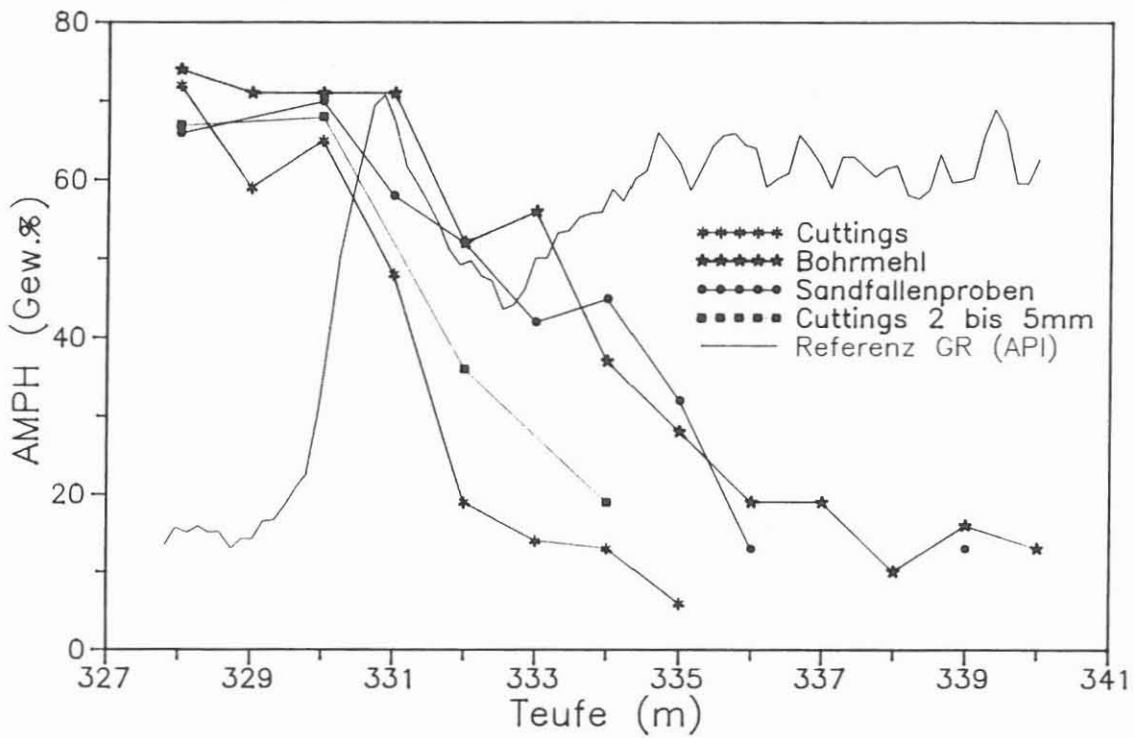


Fig. A.3.2.6: Change in amphibole content marking a lithological change from amphibolite to gneiss.



**Fig. A.4.1:** Computer-aided cuttings analysis in the KTB field laboratory.



**Fig. A.4.2:** Image-analysis of thin sections in the KTB field laboratory.

**Tab. A.4.1:** Notation of Samples from the KTB Hauptbohrung

type of sample	abbreviation	sample notation (type, depth)	date of recovery
1. core	HK	core run, core piece	-
2. side core	HSK	HSK3049	+
3. core slice	HSL	HSL0306	+
4. cuttings/cavings			
- possum belly	HF	HF0078	-
- shaker / cuttings	HC	HC0078	-
- centrifuge / rock flour	HZ	HZ0145	-
- junk basket	HR	HR3294	-
- cuttings sampler	HCS	HCS5599	-
5. mud samples	HS	HS1256	+
special samples e.g.: cuttings during hole extensions	HEC	HEC0078	-



**Fig. A.4.3:** Automatic sampling system for cuttings and drilling fluid samples (Test phase Feb./March 1992).

Order forms for KTB sample material can be got from

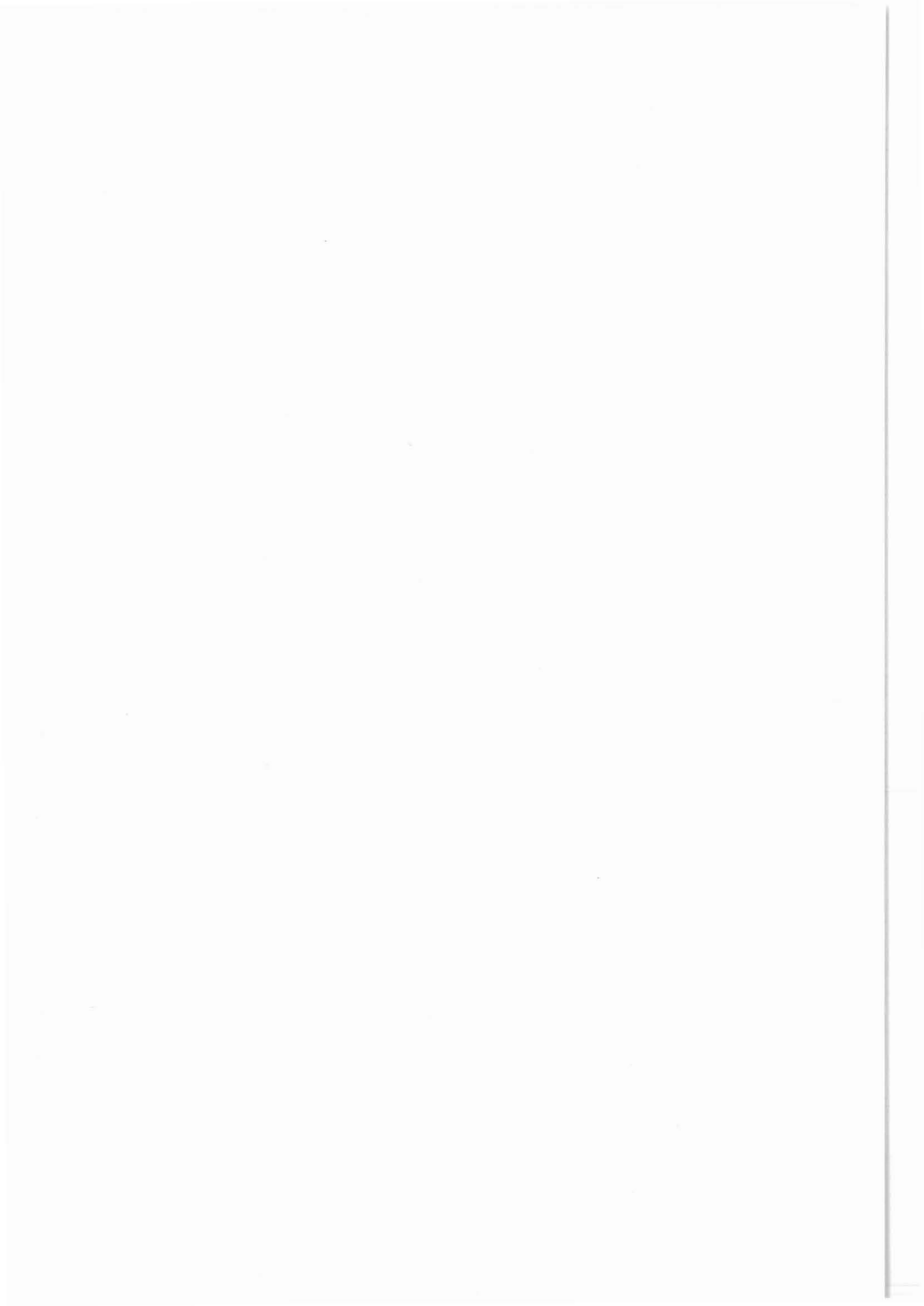
NLFB  
KTB-Feldlabor  
Postfach 67  
8486 Windischeschenbach  
Telephone 09681 / 40014  
Telefax 09681 / 40038

## A.5 References

- Bram, K. & Draxler, J. K. (eds., 1992): Grundlagenforschung und Bohrlochgeophysik (Bericht 13). Bohrlochmessungen in der KTB Oberpfalz HB, Intervall 1720.0 - 4512.0 m. - KTB Report 92-1, Hannover.
- Bram, K., Draxler, J. K. & Zoth, G. (eds., 1991): Grundlagen forschung und Bohrlochgeophysik (Bericht 11). Bohrlochmessungen in der KTB Oberpfalz HB, Intervall 0 - 1720.0 m. KTB Report 91-2, Hannover.
- Chur, C., Engeser, B. & Oppelt, J. (1990a): Das Vertikalbohrkonzept für die KTB-Hauptbohrung. - Erdöl Erdgas Kohle, 106. Jahrgang, 12, 486 - 490.
- Chur, C., Engeser, B. & Oppelt, J. (1990b): Vertical Drilling Konzept for the Mainwell. - Oil Gas, 16, 4, 26 - 29.
- Dietrich, H.-G. (1992): Aktuelle Mitteilungen aus dem KTB Feldlabor. Pilotartikel zur ständigen Rubrik KTB ab Heft 1/'92. - Die Geowissenschaften, 10. Jahrgang 1, 1-3.
- Dietrich, H.-G., Gleiß, N., Hansmann, J., Lauterjung, J. & Wöhrl, Th. (1991): Einleitung. - In: Emmermann, R., Dietrich, H.-G., Lauterjung, J. & Wöhrl, Th. (eds.). - KTB Report 91-3, A1-A26, Hannover.
- Emmermann, R. (1990): Vorstoß ins Erdinnere: Das Kontinentale Tiefbohrprogramm. - Spektrum der Wissenschaft, 60 - 70, Oktober 10/1990.
- Emmermann, R., Dietrich, H.-G., Lauterjung, J. & Wöhrl, Th. (eds., 1990), KTB Pilot Hole, Results of Geoscientific Investigation in the KTB Field Laboratory, 0 - 4000.1 m. KTB Report 90-8, Hannover.
- Emmermann, R., Dietrich, H.-G., Lauterjung, J. & Wöhrl, Th. (eds., 1991): Tiefbohrung KTB Oberpfalz HB, Ergebnisse der geowissenschaftlichen Bohrungsbearbeitung im KTB-Feldlabor, Bericht 1 zur KTB-Hauptbohrung, Teufenbereich 0 - 1720. KTB Report 91-3, Hannover.
- Emmermann, R. & Giese, P. (Hrsg., 1990): Beiträge zum 3. KTB-Kolloquium. Gießen, 28.02. - 02.03.1990. - KTB-Report 90-4, Hannover.
- Emmermann, R. & Rischmüller, H. (1990): Das Kontinentale Tiefbohrprogramm der Bundesrepublik Deutschland (KTB). Aktueller Stand und Planung der Hauptbohrung - Die Geowissenschaften, 8. Jahrgang, Nr. 9, 241 - 257.
- Heinisch, M. (1991): Das automatische Probenahmesystem für die Hauptbohrung des KTB. - In: Emmermann, R., Dietrich, H.-G., Lauterjung, J. & Wöhrl, Th. (eds., 1991). - KTB Report 91-3, I1-I3, Hannover.
- Sigmund, J. & Dietrich, H.-G. (1990): Sedimentrohr-Proben in der KTB-Vorbohrung VB1b. - In: Emmermann, R., Dietrich, H.-G., Lauterjung, J. & Wöhrl, Th. (eds., 1990). - KTB Report 90-2, H1-H9, Hannover.
- Rischmüller H. (1990): Example for Advanced Drilling Technology. - Oil Gas 16, 4, 16 - 20.
- Rischmüller H. (1991): Beitrag der Bohrprojekte der Lithosphärenforschung zur Entwicklung der Bohrtechnik für große Tiefen, dargestellt am Beispiel des KTB. - Erdöl Erdgas Kohle, 107, 1, 51 - 58.

## B. Geology

- |      |  |          |
|------|--|----------|
| B. 1 | German Continental Deep Drilling Program (KTB) – geological survey of the Hauptbohrung 0 – 6000 m<br>Susanne Lich, Johannes Duyster, Georg Godizart, Stefan Keyssner & Helga de Wall | B 1      |
| B. 2 | Drilling artifacts in cuttings samples<br>Helga de Wall & Susanne Lich   | B 43     |
| B. 3 | The geological section of the KTB Hauptbohrung – correlation with the KTB Vorbohrung and preliminary structural interpretation<br>Gottfried Hirschmann                               | B 47     |
| B. 4 | Cuttings profile 0 – 6000 m<br>Working groups Geology, Geochemistry, Geophysics  | B 53     |
|      | Compilation of geologically relevant data, 0 – 3000 m  | Appendix |





<b>KTB Report</b>	92-2	B1-B42	42 Fig.	Hannover 1992
-------------------	------	--------	---------	---------------

## **B.1 GERMAN CONTINENTAL DEEP DRILLING PROGRAM (KTB) - GEOLOGICAL SURVEY OF THE HAUPTBOHRUNG 0 - 6000 m**

**S. Lich, J. Duyster, G. Godizart, S. Keyssner & H. de Wall\***

<b>Contents</b>	<b>page</b>	
B.1. 1	INTRODUCTION	B 1
B.1. 2	METHODS	B 3
B.1. 3	GEOLOGICAL PROFILE	B 4
B.1. 4	PETROGRAPHY	B 7
B.1. 4.1	Paragneisses	B 7
B.1. 4.1.1	Evolution of fabrics and metamorphism	B 7
B.1. 4.2	Metabasic rocks	B 12
B.1. 4.2.1	Petrography	B 12
B.1. 4.2.2	Metamorphic evolution	B 19
B.1. 4.2.3	Deformation	B 20
B.1. 4.2.4	Chemical composition	B 23
B.1. 4.3	Late dykes	B 25
B.1. 4.3.1	Lamprophyres	B 25
B.1. 4.4	Aplites	B 25
B.1. 5	ORE MINERALIZATION	B 26
B.1. 5.1	Sample routine	B 26
B.1. 5.2	Ore minerals	B 26
B.1. 5.3	Age relations and aspects of formation	B 27
B.1. 5.4	Qualitative and quantitative distribution of ferrimagnetic ore minerals	B 27
B.1. 6	OPEN POROSITY AND CORRELATION WITH GAS ANALYSIS	B 31
B.1. 7	STRUCTURE	B 34
B.1. 8	SUMMARY	B 35
B.1. 9	ACKNOWLEDGEMENTS	B 37
B.1. 10	REFERENCES	B 37
B.1. 11	APPENDIX	B 39
B.1. 11.1	List of mineral abbreviations	B 39
B.1. 11.2	Description of the geological profile	B 40
B.1. 11.3	Short (preliminary) description of the cores in the KTB Hauptbohrung	B 42

### **B.1. 1. INTRODUCTION**

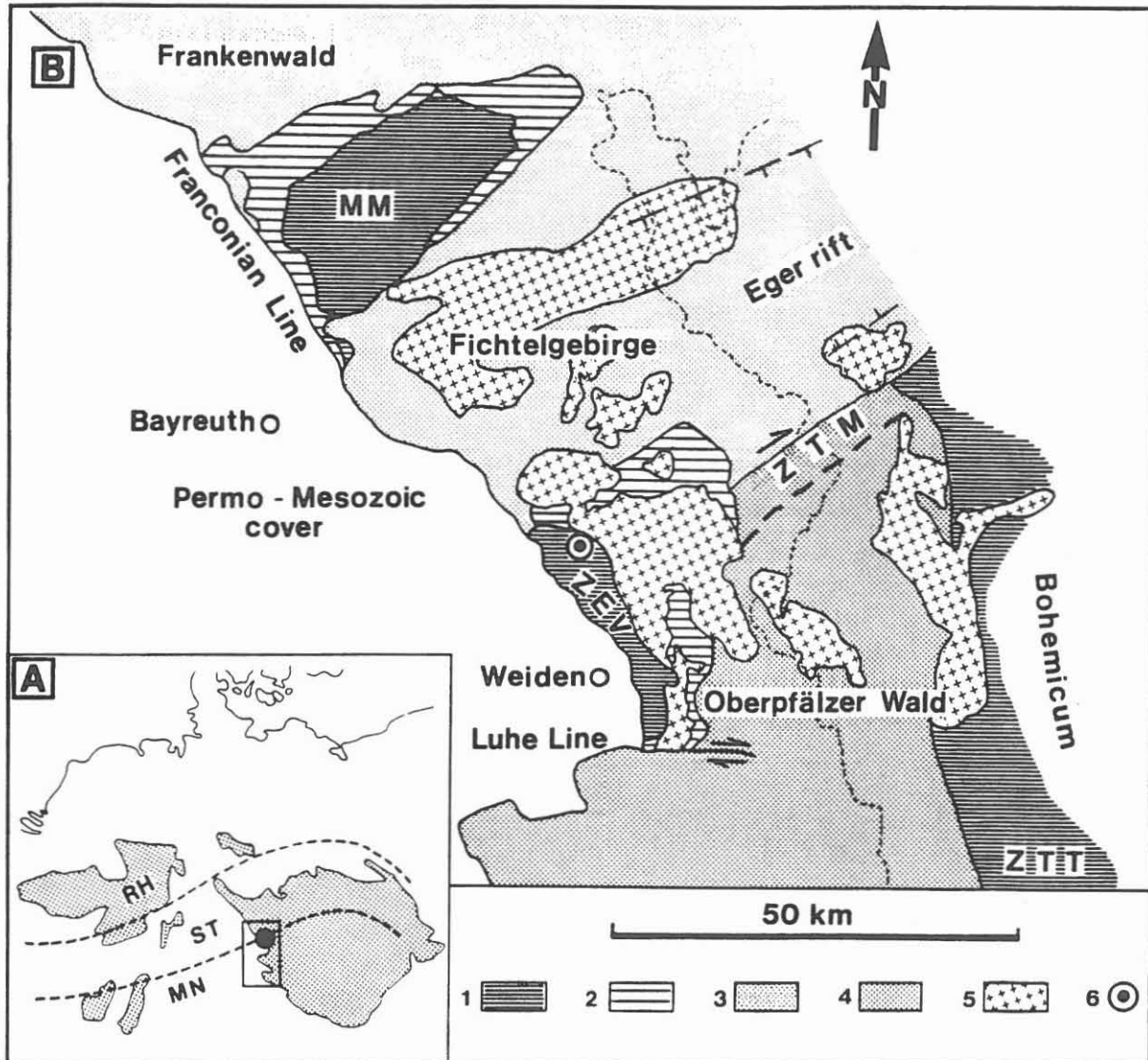
This contribution summarizes the geological aspects of the drill section 0 - 6000 m of the KTB main hole (Hauptbohrung HB). First, a short outline of the most important results

---

\* KTB Feldlabor, P.O. Box 67, D-8486 - Windischeschenbach

obtained from the KTB pilot hole (Vorbohrung VB) is given. The reader is referred to the earlier volumes of the KTB-REPORT for details. A comprehensive summary has been provided by Emmermann et al. (1990).

KTB has drilled a section of metamorphic basement, which constitutes the western Bohemian Massif (fig. B.1. 1.1). It is composed of two main rock types: paragneisses and metabasites. The paragneisses are derived from greywackes (Wimmenauer et al. 1991); a late Silurian to early Devonian age of deposition has been invoked on the base of palynology by Pflug & Prössl (1991).



**Fig. B.1. 1.1.:** Geological sketch map of the western margin of the Bohemian Massif in NE Bavaria . A: Variscan basement outcrops in Middle Europe with zones according to KOSSMAT (1927). RH: Rhenohercynian Zone; ST: Saxothuringian Zone; MN: Moldanubian Region. B: Geological map: 1,2 Münchberg Massif (MM), Zone of Erbdorf-Vohenstrauß (ZEV), Zone of Tepla-Taus (ZTT), 3: Saxothuringian; 4: Moldanubian of the Oberpfälzer Wald; 5: late- to post-tectonic granites; 6: KTB drilling site; ZTM: Zone of Tirschenreuth-Mähring(after Weber 1990)

The metabasites (metagabbros to amphibolites, minor meta-ultramafites) are essentially derived from an intrusive complex (Schalkwijk 1991) the age of which is inferred to be Ordovician on the base of Rb-Sr, U-Pb and Sm-Nd isotopic systems (v. Drach & Köhler 1990, v. Quadt 1990). These age relations would preclude that the paragneisses form the original country rock of the basic intrusions. At present, there is no independent evidence for this conclusion, however. On the contrary, a late Silurian to early Devonian sedimentation age leaves very little time for burial and metamorphism. K-Ar ages of amphibole and white mica (Kreuzer et al. 1990) range between about 380 and 385 Ma giving a lower age limit for metamorphism at high temperatures. This controversy remains to be resolved.

The rocks reveal records of a complex history in terms of deformation and metamorphism. A record of the earliest discernible stage is exclusively preserved in the metagabbros, where locally preserved parageneses require pressures up to 12 kb (Röhr et al. 1990b, Schalkwijk 1991). Subsequent to this stage of high-pressure metamorphism the rocks partially reequilibrated under granulite facies conditions. Both stages are not recorded by the paragneisses. The question whether the record has been completely wiped out due to later deformation under amphibolite facies conditions (7 kb, 675 °C, Reinhardt et al. 1989) or whether the paragneisses did not experience the early PT- history of the metabasites has to be resolved. Minor overprint under lower temperatures is localized and never goes to completion.

Unmetamorphosed lamprophyric and aplitic dykes crosscut the earlier structures.

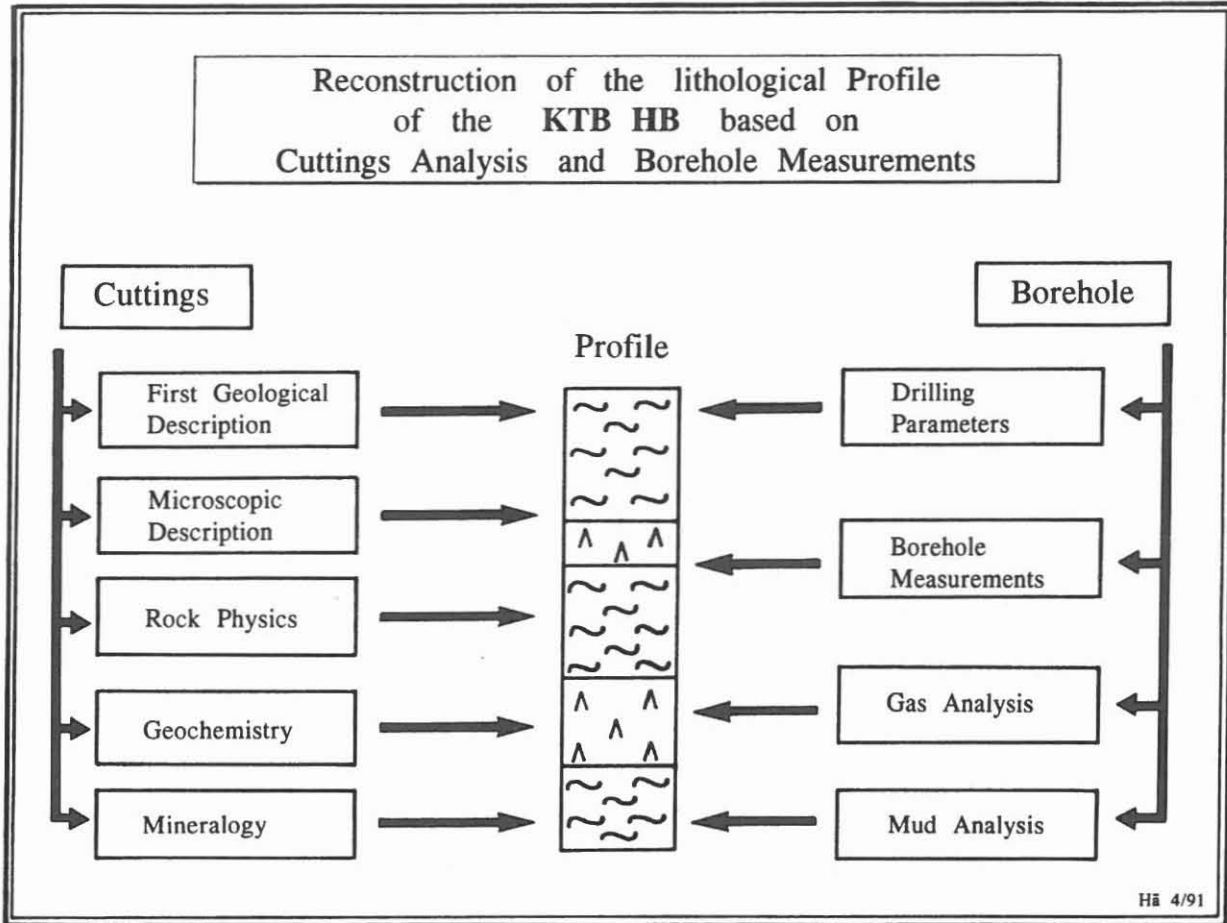
Deformation in the brittle field under high pore fluid pressure resulted in the formation of abundant cataclasites (Zulauf 1990).

The foliation in the KTB pilot hole is generally steeply inclined. It dips towards SW or NE. The observed changes in strike and dip of the foliation are interpreted to reflect large scale folds with near-horizontal NW-SE trending axis. KTB-HB has been placed into the same structure 180 m towards the East.

## **B.1. 2 METHODS**

The KTB pilot hole had been cored nearly continuously. In the KTB Hauptbohrung down to 4149 m, roller cone bits have been used. Cuttings are the only material available for this section. Between 4149 and 6000 m a total of 19 core runs has been performed with an overall core recovery of 54,8 m. Hence, the results presented in this contribution are mainly based on cutting analysis combined with well log data (fig. B.1. 2.1).

The cutting profile (contribution B.4) presents the uncorrected results of the cutting analysis, whereas the geological profile (fig B.1. 3.1) is synthesized using all available information obtained by logging and cuttings analysis. A compilation of geologically relevant data down to 3000 m is shown in the appendix. At present, structural data from the logging tool (FMI) are evaluated to this depth. The results of the deeper section will be presented in a subsequent volume.



**Fig. B.1. 2.1:** Data bases for the construction of the lithological profile

The chemical analysis carried out on cuttings are hampered by contamination (cavings, drilling artifacts) and the problem of obtaining a representative sample for a specific rock type. This requires the time-consuming preparation of separate bulk cutting material by optical examination under the microscope. For the data of the geochemical online analysis on bulk cutting samples and analytical techniques see chapter C. 3 of this report.

### B.1. 3. GEOLOGICAL PROFILE

Fig. B.1. 3.1 shows the geological profile. The drilled lithologies comprise 2834m (48%) amphibolites, 2190m (37%) garnet sillimanite-biotite gneisses, 737m (12,4%) muscovite biotite gneisses, 121m (2%) hornblende gneisses and minor amounts of lamprophyres, aplites, calc-silicate gneiss and meta-ultramafites. The profile has been synthesized from all available information. Thickness and depth of lithological boundaries are corrected using borehole logging data (mainly Caliper, Susceptibility, Gamma Ray and Electrical Resistivity) to yield the final geological profile. This explains minor discrepancies with the cutting profile (B.4). A short description of the profile is presented in the appendix B.1. 11.2.

# Geological Profile of the KTB Hauptbohrung 0 - 5908 m

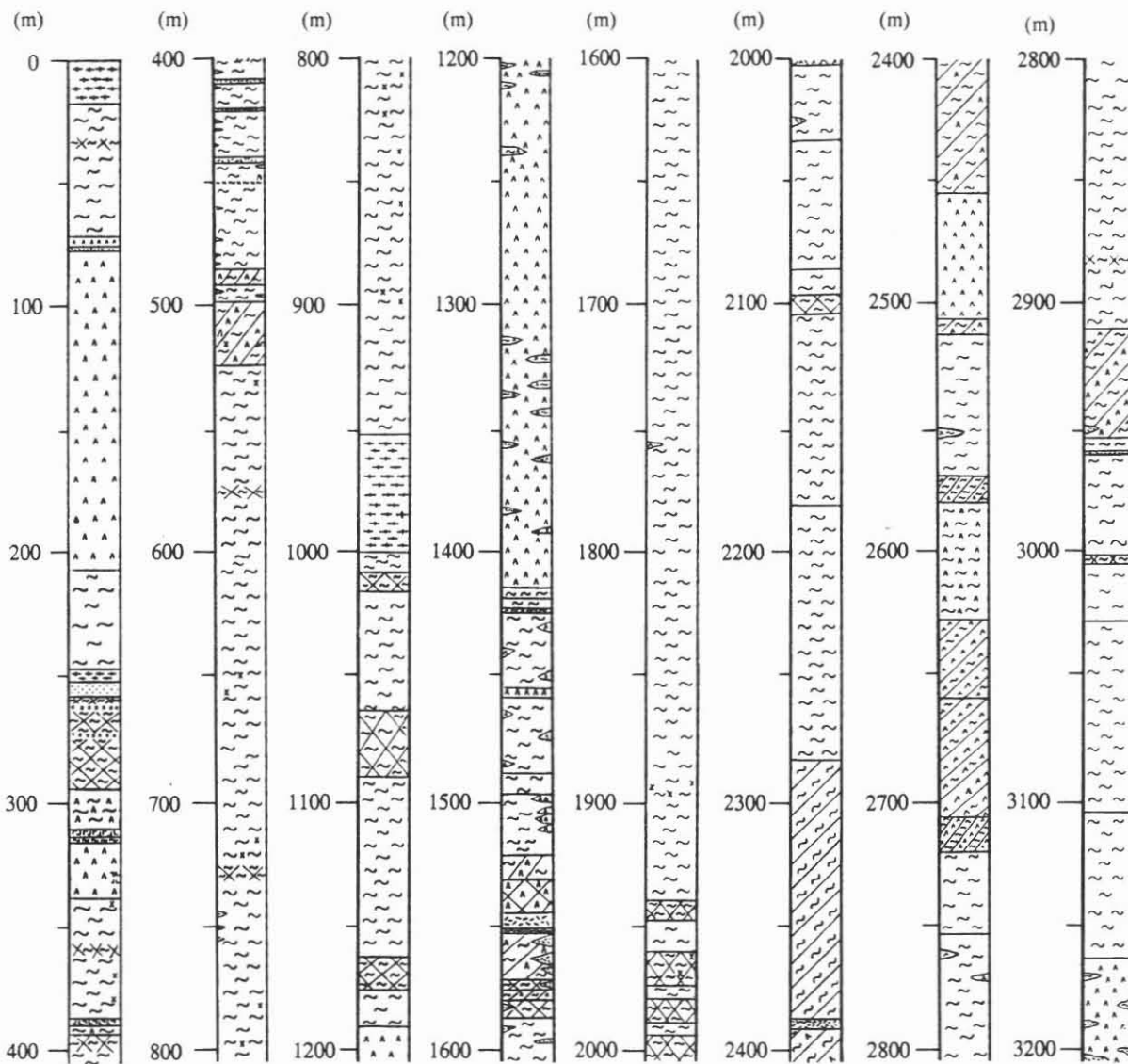
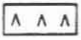



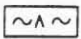


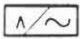




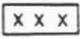
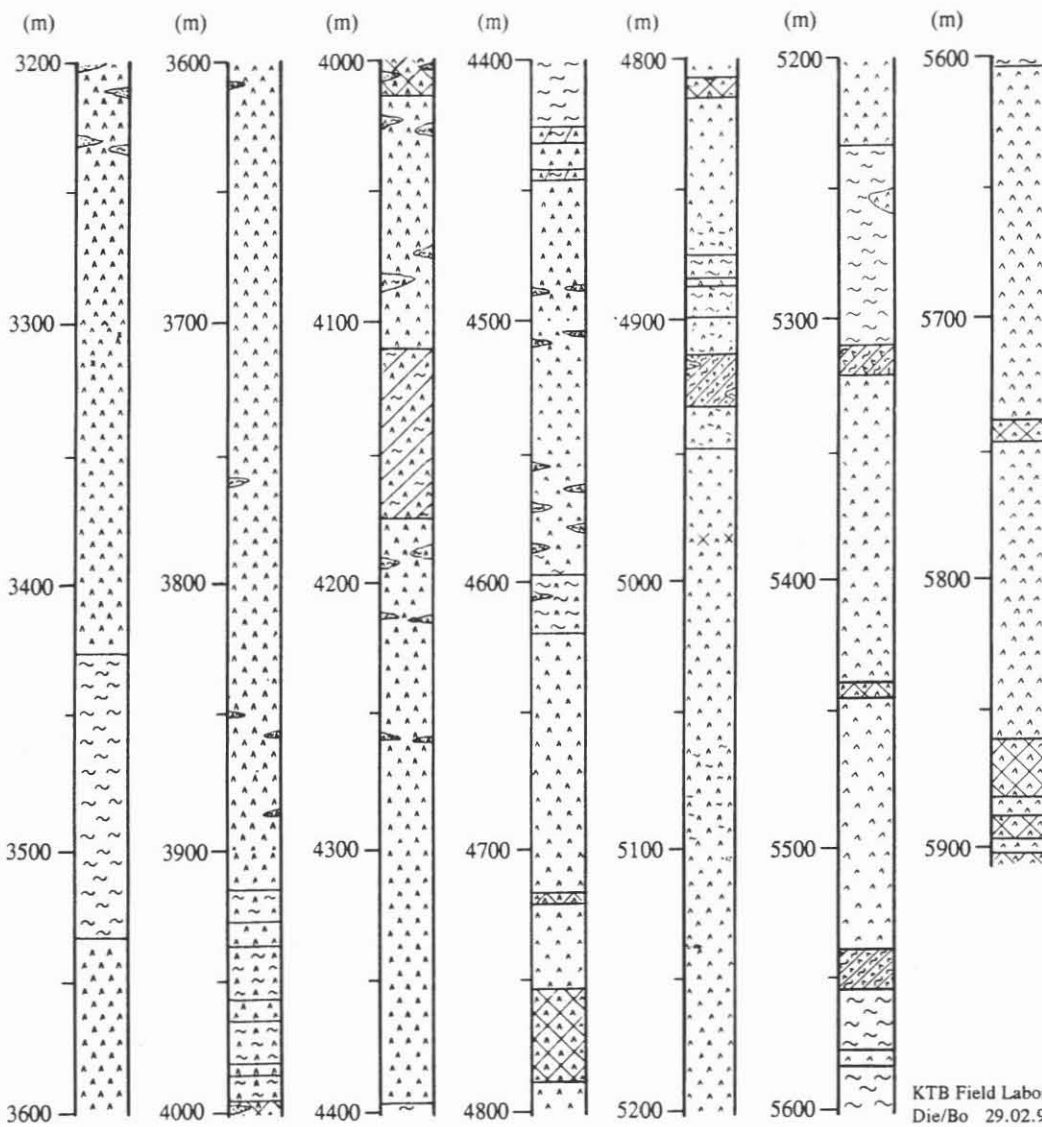


Fig B.1. 3.1: Geological Profile

**Legend :**

- |   |                         |   |   |
|---|-------------------------|---|---|
|  | Amphibolite             |    | calc-silicate bearing plagioclase rich Gneiss |
|  | Paragneiss              |    | Calc-Silicate Rock                            |
|  | Hornblende Gneiss       |    | Lamprophyre                                   |
|  | meta-ultramafic Rocks   |    | Alternation                                   |
|  | cataclastic Amphibolite |    | Cataclasite                                   |
|  | cataclastic Gneiss      |    | aplitic Dyke                                  |
|   |                         |  | Quartz Vein                                   |



## B.1. 4. PETROGRAPHY

### B.1. 4.1. Paragneisses

#### B.1. 4.1.1 Petrography

The distribution of paragneisses along the drilled section is displayed in fig. B.1. 3.1. The sequence is rather monotonous and no significant differences from top to bottom have been recognized so far. The mineralogical composition comprises plagioclase, quartz, biotite, garnet, kyanite and/or sillimanite, muscovite and various products of retrogression. The fabrics are quite variable; two basic types can be distinguished (fig. B.1. 4.1.1)

- (i) fine-grained with more or less pronounced foliation.
- (ii) coarse-grained with flaser structure or layering.

(i) is characterized by a fine-grained and equigranular *quartz-oligoclase-biotite* fabric (fig. B.1. 4.1.2). Average grain diameters of *quartz* and *oligoclase* range between 80 - 100  $\mu\text{m}$ . Grain shape is slightly oblate and the long axes defines the "ductile" lineation. *Biotite* is disseminated within the leucocratic portions or defines enriched layers with *kyanite* and *sillimanite*. The *biotite* (001) planes show a pronounced preferred orientation with a tendency to girdle textures around the lineation. Rod-shaped *quartz-oligoclase* aggregates indicate a prolate strain ellipsoid.

(ii) shows a more heterogeneous, coarse-grained fabric (fig. B.1 4.1.3). Large *quartz* and *plagioclase* blasts are embayed. *Biotite* and *fibrolite* form anastomosing layers around the leucocratic blasts. *Kyanite* occurs as round inclusions in *quartz* and *oligoclase*. Large *muscovite* blasts overgrow *fibrolite*, in places *muscovite* seems to replace *biotite*. The shape of the *quartz-oligoclase* aggregates in these types is less anisometric compared to type (i).

These types alternate along the section on various scales; the fine-grained variety predominates in the upper part, whereas the relative portion of coarse-grained rocks seems to increase with depth (de Wall 1991).

The parageneses

kyanite - garnet - biotite - plagioclase - quartz (fig. B.1. 4.1.4)

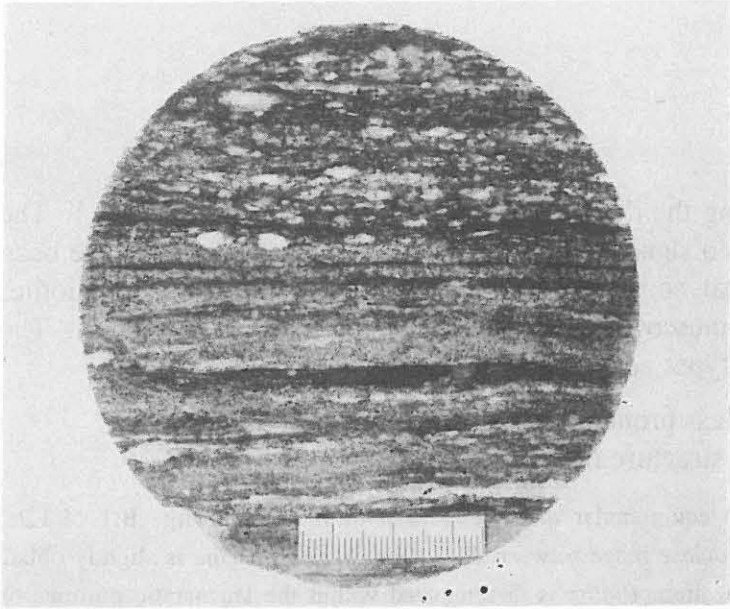
kyanite - sillimanite - garnet - biotite - plagioclase - quartz

garnet - sillimanite - biotite - muscovite - plagioclase - quartz (fig. B.1 4.1.5)

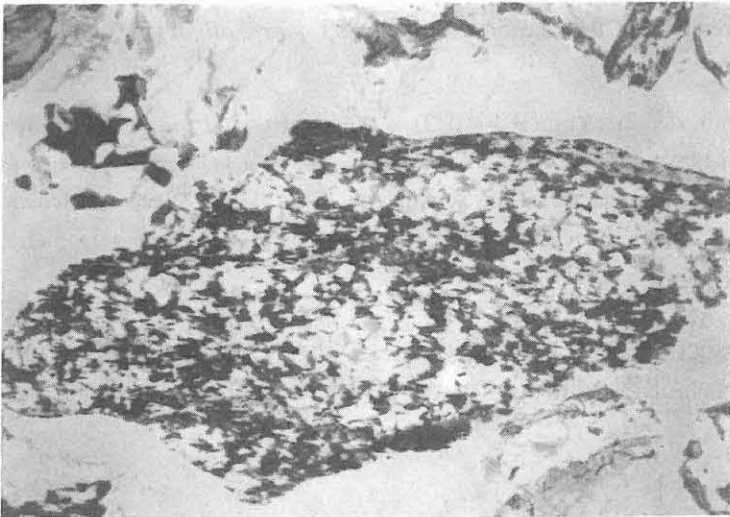
indicate equilibration under amphibolite facies conditions. Thermobarometric calculations of Reinhardt et al. (1989) yield maximum temperatures between 650 and 700 °C at pressures around 7 kbar. Minerals formed during partial reequilibration under greenschist and lower grade metamorphic conditions are chlorite, white mica, ilmenite, rutile or sphene, adularia, laumontite.

#### B.1. 4.1.2 Evolution of fabrics and metamorphism

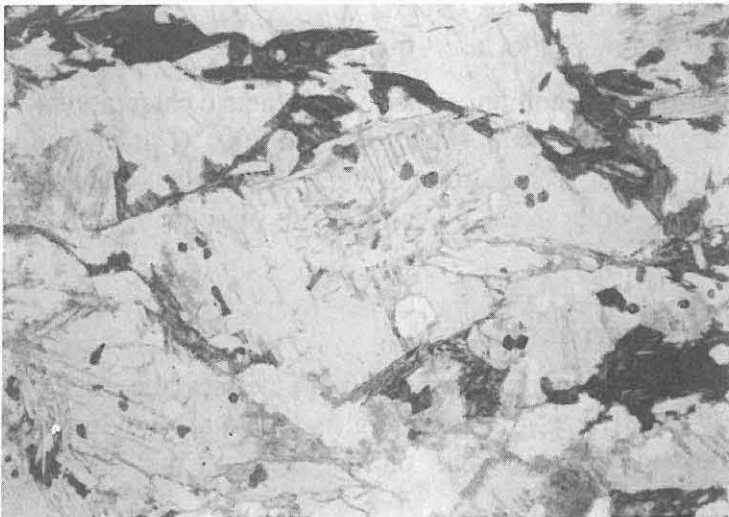
In order to reconstruct the high-temperature evolution of the paragneisses the relations between coarse-grained ("metablastic") and fine-grained ("high-temperature mylonitic", Weber 1990) rocks are to be established. This is done on the base of the following (micro)structural observations:



**Fig. B.1. 4.1.1:** Alternation of fine-grained and coarse-grained paragneiss varieties. Polished core section, KTB Vorbohrung (408C1h, depth 1813,5 m, cm scale bar )

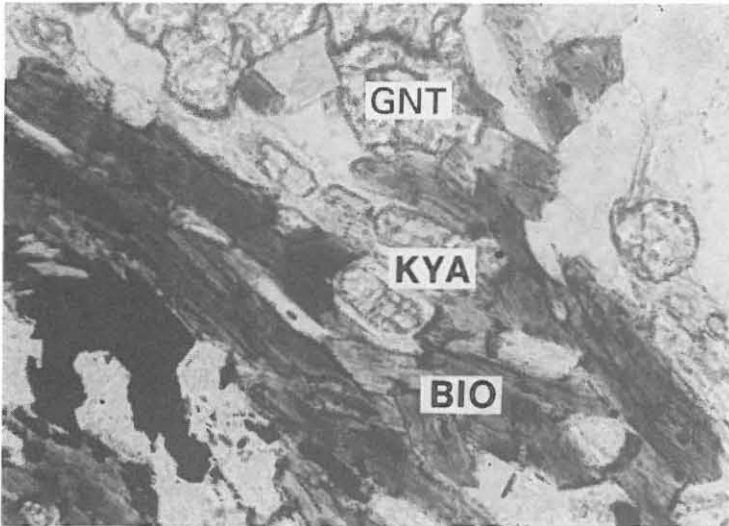


**Fig. B.1. 4.1.2:** Fine-grained paragneiss with equigranular quartz-oligoklas-biotite fabric. (HC2106, depth 2106 m, thinsection, parallel nicols, width of view 6 mm)

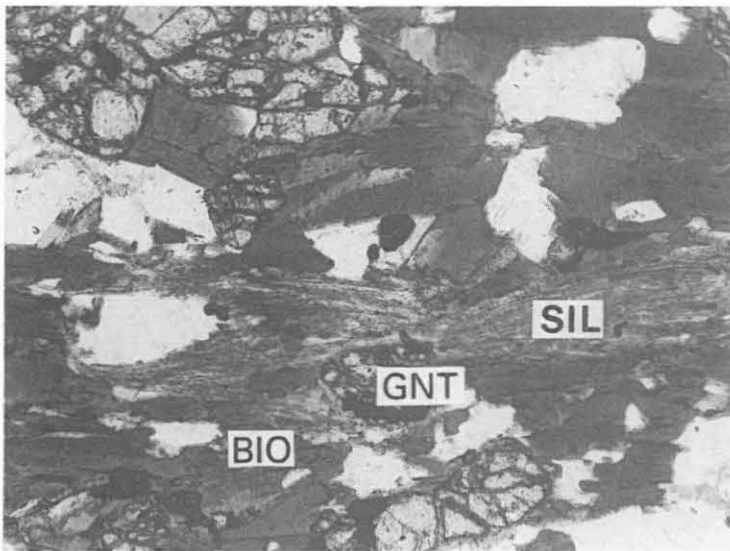


**Fig. B.1. 4.1.3:** Coarse-grained paragneiss, Coarse oligoclase blasts with muscovite and quartz inclusions are surrounded by muscovite and biotite. (HCS5530,4/1, thinsection, parallel nicols, width of view 6 mm)





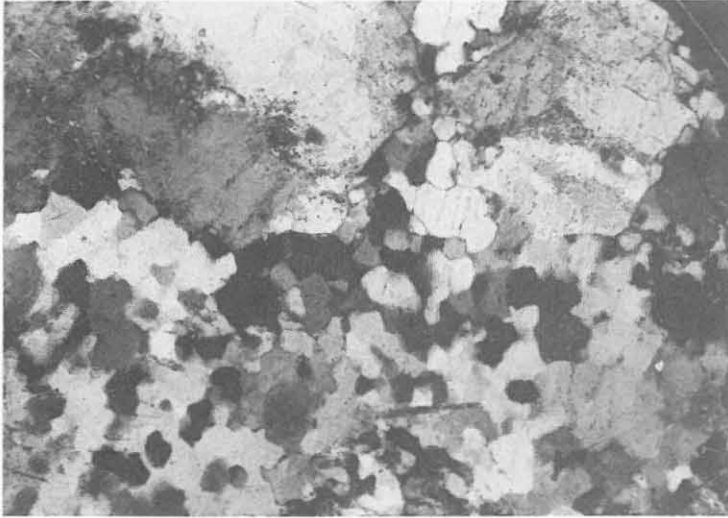
**Fig. B.1. 4.1.4:** Kyanite-garnet-biotite-plagioclase-quartz paragenesis in fine grained paragneiss. (HC2106, depth 2106 m, thinsection, parallel nicols, width of view 0.6 mm)



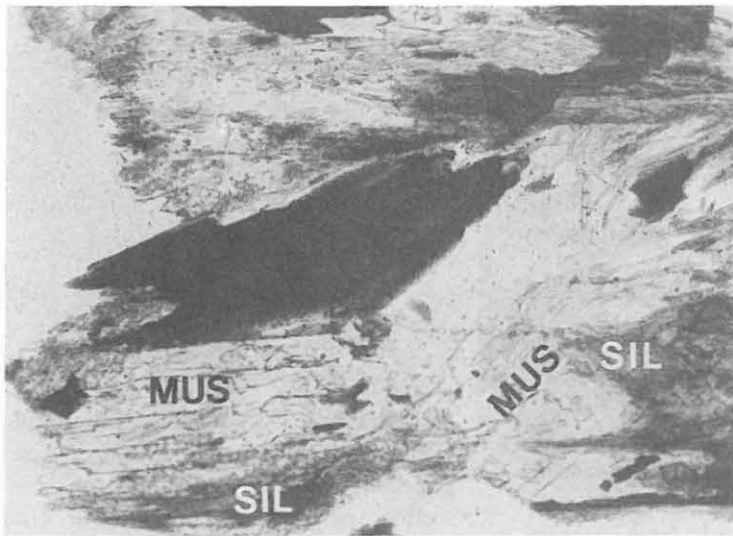
**Fig. B.1 4.1.5:** Garnet-fibrolite-biotite-plagioclase-quartz paragenesis in coarse-grained paragneiss (HCS5530,4/4, thin-section, parallel nicols, width of view 2.5 mm)



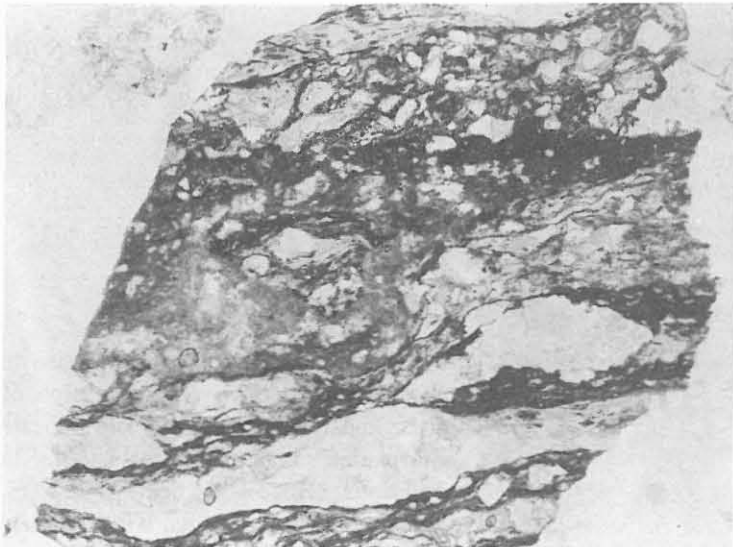
**Fig. B.1 4.1.6:** Discordant shearzone in paragneiss. Dynamic recrystallisation of quartz and formation of chlorite indicate deformation under greenschist facies conditions (H013B14, depth 5282 m, thinsection, crossed nicols, width of view 5.5 mm)



**Fig. B.1. 4.1.7:** Mosaic recrystallisation of quartz in diaphthoritic muscovite-biotite gneiss . Plagioclase clasts show no crystalplastic deformation. (HC5316, depth 5316 m, thinsection, crossed nicols, width of view 2 mm)



**Fig. B.1. 4.1.8:** Muscovite blasts overgrow sillimanite within muscovite-biotite gneiss (HC3178, depth 3178 m, thinsection, parallel nicols, width of view 2 mm)



**Fig. B.1. 4.1.9:** Graphite-bearing cataclastic shearzone in muscovite-biotite gneiss (HC5244, depth 5244 m, thinsection, parallel nicols, width of view 3 mm)

- (1) Foliation and stretching lineation, developed during high-temperature deformation show identical attitude in both types (cores from KTB-VB, de Wall 1991).
- (2) Millimeter-sized plagioclase blasts grew prior to the respective deformation; they tend to be recrystallized in the fine-grained and preserved in the coarse-grained variety.
- (3) The same holds for plagioclase-quartz mobilisates.

These relations suggest that the fine-grained variety is the result of enhanced deformation which caused extensive recrystallization of plagioclase. The inhomogeneity of deformation may be related to some primary compositional differences, suggested by the following observations:

- (1) Kyanite predominates in the fine-grained variety and is rarely found in the coarse-grained rocks.
- (2) Sillimanite, on the contrary, is a major component of the coarse-grained variety, occurring as fibrolite.
- (3) Like sillimanite, large muscovite crystals are much more abundant in the coarse-grained rocks; microstructural relations indicate that they have grown after cessation of high-temperature flow at the expense of sillimanite (and K-feldspar?).

The quantitative and qualitative differences in the mineral assemblage are related to differences in bulk composition. These, in turn, should have caused differences in the respective reaction paths. This is reflected by the  $Al_2SiO_5$  forming reactions, which have seemingly proceeded under differing conditions, hence in different stability fields (kyanite versus sillimanite), along the p-T-path common for both rock types.

Later deformation took place under greenschist to zeolite facies conditions. The intensity of the greenschist facies overprint tends to increase with depth. Nevertheless, the phase assemblage and microstructures adjusted under high-temperature conditions are generally not completely obliterated, with the exception of some shear zones (fig. B.1. 4.1.6) up to one meter wide. The quartz microfabric reveals evidence of dislocation creep accompanied by dynamic recrystallization; feldspars show features of minor crystal plastic deformation and some fracturing (fig. B.1. 4.1.7). Formation of chlorite and Ti-phases at the expense of biotite and replacement of sillimanite by fine-grained white mica (fig. B.1. 4.1.8) are related to this deformation.

After further cooling deformation proceeded in the brittle field under high pore-fluid pressure; abundant cataclasites (fig. B.1. 4.1.9) along fault and fracture zones are the result (Zulauf 1990). The variety of structures and mineralization suggests that cataclasite formation took place over a considerable span of time and conditions. Nevertheless, no systematic differences with depth could be established on the base of the available material down to 6000 m so far.

## **B.1.4.2 Metabasic rocks**

### **B.1.4.2.1 Petrography**

The results of the thorough analysis of the metabasites in the KTB Vorbohrung can be summarized as follows:

The metabasic series is built up mainly of metagabbros with thin layers of mafic cumulates, fine-grained and coarse-grained amphibolites.

The protoliths of the metabasic rocks formed during late-Ordovician times (v. Quadt 1990, v. Drach & Köhler 1990). The preserved magmatic fabrics indicate their intrusive nature and point to a shallow level of intrusion (Schalkwijk 1991). An effusive nature of the protoliths is possible for the section down to 460 m, and cannot be ruled out for some of the amphibolite-hornblendegneiss layers. Talc-chlorite-amphibole felses are interpreted as metamorphosed mafic cumulates (v. Gehlen et al. 1991).

The chemical compositions of the metabasites range from subalkaline tholeiitic to transitional basalts. The different trace element characteristics of the various metabasic units (Patzak et al. 1991) do not allow for the unequivocal derivation of the tectonic setting. Generation in an anomalous oceanic ridge environment or in a back-arc basin has been discussed by Patzak et al. (1991). Schalkwijk (1991) demonstrates that the chemical composition is compatible to a continental within-plate tectonic environment.

The original magmatic fabrics have been destroyed in most rocks by high-grade metamorphism and polyphase deformation. An early high pressure metamorphic stage can be deduced from inclusions of  $Al_2SiO_5$  and zoisite in corona garnet. Metamorphism under garnet granulite facies conditions is documented by the paragenesis clinopyroxene-garnet-plagioclase-hornblende. Deformation under high-grade amphibolite facies conditions was followed by partial melting, resulting in the formation of coarse-grained amphibolites rich in plagioclase-quartz mobilisates. Later high-temperature deformation is restricted to ductile shear zones. Syntectonic fabrics were generally annealed (Schalkwijk 1991).

The complex late to post-Variscan deformation history under greenschist and zeolite facies conditions has been discussed in detail by Zulauf (1990).

The distribution of metabasic series intersected in the KTB Hauptbohrung is shown in fig. B.1.3.1.

The metabasic rocks from the KTB Hauptbohrung can be classified as

- (1) metagabbros,
- (2) amphibolites,
- (3) mafic cumulates and
- (4) hornblende gneisses.

For the KTB Hauptbohrung the use of this classification is restricted to the core samples between 4130 and 6000 m. However, characteristic features of each variety were recognized in cuttings throughout the entire drilled section.

### (1) Metagabbros

Metagabbros are massive and medium to coarse grained. They are characterized by their relictic magmatic ophitic textures or corona fabrics (coronitic metagabbros). The metagabbros are not foliated except in ductile shear zones.

Main constituents are clinopyroxene, garnet, amphibole and plagioclase together with minor amounts of biotite and quartz. Rutile, ilmenite, apatite and occasionally zircon are accessories.

*Clinopyroxene* occurs as mm sized phenocryst with plagioclase inclusions or in symplectitic intergrowth with plagioclase. It is partially or completely replaced by hornblende. *Garnet* forms coronas around clinopyroxene-plagioclase symplectites or occurs pseudomorphically after plagioclase inclusions in clinopyroxene. Brown *hornblende* is formed by amphibolitization of clinopyroxene. It occurs intergrown with symplectitic clinopyroxene, as fine-grained aggregates or as mm sized single crystals. Primary magmatic *plagioclase* forms lath-like inclusions in clinopyroxene. It is completely saussuritized or pseudomorphically replaced by garnet.

Common retrograde reactions are replacement of hornblende by actinolite, transformation of clinopyroxene-plagioclase symplectites to hornblende-plagioclase-quartz symplectites, poikilitic hornblende and finally to actinolite and/or chlorite. Garnet is replaced by chlorite, biotite is replaced by chlorite and sphene.

The mineral chemistry of metagabbros from the KTB Vorbohrung is described in detail by Schalkwijk (1991). Characteristic microscopic fabrics of metagabbros are shown in figs. B.1.4.2.1-4.

### (2) Amphibolites

The following types of amphibolites were observed:

- (a) fine-grained, homogenous amphibolites
- (b) coarse-grained amphibolites
- (c) foliated amphibolites with a pronounced compositional layering.

In all three types, the main rock forming minerals are hornblende, plagioclase and garnet together with minor quartz and biotite. Accessories are Ti-phases, opaques (see B.1.5 Ore mineralization), K-feldspar, apatite and some zircon.

Green *hornblende* and *plagioclase* form mm sized blasts or equal-grained aggregates with straight high-angle grain boundaries. *Garnet* contents are highly variable. Occasionally, garnet is replaced pseudomorphically by hornblende, plagioclase and minor biotite. *Ti-phases* include sphene, rutile, ilmenite (often rimmed by sphene) and mm sized idiomorphic sphene. Ilmenite-hornblende symplectites grown at the expense of sphene are found throughout the whole drilled section (fig. B.1.4.2.5).

Chlorite, sphene and epidote are retrograde reaction products. Quartz, actinolite, epidote/clinozoisite, prehnite, adularia and laumontite occur as vein minerals both within metagabbros and amphibolites.

In the fine-grained type (a) amphibolites, relics of clinopyroxene and clinopyroxene-plagioclase symplectites are commonly observed. They are lacking in type (b) and type (c) amphibolites.

The coarse-grained type (b) amphibolites generally are associated with undeformed quartz-feldspar mobilisates. They are not foliated except in localized ductile shear zones.

The fine-grained type (a) amphibolites and the coarse-grained type (b) amphibolites show the following relations:

The foliation in fine-grained type (a) amphibolites is cut by unfoliated quartz-plagioclase mobilisates. Foliated fine-grained amphibolites form blocks enclosed by coarse-grained amphibolites and quartz-plagioclase mobilisates. At the contacts between type (a) and type (b) amphibolites, coarsening of hornblende can be observed (figs. B.1.4.2.6-8). In areas of extensive hornblende blastesis localized depletion in felsic components occurs.

Type (c) amphibolites generally are strongly foliated. They show a distinct compositional layering. Quartz-feldspar layers contain hornblende-clasts of grain-sizes similar to those occurring in the coarse-grained amphibolites. These felsic layers alternate with more mafic layers (fig. B.1.4.2.9).

### **(3) Mafic Cumulates**

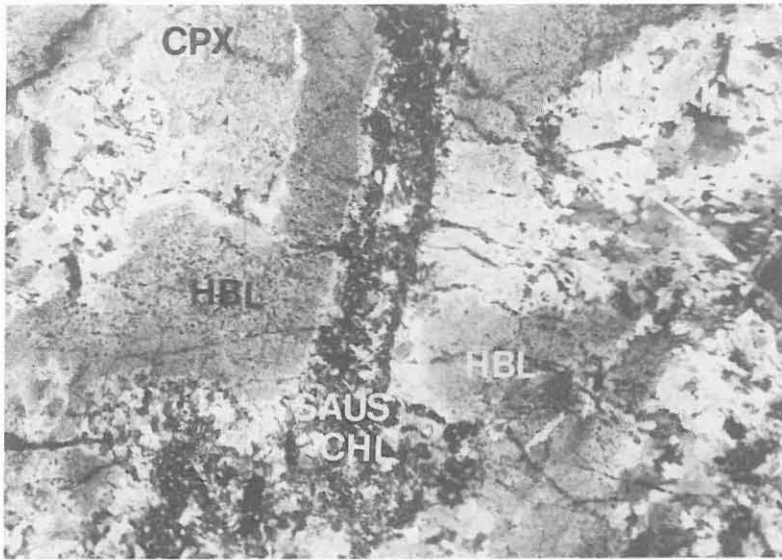
Mafic cumulates were found in core run H011 (depth 5014 m) and at 4975 m depth (detected by high concentrations of Cr, Ni and MgO during routine XRF cutting analysis). Textures and mineral compositions are quite variable, including fine to medium grained hornblendites and (talc)-chlorite-hornblende felses. The main rock-forming minerals are hornblende (with inclusions of relictic clinopyroxene), chlorite, actinolite and minor amounts of talc.

For the chemical composition see chapter B.1.4.2.4.

### **(4) Hornblende gneisses**

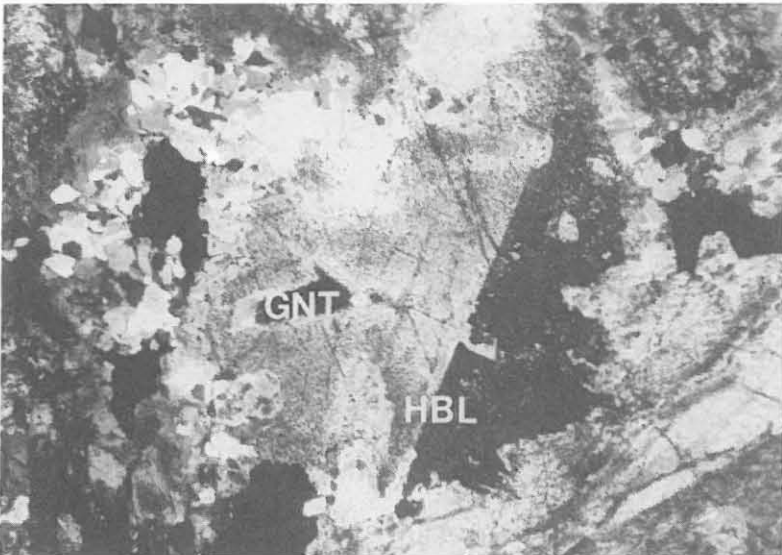
Hornblende gneisses consist of the same minerals and show the same retrograde reactions as the amphibolites. They are richer in quartz, plagioclase and biotite. Occasionally clinopyroxene included in hornblende and clinopyroxene-plagioclase symplectites occur. They are well foliated. Shape and distribution of mafic and felsic phases suggest a coarse-grained intrusive protolith.

An example for the quartz fabrics in hornblende gneisses is presented in B.1.4.2.3.



**Fig. B.1.4.2.1:** Metagabbro: Ophitic intergrowth of clinopyroxene (mostly replaced by brown hornblende) and completely saussuritized plagioclase.

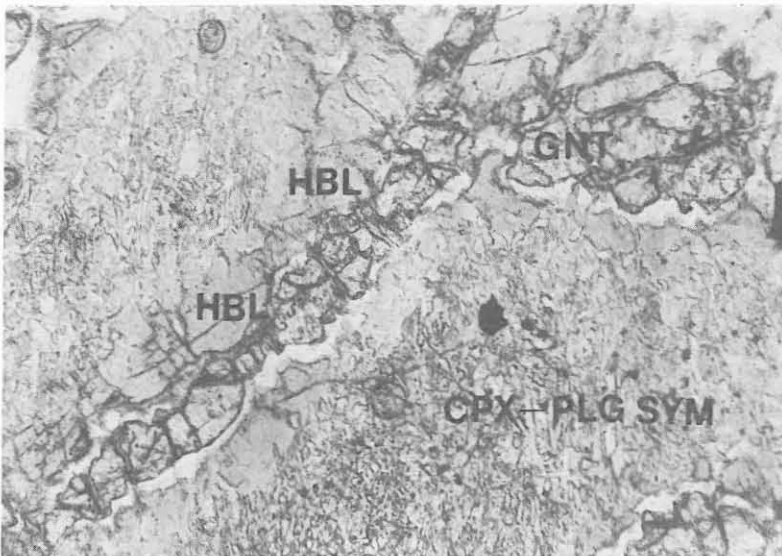
(Thin section H014E32d3, crossed nicols, depth 5380.9 m, width of view 5.6 mm).



**Fig. B.1.4.2.2:** Metagabbro:

A former clinopyroxene phenocryst is completely replaced by brown hornblende. Magmatic plagioclase is pseudomorphed by garnet.

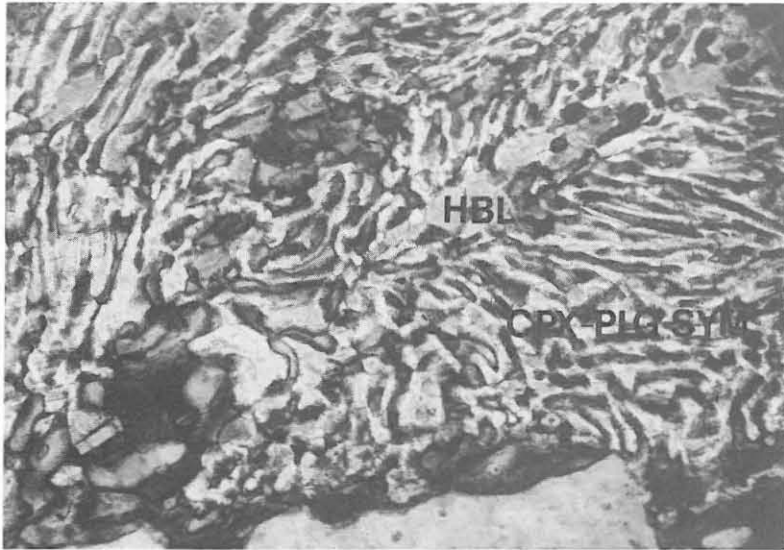
(Thin section H014E32d4, crossed nicols, depth 5381 m, width of view 4.7 mm).



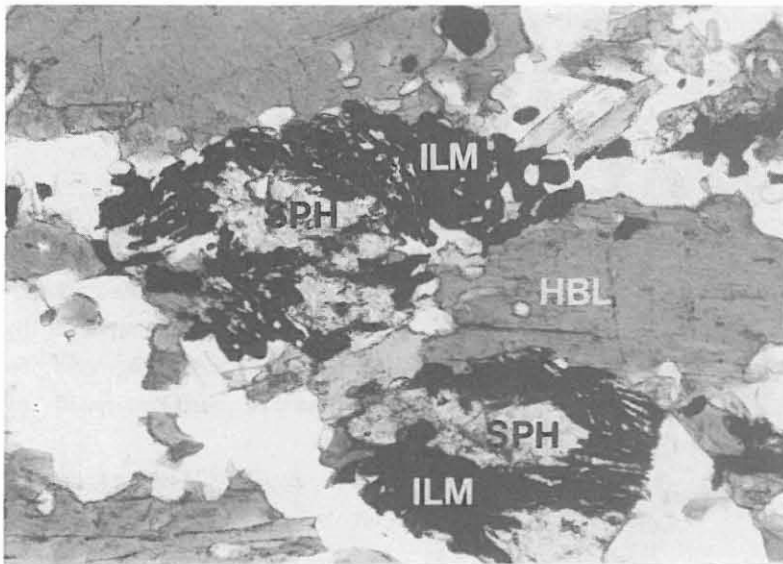
**Fig. B.1.4.2.3:** Coronitic metagabbro:

Former clinopyroxene phenocrysts replaced by clinopyroxene-plagioclase symplectites and brown hornblende, surrounded by garnet coronas.

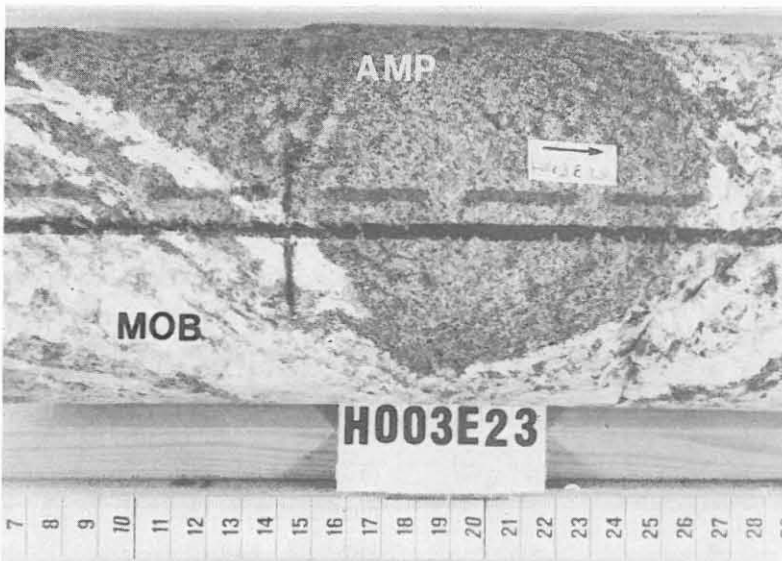
(Thin section HC3328, parallel nicols, depth 3328 m, width of view 1.25 mm).



**Fig. B.1.4.2.4:** Coronitic metagabbro:  
Fine-grained clinopyroxene-plagioclase symplectite, intergrown with brown hornblende.  
(Thin section HC3568, parallel nicols, depth 3568 m, width of view 0.64 mm).

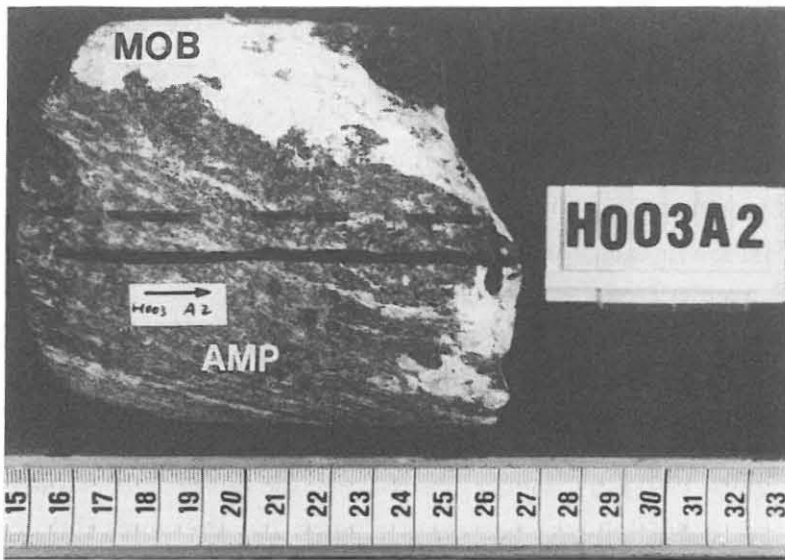


**Fig. B.1.4.2.5:** Ilmenite-hornblende symplectite at the expense of sphene.  
(Thin section H006A6R, parallel nicols, depth 4512.2 m, width of view 1.8 mm).

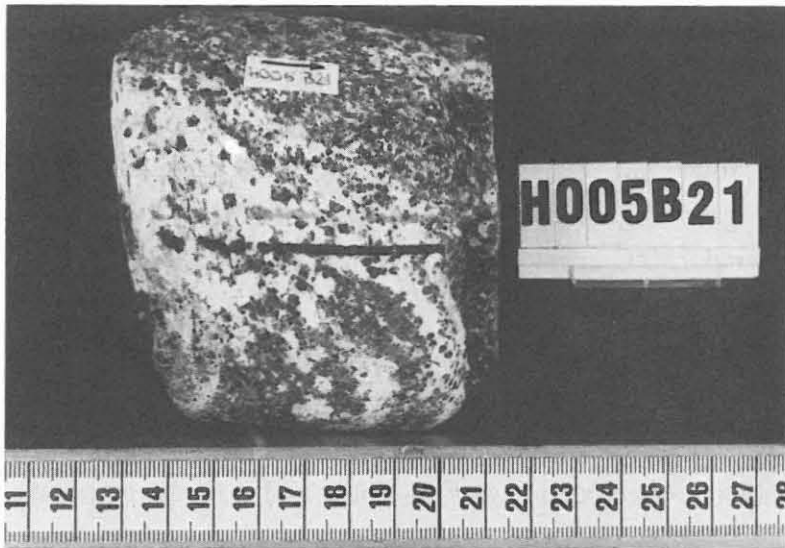


**Fig. B.1.4.2.6:** Fine-grained type (a) amphibolites form blocks enclosed in quartz-plagioclase mobilisates.  
(Sample H003E23, depth 4524 m)





**Fig. B.1.4.2.7:** Foliation in fine-grained type (a) amphibolite is cut by quartz-plagioclase mobilisates. (Sample H003A2, depth 4251 m).



**Fig. B.1.4.2.8:** Coarse-grained type (b) amphibolite with mm sized hornblende blasts in quartz-plagioclase mobilisates. (Sample H005B21, depth 4449 m)



**Fig. B.1.4.2.9:** Strongly foliated type (c) amphibolite showing compositional layering and mm sized hornblende clasts within quartz-feldspar layers. (Sample H006A10, depth 4513 m)

#### **B.1.4.2.2 Metamorphic evolution**

The metabasic rocks reveal a complex metamorphic evolution of

- (1) early high pressure metamorphism, documented in sparse relics,
- (2) garnet-granulite facies metamorphism, recorded in coronitic metagabbros,
- (3) pervasive amphibolite facies metamorphism with partial melting and
- (4) partial to localized greenschist facies retrogression.

##### **(1) High pressure metamorphism**

Inclusions of zoisite,  $\text{Al}_2\text{SiO}_5$  and omphacitic pyroxene in corona garnets were reported by Röhr et al. (1990b) and Schalkwijk (1991) for metagabbros from the KTB Vorbohrung. They are evident for the high pressure breakdown reaction of plagioclase. Pressures did not exceed 12 kbar (Schalkwijk 1991).

##### **(2) Garnet granulite facies metamorphism**

In the coronitic metagabbros, the paragenesis garnet-clinopyroxene-plagioclase-hornblende-Ti-phase (ilmenite or rutile) is found in garnet coronas around clinopyroxene. This documents metamorphism under garnet granulite facies conditions. Thermobarometric calculations yield temperatures around 750°C at minimum pressures of 12 kbar (Schalkwijk 1991).

##### **(3) Amphibolite facies metamorphism**

Subsequently, most rocks underwent deformation under amphibolite facies conditions. The stable mineral assemblage is hornblende-plagioclase-(garnet)-biotite and ilmenite or rutile.

The relations between fine-grained type (a) and coarse-grained type (b) amphibolites discussed above, indicate in-situ partial melting processes. Fine-grained type (a) amphibolites (palaeosome) were transformed into coarse-grained type (b) amphibolites (neosome) rich in quartz-plagioclase mobilisates. Partial melting, induced by the influx of water, occurred at high-grade amphibolite facies conditions. No significant differences in mineral chemistry and derived pressure and temperature conditions between palaeosome and neosome were observed in the KTB Vorbohrung (Schalkwijk 1991). This indicates pervasive amphibolite facies reequilibration. Amphibolite facies metamorphism took place over a considerable temperature and pressure range. At high-grade amphibolite facies conditions garnet is present in the critical assemblage and partial melting occurs. Under low-grade amphibolite facies conditions, garnet is replaced by hornblende, plagioclase and some biotite. Rims of sphene are formed around ilmenite or rutile.

#### **(4) Greenschist facies metamorphism**

Except for local shear zones, the greenschist facies overprint has never gone to completion. Clinopyroxene and hornblende are replaced by actinolite. Hornblende and garnet are replaced by chlorite and epidote. Biotite reacts to chlorite and sphene. Plagioclase is sericitized and saussuritized.

##### **B.1.4.2.3 Deformation**

Metagabbros and amphibolites developed at least partly from the same protoliths. Their different fabrics and the intimate interlayering of strongly deformed mylonitic amphibolites, undeformed amphibolites and metagabbros document highly inhomogenous deformation.

Metagabbros partly survived unstrained and preserved their magmatic fabrics despite extensive metamorphic reequilibrations. Strain is localized in narrow shear zones in which a flaser fabric has developed. Within these shear zones plagioclase and hornblende are completely recrystallized to fine-grained aggregates.

In fine-grained type (a) amphibolites inhomogenous deformation results in the formation of weakly to strongly foliated varieties.

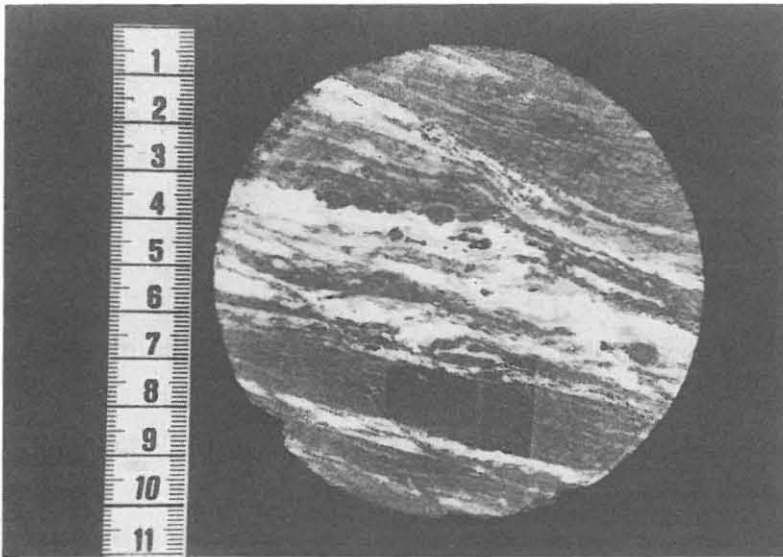
Amphiboles show varying degrees of recrystallization. Some grains are marginally recrystallized, some are completely recrystallized. Amphibolites with strong mylonitic fabrics developed in localized ductile shear zones, e.g. in areas of higher strain concentrations. The foliation is defined by dimensional and crystallographic preferred orientation of completely recrystallized fine-grained hornblende, plagioclase, biotite and ore minerals.

These shear zones are cut by undeformed quartz-plagioclase mobilisates and undeformed coarse-grained type (b) amphibolites. Therefore, this first shear zone generation formed during a ductile deformation older than the partial melting event.

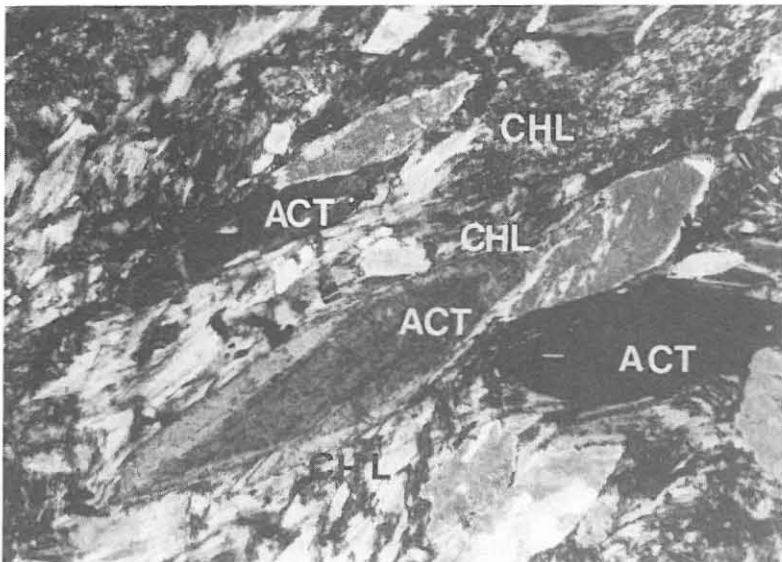
After partial melting further ductile deformation took place. A second generation of shear zones disrupts both palaeosome and neosome (fig. B.1.4.2.10). Deformation resulted in the mylonitization of both type (a) and type (b) amphibolites and quartz-plagioclase mobilisates. The strongly foliated and banded type (c) amphibolites seem to be the product of this second stage of ductile deformation.

Later deformation took place under low-temperature conditions (figs. B.1.4.2.11-12).

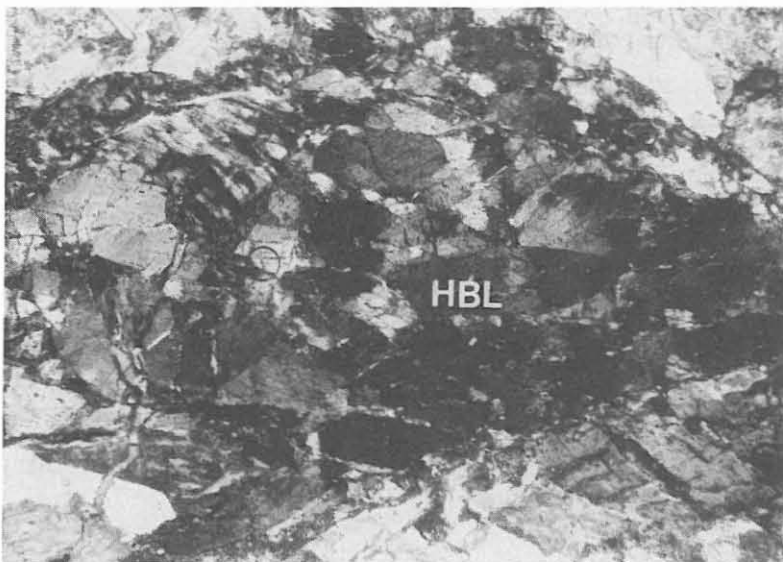
In most rocks syntectonic fabrics adjusted during high-temperature deformation were annealed. Hornblende and plagioclase are completely recrystallized to fine-grained aggregates. Thermobarometric calculations indicate amphibolite facies conditions during both stages of deformation (Schalkwijk 1991).



**Fig. B.1.4.2.10:** Second generation shear zone, disrupting both palaeosome and neosome.  
(Sample H003A5, depth 4251 m).



**Fig. B.1.4.2.11:** Crystallization of idiomorphic actinolite and chlorite in greenschist facies shear zone.  
(Thin section H011D32, crossed nicols, depth 5014 m, width of view 2.2 mm).



**Fig. B.1.4.2.12:**  
Intensively fragmented hornblende in cataclastic shear zone.  
(Thin section H011D37T, crossed nicols, depth 5014 m, width of view 2.8 mm).

Quartz lenses in some amphibolites reveal characteristic microfabrics. An example of the second ductile deformation is sample H003 A5 from a depth of 4251 m.

The foliation dips about 60°; the lineation, defined by stretched plagioclase clasts is subhorizontal. Azimutal values are lacking, because the core has not yet been oriented. The amphibolite contains deformed mobilisates consisting of plagioclase and quartz. Quartz is concentrated in lenses and asymmetric pressure shadows around plagioclase-clasts. The asymmetry reflects a certain sense of shear. Grain sizes vary between 40 µm and 1 mm in size, with an average of 230 µm (equivalent circle-area diameters). The grains show almost no undulose extinction; the grain boundaries are straight to slightly curved. The trace of rare subgrain boundaries are oriented mostly parallel or at small angles to the lineation.

The c-axis distribution (fig. B.1.4.2.13a) shows two asymmetric maxima (>10 mrd and >6 mrd) at small angle to the lineation. This type of preferred orientation has been observed exclusively in high temperature tectonites, eg. Blumenfeld et al. (1986), Mainprice et al. (1986), Kruhl & Huntemann (1991). The pattern analyzed in sample H003 A5 is significantly more pronounced than all similar patterns published previously. It is interpreted to reflect the predominance of prism <c> slip. Activation of this glide system requires high temperatures. Thus the quartz fabric has been adjusted during high temperature deformation after the formation of mobilisates.

Hornblende gneisses, too, show fabrics indicative of high temperature deformation.

Sample H001 E37c is a typical hornblende gneiss from a depth of 4152 m.

Foliation dips with 50°, the lineation is subhorizontal. Macroscopically the hornblende gneiss shows a strongly prolate fabric, marked by stretched finely recrystallized plagioclase and quartz rods about 2 cm in length and few millimeters in height and width. Possibly these rods are highly strained magmatic grains. The xz thin-section shows a well developed foliation, defined by hornblende/biotite-rich and quartz/feldspar-rich layers. In the yz section the trace of the xz plane is exclusively marked by flattened quartz aggregates.

Quartz c-axis orientation distributions (fig. B.1.4.2.13b) show an asymmetric cross girdle with a maximum near y (4.85 times uniform). This indicates activation of rhomb <c+a> and prism <a> slip (Bouchez & Pechez 1981). According to Hobbs (1985) these slip-systems are activated at elevated temperatures. The observed pattern matches very closely c-axes patterns shown by Price (1985, sample 70) which developed in quartzites exhibiting constrictive strain.

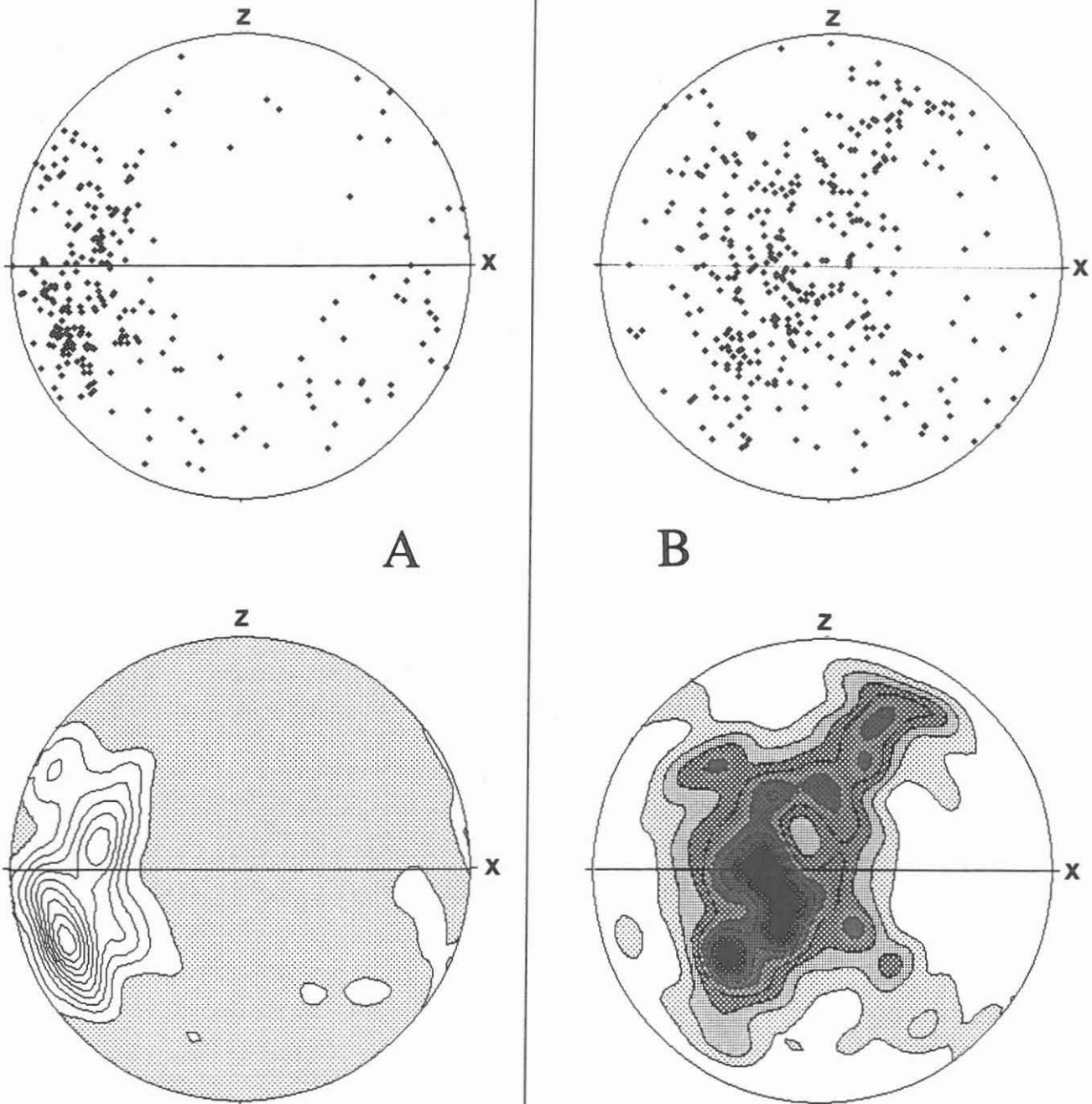
From the observations the following succession of events can be deduced:

A first shear zone generation is formed by ductile deformation prior to partial melting.

A second shear zone generation cuts both palaeosome and neosome. It formed after the partial melting event.

The related quartz fabrics document high temperatures during deformation, as do the phase equilibria.

Semi-brittle and brittle deformation during lower p-T-conditions is restricted to cataclastic shear zones.



**Fig. B.1.4.2.13:** Quartz c-axis distributions

a) Sample H003A5, Amphibolite, 256 measurements. Contours at 1,2,3... multiples of random densities (mrd). Maximum at 10.5 mrd. Densities < 1 mrd are grey.

b) Sample H001E37c, Hornblende-Gneiss, 357 measurements. Contours at 0.5, 1, 1.5... multiples of random densities (mrd). Maximum at 4.85 mrd. Darker greyvalues indicate increasing densities.

All Diagrams: Equal area projection, lower hemisphere, z is the pole of foliation, x is the lineation. Quartz c-axis orientations were measured with a U-stage, the grain area, shape and position were determined with an image analysis system. Orientation distributions were calculated weighing each measurement with the area of the measured grain.

#### B.1.4.2.4 Chemical composition

Compositions of the metabasites range from subalkaline tholeiitic and transitional to mildly alkaline rocks. Abundances of the high-field-strength (HFS) elements Ti, Zr, Y and Nb correspond to those of modern E-type MORB and within-plate (tholeiitic) basalts. The wide range of Mg-values ( $100 \cdot \text{Mg}/(\text{Mg} + \text{Fe}_{\text{TOTAL}})$ ), Cr and Ni and negative correlations of these parameters with the HFS elements indicate that chemical variations can partly be attributed to accumulation and fractionation processes. Increase of Ti and V with increasing  $\text{FeO}_{\text{TOTAL}}/\text{MgO}$  points to a tholeiitic fractionation trend. Highly variable concentrations of the large-ion lithophile (LIL) elements Sr, K and Rb probably reflect redistribution of these elements by hydrothermal alteration and metamorphism.

Until now, only few analyses of cutting separates and core samples (depth 4130-6000 m) are available. MORB-normalized variation diagrams for these samples and some representative XRF routine cutting samples are shown in fig. B.1.4.2.15a-d. All patterns show a distinct enrichment of the LIL elements Sr, K and Rb and slight to moderate enrichment from Zr to Nb with respect to N-type MORB.

In the  $\text{TiO}_2$  vs. Zr discrimination diagram of Pearce (1982) most data points lie in the field of within-plate lavas, some plot in the field of arc lavas (fig. B.1.4.2.15e). Positions of data points of the metabasic series 69-203 m and 1183-1410 m are shown for comparison (hatched area, XRF routine cutting analyses). Ti/V ratios vary between 30 and 55 and are in the range reported by Shervais (1982) for MORB and within-plate tholeiites (fig. B.1.4.2.15f).

The mafic cumulates are high in Cr (1160-2278 ppm), Ni (360-670 ppm) and MgO (15-22 wt.-%) and low in incompatible trace elements.  $\text{SiO}_2$  and  $\text{Al}_2\text{O}_3$  concentrations are in the range 44-46 and 9-14 wt.-% respectively (calculated volatile-free).

The normative mineralogy (CIPW norm) is shown in the cpx-opx-ol and cpx-opx-(an+ab) ternary diagrams in fig. B.1.4.2.14.

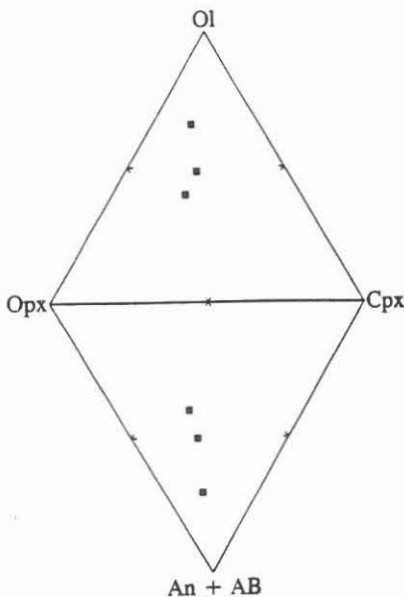
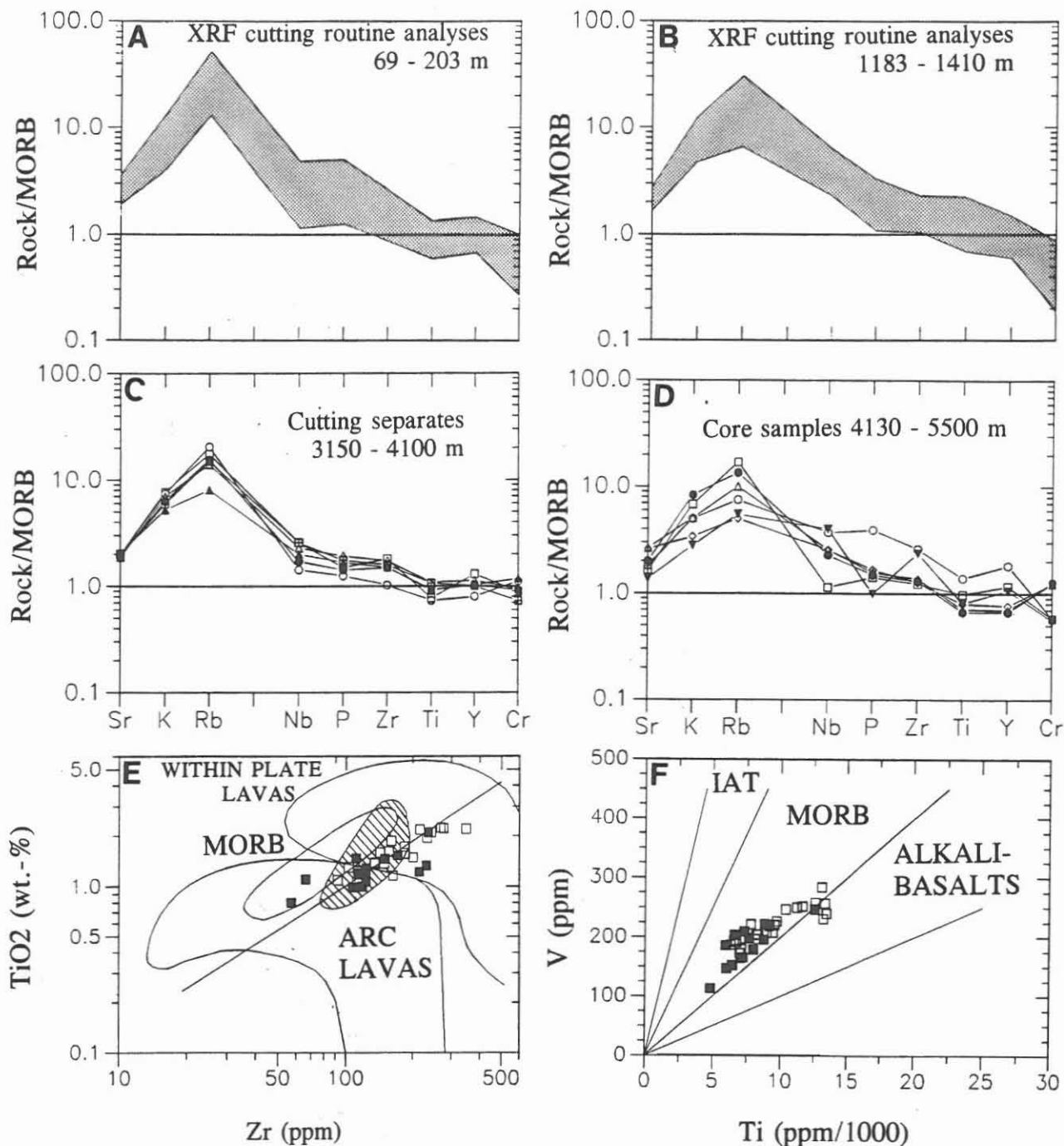


Fig. B.1.4.2.14: Normative compositions (CIPW norms) of mafic cumulates, shown in Cpx-Opx-Ol and Cpx-Opx-(An+Ab) ternary diagrams.



**Fig. B.1.4.2.15:** Chemical compositions of representative metabasites (cutting separates, core samples and selected XRF routine samples) shown in MORB-normalized variation diagrams (a-d) and TiO<sub>2</sub> vs. Zr (Pearce 1982) and Ti vs. V (Shervais 1982) discrimination diagrams (e-f).  
 Open squares = cutting separates (3150 - 4100 m), closed squares = core samples (4130 - 6000 m).  
 Data: working group Geochemistry.



### B.1. 4.3. Late dykes

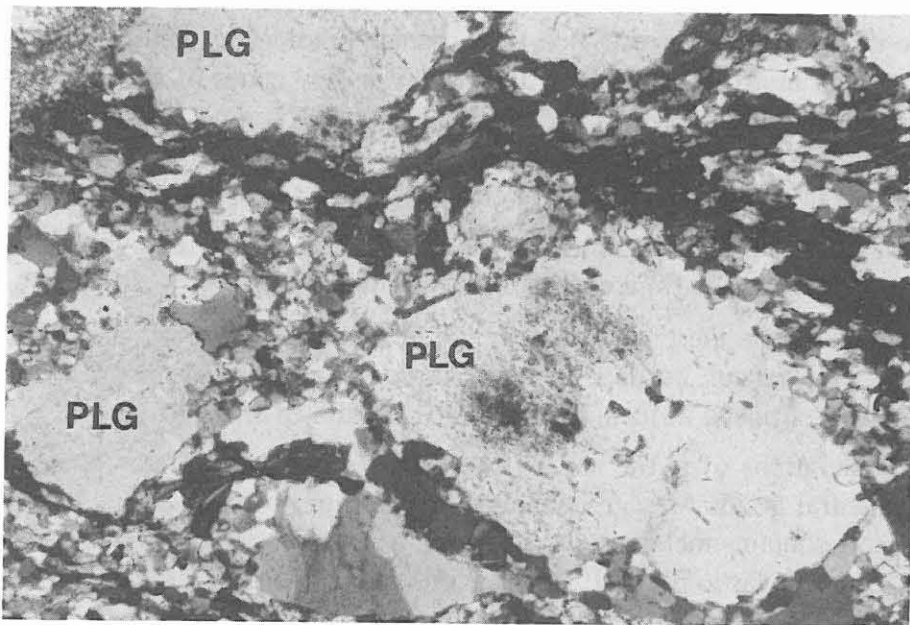
#### B.1. 4.3.1 Lamprophyres

Lamprophyres are found throughout the entire drilled section. No informations about the structural relations between dykes and host rocks can be obtained from the cutting material. In the KTB pilot hole, lamprophyres containing xenoliths of cataclastic host rocks were observed. Therefore, the lamprophyre intrusions must be younger than at least early stages of cataclastic deformation (Röhr et al. 1990). Plagioclase, K-feldspar, hornblende and biotite are the main constituents. Low grade alteration is commonly observed. Olivine is generally pseudomorphed by carbonate, chlorite, actinolite and sheet silicates. Actinolite, epidote/clinozoisite, prehnite, calcite, quartz and adularia have formed along fractures. The occurrence of both extremely fine-grained and coarser grained varieties in some cutting samples points to the existence of chilled margins.

The lamprophyres from the KTB main hole can be classified after Rock (1984) and Streckeisen (1979) as calc-alkaline lamprophyres (kersantites and spessartites). Complete XRF and XRD analyses of cutting separates can be obtained on request from the authors.

#### B.1. 4.3.2 Aplites

In the KTB main hole undeformed aplites occur at a depth of 3609 m. The main constituents are plagioclase, quartz with minor biotite and chlorite. At a depth of 3413 - 3427 m plagioclase-mylonites are observed (Fig: B.1. 4.3.1). Zoned plagioclase clasts are embedded within a matrix of fine-grained recrystallized plagioclase, minor quartz and chlorite. They are regarded as deformed aplites similar to those recorded from the KTB pilot hole.



**Fig: B.1. 4.3.1:** Plagioclase mylonite, plagioclase marginally recrystallized. HC4318, depth 4318m, thin-section, crossed nicols.

## **B.1.5 ORE MINERALIZATION**

### **B.1.5.1 Sample routine**

Composite polished sections of cuttings were studied at 20 m intervals, regularly. The hand-picked material in a particular polished section either represents lithological units, rock components or ore mineral separates from representative rock units and especially from cataclastic or shear zones, vein mineralization, and geochemical and/or geophysical anomalies.

The distribution of scheelite has been determined under UV light in metabasic sections. Ferromagnetic minerals have been investigated by applying a magnetic colloid to the surface of polished sections.

### **B.1.5.2 Ore minerals**

Ore minerals identified so far include

- (1) sulphides (in decreasing order of abundance):  
pyrite, pyrrhotite, chalcopyrite, sphalerite, marcasite, pentlandite, galena, molybdenite, arsenopyrite, millerite, covellite and
- (2) oxides:  
ilmenite, rutile, anatase, leucosene, magnetite, goethite, hematite, lepidocrocite, spinel, and scheelite.

Furthermore sphene, graphite, and zircon were found.

The ore mineral association is generally similar to that determined for the pilot hole. There, few additional opaque phases have been identified by microprobe analyses (Friedrich et al. 1991; Röhr et al. 1990a; Godizart et al. 1991).

Most opaque minerals are not restricted to particular lithologies; they occur, sometimes as minor components, in all different rock units. Only in few zones of alteration or cataclasis, ore mineralization (disseminated sulphides, mainly pyrite) becomes abundant. Within gneisses the distribution is commonly foliation-controlled whereas metabasic rocks are characterized by rather erratic ore mineral occurrences.

Oxidation of sulphides to Fe-oxides and -hydroxides is caused by supergene alteration close to the present-day surface or fluid circulation along fault zones.

Pyrite and pyrrhotite are the prevailing sulphidic ore minerals within paragneisses and metabasic rocks. They occur as disseminated single grains or aggregates within the rock groundmass or are enriched in form of erratically distributed small lenses.

At least two generations of pyrite and pyrrhotite can be distinguished. Pyrite I consists of euhedral to anhedral grains with grain sizes ranging from several microns to a few hundred microns. Pyrite I contains inclusions of chalcopyrite and minor pyrrhotite (I), which are locally cogenetic. Metablastic pyrite II forms aggregates of euhedral to subhedral grains. Oriented inclusions of silicate, graphite and zircon may be present in gneissic units; intergrowths of altered ilmenite with rutile and sphene inclusions and rims in pyrite II occur in metabasic sections. Cataclastic deformation of pyrite II and fissure fillings by

chalcopyrite and minor galena are typical features. Disseminations or lens-like mobilisations of pyrrhotite II show intergrowths with chalcopyrite, sphalerite and galena.

Graphite is abundant mostly in form of elongated and kinked laths in paragneiss; exceptionally, it is found with a sphaerolitic shape in metabasic units (fig. B.1.5.1). Local replacement (?) of ilmenite by graphite was observed (fig. B.1.5.2).

Amphibolites and metagabbros are characterized by an abundance of oxidic opaque minerals. Large rounded to tabular ilmenite is prevailing (fig. B.1.5.2) with more or less alteration to Fe-/Ti-oxides (e.g. rutile, sphene, formed along cleavage planes in chlorite). Minor amounts of scheelite are distributed irregularly within cuttings from metabasites. Small discordant fissures filled with chalcopyrite, pyrrhotite, sphalerite, galena and arsenopyrite as well as quartz and calcite are in good agreement with vein-like sulphide mineralization in the KTB Vorbohrung.

### **B.1.5.3 Age relations and aspects of formation**

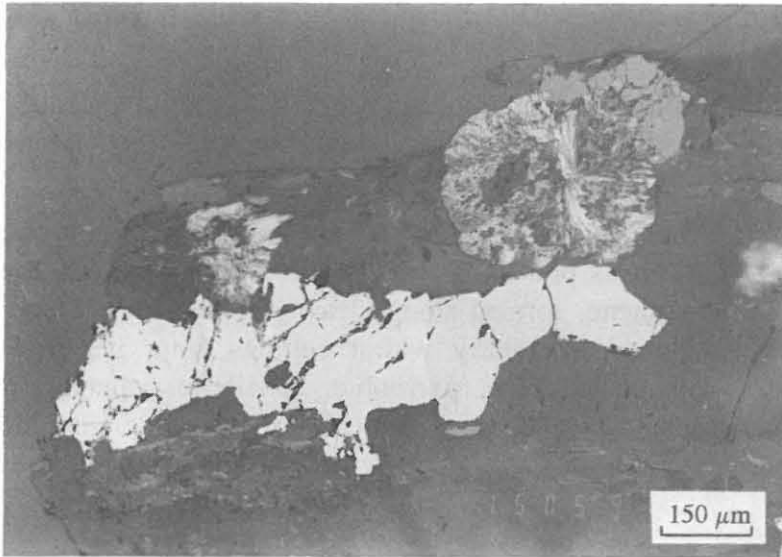
Determinations of age relationships of ore mineral associations are limited by the complex tectono-metamorphic history of the host rocks. At least four different types of mineralization have been described for the Vorbohrung by Kontny et al. (1990): intra-magmatic, metamorphically overprinted, metamorphically mobilized, post-metamorphic hydrothermal. Micro-analytical investigations are necessary for a distinction of different mineralization types concerning individual ore minerals.

The bulk of the sulphides proves to be relatively young as indicated by textural aspects and mineral intergrowths (Kontny et al. 1990; Godizart et al. 1991). They are products of mobilization/recrystallization and mineral alteration during the retrograde metamorphism, hydrothermal activity or cataclastic overprint. Cogenetic inclusions of chalcopyrite and pyrrhotite in pyrite I indicate formation temperatures of  $334 \pm 17^\circ\text{C}$  based on the calibrations of Yund & Kullerud (1966) resp.  $328 \pm 5^\circ\text{C}$  (Sugaki et al. 1975). The association of pyrite (II?) with arsenopyrite will enable thermometric conclusions (Kretschmar & Scott 1976) after microprobe analyses. Late chalcopyrite and galena fill cracks in relatively elder pyrite II. Pyrite II is younger than euhedral sphene of metabasic sections.

Oxidic opaque minerals in metabasic rocks (disseminated ilmenite and rutile) document an earlier stage of formation. Alteration of ilmenite to rutile, anatase and sphene and minor sulphides (mostly pyrrhotite) took place during retrograde metamorphism. Magnetite and goethite as alteration products of ilmenite (fig. B.1.5.3) and sulphides are young mineralization products in active zones of fluid inflow into the borehole (cf. Chap. C). Late pyrrhotite mobilises surround or replace ilmenite, leaving behind large rutile grains as products of metasomatism (fig B.1.5.4). Pyrrhotite itself is partially replaced by chalcopyrite.

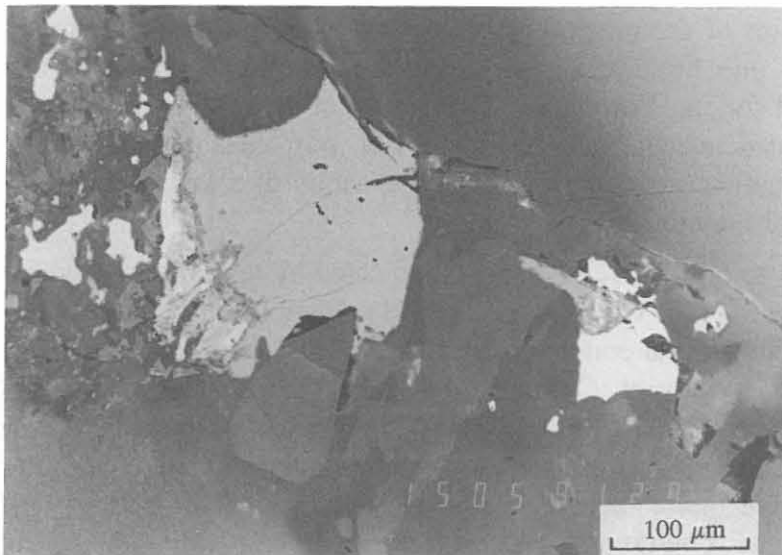
### **B.1.5.4 Qualitative and quantitative distribution of ferromagnetic ore minerals**

Pyrrhotite and magnetite represent the ferromagnetic minerals identified microscopically. Pyrrhotite, which has been confirmed causing the regional magnetic anomaly (Pucher 1986; Bader & Stettner 1990; Pohl et al. 1992; Keyssner 1992), is abundant in the entire rock sequence. A distinctive predominance of ferrimagnetic pyrrhotite relative to antiferromagnetic pyrrhotite is evident (fig. B.1.5.5).



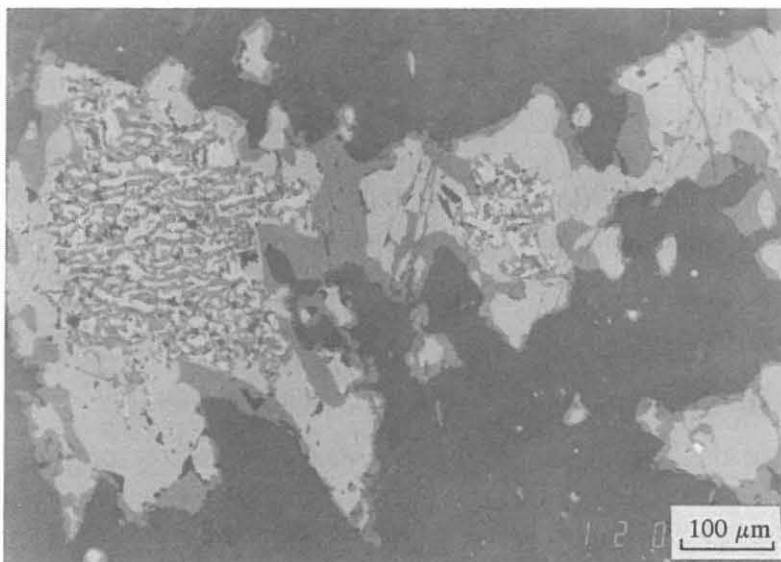
**Fig. B.1.5.1:** Large sphaerolitic individuals of graphite together with pyrrhotite with a distinct bireflectance.

(HC2700K, 2700 m, // Nic., air).



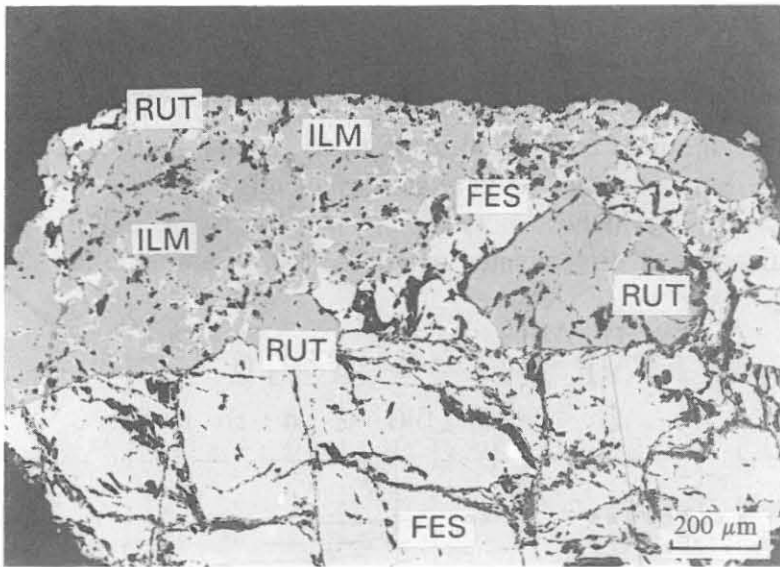
**Fig. B.1.5.2:** Tabular ilmenite aggregate (grey) with thin rim of sphene (dark grey) and replacement (?) of graphite (diffuse grey); white sulfide grains are pyrrhotite, which partially formed by ilmenite alteration.

(HC2680K I, 2680 m, // to + Nic., air).

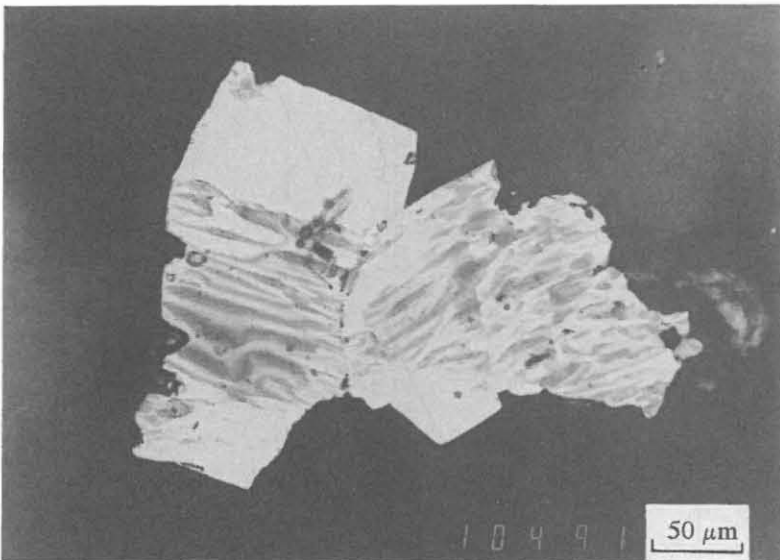


**Fig. B.1.5.3:** Anhedral ilmenite aggregates (grey) with rims of and replacement by sphene (dark grey) and rutile (light grey). Replacement by magnetite in form of dark grey strings is visible due to a magnetic colloid; white sulphide grain is pyrrhotite.

(HC3380K I, 3380 m, // Nic., air).

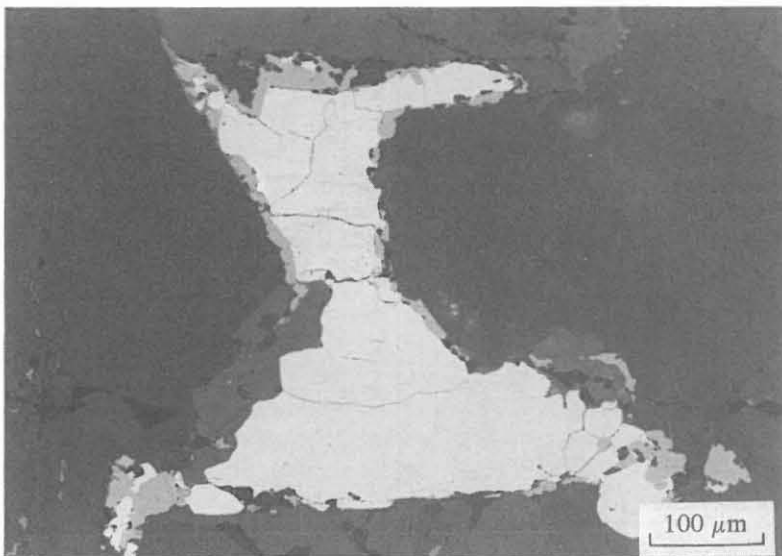


**Fig. B.1.5.4:** Mobilized pyrrhotite (FES) replaces ilmenite (ILM). The remaining Ti-content is fixed in locally large rutile (RUT) grains. (HC3640K II, 3640 m, // Nic., air).



**Fig. B.1.5.5:** Pyrrhotite aggregate showing the association of a ferromagnetic (brown haze) and anti-ferromagnetic type by application of a magnetic colloid.

(HC2400K, 2400 m, // Nic., air).



**Fig. B.1.5.6:** Pyrite (white) with chalcopyrite inclusions (light grey) is surrounded by magnetite (medium grey). High amounts of disseminated magnetite were also identified in this section causing the highest values of magnetic susceptibility detected so far in the Hauptbohrung (c.f. fig. B.1.5.7).

(HC4480K II, 4480 m, // Nic., air).

Pyrrhotite shows ferri- and antiferromagnetic types as documented by investigation of the Vorbohrung (Keyssner 1992). Microprobe analyses to distinguish between pyrrhotite types in relation to lithology, depth, and rock temperatures have not yet been carried out

Magnetite is quite rare above 3000 m and is considered to be of secondary origin. Below 3000 m depth its content increases. Magnetite can be correlated frequently with recently active fluid circulation (c.f. Chap. C). The highest value of the magnetic susceptibility at about 4500 m is due to higher amounts of disseminated magnetite within amphibolite (cf. fig. B.1.5.6, 1.5.7 and Chap. D).

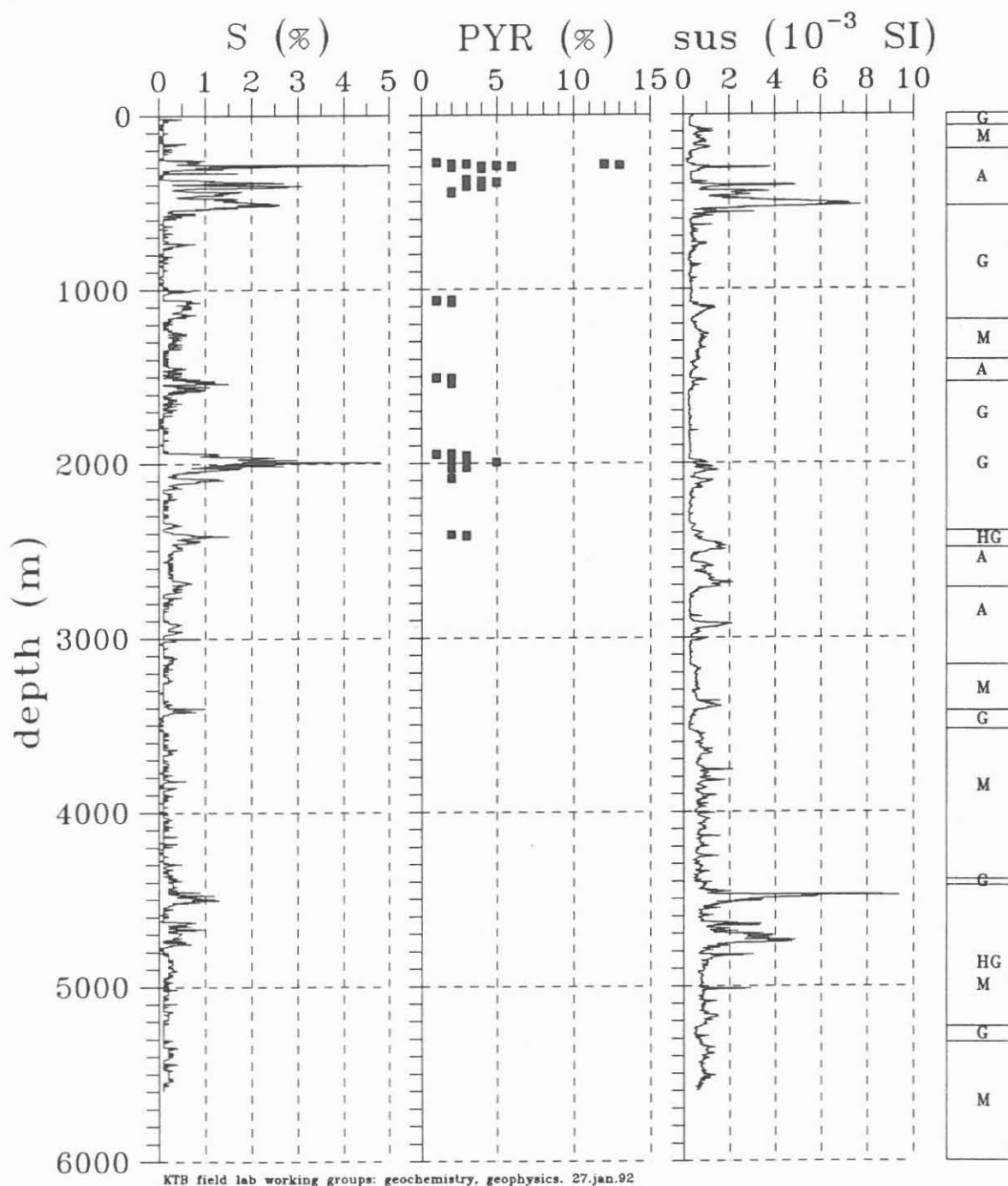


Fig. B.1.5.7: Depth related quantitative distribution of sulfur (XRF) and pyrite (XRD) in comparison with magnetic susceptibility measured on cuttings (S and pyr in weight-%).

Analytical results concerning the depth-dependent distribution of sulphur (S) and pyrite (pyr) determined by XRF and XRD are compared with the magnetic susceptibility (fig B.1.5.7; cf. Chap. C and D). Sulphur enrichment down to 2000 m correlates with pyrite concentrations in cataclastic zones (250 - 500, 1100, 1550, and 2000 m). A very high value near 500 m originates in pyrrhotite enrichment. Below 2500 m, frequent peaks in susceptibility indicate that more sulphur is present in form of ferrimagnetic pyrrhotite.

Sections with lower "background" susceptibilities between 1600 - 3100 m represent gneissic units with a dominance of pyrite or antiferromagnetic pyrrhotite. Higher susceptibilities between 2000 - 3000 m are caused by enrichment of ferrimagnetic pyrrhotite in prominent cataclastic zones around 2000 m or metabasic intercalations (2500 and 2700 m).

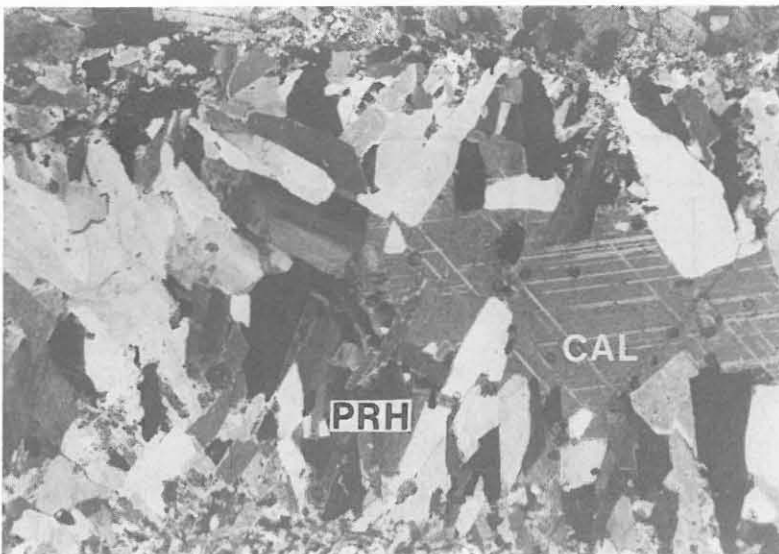
### B.1. 6 OPEN POROSITY AND CORRELATION WITH GAS-ANALYSIS

Idiomorphous crystals of prehnite, laumontite, epidote, calcite, actinolite and quartz have been found during continuous cutting-analysis (see fig. B.1. 6. 1-3). The following fissure mineral associations are observed.

- prehnite - calcite - chlorite - quartz
- prehnite - actinolite - clinzoisite - calcite - quartz
- laumontite - calcite - quartz
- epidote - calcite - quartz
- adularia - calcite - quartz

The idiomorphous shape indicates growth from solution into porous zones and open fissures. Minimum widths of the opened fissures can be deduced from the size of the crystals, amounting to several millimeters.

Open fissures and porous zones were also observed within the KTB pilot hole (Borchardt et al. 1990, Behr et al. 1991, Zulauf 1991a/b). Behr et al. (1990) analysed the palaeofluids of fissure minerals (calcite, quartz, epidote) in cores of the KTB pilot hole. They detected a system of fluid inclusions with high salinity (Na-Ca-Cl). This system developed at temperatures between 200 - 250°C during a hydrothermal event. Two different generations



**Fig. B.1. 6.4:** Fissure mineralisation. Idiomorphous prehnite and younger calcite filling (H010A7, depth 4820.5 m thinsection, crossed nicols, width of view 5,5 mm)

of fluid inclusions were observed, which both homogenize at temperatures of about 100°C. The investigation of fluid inclusions in fissure minerals of the KTB Hauptbohrung (Topp, pers. com.) yields the same results. Porous zones filled with calcite have been observed in cuttings and core samples of the KTB HB (fig. B.1. 6.4) as well as in core samples of the KTB VB (Röhr et al. 1991a). This also might indicate calcite-rich fluid migration.

Within the KTB pilot hole Borhardt (1990) differentiates various time and p/T- dependent stages of fissure mineral formation. With decreasing temperature (350 - 200°C), age (postvariscian to late cretaceous and tertiary) and depth of the pilot hole following generations were defined: Actinolite/epidote-chlorite-quartz/adularia-prehnite-calcite-laumontite.

There is a distinct correlation of gas inflow and the occurrence of fissure minerals in cuttings samples (see fig. B.1. 6.5). A mixture of gas (mainly nitrogen, methane, helium and radon) and fluid (Na-, Ca-, Sr-chlorides) has been detected in these zones (see chapter C).

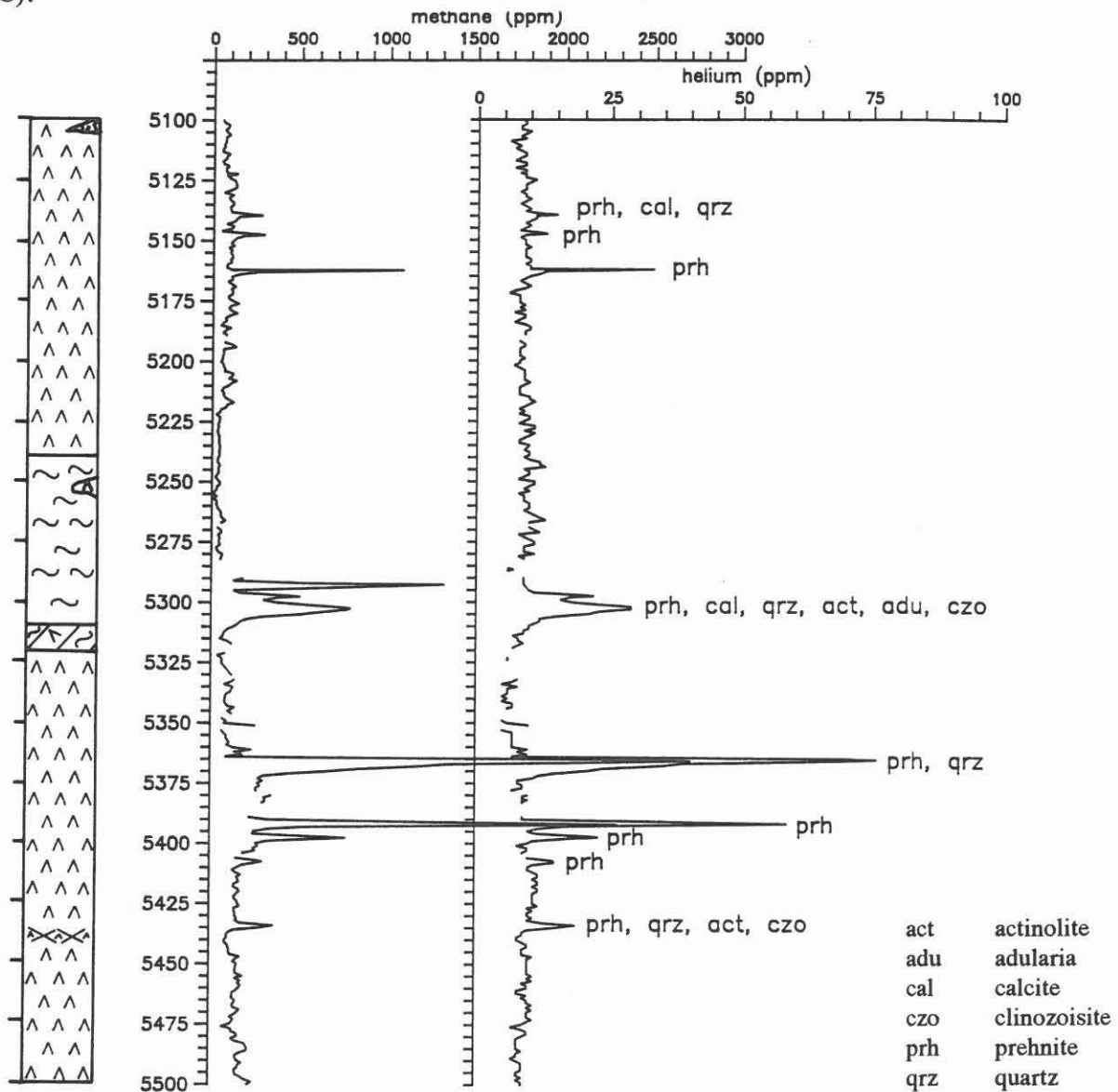
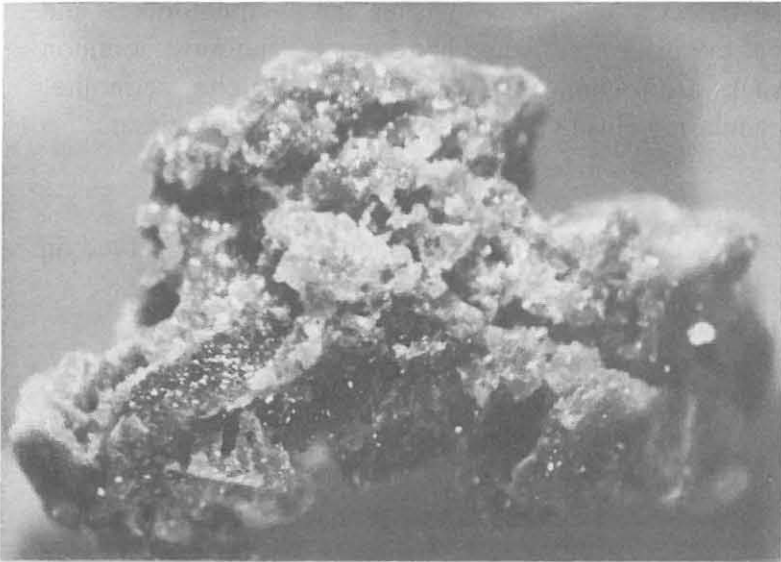
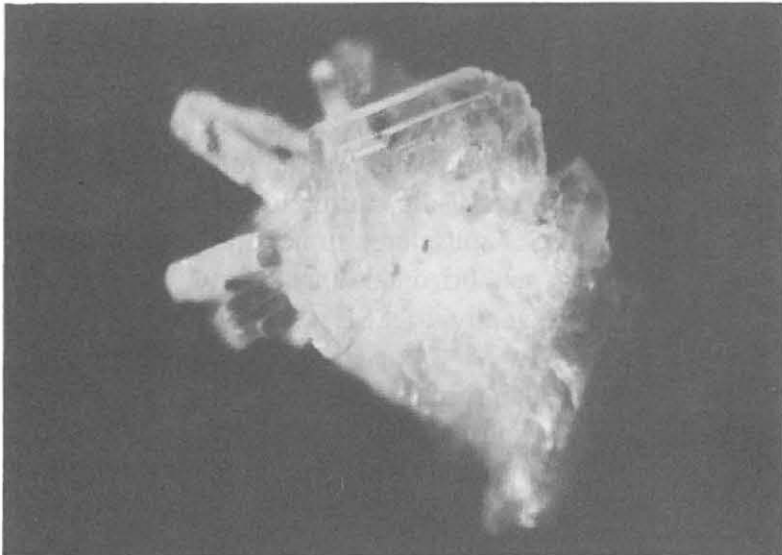


Fig. B.1. 6.5: Correlation between lithology, influx (mainly methane and helium) and fissure mineralization of the depth interval 5100 - 5500 m in the KTB Hauptbohrung (cf. legend in B.4)

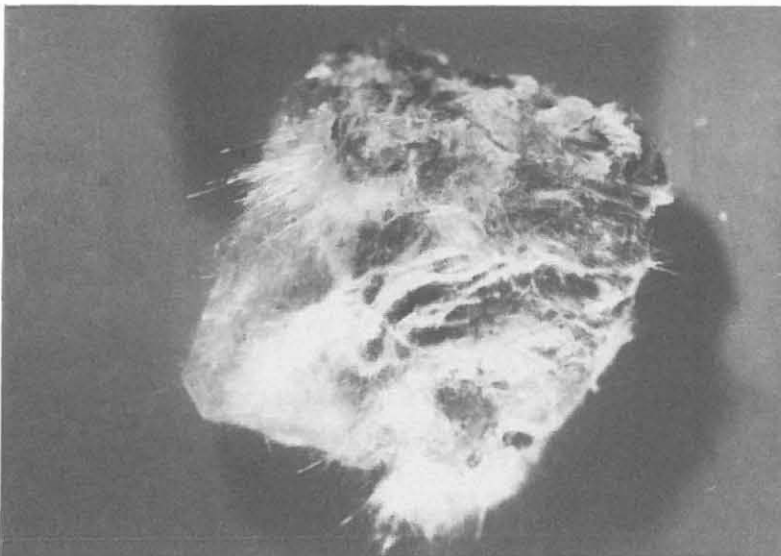




**Fig. B.1. 6.1:** Open fissure mineralization: porous epidote aggregate. (HC3394, depth 3394 m, width of view 6 mm)



**Fig. B.1 6.2:** Open fissure mineralization: idiomorphous prehnite. (HC4117, depth 4117 m, width of view 3 mm)



**Fig. B.1 6.3.:** Open fissure mineralization: tabular idiomorphous prehnite, overgrown with fibrous zeolite. (HC3866, depth 3866 m, width of view 6 mm)

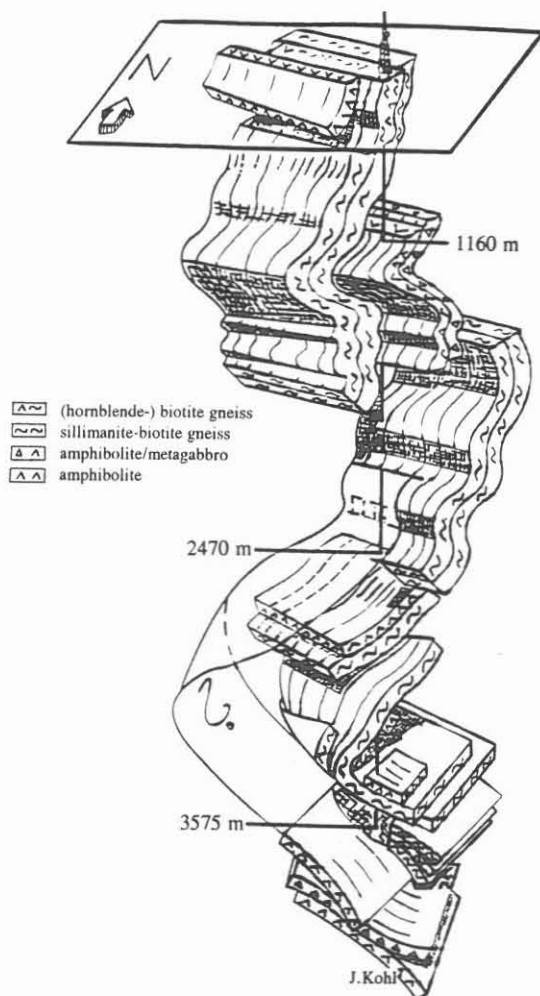
Most porous zones and fissures are detected within metabasites since amphibolites and metagabbros behave brittle throughout the respective temperature range. The most common fissure minerals occurring in these rocks are prehnite, epidote, adularia, calcite, actinolite, laumontite, clinozoisite. Quartz and adularia-veins predominate within the paragneisses.

### Conclusions

- porous zones and open fissures are identified by idiomorphous crystals observed in cuttings samples
- these zones correlate with zones of enhanced influx
- the fissure mineralisation is controlled by lithology

### B.1. 7 STRUCTURE

For the KTB Vorbohrung the structures were measured directly on core material. Cores were reoriented using Borehole Televiewer (BHTV) and Formation MicroScanner Tool (FMST) logs (Draxler & Hänel 1987, 1988, Schmitz et al. 1989).



Down to 2500 m the foliation is steeply inclined with the dip direction switching between SSW and NNE. In section 2500 to 3300 m the orientation of the foliation flattens gradually and dip turns towards SE. The structure is considered to be a large open fold with a subhorizontal axial plane. The axis plunges gently to SSE (Röhr et al. 1990a) (fig. B.1. 7.1). For the KTB Hauptbohrung structural information is only available from well logging data and few cores. To a depth of 1720 m the Formation MicroScanner tool (FMST), further down a Formation Micro Imager (FMI)\* was employed . Both tools register formation resistivity in four perpendicular directions (four-pad tool) of the hole wall.

Fig. B.1. 7.1: Structural model of the KTB Vorbohrung (Röhr et al. 1990a).

\* FMI (from SCHLUMBERGER) is an improved FMST with an increased coverage of the hole wall (e.g. for 14 3/4" diameter: FMI covers 43 %, FMST 21,5%)

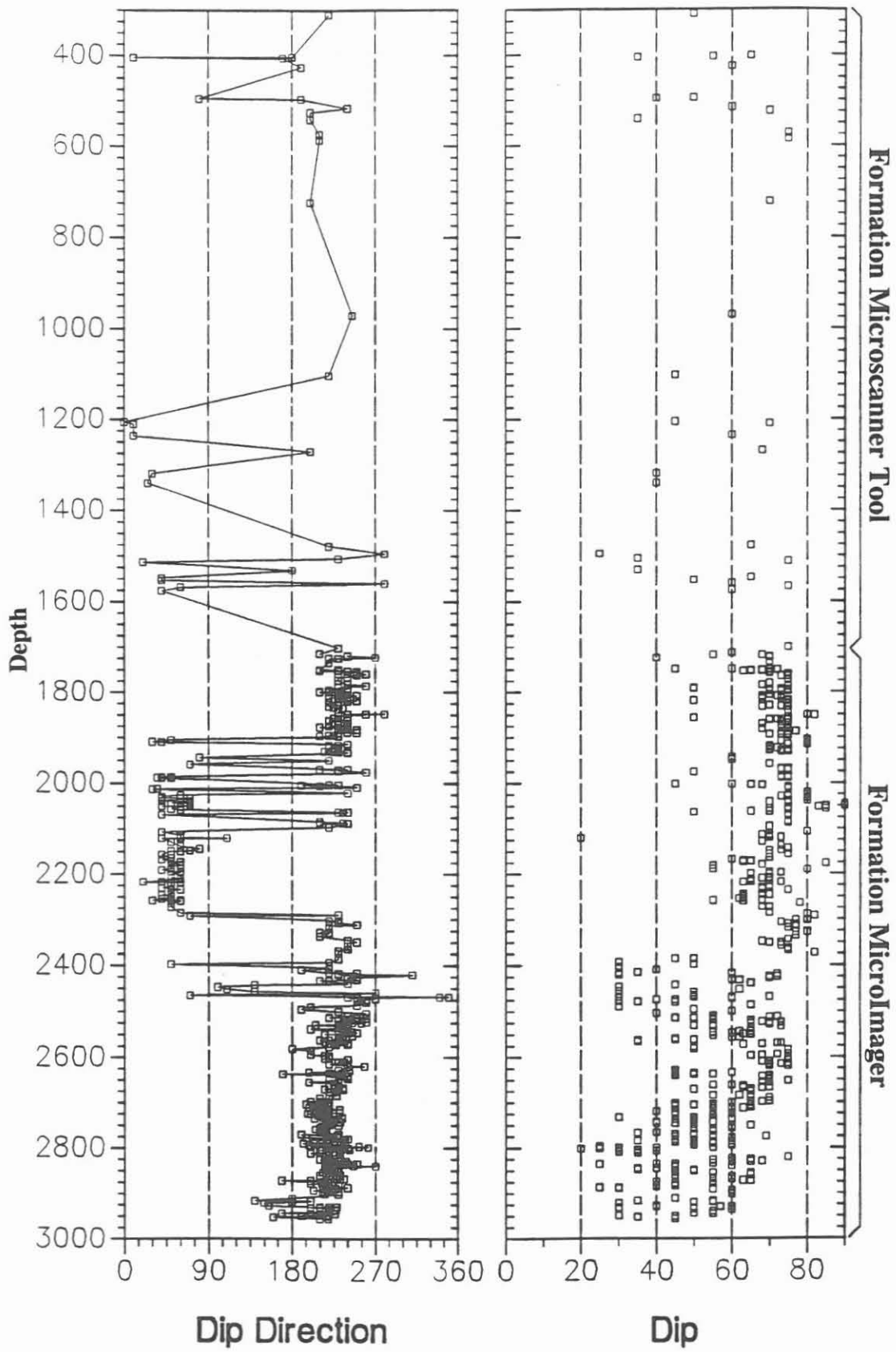


Fig. B.1. 7.2: Dip of the foliation in the KTB Hauptbohrung

Electric resistivity is very high in metamorphic rocks. Open porosity filled with conductive material leads to high resistivity contrasts. Paragneisses and metabasites show different conductivity patterns in the FMI-logs:

- In paragneisses rockfoliation is generally reproduced. This is due to fluid filled microcracks parallel to micaceous layering. Fracture sets oriented parallel to the foliation are abundant. In altered parts rock is disintegrated and becomes more porous. Thus, in these parts resistivity contrasts are reduced and the foliation is often not detectable.
- In metabasic rocks, the foliation does not represent a plane of low tensional strength and is not as obvious as in paragneisses. Cracks often crosscut the foliation. Conjugate fracture sets are abundant.

Structural data have been evaluated down to 3000 m yet. Selected values are displayed in the geologically relevant data (appendix). Foliation dips generally SW, switching towards NE in steep inclined sections (fig. B.1. 7.2.) Below 2400m the foliation slightly flattens. This structure corresponds exactly with the structure reported for the KTB pilot hole.

#### **B.1. 8 SUMMARY**

Down to 6000m the KTB main hole has cut through one coherent section of continental crust belonging to the Zone of Erbendorf-Vohenstrauß (ZEV). The drilled section is essentially composed of two petrogenetic units: paragneisses and metabasites. It is transected by numerous faults and cataclastic shear zones, as well as aplitic and lamprophyric dykes.

Protoliths of most metabasites are mainly mafic intrusives emplaced at shallow crustal levels. Paragneisses are derived from greywackes to mudstones.

The metamorphic foliation dips steeply to SSW or NNE. The ductile stretching lineation is subhorizontal. Indicators for non-coaxial deformation were observed in some shear zones only. Both units show a complex metamorphism and deformation history. High temperature deformation is older than 380ma. The earliest preserved stages are high pressure and garnet-granulite facies metamorphism in the metabasites. The highest metamorphic grade preserved in paragneisses is high amphibolite facies, however. Both, paragneisses and metabasites, suffered inhomogeneous deformation under high-temperature conditions. Both are partially overprinted under greenschist facies conditions.

The borehole has reached 6000m at ambient temperatures close to 180° C. The thermal gradient should have been higher during late-Variscan times. Consequently the drill hole should reveal a profile covering a temperature range considerably wider than today. Nevertheless, phenomena related to deformation and fluid activity at low temperatures and pressures, like vein mineralizations, retrogressive overprint and alteration, do not vary significantly throughout the drilled section.

The ZEV has been interpreted as a supra-crustal nappe (Weber & Vollbrecht 1989). The base of this structure has not been reached yet.

## B.1. 9 ACKNOWLEDGEMENTS

B. Stöckhert, K. v Gehlen and P. Herzig improved this manuscript by discussion and critical reading. J. Lauterjung & M. Larvin improved the english text.

We thank J. Topp for fluid inclusions data, U. Pieper for SEM/EDX analyses and R. Borchardt for microprobe analyses.

We also thank the technical staff at the KTB-Fieldlaboratory.

## B. 1. 10 REFERENCES

- BADER, K. & STETTNER, G. (1990): Zur Ursache der aeromagnetischen Anomalie von Windischeschenbach und Vohenstrauß (Nordost-Bayern).- Geol. Jb., **E44**, 15-35, Hannover.
- BEHR, H.J., GERLER, J., HORN, E.E., REUTEL, Ch. & TOPP, J (1991): Paläofluide in Mineralien und Gesteinen der KTB-Vorbohrung. -KTB Report **91-1**, 346-358.
- BLUMENFELD, P., MAINPRICE, D. & BOUCHEZ, J. L. (1986): C-Slip in quartz from subsolidus deformed granite. - Tectonophysics, **127**, 97-115.
- BORCHARDT, R., ZULAUF, G., EMMERMANN, R., HOEFS, J. & SIMON, K. (1990): Abfolge und Bildungsbedingungen von Sekundärmineralien in der KTB-Vorbohrung.-KTB Report, **90-4**, 76-88.
- DRACH, V. von & KÖHLER, H. (1990): Sr- und Nd-Isotopensystematik an Proben der KTB-Vorbohrung. - In: Emmermann, R. & Giese, P. (eds.): Beiträge zum 3. KTB-Kolloquium, Gießen, 28.2. bis 2.3.1990. - KTB Report **90-4**, 548, Hannover.
- DRAXLER & HÄNEL, Grundlagenforschung und Bohrlochgeophysik (Bericht 3) Bohrlochmessungen in der KTB -VB.-KTB-Report, **87-4**, 88-4
- EMMERMANN, R., DIETRICH, H.-G., LAUTERJUNG, J. & WÖHRL, TH. (eds.), (1990): KTB Pilot Hole, Results of Geoscientific Investigation in the KTB Field Laboratory, 0 - 4000.1 m. - KTB-Report **90-8**, Hannover.
- FRIEDRICH, G., HERZIG, P., KONITNY, A., VOGTMANN-BECKER, J. & KEYSNER, S (1991): Erzpetrologie in der KTB-Vorbohrung. - In: Emmermann, R. & Lauterjung, J. (eds.): Forschungsergebnisse im Rahmen des DFG-Schwerpunktprogramms "KTB", 1986-1990, KTB Report **91-1**, 136 - 155, Hannover.
- KEYSSNER S. (1991): Erzpetrologie in der KTB-Vorbohrung.- In: Emmermann, R. & Lauterjung, J. (eds.): Forschungsergebnisse im Rahmen des DFG-Schwerpunktprogramms "KTB", 1986-1990.- KTB Report **91-1**, 136-155, Hannover.
- GEHLEN, K. von, MATTHES, S., OKRUSCH, M., RICHTER, P., RÖHR, C. & SCHÜSSLER, U. (1991): Ultramafische Einschaltungen in Metabasiten der KTB-Vorbohrung. - In: Emmermann, R. & Lauterjung, J. (eds.): Forschungsergebnisse im Rahmen des DFG-Schwerpunktprogramms "KTB", 1986-1990, KTB Report **91-1**, 83-95, Hannover.
- GODIZART, G., GLEISS, N., HANSMANN, J., HÄUSSINGER, H., KEYSNER, S., KOHL, J. & LAPP, M. (1991): Tiefbohrung KTB Oberpfalz HB, Ergebnisse der geowissenschaftlichen Bohrungsbearbeitung im KTB-Feldlabor (Windischeschenbach), Teufenbereich von 0 bis 1720 m: B. Geologie.- In: Emmermann, R., Dietrich, H.-G., Lauterjung, J. & Wöhr, Th. (eds.): Tiefbohrung KTB-Oberpfalz HB, Bericht 1 zur KTB-Hauptbohrung, Teufenbereich von 0 - 1720 m, KTB Report **91-3**, B1-B83, Hannover.
- HOBBS, B. (1985): The Geological Significance of Microfabric Analysis. - In: Wenk, H. R. (ed): Preferred Orientation in Deformed Metals and Rocks: An Introduction to Modern Texture Analysis. 463-484, Academic Press.

- KEYSSNER, S. (1992): Pyrrhotin in der 4000 m tiefen Kernbohrung "KTB OBERPFALZ VB" - optische, mineralchemische und magnetische Eigenschaften.- Diss. RWTH Aachen, 117 p. (unpubl.).
- KONTNY, A., FRIEDRICH, G., HERZIG, P., KEYSSNER, S. & VOGT-MANN-BECKER, J. (1990): Erzmineralparagenesen und Mineralisationstypen in der KTB-Vorbohrung.- In: Emmermann, R. & Giese, P. (eds.): Beiträge zum 3. KTB-Kolloquium, Giessen, 28.2.-2.3.1990.- KTB Report **90-4**, 65-75, Hannover.
- KREUZER, H., MÜLLER, P., CARL, C., EBADI, A., HÖHNDORF, A. & PATZAK, M. (1990): Mineral dating on core samples from 500 to 2000 m depth of the KTB drill hole. - In: Emmermann, R. & Giese, P. (eds.): Beiträge zum 3. KTB-Kolloquium, Gießen, 28.2.-2.3.1990.- KTB Report **90-4**, 546, Hannover.
- KRETSCHMAR, U. & SCOTT, S.D. (1976): Phase relations involving arsenopyrite in the system Fe-As-S and their application.- *Canad. Mineral.*, **14**, 364-386.
- KRUHL, J. H. & HUNTEMANN, T. (1991): The structural state of the former lower continental crust in Calabria (S. Italy). - *Geol. Rundschau*, **80-2**, 289-302, Stuttgart.
- MAINPRICE, D., BOUCHEZ, J. L., BLUMENFELD, P. & TUBIA, J. M. (1986): Dominant c-slip in naturally deformed quartz: implications for dramatic plastic softening at high temperature. - *Geology*, **14**, 819-822.
- QUADT, A. von (1990): U-Pb-zircon and Sm-Nd analyses on metabasites from the KTB pilot borehole. - In: Emmermann, R. & Giese, P.: Beiträge zum 3. KTB-Kolloquium, Gießen, 28.2. bis 2.3.1990. - KTB Report **90-4**, 545, Hannover.
- PATZAK, M., OKRUSCH, M. & RÖHR, CH. (1991): Die Metabasite der KTB-Vorbohrung: Petrographie, Geochemie, Mineralchemie und Metamorphoseentwicklung. - In: Emmermann, R. & Lauterjung, J. (eds.): Forschungsergebnisse im Rahmen des DFG-Schwerpunktprogramms "KTB", 1986 - 1990. - KTB Report **91-1**, 63-82, Hannover.
- PEARCE, J. R. (1982): Trace-element characteristics of lavas from destructive plate boundaries.-In: Thorpe, R. S (ed.): *Andesites*.-Wiley and Sons, 525-548, New York.
- PFLUG, H.D. & PRÖSSL, K.F. (1991): Palynology in the Pilot Hole of the Continental Deep Drilling Program: Results and Implications. - In: Emmermann, R. & Lauterjung, J. (eds.): Forschungsergebnisse im Rahmen des DFG-Schwerpunktprogramms "KTB", 1986-1990. - KTB Report **91-1**, 239-258, Hannover.
- POHL, J., PÄTZOLD, T., SOFFEL, H., ROLF, C. & WORM, H.-U. (1992): A rock magnetic log of the KTB pilot borehole.- *Scientific Drilling*, **2**, 110-122.
- PRICE, G. P. (1985): Preferred Orientations in Quartzites. - In: Wenk, H. R. (ed): *Preferred Orientation in Deformed Metals and Rocks: An Introduction to Modern Texture Analysis*. 385-406, Academic Press.
- PUCHER, R. (1986): Interpretation der magnetischen Anomalie von Erbdorf (Oberpfalz) und dazugehörige gesteinsmagnetische Untersuchungen.- *Geol. Jb.*, **E33**, 32-52, Hannover.
- REINHARDT, J., KLEEMANN, U., BLÜMEL, P. & SCHREYER, W. (1989): Geothermobarometry of metapelites as a key to the pressure and temperature history of the ZEV (Zone von Erbdorf-Vohenstrauß), NE Bavaria. - In: Emmermann, R. & Giese, P. (eds.): Beiträge zum 2. KTB-Kolloquium, Gießen, 15. bis 17.3.1989. - KTB Report **89-3**, 24-32, Hannover.
- ROCK, N.M.S. 1984. Nature and origin of calc-alkaline lamprophyres: minettes, vogesites, kersantites and spessartites. *Trans. R. Soc. Edinburgh*, **74**, 193-227, 1984.
- RÖHR, C., KOHL, J., HACKER, W., KEYSSNER, S., MÜLLER, H., SIGMUND, J., STROH, A. & ZULAUF, G. (1990a): German Continental Deep Drilling Program (KTB) - Geological survey of the pilot hole "KTB OBERPFALZ VB".- In: Emmermann, R., Dietrich, H.-G., Lauterjung, J. & Wöhrl, Th. (eds.): *KTB Pilot Hole, Results of Geoscientific Investigation in the KTB Field Laboratory, 0 - 4000.1 m*. - KTB Report **90-8**, B1-B55, Hannover.

- RÖHR, C., PATZAK, M. & OKRUSCH, M. (1990b): Metamorphose-Entwicklung der Metabasite in der KTB-Vorbohrung.- In: Emmermann, R., & Giese, P. (eds.): Beiträge zum 3. KTB-Kolloquium, Gießen, 28. 2.- 2. 3. 1990. - KTB Report **90-4**, 532-533, Hannover.
- SCHALKWIJK, G. (1991): Metabasites in the pilot borehole of the German Continental Deep Drilling Project, Windischeschenbach, Eastern Bavaria. Structures and fabrics as documents of crustal evolution. - Diss., Universität Bochum, 203 S.
- SCHMITZ, D., HIRSCHMANN, G, KOHL, J. & WOHLGEMUT, L (1989). Die Orientierung von Bohrkernen in der KTB-Vorbohrung.-KTB Report, **89-3**, 468-468, Hannover
- SHERVAIS, J. W. (1982): Ti-V plots and the pretrogenesis of modern and ophiolitic lavas.- Earth Planet. Sci. Lett., **59**, 101-118.
- STRECKEISEN A., 1979. Classification and nomenclature of volcanic rocks, lamprophyres, carbonatites and melilitic rocks.- *Geology*, **7**, 331-335.
- SUGAKI, A., SHIMA, H., KITAKAZE, A. & HARADA, H. (1975): Isothermal phase relations in the system Cu-Fe-S under hydrothermal conditions at 350°C.- *Econ. Geol.*, **70**, 806-823, El Paso.
- TOPP, J :Diss. in prep.- Univ. Göttingen
- WALL, H. de (1991): Die Gefüge der Paragneise in der KTB-Vorbohrung und ihr Einfluß auf gesteinsphysikalische Eigenschaften. - Diss. (unpubl.), Universität Göttingen, 101 S.
- WEBER, K. (1990): Observations on the ductile deformation path of the paragneisses of the KTB pilot hole. - In: Emmermann, R., Dietrich, H.-G., Lauterjung, J. & Wöhl, Th. (eds.): KTB Pilot Hole, Results of Geoscientific Investigation in the KTB Field Laboratory, 0 - 4000.1 m. - KTB Report **90-8**, J1-J19, Hannover.
- WIMMENAUER, W. (1991): Geochemie der metamorphen Sedimentgesteine in der Kontinentalen Tiefbohrung und ihrem Umfeld. - In: Emmermann, R. & Lauterjung, J. (eds.): Forschungsergebnisse im Rahmen des DFG-Schwerpunktprogramms "KTB", 1986-1990. - KTB Report **91-1**, 106-135, Hannover.
- YUND, R.A. & KULLERUD, G. (1966): Thermal stability of assemblages in the Cu-Fe-S-system.- *J. Petrol.*, **7**, 454-488.
- ZULAUF, G. (1990): Spät- bis postvariszische Deformationen und Spannungsfelder in der nördlichen Oberpfalz (Bayern) unter besonderer Berücksichtigung der KTB-Vorbohrung. - *Frankfurter geowiss. Arb., Serie A (Diss.)* Bd. 8: 1-285; Frankfurt a. M.
- ZULAUF, G. (1991b): Zur spät- bis postvariszischen Krustenentwicklung in der nördlichen Oberpfalz.-KTB Report 91 - 1, 41-62

## B.1. 11 APPENDIX

### B.1. 11.1 List of Mineral Abbreviations

ACT	actinolite	KYA	kyanite	SAUS	saussuritization
BIO	biotite	LAU	laumontite	SIL	sillimanite
CAL	calcite	MOB	mobilisate	SPH	sphene
CHL	chlorite	MUS	muscovite	SYM	symplectite
CPX	clinopyroxene	PLG	plagioclase	WMIC	white mica
GNT	garnet	PRH	prehnite		
ILM	ilmenite	QRZ	quartz		

### B.1. 11.2 Description of the geological profile

- 0000.0 - 0016.0 m: **Calc-silicate bearing plagioclase rich gneiss.**
- 0016.0 - 0069.0 m: **Muscovite-biotite gneiss**, completely chloritized.
- 0069.0 - 0203.0 m: **Amphibolite**, weakly to strongly altered.
- 0203.0 - 0290.0 m: **Garnet-sillimanite-biotite gneiss** with intercalations of calc-silicate bearing and plagioclase rich gneiss (243 - 247 m) and cataclasites (247 - 254 m).
- 0290.0 - 0522.0 m: Variegated alternation between **muscovite-biotite gneiss / calc-silicate bearing and plagioclase rich gneiss / garnet-kyanite/sillimanite-biotite gneiss** and **metabasites** (309 - 329 m).
- 0522.0 - 1183.0 m: **Garnet-sillimanite-biotite gneiss** with **calc-silicate bearing plagioclase rich gneiss** (947 - 994 m).
- 1183.0 - 1410.0 m: **Amphibolite** with few thin intercalations of **garnet-biotite-hornblende gneiss**; locally with cataclastic overprint.
- 1410.0 - 1573.0 m: Variegated alternation of **muscovite-biotite gneiss**, **garnet-sillimanite-biotite gneiss**, **metabasite**; **lamprophyres** between 1540 - 1590 m.
- 1573.0 - 2277.0 m: **Garnet-sillimanite-biotite gneiss** with intercalations of **muscovite-biotite gneiss** (2031 - 2082, 2175 - 2277 m); weakly altered; strong cataclastic overprint between 1920 - 2100 with intercalations of cataclastic gneiss in the vicinity of prominent faults (1937 - 1945, 1957 - 1970, 1975.5 - 1985, 1990 - 2000 m).
- 2277.0 - 2380.0 m: Alternation of **garnet-sillimanite-biotite gneiss** and **muscovite-biotite gneiss**; weakly altered.
- 2380.0 - 2384.0 m: **Lamprophyre.**
- 2384.0 - 2453.0 m: Alternation of **garnet-sillimanite-biotite gneiss / biotite-hornblende gneiss**; weakly altered.
- 2453.0 - 2502.0 m: **Amphibolite**, weakly altered.
- 2502.0 - 2510.0 m: Alternation of **amphibolite / garnet-sillimanite-biotite gneiss.**
- 2510.0 - 2564.0 m: **Garnet-sillimanite-biotite gneiss** with locally cataclastic overprint; intercalation of **hornblende-biotite gneiss** at 2547 m.
- 2564.0 - 2574.0 m: Alternation of **garnet-sillimanite-biotite gneiss / hornblende-biotite gneiss** with epidote.
- 2574.0 - 2626.0 m: **Hornblende-biotite gneiss**, weakly altered.
- 2626.0 - 2656.0 m: Alternation of **hornblende-biotite gneiss / amphibolite.**
- 2656.0 - 2701.0 m: Alternation of **amphibolite / hornblende gneiss.**
- 2701.0 - 2718.0 m: Alternation of **garnet-sillimanite-biotite gneiss** and **amphibolite**, locally strongly altered.
- 2718.0 - 2747.0 m: **Muscovite-biotite gneiss**, strongly altered.
- 2747.0 - 2906.0 m: **Garnet-sillimanite-biotite gneiss** with local **amphibolite** intercalations (2756, 2763 m); strongly altered between 2770 - 2820 and 2870 - 2880 m; locally with cataclastic overprint.
- 2906.0 - 2950.0 m: Alternation of **garnet-sillimanite-biotite gneiss / biotite-hornblende gneiss / amphibolite**; **lamprophyre dyke** at 2948 m.
- 2950.0 - 3160.5 m: **Garnet-sillimanite-biotite gneiss**, locally strongly altered and with cataclastic overprint (e.g. 3145 - 3160 m); **lamprophyres** at 3093, 3104 - 3107 and 3153 m.



- 3160.5 - 3413.5 m: **Amphibolite**, strong to complete cataclastic overprint in the upper part, **lamprophyres** above 3240 m.
- 3413.5 - 3427.0 m: **Feldspar mylonites**.
- 3427.0 - 3534.0 m: **Muscovite-biotite gneiss**, below 3490 m increase of alteration.
- 3534.0 - 3877.0 m: **Amphibolite**; cataclastic section between 3580 - 3600 m and 3805 and 3830 m, open fissures from 3700 - 3760 m; **aplite** between 3608 - 3610 m.
- 3877.0 - 3898.0 m: **Amphibolite**, strongly altered, alternating with minor hornblende-biotite gneiss.
- 3898.0 - 3941.0 m: **Amphibolite**, generally less altered, with intercalated hornblende-biotite gneiss at 3924.0 m.
- 3941.0 - 3950.0 m: **Hornblende-biotite gneiss**.
- 3950.0 - 4108.0 m: **Amphibolite**, generally severely altered; with cataclastic overprint between 3950 - 4006 m.
- 4108.0 - 4129.5 m: **Biotite-hornblende gneiss / amphibolite** alternations.
- 4129.5 - 4394.5 m: **Amphibolite**, strongly altered with intercalations of biotite-hornblende gneiss at 4148.5 and 4237 m; open fissures at 4272- 4290 m, 4350 - 4395 m.
- 4394.5 - 4422.5 m: **Garnet-sillimanite-biotite gneiss**.
- 4422.5 - 4596.5 m: **Amphibolite** with intercalations of biotite-hornblende gneiss.
- 4596.5 - 4605.5 m: **Biotite-hornblende gneiss**.
- 4605.5 - 4911.5 m: **Amphibolite**, strong alteration or cataclastic overprint (4627 - 4631, 4670 -4680, 4720 - 4750, 4845 - 4855 m); cataclastic amphibolite at 4764 - 4775 and 4803 - 4817 m; lamprophyres at 4810 - 4813 m, 4835, 4856 and 4868 m.
- 4911.5 - 4939.0 m: **Garnet-biotite gneiss**, garnet-hornblende-biotite gneiss and amphibolite, alternating.
- 4939.0 - 5224.5 m: **Amphibolite**, weakly or strongly altered; increased cataclastic overprint at 4956 - 4990, 5005 - 5015 m porous zones and gas inflows; meta-ultramafic intercalation at 4975 m.
- 5224.5 - 5300.0 m: **Muscovite-biotite gneiss**, strongly altered with intercalation of amphibolite at 5245 m; cataclastic gneiss with minor pyrite content at 5285 - 5295 m.
- 5300.0 - 5311.0 m: **Amphibolite**, strongly altered.
- 5311.0 - 5320.5 m: **Muscovite-biotite gneiss**, strongly altered.
- 5320.5 - 5541.0 m: **Amphibolite**, generally strongly altered, locally with intensive cataclastic overprint; intercalations of hornblende-biotite gneiss at 5354 and 5404 m and of meta-gabbro at 5380 m; cataclastic, sulphide bearing amphibolite at 5445 - 5450 m; porous fault zones at 5375 - 5380 m; below 5360 m increase of porous zones.
- 5541.0 - 5609.0 m: **Muscovite-biotite and muscovite-chlorite gneiss**, strongly altered, decreasing alteration with depth; intercalations of partially cataclastic amphibolite at 5578 - 5582 and 5584.5 - 5592.0 m; fault zone with high amounts of pyrite cataclasites at 5592 m.
- 5609.0 - 5900.0 m: **Amphibolite**, strongly altered, locally strong cataclastic overprint.

**B.1. 11.3 Short (preliminary) description of the cores in the KTB Hauptbohrung**

Core	Core Run	Recovery (m)	Lithology	Dip of Foliation (°)
H001	4149.0 - 4156.8	5.30	<b>Amphibolite</b> , fine grained, well foliated with intercalations of strongly deformed <b>Biotit-Hornblende-Gneiss</b> , laumontite mineralization on joints.	50-70
H002	4195.0 - 4202.2	3.90	<b>Amphibolite</b> , fine grained, well foliated locally massive with <b>metagabbro</b> intercalations, partially strongly altered, in the lower part of the core run strongly deformed <b>hornblende gneiss</b> .	40-85
H003	4251.0 - 4260.3	4.05	<b>Amphibolite</b> , fine grained, well foliated, alternating with strongly foliated <b>hornblende gneiss</b> , locally high contents of biotite-bearing quartz-feldspar mobilisate.	40-80
H004	4341.3 - 4350.6	2.30	<b>Amphibolite</b> , medium grained, locally garnet-bearing, partially strongly altered.	35-70
H005	4447.2 - 4456.2	2.90	<b>Amphibolite</b> fine to medium grained, massive, locally well foliated, locally rich in mobilisates with hornblende blasts	50-70
H006	4512.0 - 4521.0	5.10	<b>Garnet Amphibolite</b> fine to medium grained, with <b>metagabbro</b> -intercalations, locally well foliated with garnet rich boudins, partially strongly altered.	40-60
H007	4592.3 - 4601.6	3.84	<b>Hornblende-gneiss / amphibolite</b> , locally strongly altered with epidote, open fissures.	50-60
H008	4646.2 - 4655.5	3.10	<b>Amphibolite</b> , massive, locally strongly foliated, locally strongly altered, weakly jointed.	60-90
H009	4684.7 - 4692.4	4.15	<b>Amphibolite / Garnet Amphibolite</b> , ductile, steep shear zones in the lower part of the core run.	60
H010	4820.0 - 4826.6	3.50	<b>Amphibolite</b> , massive with quartz-feldspat mobilisates, locally garnet and titanite bearing, local cataclastic overprint, two <b>gneiss intercalations</b> .	55-65
H011	5012.0 - 5018.0	2.50	<b>Amphibolite</b> , strongly to completely altered, cataclastic overprint, fault gouge in the lower part.	45-80
H012	5082.0 - 5089.0	3.90	<b>Amphibolite</b> , weakly altered, well foliated to massive, locally thin deformed mobilisate layers.	50-90
H013	5282.0 - 5288.0	1.35	<b>Muscovite-biotite-Gneiss</b> , strongly altered and cataclastically overprinted, graphit bearing shear zones.	~60
H014	5378.0 - 5387.4	4.70	<b>Amphibolite</b> , weakly to strongly altered with thin <b>hornblende-gneiss</b> intercalations	20-30
H015	5502.5 - 5511.1	0.15	<b>Amphibolite</b> , fine grained, cataclastic overprint.	55
H016	5523.2 - 5530.4	1.85	<b>(Garnet-)Amphibolite</b> , fine grained, weakly foliated, with quartz feldspar mobilisates	35-65
H017	5555.5 - 5561.5	0.00		
H018	5705.0 - 5706.0	0.00		
H019	5778, 5 - 5782, 5	2.25	<b>Amphibolite</b> , partially strongly altered, massive to strongly foliated,	40-60

KTB Report	92-2	B43-B46	3 Fig.	Hannover 1992
------------	------	---------	--------	---------------

## B.2 DRILLING ARTIFACTS IN CUTTINGS SAMPLES

Helga de Wall & Susanne Lich  
 KTB Feldlabor, P.O. Box 67, D-8486 Windischeschenbach

In the KTB Hauptbohrung the scientific investigations are based mainly on cuttings material. This contribution concentrates on drilling artifacts and drilling induced structures in this material and its influence on petrophysical and geochemical analyses.

### B.2. 1. Bit-Metamorphism

During sample analysis under the binocular microscope a special kind of cutting which differ from other cuttings is observed. They are shelly with convex and concave shape and lighter in colour. At the concave part a metallic striation is abundant. Bursting while treating with tweezers indicates an intense reduction in mechanical strength.

This drilling induced change in cutting material is called "bit-metamorphism", a well known phenomenon in drilling. In the KTB Hauptbohrung insert-bits have been used with weights on bit up to 250 kN in the 14 3/4" drilling phase. There is no information about exact temperature conditions at the bit-rock contact. But they are expected to be high.

A dependance of Bit-metamorphism on lithology (high in metabasites, low or absent in gneisses) and drilling processes is observed. Especially drilling with a thruster\* leads to strong bit-metamorphism. Maximum values reach up to 20 %.

The influence on mineral composition and petrophysical properties by this phenomenon has been examined.

- X-ray diffractometry and microcopic analysis of thin sections show no change in mineral composition in bit-metamorphic cuttings (see fig. B.2. 1.2).
- Rock density is slightly decreased as volume increases through cracking (see tab. B.2. 2.1).
- Rock susceptibility increases due to the metallic striation. (see below and chapter D 4).

The influence on natural gamma-ray activity and thermal conductivity has not been measured due to lack of sufficient material. No influence can be expected since there is no change in mineral composition.

Sample	Density (g/cm)		
	<i>bulk sample</i>	<i>bit-met. cut.</i>	<i>difference</i>
HC 3370	2,9160	2,8965	0,0195
HC 3372	2,8969	2,8728	0,0241
HC 3866	2,9419	2,9307	0,0112

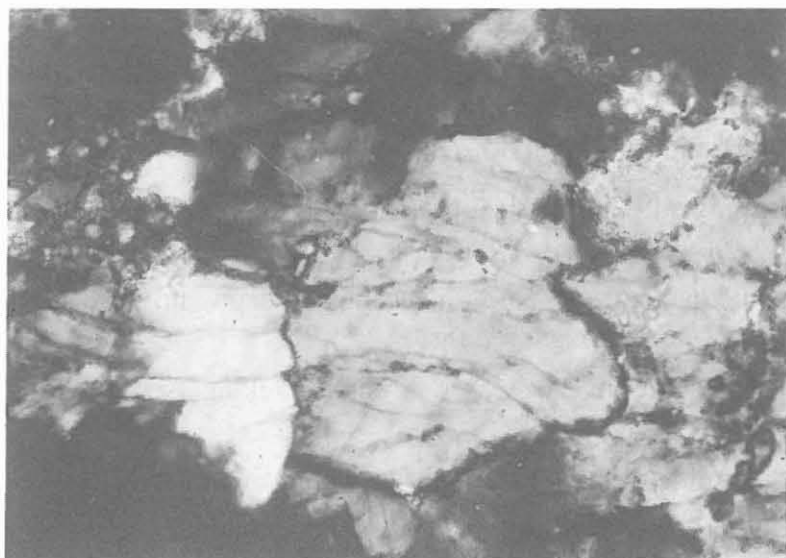
Tab. B.2. 2.1: Density values for amphibolite bulk samples and separated bit-metamorphic amphibolites

\* A thruster is a part of drilling equipment, which allows the driller to apply an increased and constant weight immediately above the bit by using mud hydraulics.

Microscopic studies on thin sections show the accumulation of transgranular microcracks especially in quartz, plagioclase and amphibole (see fig. B.1.2. 2). The microcracks are mainly oriented in subparallel sets (see fig. B.1.2. 1).



**Fig. B. 2. 2.1:** Subhorizontal crack sets in a bit-metamorphic amphibolite cutting (HC 3370), crossed nicols, width of view 2mm



**Fig. B. 2. 2. 2:** Crackpattern in quartz and plagioclase treated by bit-metamorphism (HC 3370), crossed nicols, width of view 0,5mm

## Conclusion

Extreme PT-conditions at bit-rock contact are so short-timed that they cause no change in mineral composition. Reduction in mechanical strength can be ascribed to intense microcracking. The crack pattern leads to the conclusion that bit pressure has induced the cracking. Cracking by thermal stresses seems to be less important. Amphibolites (massive, high strength) and gneisses (well foliated, lower strength) show different response to

mechanical bit treatment. Weights on bit during drilling differ much between amphibolites (100 - 200 kN) and gneisses (20 - 80 kN). This explains the rare occurrence of Bit-Metamorphism in the gneisses. We propose to avoid the term "metamorphism" for this phenomenon as it is incorrect in the sense of geosciences. The effect is purely mechanical.

### B.2. 2. Metal content

Drilling the KTB Hauptbohrung has revealed that amphibolites are hard to penetrate with roller cone insert bit. This rock type (strength values between 200 - 300 MPa, see chapter E) requires high weights on bit (s.a.). Especially the metabasic rock sequence below 3160 m leads to high bit-abrasion in noncataclastic and only weakly altered parts. An early breaking off of the inserts can be followed from the detection of non abraded inserts found in the lowest part of the borehole assembly (e.g. junk sub, cutting sampler, shock absorber). Some bits show high caliper reduction.

In cutting samples metallic artifacts (splinters, rusty scrap) are observed. We examined the influence of this artifacts on rock susceptibility and geochemistry.

From a defined volume of bulk cutting material (10 ml) the magnetic portion was separated and weighed. The magnetic portion consists of metallic artifacts (s.a.), bit-metamorphic cuttings with metallic application (see chapter B.2. 1) and magnetic cuttings (with ore mineralization). Measurements have been carried out for the section 3744 - 4340 m. The magnetic portion is plotted versus depth separated for the bit runs (fig. D.4.4) .

It could be observed that

- the metallic portion is not randomly distributed with depth (fig. D.4. 4).
- a high content is observed (fig. B.2. 2.1)
  - at the beginning of a new bit run due to scrapping on casing during trip in/trip out (A)
  - when sticking of the assembly requires jarring (B)
  - at the end of a run if the bit is worn (C)

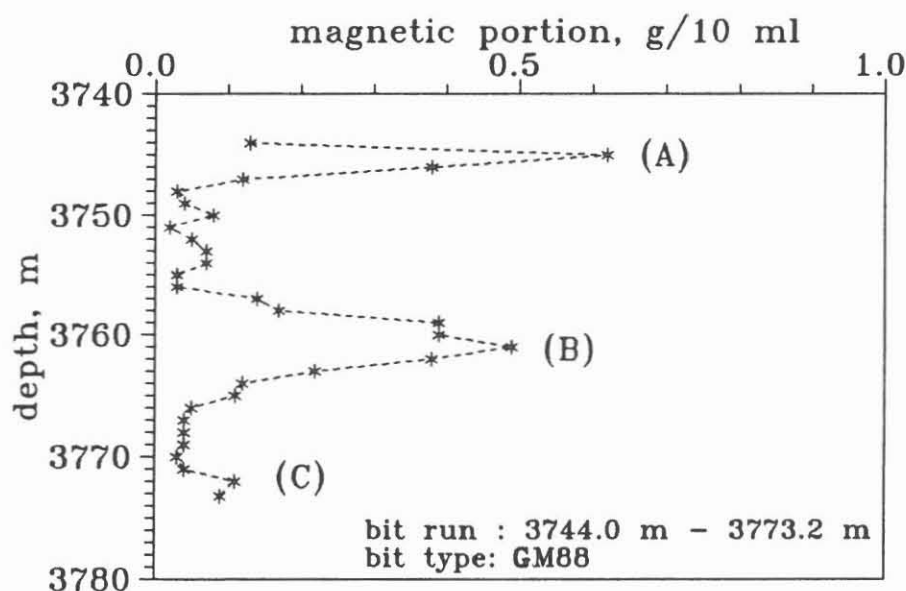


Fig. B.2. 2.1: Magnetic portion in cuttings samples shown for a selected bit run

A comparison of magnetic portion with susceptibility data of bulk cutting material shows a correlation of portion peaks with high susceptibility values. This positive correlation is also valid for selected geochemistry data ( $\text{Fe}_2\text{O}_3$ , sulfur, zinc, copper).

### **Conclusion**

Metallic abrasion of the borehole assembly spoils the cutting material. Especially the samples taken the first three meters of a new bit run show a high content of metallic artifacts. This should be taken into account if susceptibility and geochemistry are interpreted. As shown in chapter D.4. 4 a correction is possible by quantifying the abraded metal content.

### **Acknowledgements**

We are grateful to the KTB drilling engineers C. Chur, L. Wohlgemuth, R. Jatho for their cooperation. Thanks to T. TranViet for critical reading the manuscript.

KTB Report	92-2	B47-B52	3 Fig.	Hannover 1992
------------	------	---------	--------	---------------

### **B.3 THE GEOLOGICAL SECTION OF THE KTB HAUPTBOHRUNG - CORRELATION WITH THE KTB VORBOHRUNG AND PRELIMINARY STRUCTURAL INTERPRETATION**

G. Hirschmann \*

The pilot hole (Vorbohrung - VB) down to its final depth of 4000,1 m as well as the main borehole (Hauptbohrung - HB) down to its present depth of 5900 m has penetrated into a succession of gneisses alternating with metabasites (Emmermann et al. 1990, Lich et al. 1992). This succession corresponds very well with the composition and distribution of rock types at the surface in the location area. Here, amphibolites and hornblende gneisses (amphibole gneisses) form several NW-SE trending and SW-dipping belts within the biotite- and muscovite-biotite paragneisses. This rock association in connection with some minor intercalations (calcsilicates, carbonatic and graphite bearing rocks, orthogneisses) is characteristic for the Zone of Erbendorf-Vohenstrauß (ZEV).

The geological situation in the immediate vicinity of the drill site is complicated by a prominent NNW-SSE fault zone (Nottersdorf fault zone) which is steeply dipping to the ENE and causes a considerable offset of the geological units. Furthermore, this fault zone is characterized by dykes of quartz, aplitic granite, pegmatite and lamprophyre (Fig. B.3.1). The pilot hole is situated within this fault zone, the main borehole immediately east of it. Probably, the fault crossing the drill site between the two boreholes is the most important one.

With a few exceptions, the geological sections of the pilot hole and the main borehole are very similar regarding both the lithological succession and the principal structural features (Fig. B.3.2 and B.3.3). The sections of both boreholes show a characteristic lithostratigraphic sequence. The alternating gneissic and metabasic units have apparent thicknesses of several hundreds of metres (up to more than 2000 m). The metabasic units are composed of amphibolites, garnetiferous amphibolites, calcsilicate amphibolites, metagabbros, biotite-amphibole gneisses and rare meta-ultramafic rocks. The individual units can be distinguished by proportion and distribution of these rock types and, partly, by chemical differences. Most of the metabasites were derived from mafic magmatites (basalts and gabbros). Some types, supposedly, represent former volcanoclastics or tuffogenic sediments. Occasionally, transitions from paragneisses to metabasites are observable. Most of the biotite- to muscovite-biotite gneisses are paragneisses and represent former metapelitic and metapsammitic sediments of greywacke composition in varying proportions (Emmermann et al. 1990). Plagioclase-rich and epidote-bearing gneisses of uncertain origin (orthogneisses?) occur as minor intercalations in the main borehole and at the surface.

The lithological units of the pilot hole (VB) and the main borehole (HB) and their correlation are shown in Fig. B.3.2.

---

\* Niedersächsisches Landesamt für Bodenforschung, Stilleweg 2, W-3000 Hannover 51, FRG

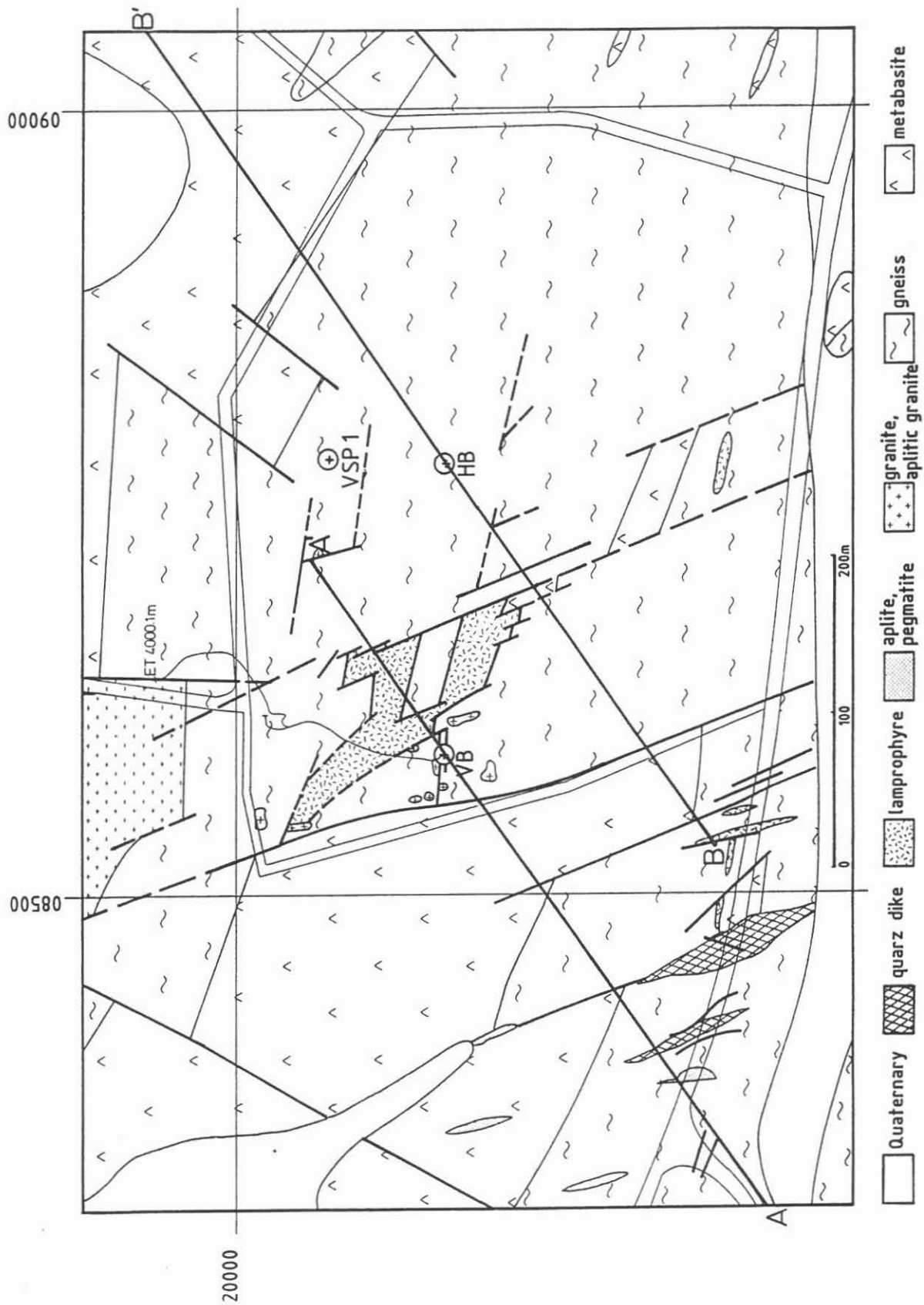


Fig. B.3.1: Geological map of the drill site and its immediate surroundings (mainly after Rohrmüller 1987, Stettner et al. 1990). A - A' and B - B' section lines of Fig. B.3.3



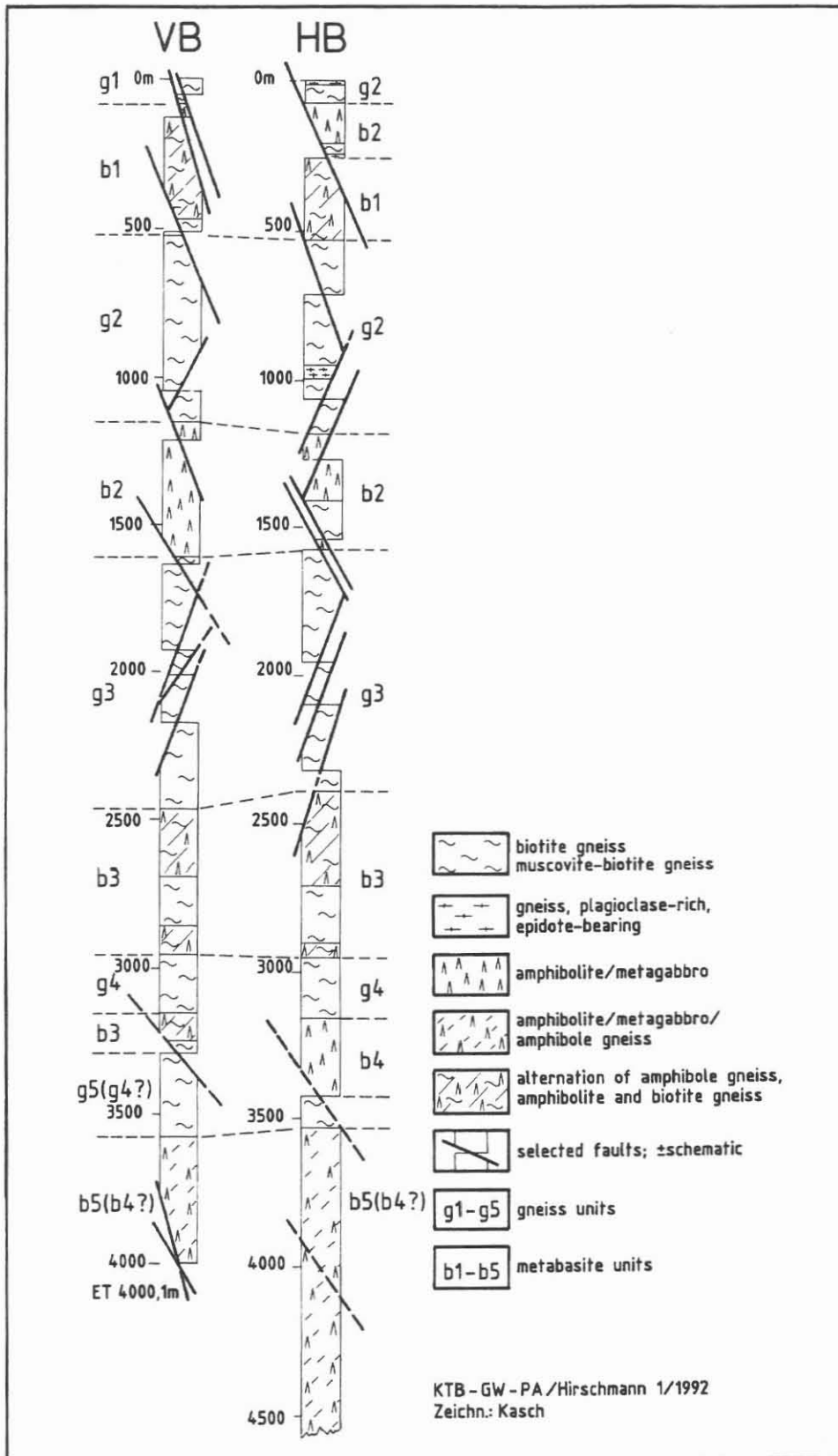


Fig. B.3.2: Correlation of main lithologic units and some major faults.

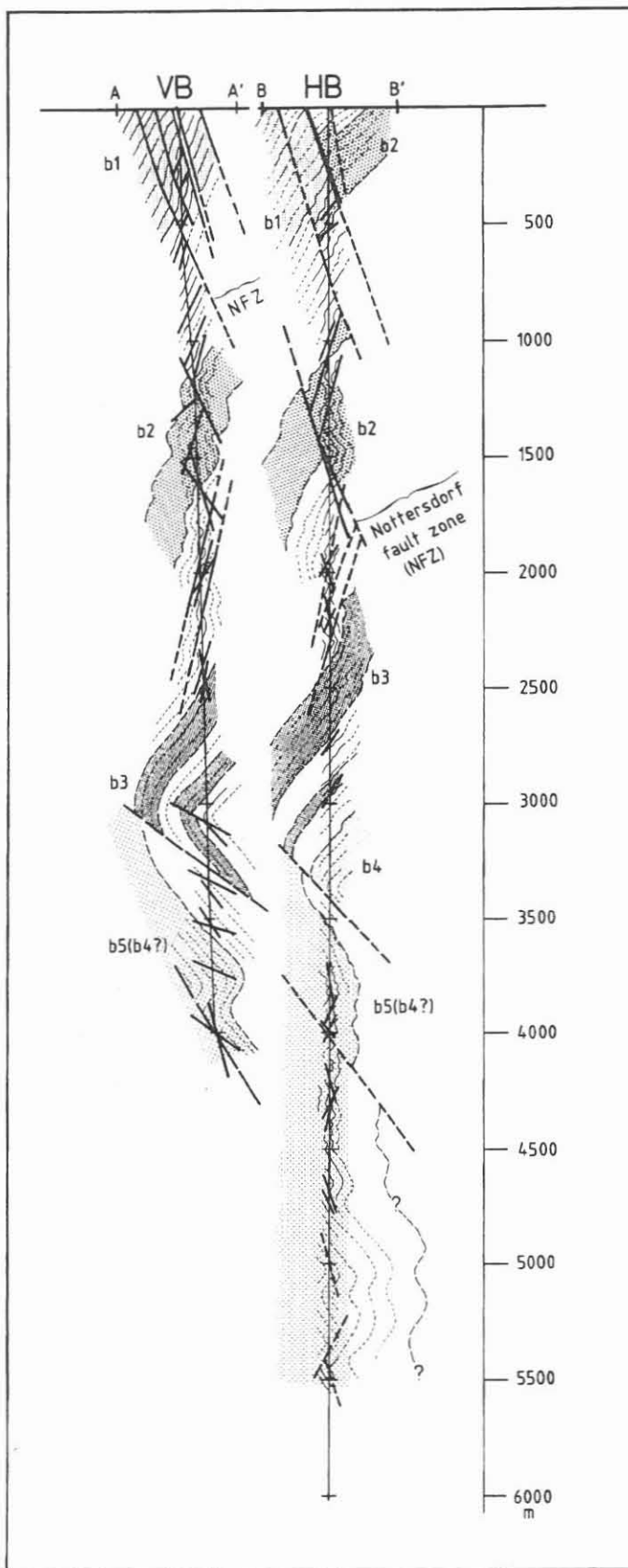


Fig. B.3.3: Preliminary structural interpretation. Numbering of lithologic units corresponds to Fig. B.3.2. Position of section lines A - A' and B - B' see Fig. B.3.1

A provisional numbering of the units (from top to bottom; gneisses g1,g2 .., metabasites b1,b2 ..) serves for easier identification and correlation. The following units can be distinguished:

**Gneiss unit g1:** (muscovite-)biotite gneisses overlying the metabasites b1 (VB: ?0 - 81m)

**Metabasite unit b1:** alternating sequence of hornblende gneisses, amphibolites, biotite gneisses and calcsilicate rocks, locally marble (VB: 81 - 460/527 m, HB: 290 - 522 m)

**Gneiss unit g2:** garnet-kyanite/sillimanite-biotite gneisses between b1 and b2 (VB: 460/527 - 1160 m, HB: 0 - 69 m, 203 - 247 m?, 522 - 1183 m), in the lower part intercalated by plagioclase-rich epidote-bearing gneiss g2\* (HB: 0 - 16 m, 243 - 247 m, 947 - 994 m)

**Metabasite unit b2:** amphibolites/garnetiferous amphibolites and metagabbros with rare meta-ultramafic rocks (VB: 1160 - 1610 m, HB: 69 - 203 m, 1183 - 1410/1573 m)

**Gneiss unit g3:** garnet-sillimanite/kyanite-biotite gneisses between b2 and b3, locally containing small intercalations of amphibolites (VB: 1610 - 2469 m, HB: 1573 - 2391 m)

**Metabasite unit b3:** three intervals of alternating amphibole gneisses, amphibolites and calcsilicate rocks, separated by intervals of garnet-sillimanite/kyanite-biotite gneisses with rare intercalations of amphibolite and amphibole gneiss (VB: 2469 - 2955m, 3155 - ?3290 m, HB: 2391 - 2951 m)

**Gneiss unit g4:** garnet-sillimanite-(muscovite-)biotite gneisses (VB: 2955 - 3155 m, fold hinge interval between the two occurrences of b3, HB: 2951 - 3160 m between b3 and b4)

**Metabasite unit b4:** amphibolites and metagabbros (HB: 3160 - 3426 m)

**Gneiss unit g5 (g4?):** (garnet-)sillimanite-(muscovite-) biotite gneisses overlying b5 (b4?) (VB: ?3290 - 3574 m, HB 426 - 3531 m)

**Metabasite unit b5 (b4?):** amphibolites/metagabbros, frequently alternating with hornblende gneisses, rare meta-ultramafic rocks, some intercalations of muscovite-biotite gneisses or garnet-sillimanite-biotite gneisses (VB: 3574 - 4000,1 m, HB: below 3531 m)

The interpretation of the geological section is dependent on structural assumptions. Fig. B.3.3 presents a preliminary structural interpretation. In general, the upper parts of the pilot hole and of the main borehole are characterized by a steep to moderate dip of the foliation to the SW (see chapter B.1. 7). Exceptions are the metabasite b2 interval with a fold-related variability of the azimuth and the dip of foliation and the interval from 1900 to 2500 m with repeated bending of foliation from SW to NE which is, probably, due to fault tectonics. In the pilot hole at a depth of 3050 m (gneiss unit g4) and in the main borehole at a depth of approximately 3350 m (metabasite unit b4) the foliation is generally bending from SW to NE or E and thus represents, presumably, a major fold hinge. According to preliminary and incomplete structural data, below this fold hinge down to the final depth of the VB and the

present depth of the HB the structure is determined by intensive folding with a predominant dip of foliation to the east.

The structural picture is characterized by a great number of faults of different type, direction, dip and age. At least, some of the most important fault zones of the two boreholes can be correlated.

The Nottersdorf fault zone represents a bundle of NNW-SSE striking and steeply ENE dipping faults which were met in the uppermost section of the pilot hole (0 - 515 m) and between 247 and approximately 1570 m in the main borehole. The uppermost parts of the main borehole (above the fault between 247 and 253 m) belong to the tectonic block east of the Nottersdorf fault zone. The following fault-bounded units (VB: 0 - 515 m, HB: 253 - ?~1570 m) belong to the Nottersdorf fault zone, whereas the underlying portions of both boreholes are parts of the tectonic block west of the Nottersdorf zone. The offset of lithological units is considerable (upthrust of b2 in the order of 500 to 1000 m).

An important steeply SW dipping fault zone crosses both boreholes between 1900 and 2300 m. The offset of lithological units is unknown.

A correlation of a moderately E-dipping ( $30 - 60^\circ$ ) fault zone at approximately 3300 m in the pilot hole and at 3426 m in the main borehole seems likely. This fault zone might be responsible for a considerable reduction of the lithostratigraphic sequence in the lower limb of the large fold structure with the result that the lithologic units above and below this fault zone cannot be correlated. This assumption is supported by the different composition and lithologic character of the metabasic complex b5 in comparison with the complexes b1, b2 and b3 whereas a partial correlation with b4 (fold hinge in the HB) cannot be excluded. Furthermore, correlations are possible between individual NE dipping faults at a depth of approximately 4000 m in the main borehole and the prominent fault zone at the bottom of the pilot hole with its strong inflow of saline formation fluids. For this fault zone the offset of lithologic units is unknown.

## References

- EMMERMANN, R. , DIETRICH, H.-G., LAUTERJUNG, J. & WÖHRL, TH. (eds), (1990): KTB Pilot Hole, Results of Geoscientific Investigation in the KTB Field Laboratory, 0 - 4000,1 m. - KTB Report 90-8, Hannover.
- LICH, S., DUYSER, J., GODIZART, G., KEYSNER, S. & DE WALL, H. (1992): German Continental Deep Drilling Program (KTB)- Geological Survey of the Hauptbohrung 0 - 5900 m. - KTB Report 92-2, Hannover.
- ROHRMÜLLER, J. (1988): Die Geologie im Umfeld der KTB-Bohrlokation Windischeschenbach, Oberpfalz - Geologisch-Petrographisch-Tektonische Untersuchungen im Gebiet zwischen Windischeschenbach, Burggrub und Bach. - Diplomarbeit, Ludwig-Maximilians-Universität München (unpublished).
- STETTNER, G. mit Beiträgen von BURGER, R., ROHRMÜLLER, J. & TROLL, G. (1990): Geologische Karte des KTB-Umfeldes Oberpfalz 1 : 10000. Blatt 6 Krummennaab. - Hannover 1990.

KTB Report	92-2	B53-B83	30Fig.	Hannover 1992
------------	------	---------	--------	---------------



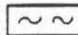










## B.4 CUTTING PROFILE

Working Groups Geology, Geochemistry and Geophysics

KTB-Feldlabor, Postfach 67, W 8684 Windischeschenbach, FRG

The Cutting Profile shows the preliminary lithological profile, the gamma ray profile and selected results from XRD/XRF analysis. Complete geochemical data are listed in chapter C.3. All data are based on measurements of cuttings. Cuttings are sampled at meter intervals. As first step every cutting-sample is analyzed under the binocular. Cutting samples consist of rock fragments mostly from different lithologies. Their relative portions, the degree of alteration and cataclasis is estimated. Also mineralizations, open fissures and drilling artifacts can be detected (see B.1.6, B.2). Thin sections and polished sections of cuttings are prepared and analyzed at four meter intervals, in zones of special interest more frequently. The recorded informations are stored in the central KTB database. Gamma ray measurements and XRD/XRF measurements on cuttings are described in chapters D3 and chapter C.3. Cutting samples may be contaminated with material broken out from the drill-hole wall above (cavings). Since the exact depth of the drilling-bit is not known, the lithological boundaries may vary within 6-8 m. The cutting-profile combines the information available from this data-set and is kept topical daily. This preliminary lithological profile is later corrected to the final geological profile (fig. B.1. 3) mainly through additional information obtained from well logging data.

### Legend

	Amphibolite		calc-silicate bearing plagioclase rich Gneiss
	Paragneiss		Calc-Silicate Rock
	Hornblende Gneiss		Lamprophyre
	meta-ultramafic Rocks		Alteration
	cataclastic Amphibolite		Cataclasite
	cataclastic Gneiss		aplitic Dyke
			Quartz Vein

Alteration:                    1 fresh                    2 weak                    3 strong                    4 complete.

Mineral abbreviations:    **Cal** calcite, **Ccc** graphite, **Epd** edidote, **FeS** pyrrhotine,  
**Fsp** feldspar, **Hbl** hornblende, **Lau** laumontite, **Plg** plagioclase  
**Prh** prehnite, **Pyr** pyrite, **Qrz** quartz, **Sul** sulfide.

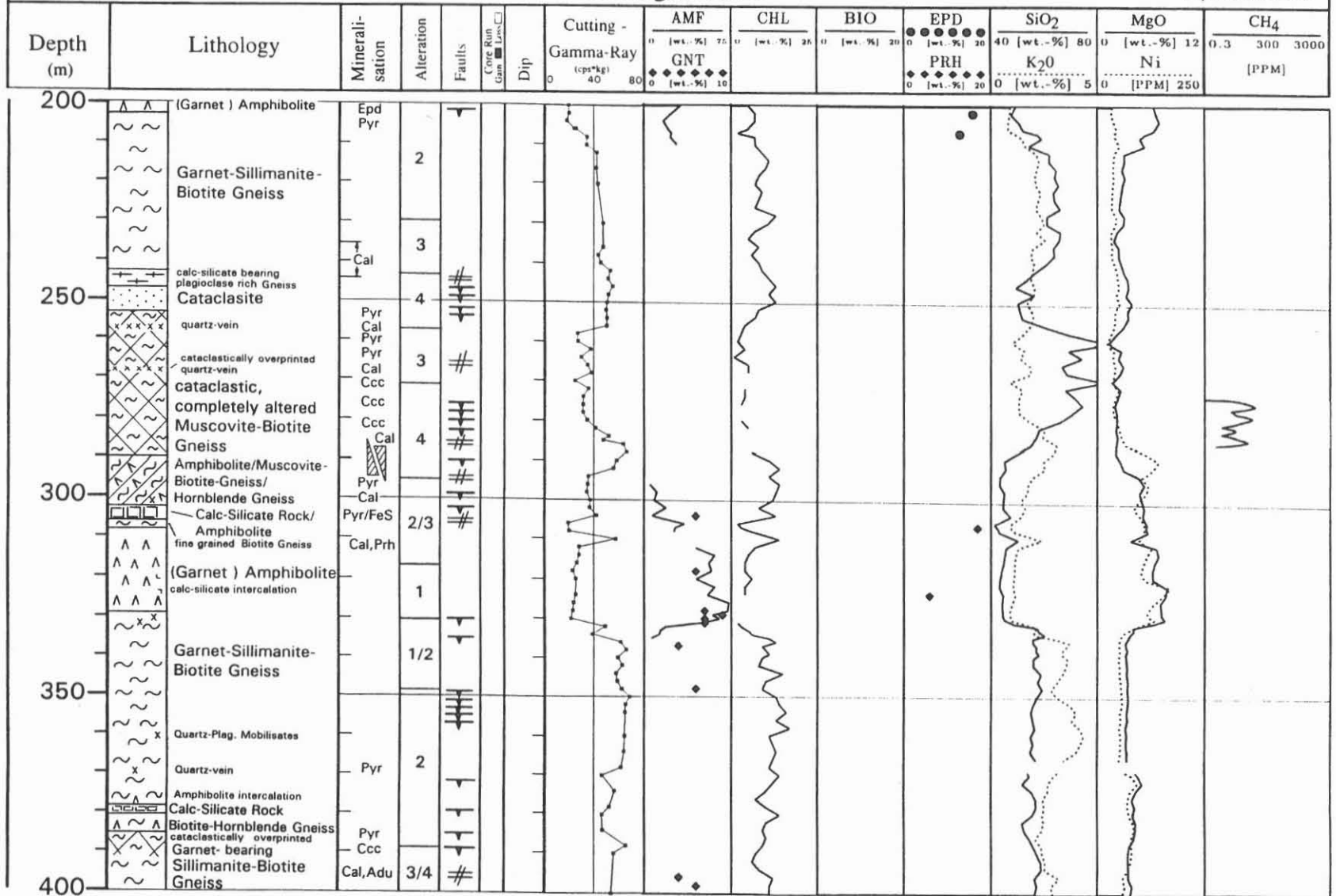


# KTB Hauptbohrung Oberpfalz

## Cuttings Profile

State: February 1992

Explanations in Text

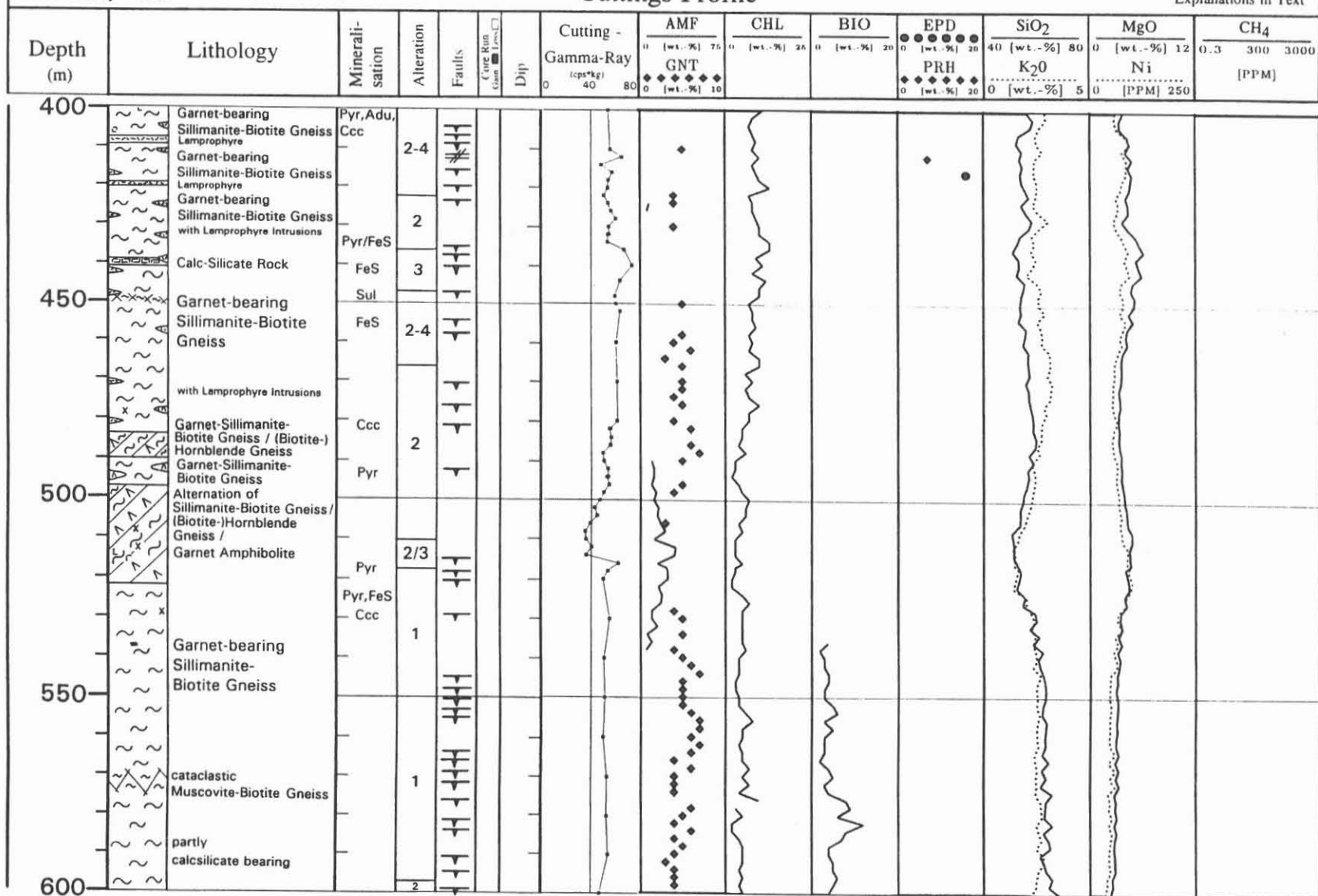


# KTB Hauptbohrung Oberpfalz

## Cuttings Profile

State: February 1992

Explanations in Text



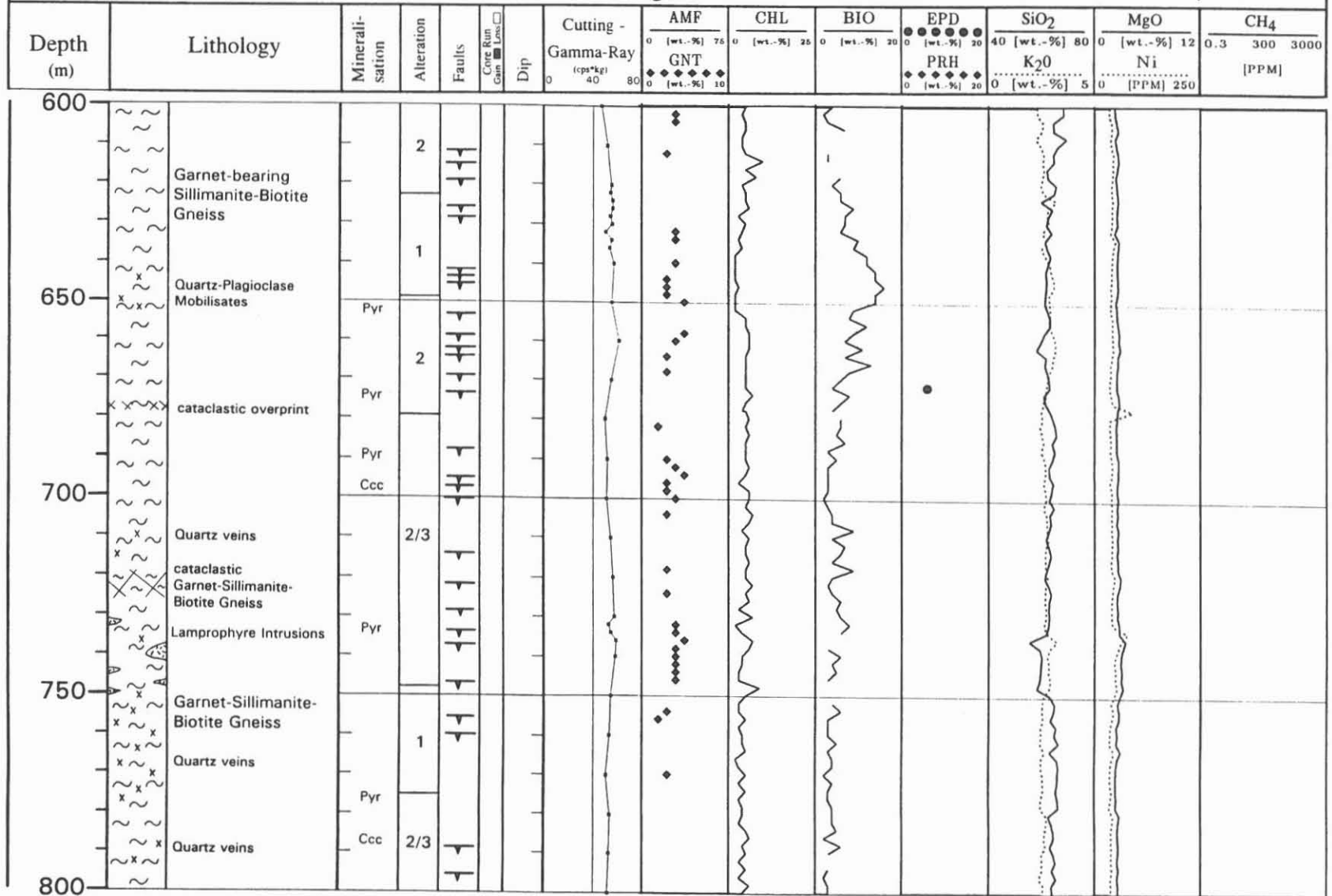


# KTB Hauptbohrung Oberpfalz

## Cuttings Profile

State: February 1992

Explanations in Text

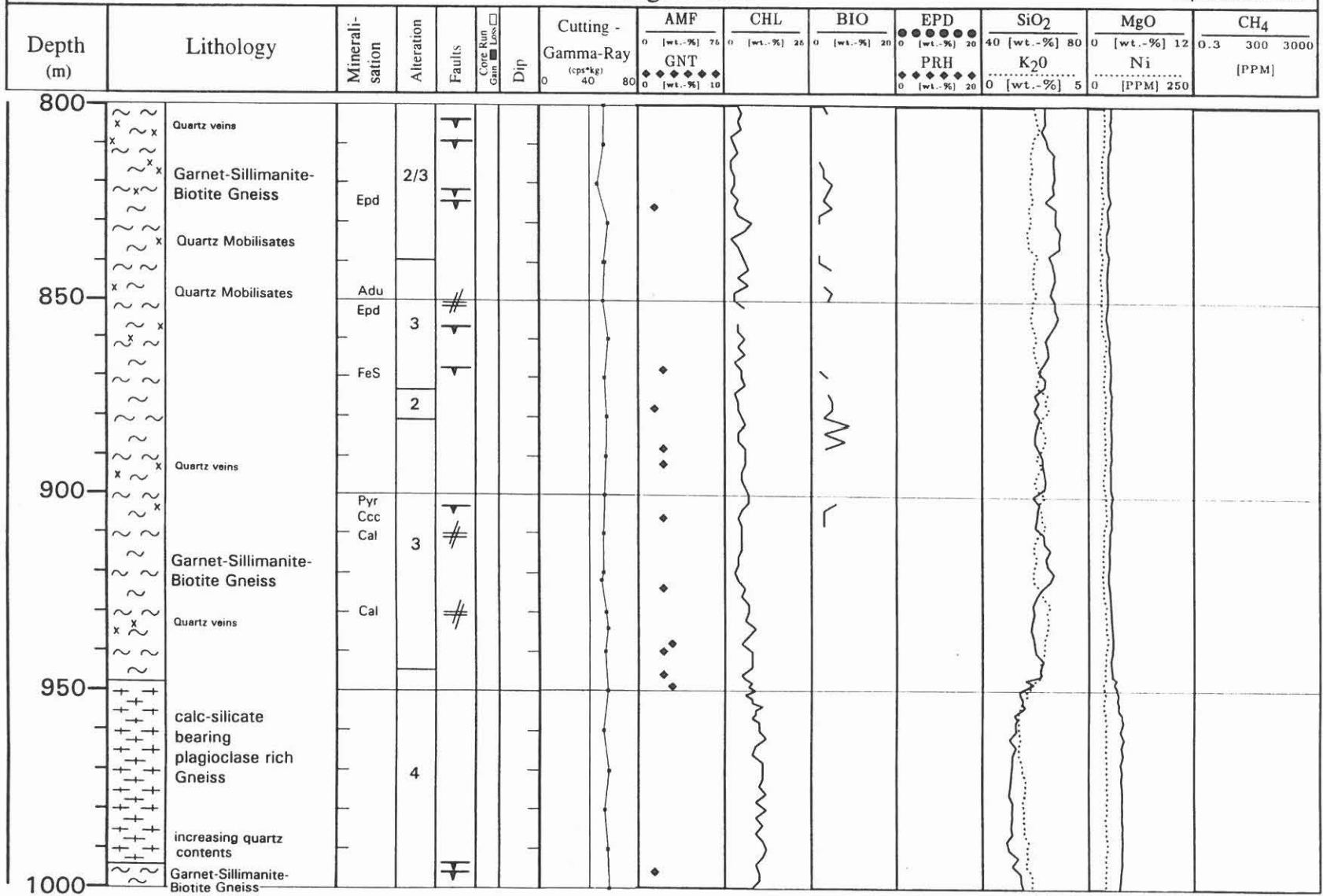


# KTB Hauptbohrung Oberpfalz

## Cuttings Profile

State: February 1992

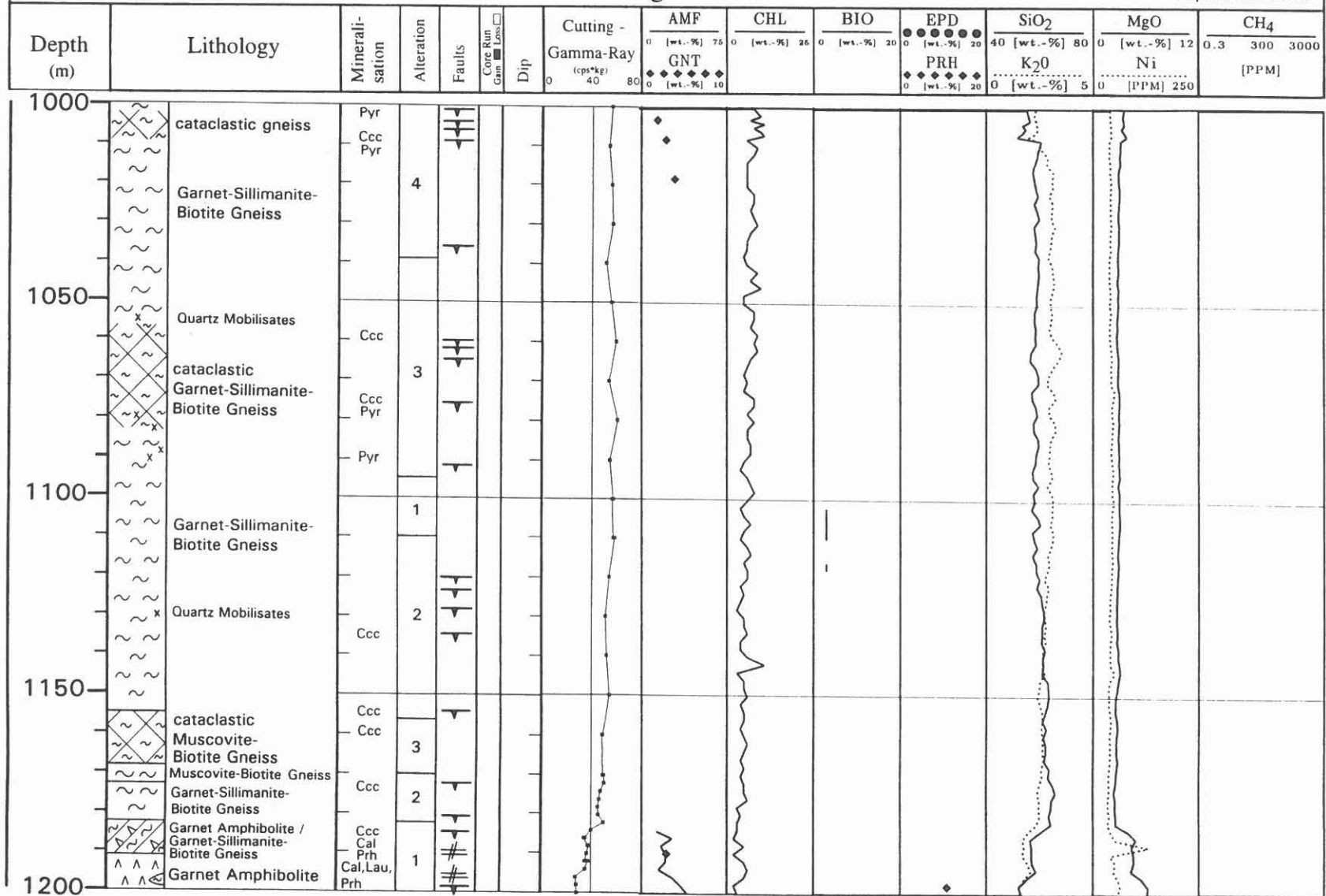
Explanations in Text



# KTB Hauptbohrung Oberpfalz Cuttings Profile

State: February 1992

Explanations in Text

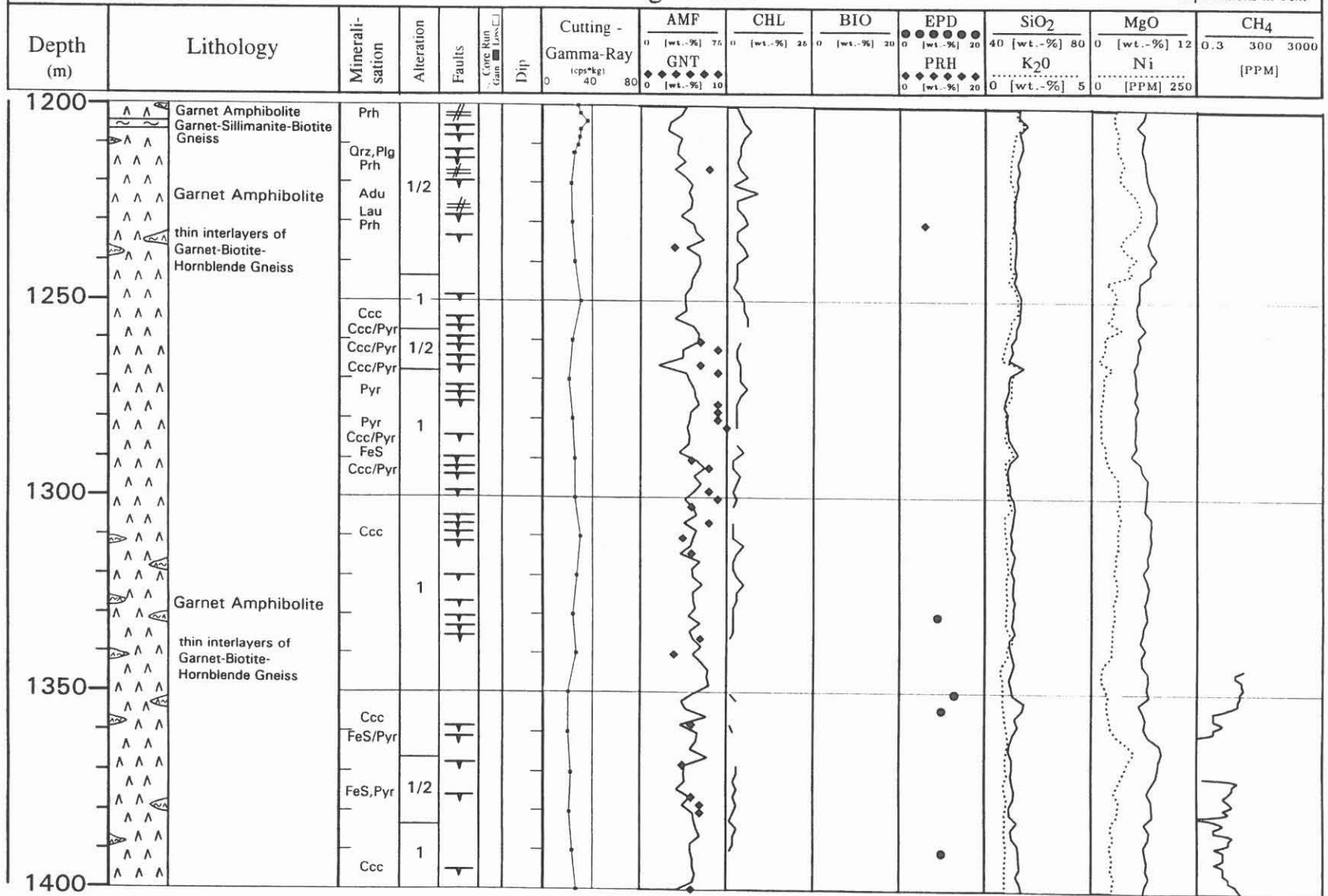


# KTB Hauptbohrung Oberpfalz

## Cuttings Profile

State: February 1992

Explanations in Text



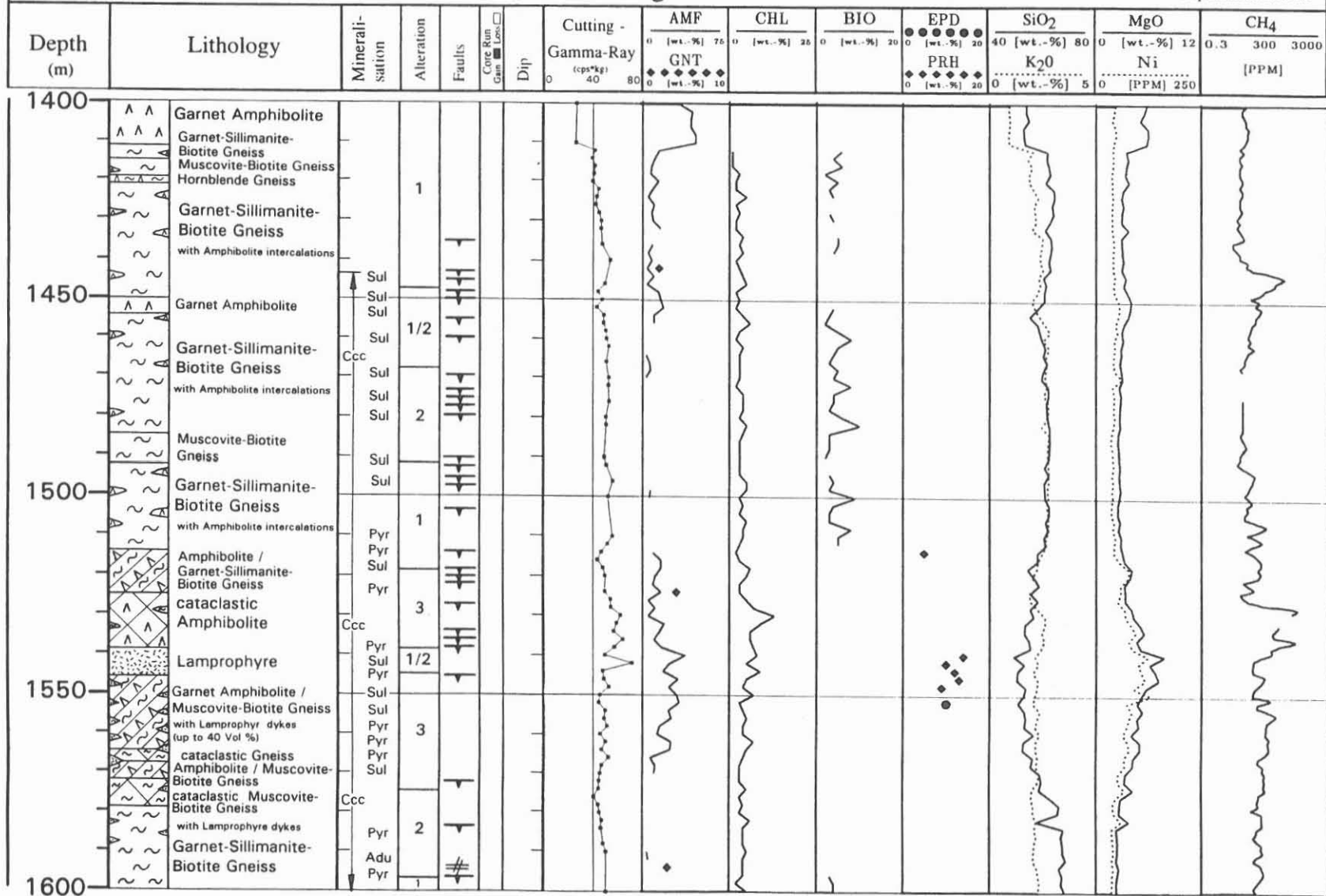
-B 60-

# KTB Hauptbohrung Oberpfalz

## Cuttings Profile

State: February 1992

Explanations in Text



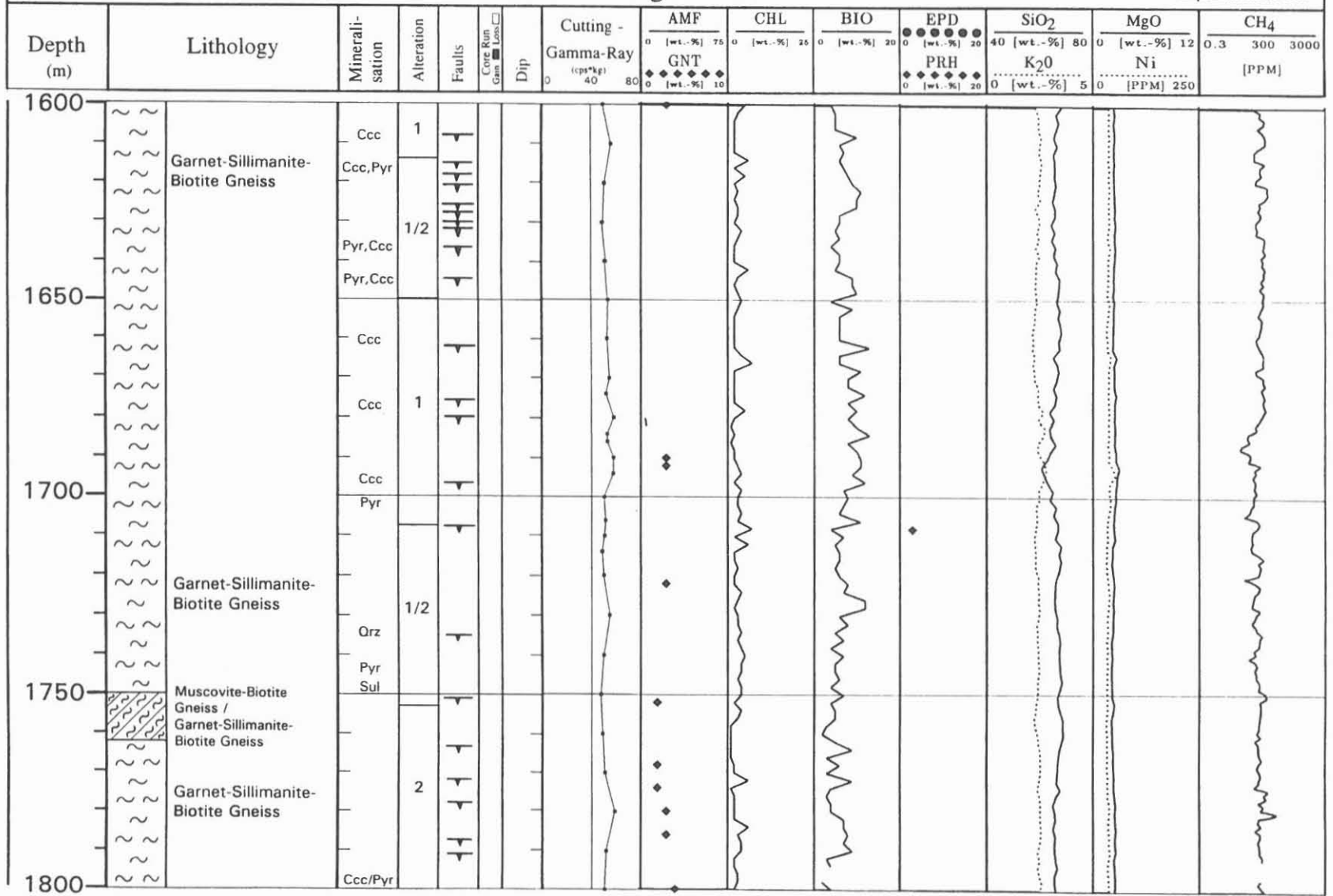
-B 61-

# KTB Hauptbohrung Oberpfalz

## Cuttings Profile

State: February 1992

Explanations in Text

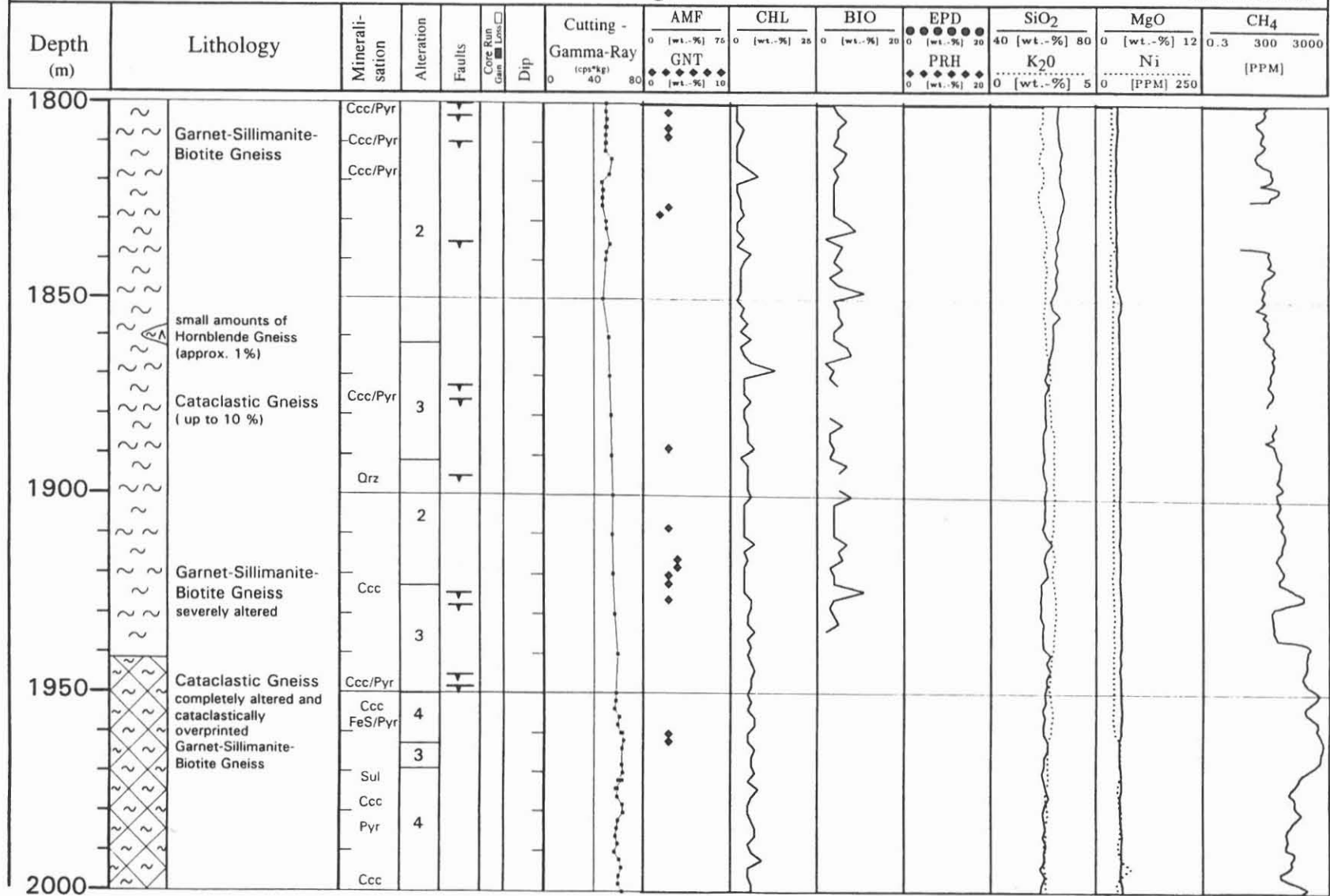


-B 62-

# KTB Hauptbohrung Oberpfalz Cuttings Profile

State: February 1992

Explanations in Text

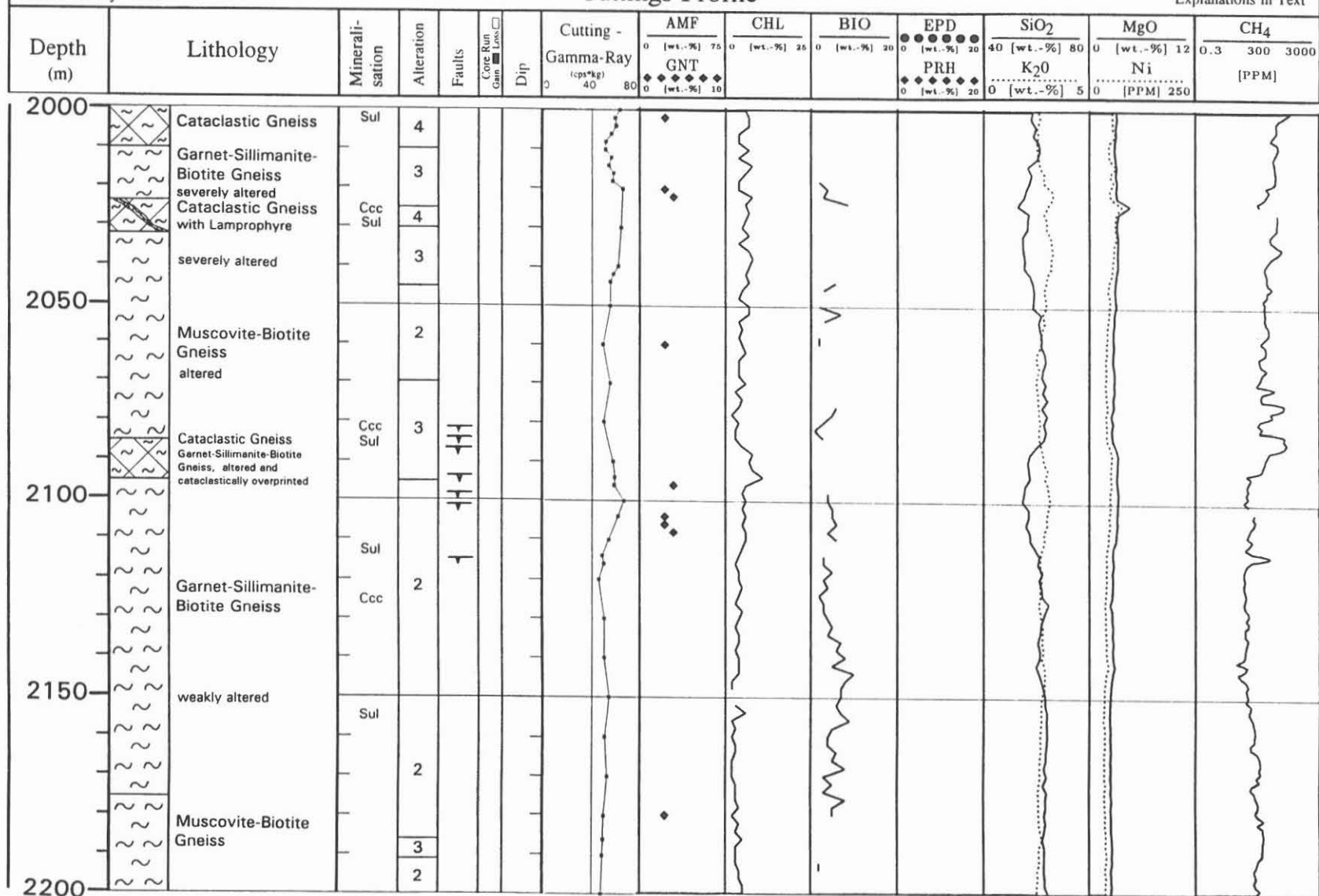


# KTB Hauptbohrung Oberpfalz

## Cuttings Profile

State: February 1992

Explanations in Text

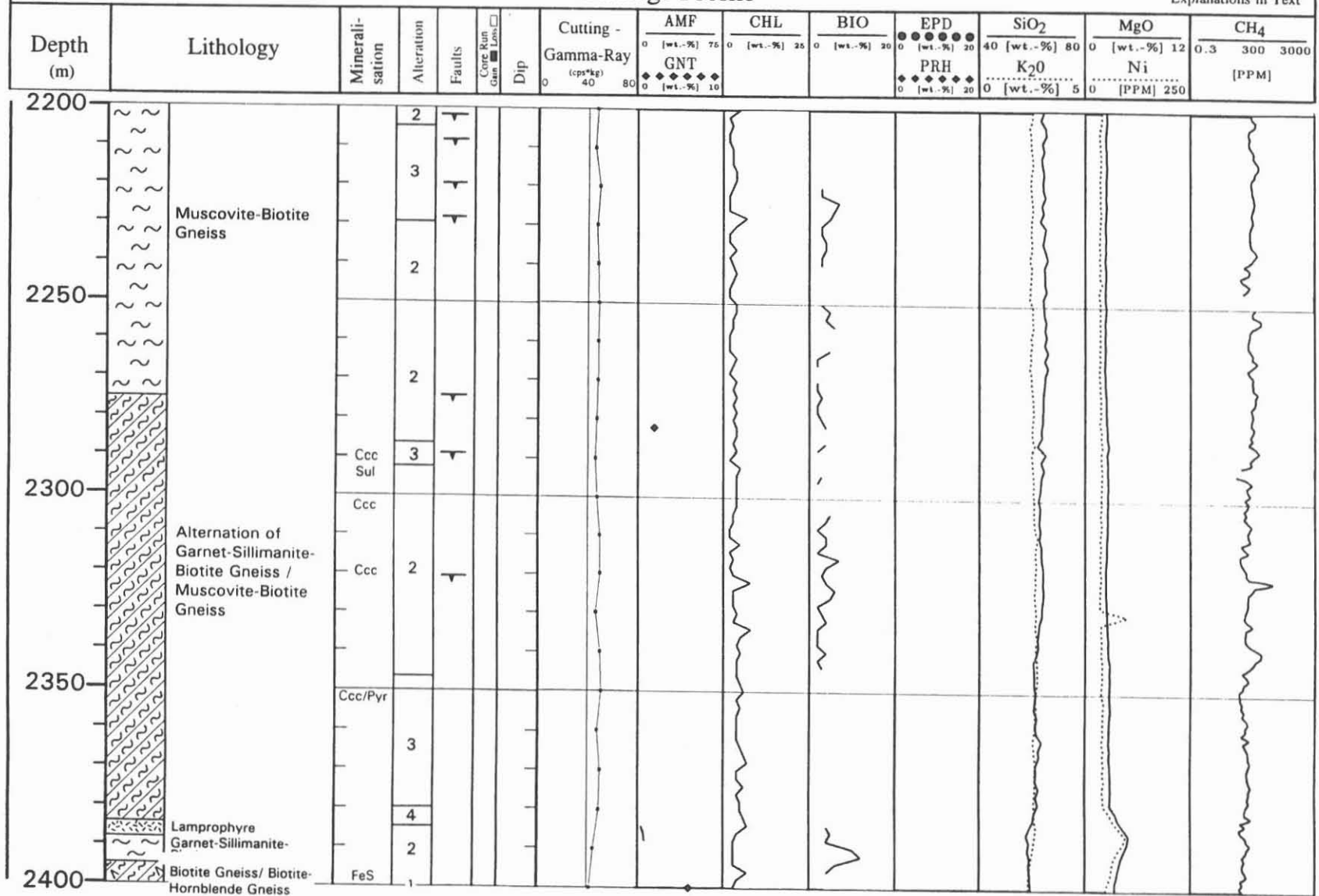




# KTB Hauptbohrung Oberpfalz Cuttings Profile

State: February 1992

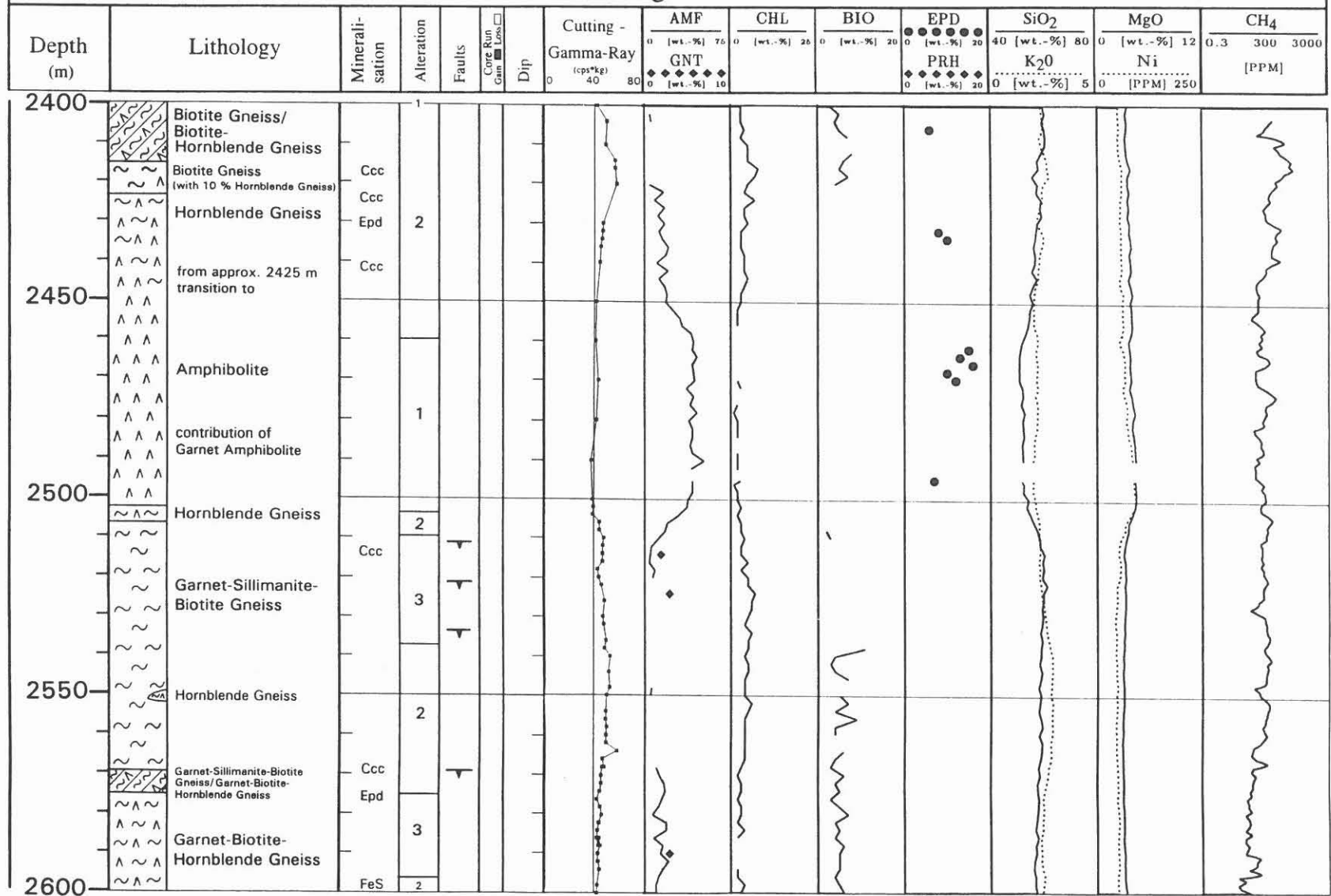
Explanations in Text



# KTB Hauptbohrung Oberpfalz Cuttings Profile

State: February 1992

Explanations in Text

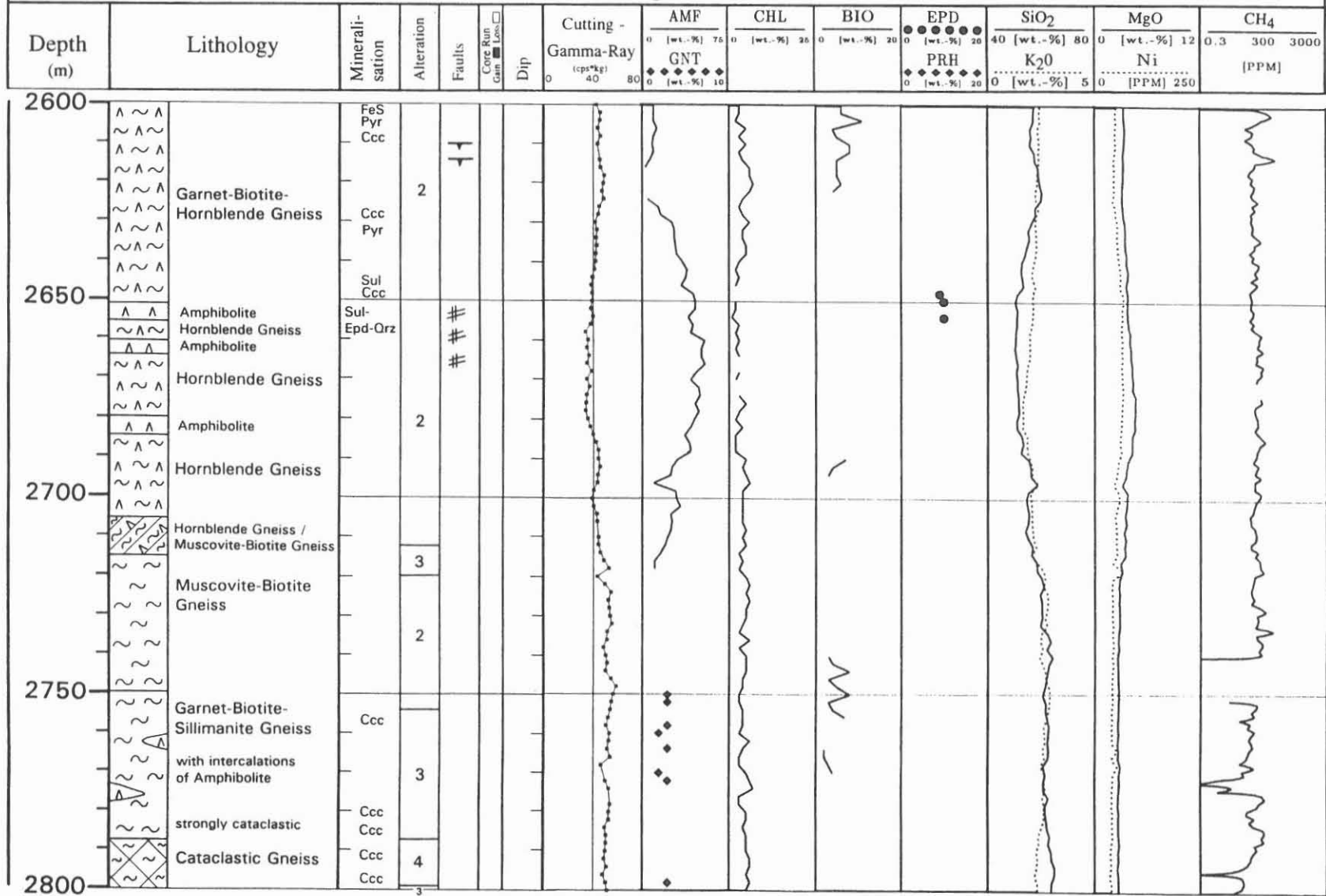


# KTB Hauptbohrung Oberpfalz

## Cuttings Profile

State: February 1992

Explanations in Text



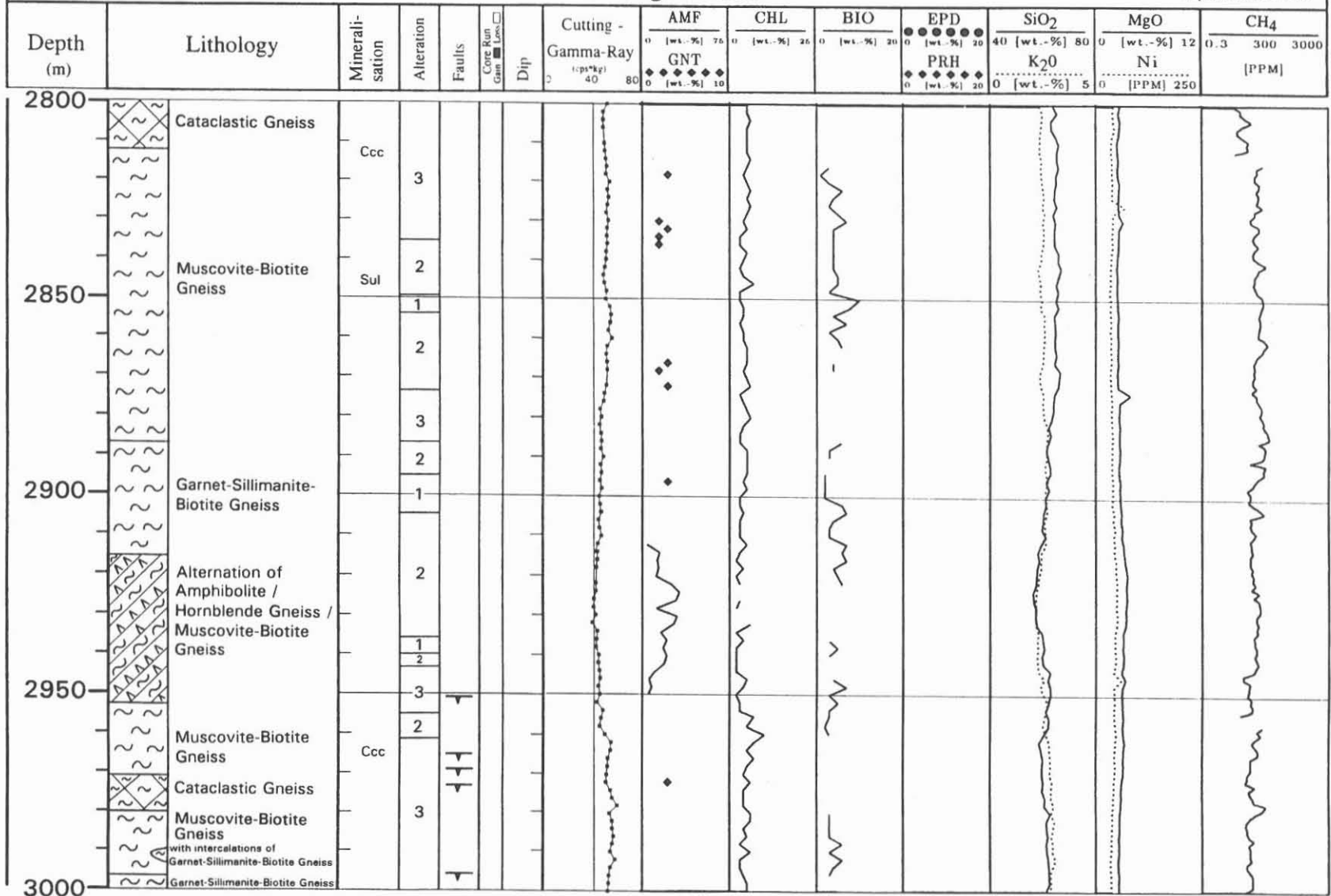
-B 67-

# KTB Hauptbohrung Oberpfalz

## Cuttings Profile

State: February 1992

Explanations in Text

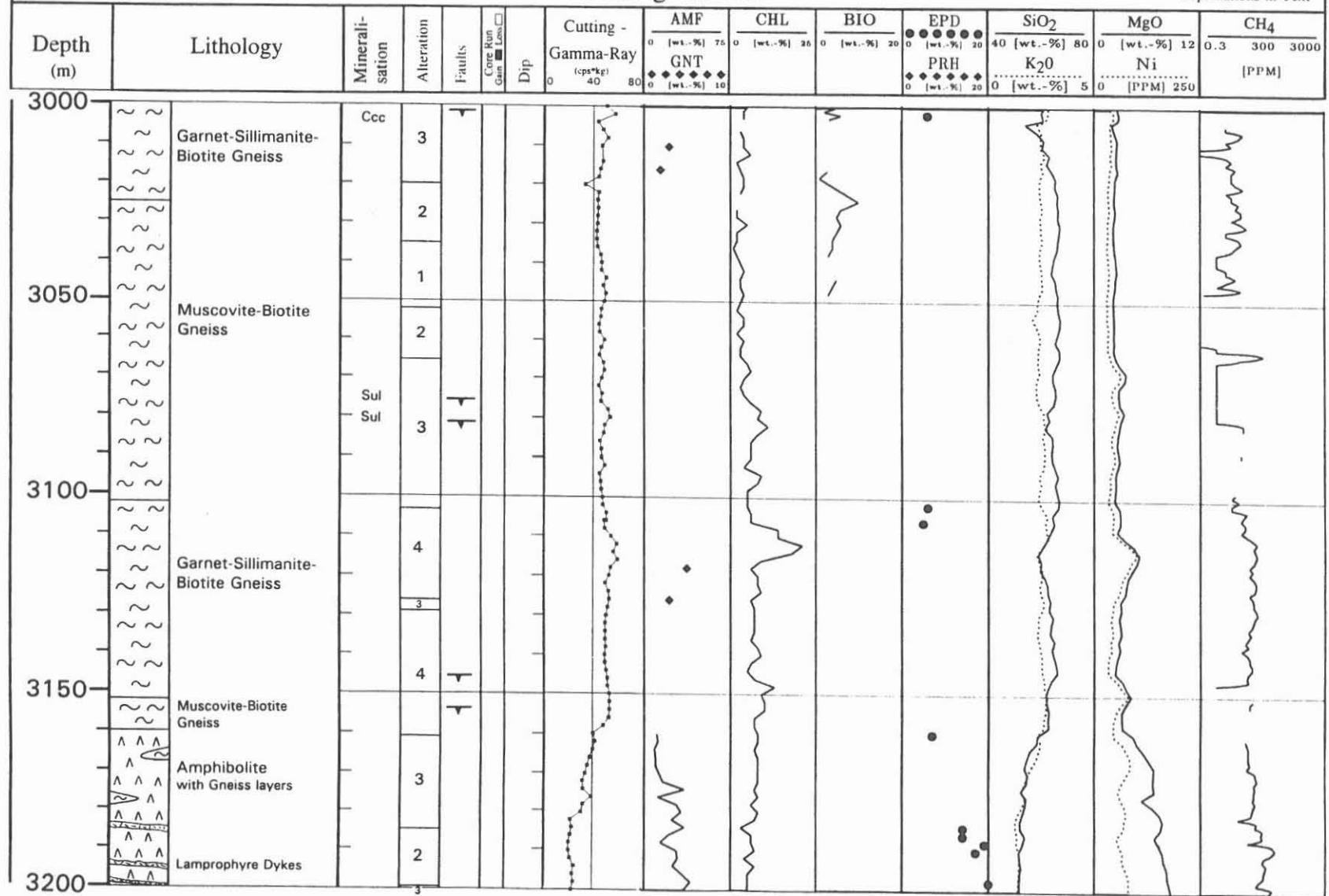


# KTB Hauptbohrung Oberpfalz

## Cuttings Profile

State: February 1992

Explanations in Text

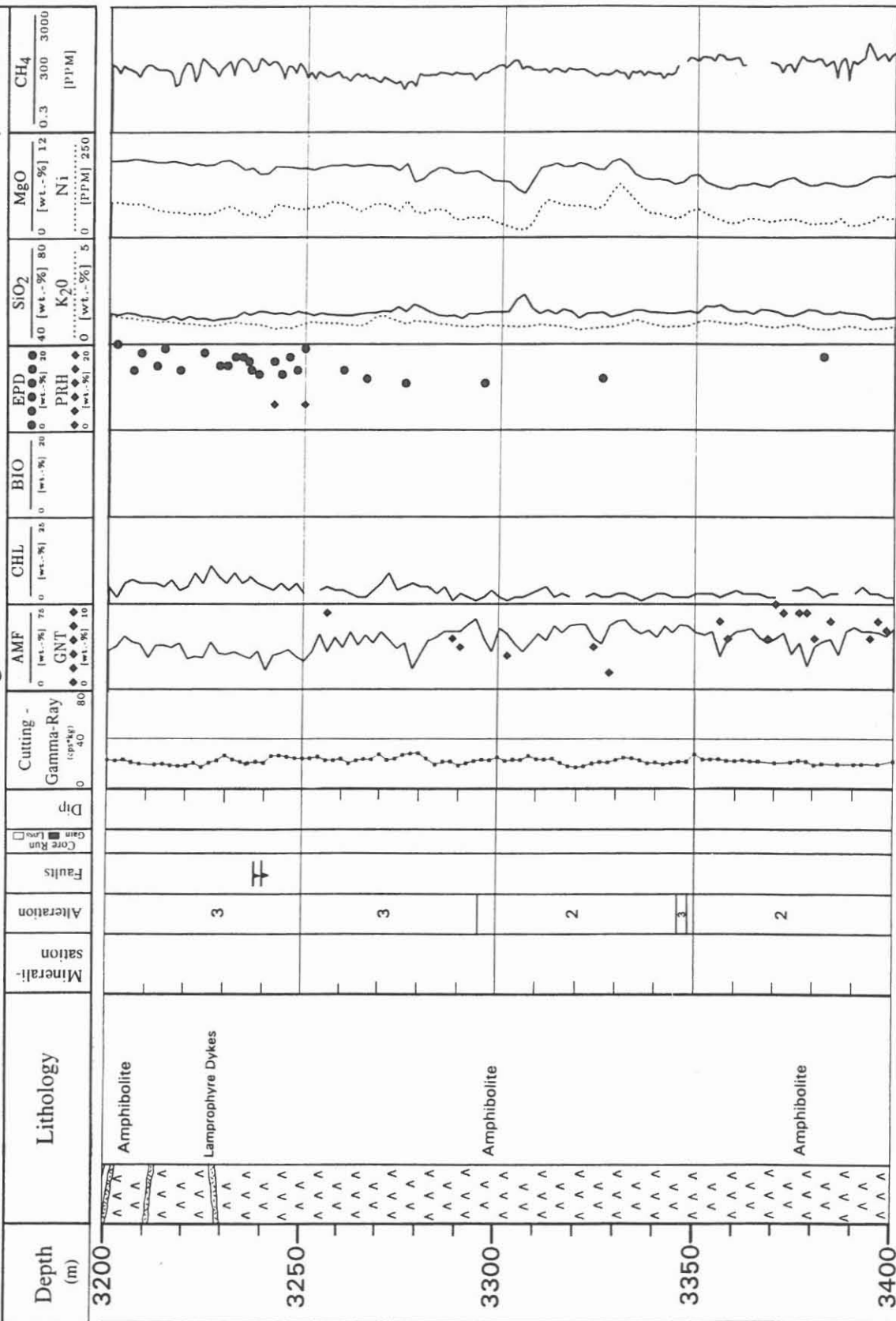


# KTB Hauptbohrung Oberpfalz

## Cuttings Profile

State: February 1992

Explanations in Text

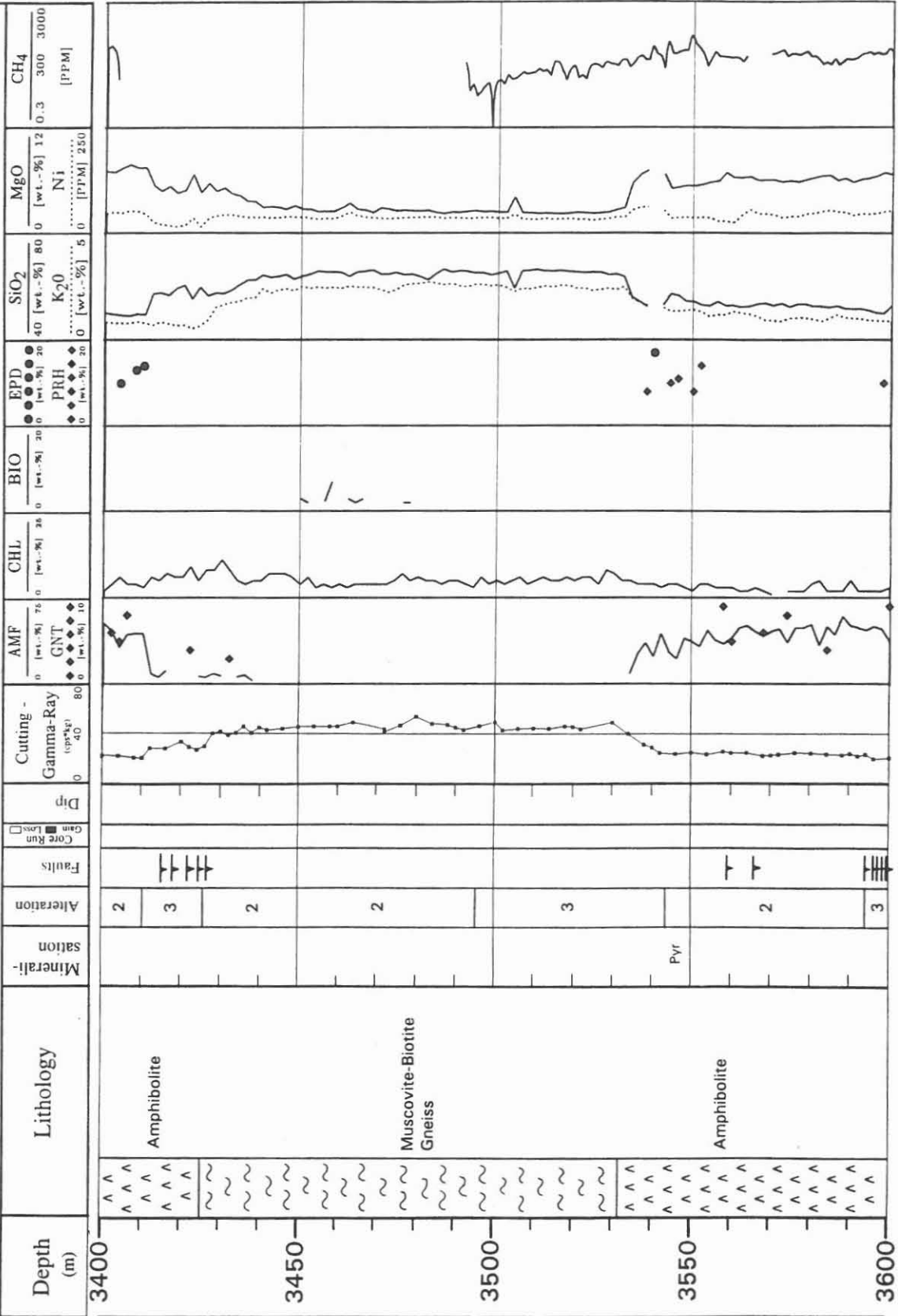


# KTB Hauptbohrung Oberpfalz

## Cuttings Profile

State: February 1992

Explanations in Text

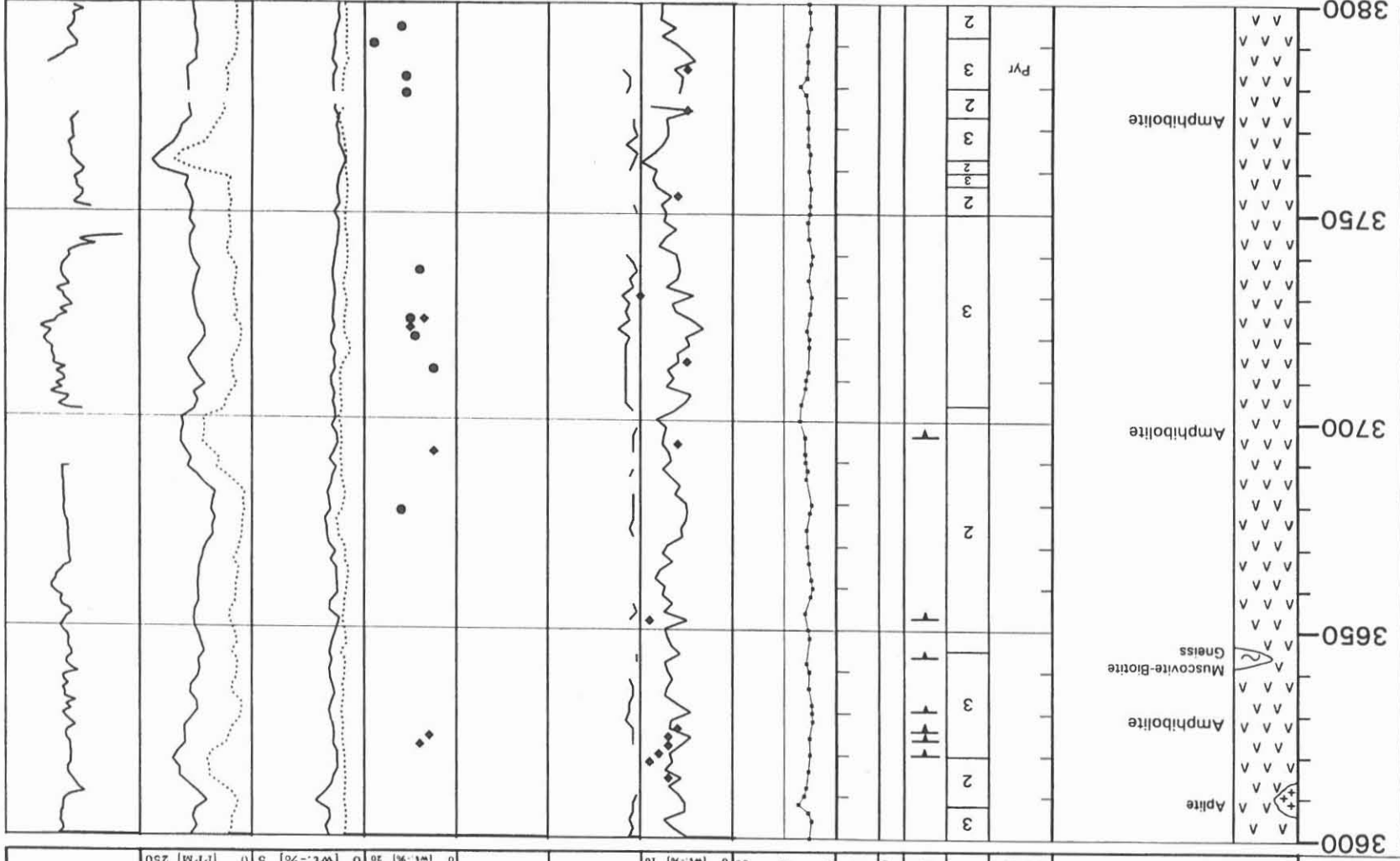


# KTB Hauptbohrung Oberfalz

State: February 1992

Explanations in Text

Depth (m)	Lithology	Mineralisation	Alteration	Faults	Core Run Gan <input type="checkbox"/> Ures <input type="checkbox"/>	Dip	Cutting - Gamma-Ray (cp% <sup>100</sup> )	Cutting - AMF GNT GNT	CHL	BIO	EPP PRH PRH	SiO <sub>2</sub> K <sub>2</sub> O	MgO Ni	CH <sub>4</sub> [ppm]
							0 [wt.-%] 20 40 [wt.-%] 80	0 [wt.-%] 20 40 [wt.-%] 80	0 [wt.-%] 20 40 [wt.-%] 80	0 [wt.-%] 20 40 [wt.-%] 80	0 [wt.-%] 20 40 [wt.-%] 80	0 [wt.-%] 5 12 [ppm] 250	0.3 300 3000	

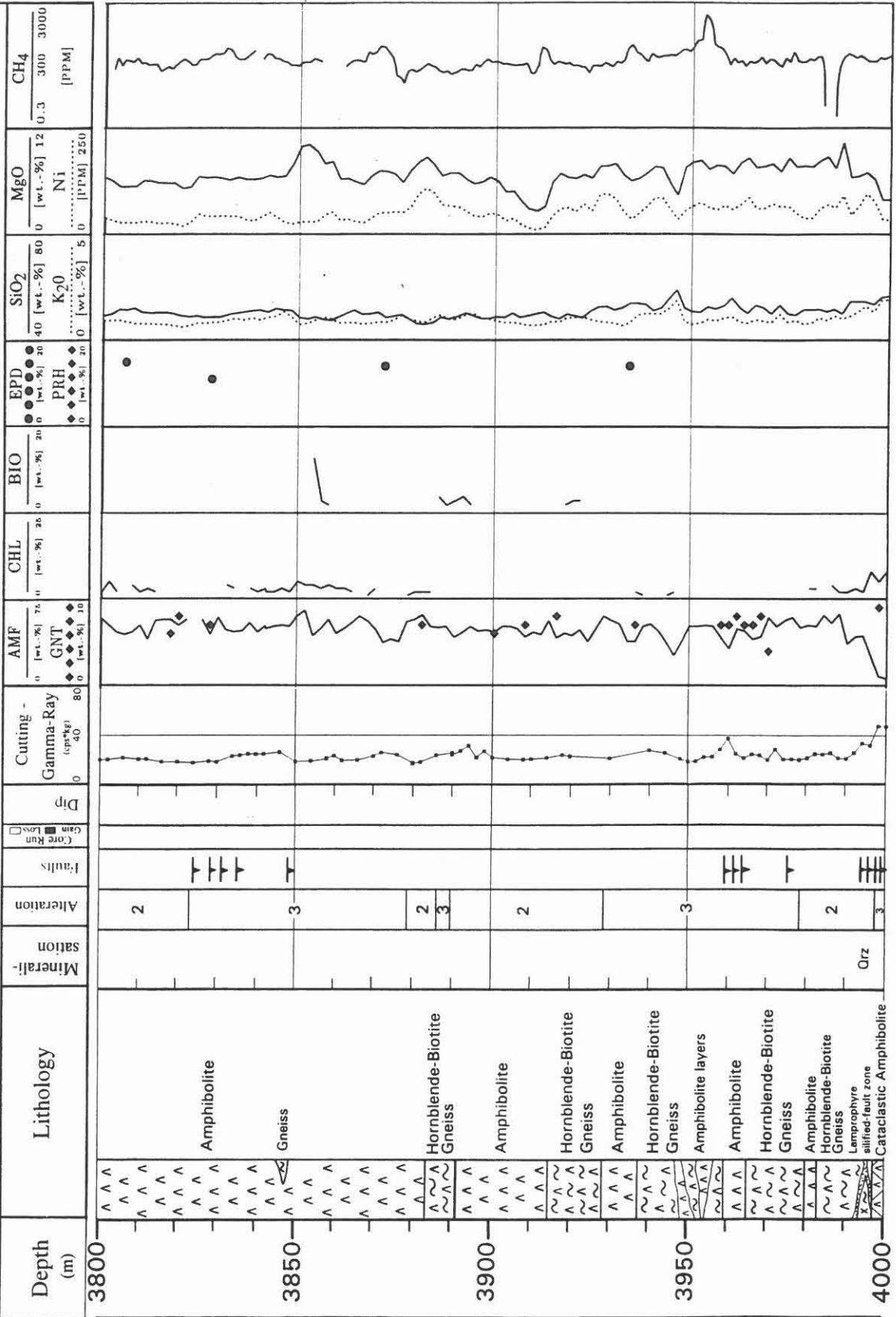




# KTB Hauptbohrung Oberpfalz Cuttings Profile

State: February 1992

Explanations in Text

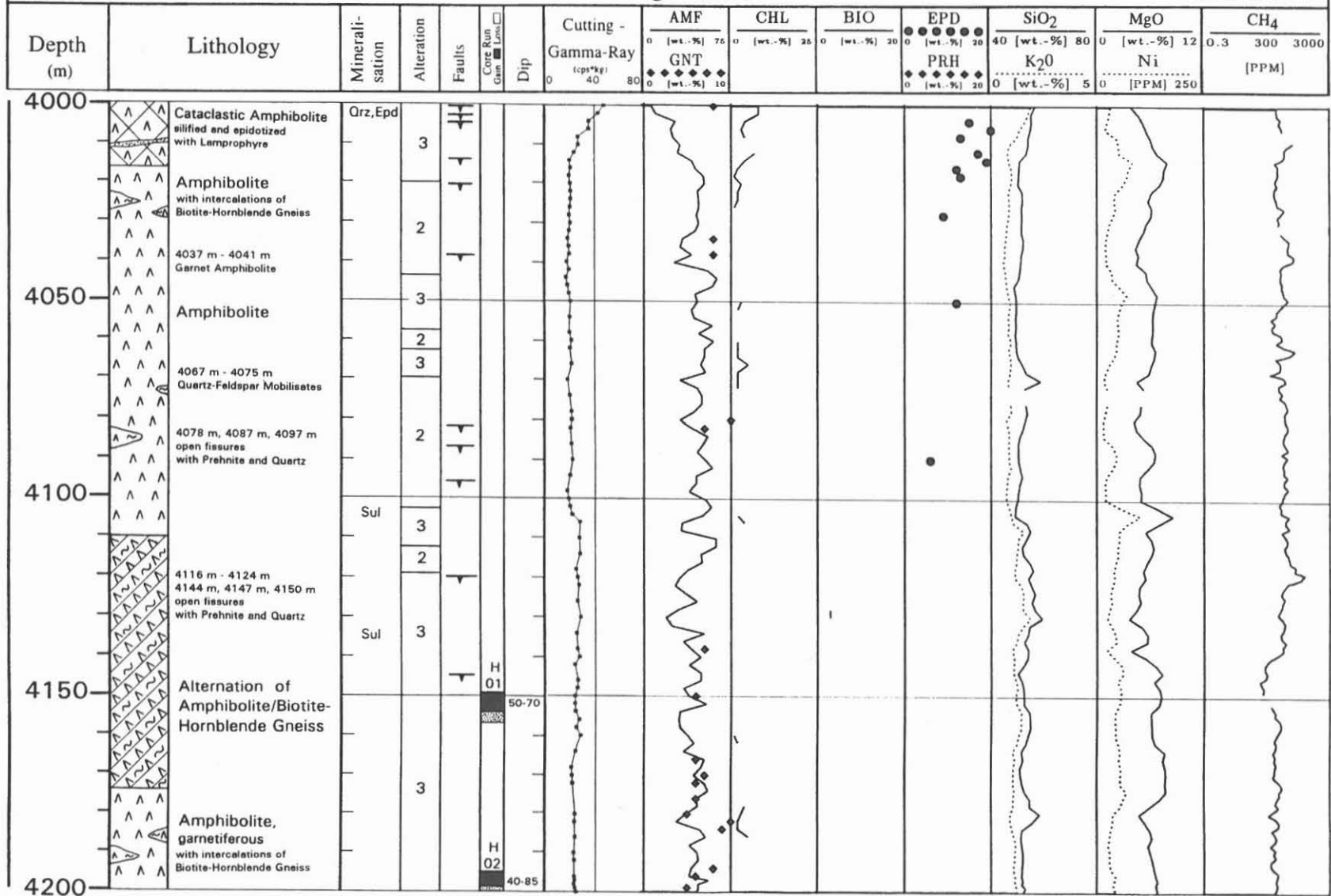


# KTB Hauptbohrung Oberpfalz

## Cuttings Profile

State: February 1992

Explanations in Text

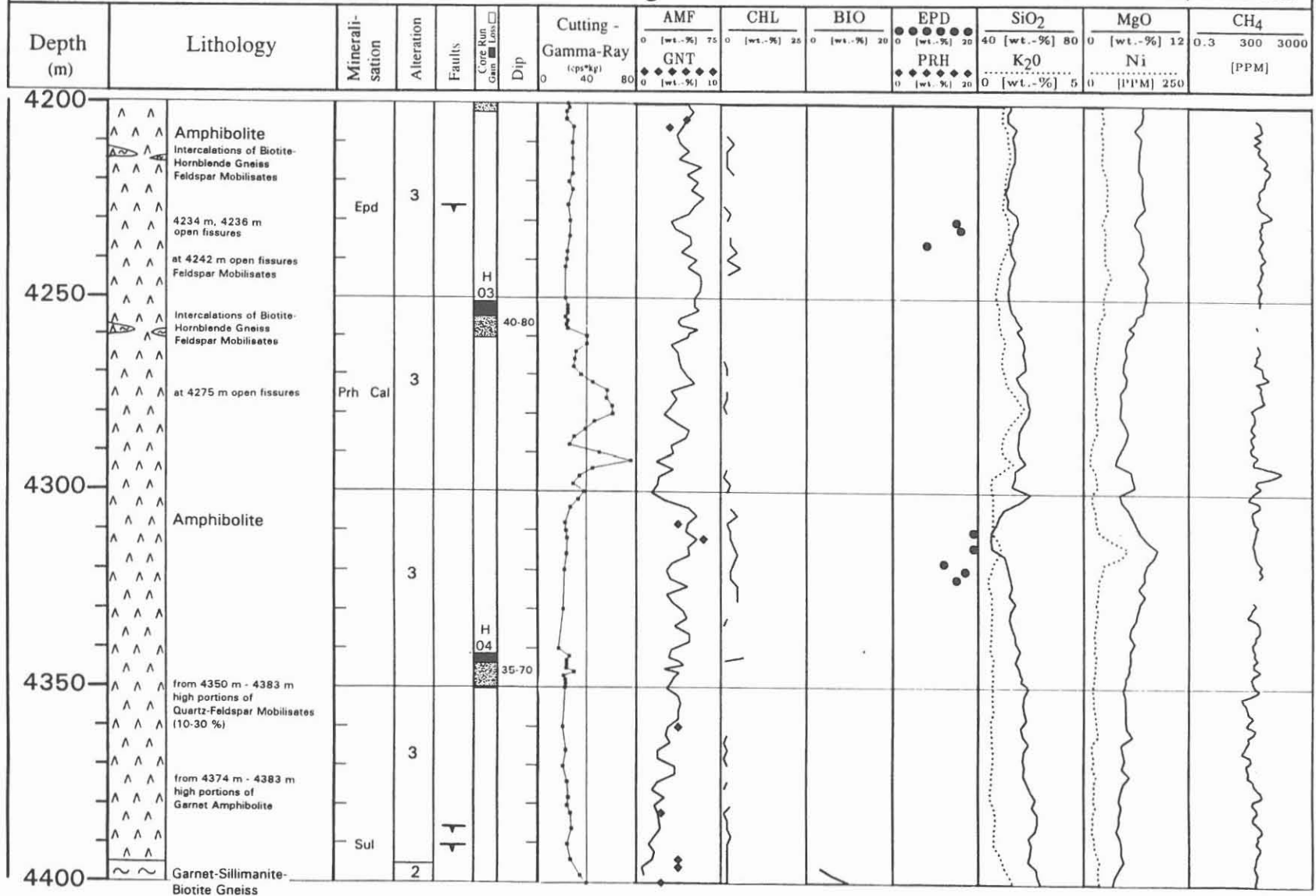


# KTB Hauptbohrung Oberpfalz

## Cuttings Profile

State: February 1992

Explanations in Text



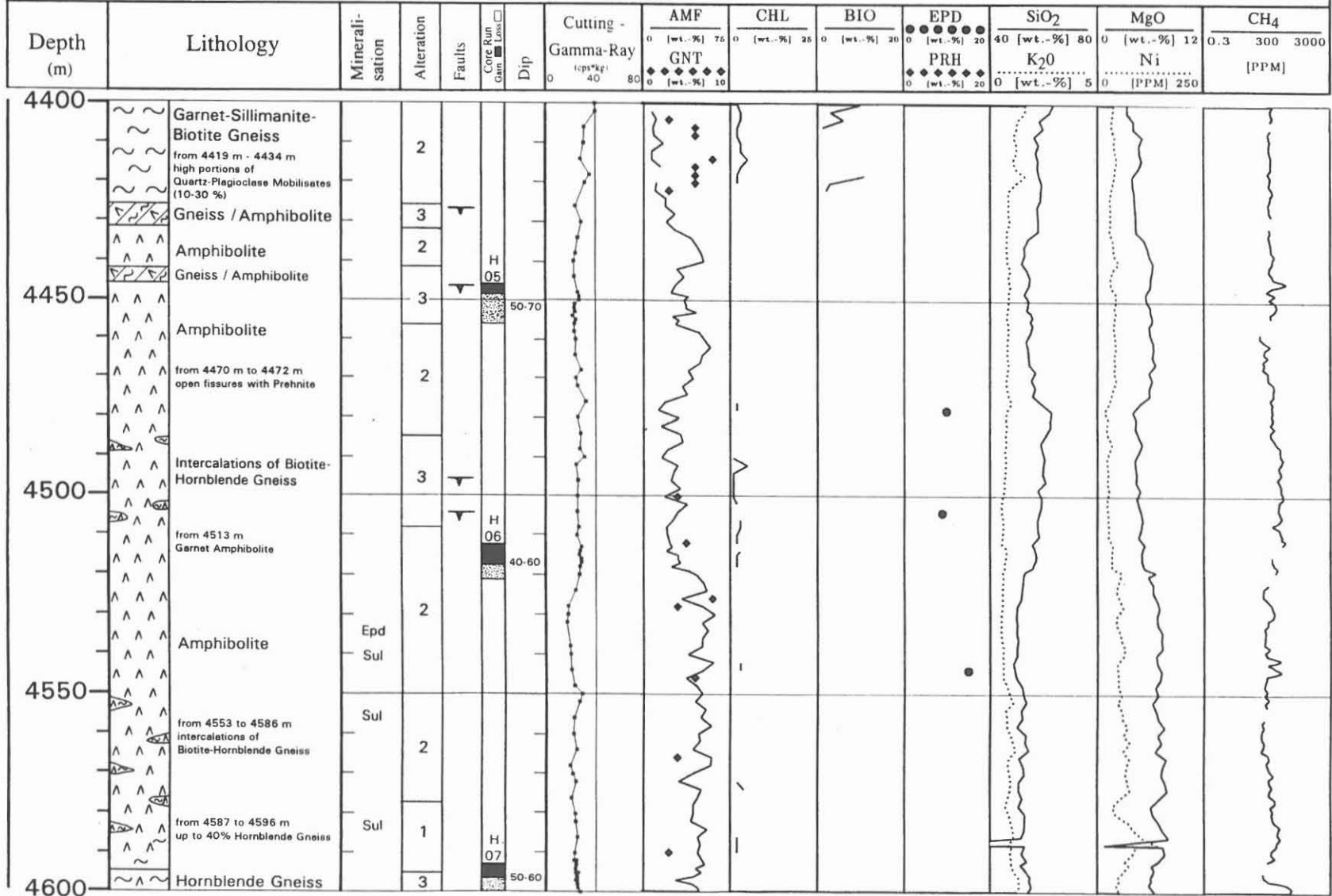
-B 75-

# KTB Hauptbohrung Oberpfalz

## Cuttings Profile

State: February 1992

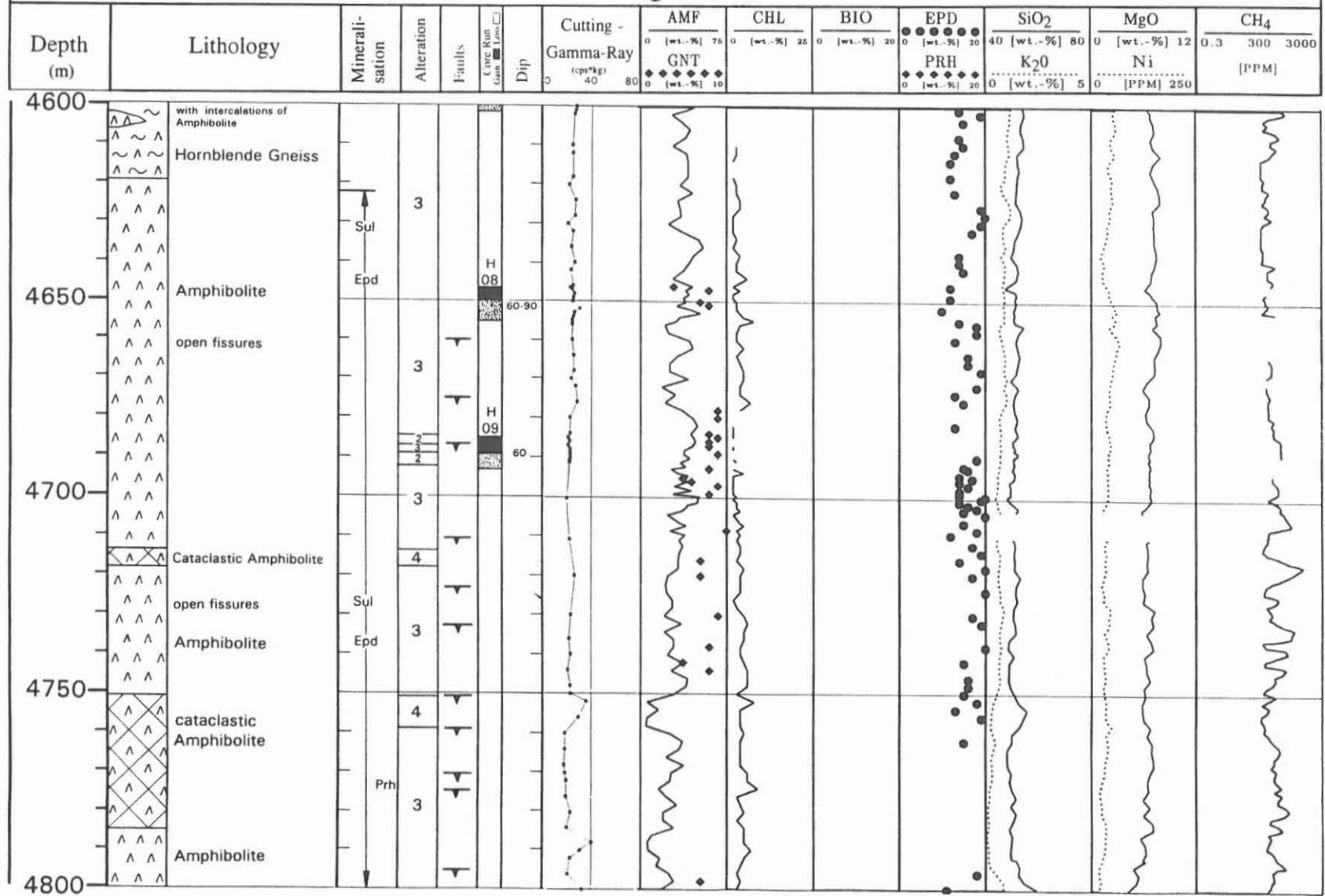
Explanations in Text



# KTB Hauptbohrung Oberpfalz Cuttings Profile

State: February 1992

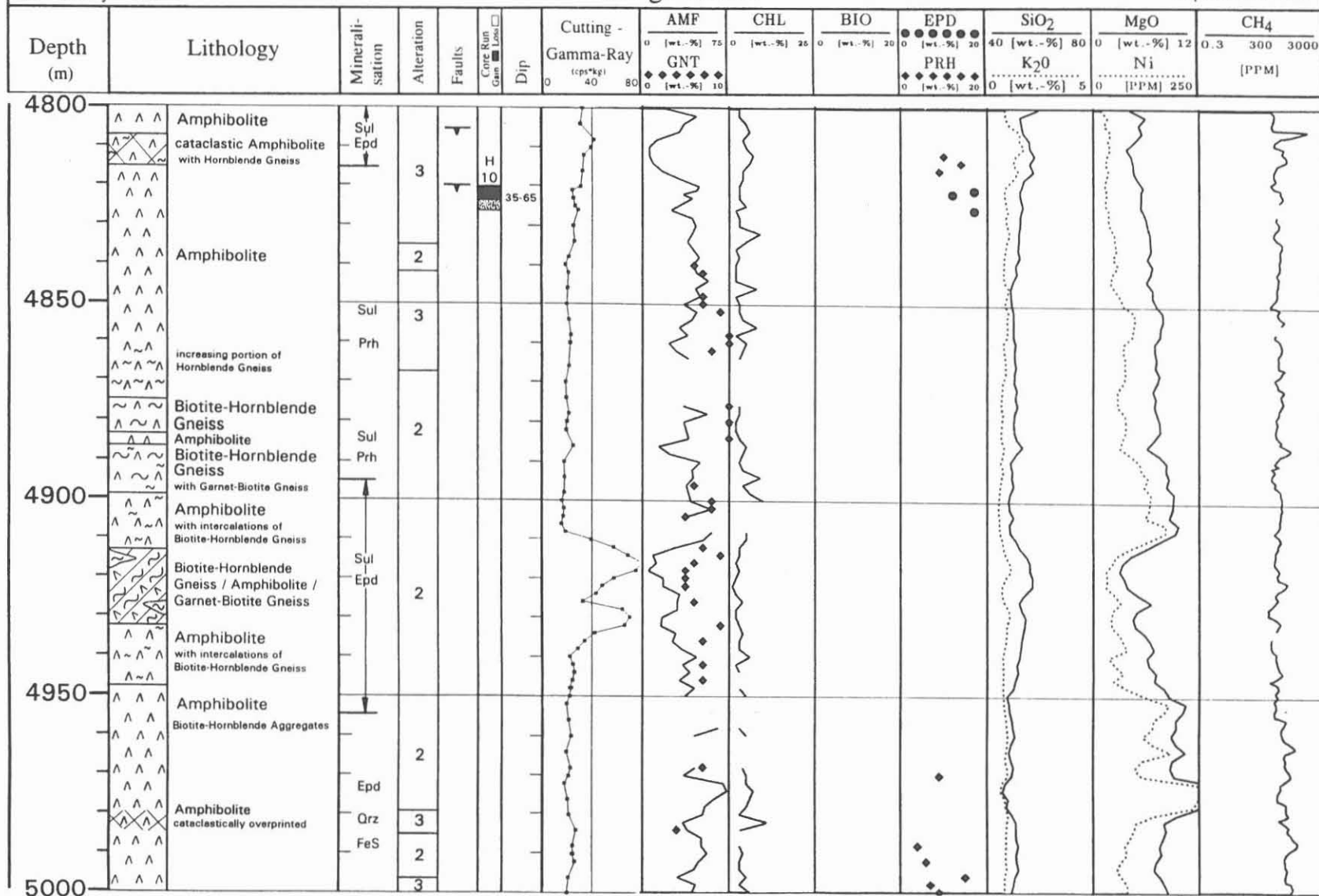
Explanations in Text



# KTB Hauptbohrung Oberpfalz Cuttings Profile

State: February 1992

Explanations in Text

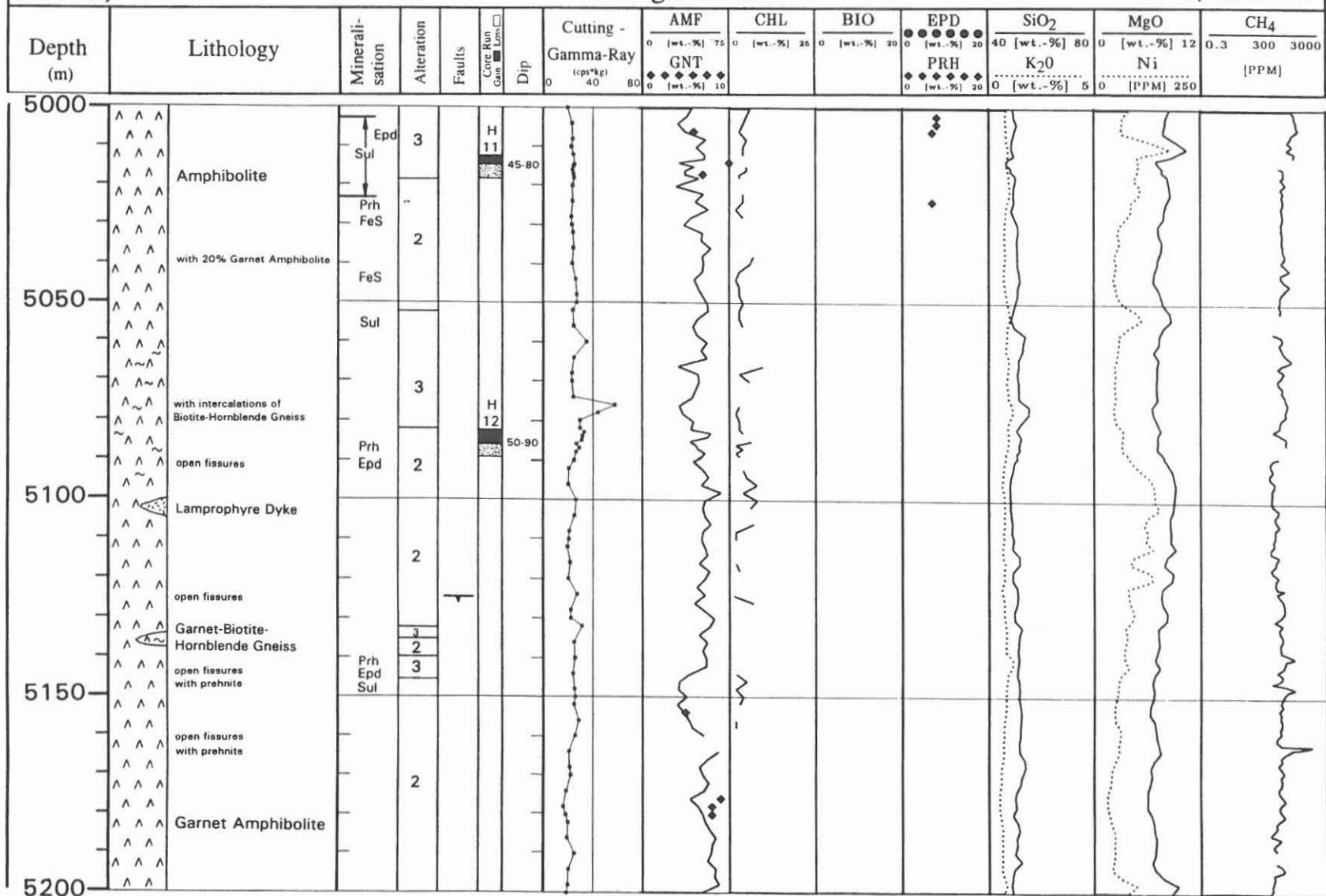


# KTB Hauptbohrung Oberpfalz

## Cuttings Profile

State: February 1992

Explanations in Text

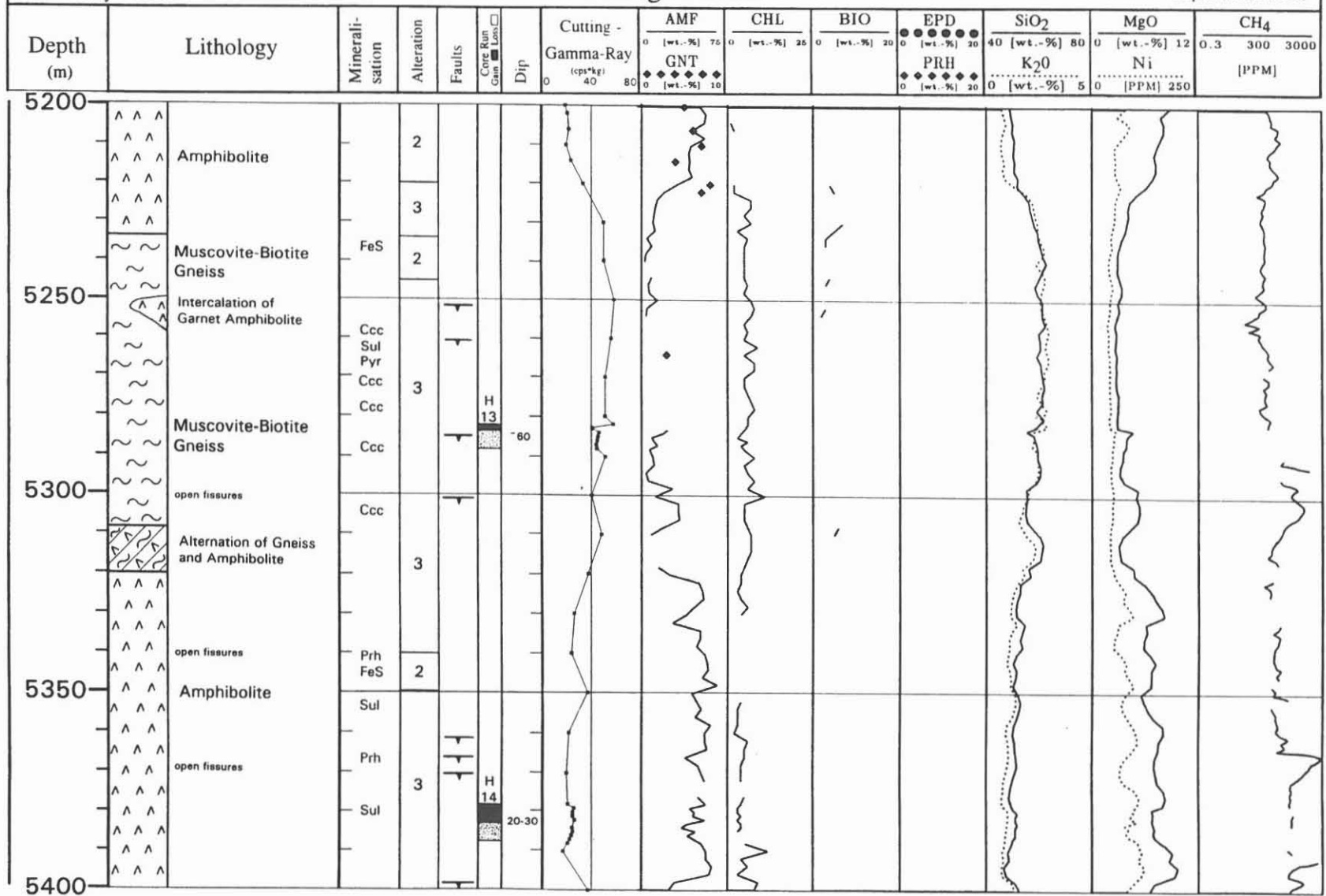


# KTB Hauptbohrung Oberpfalz

## Cuttings Profile

State: February 1992

Explanations in Text

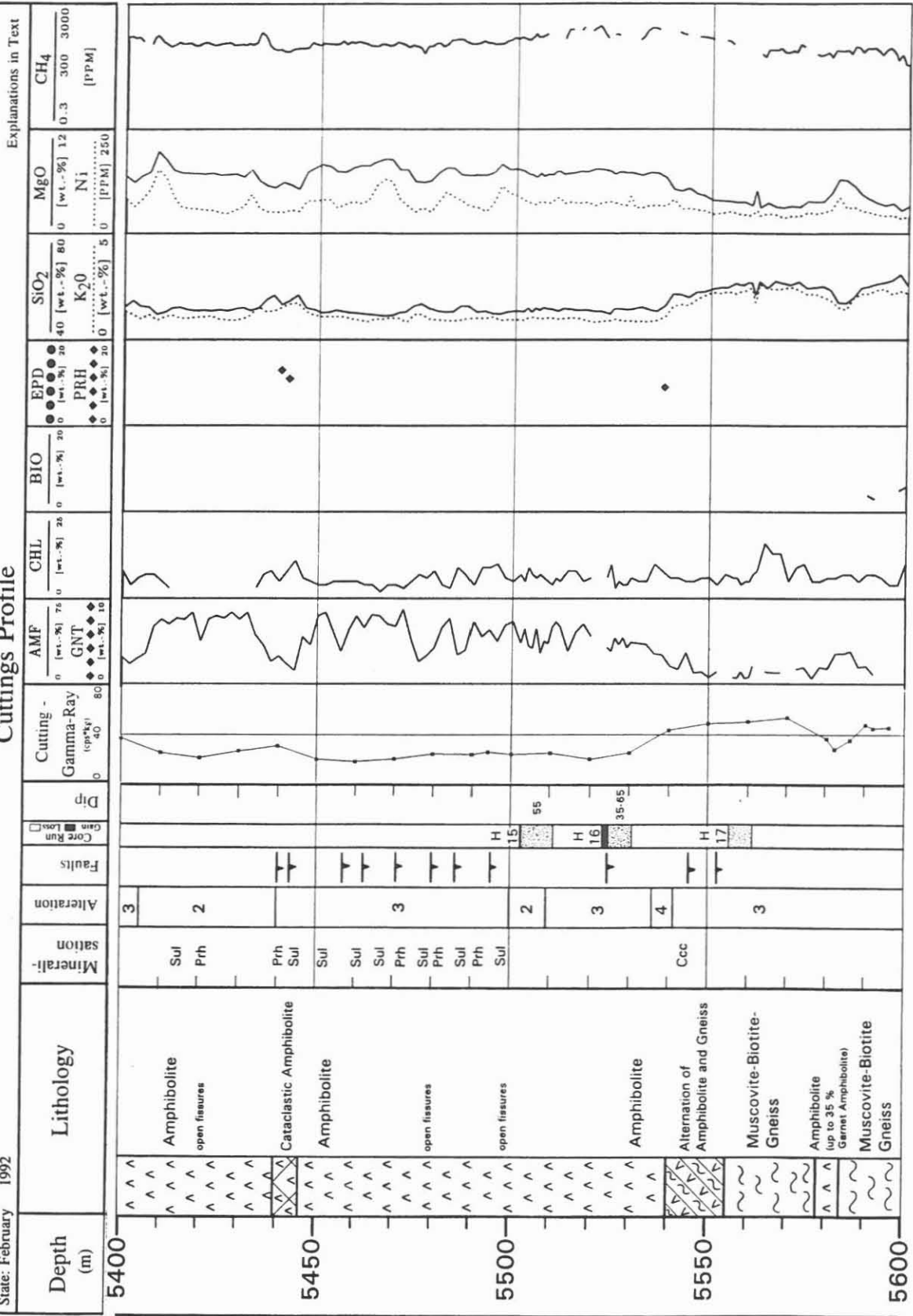


-B 80-



# KTB Hauptbohrung Oberpfalz Cuttings Profile

State: February 1992

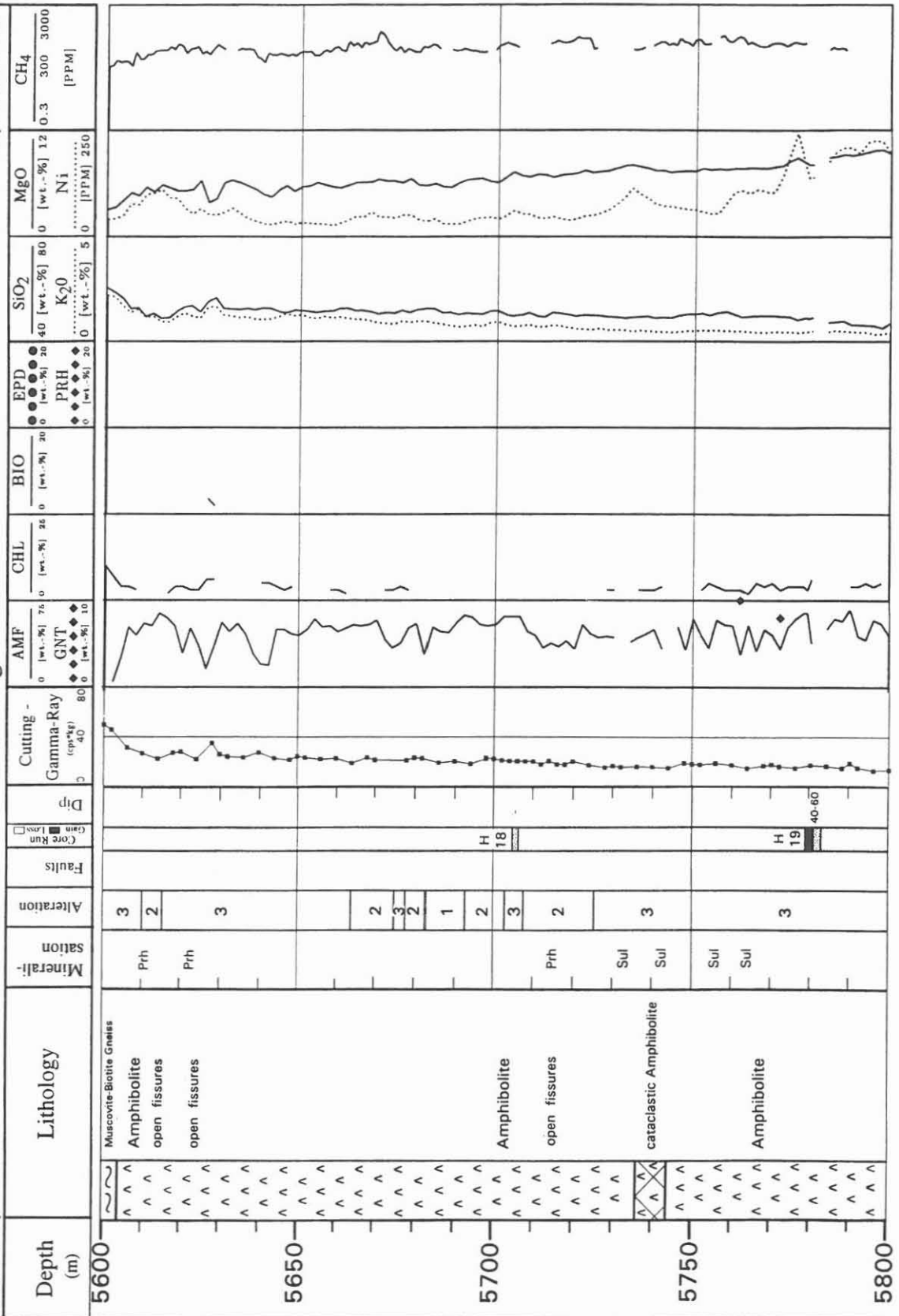


# KTB Hauptbohrung Oberpfalz

## Cuttings Profile

State: February 1992

Explanations in Text



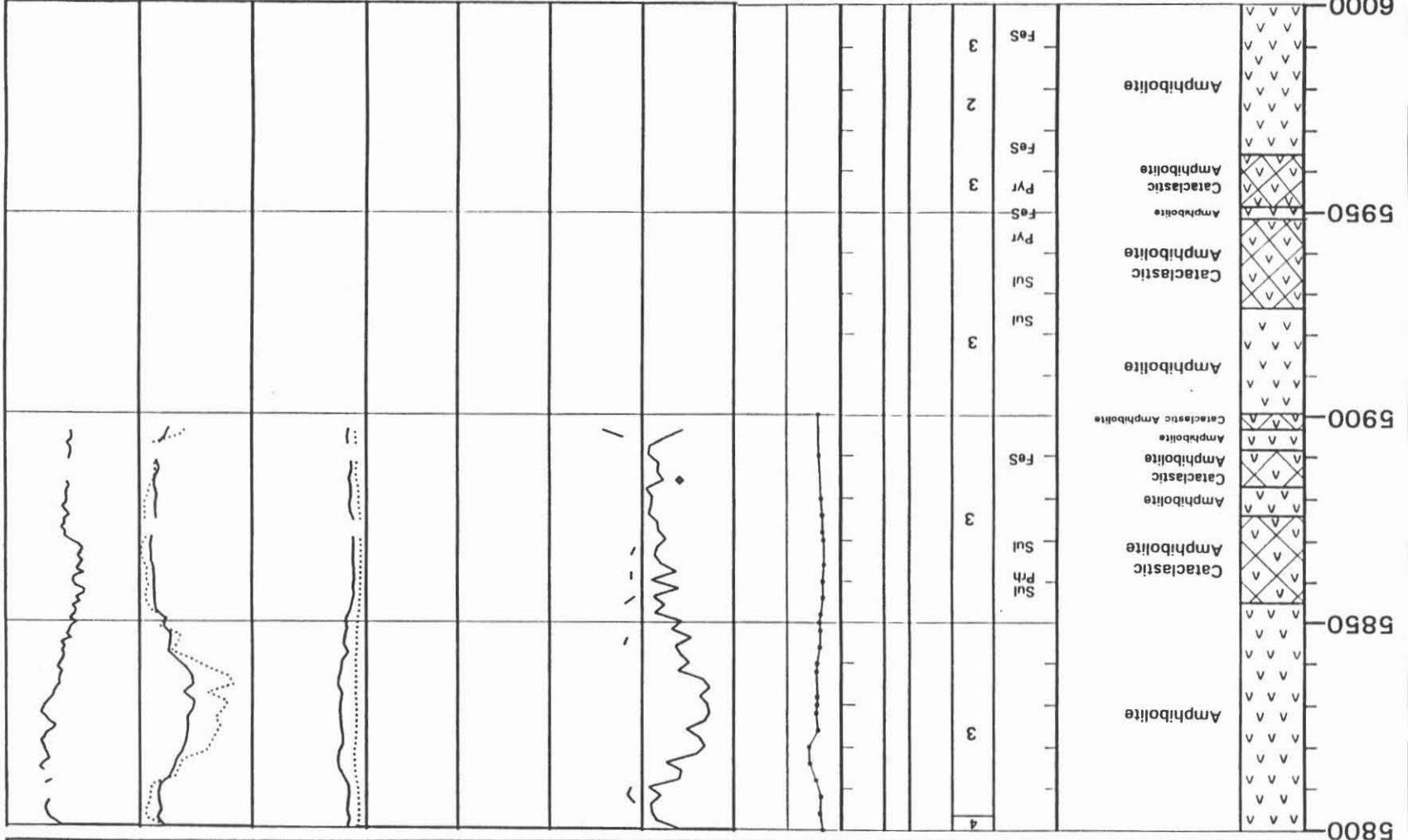
# KTB Hauptbohrung Oberpfalz

State: March 1992

## Cuttings Profile

Explanations in Text

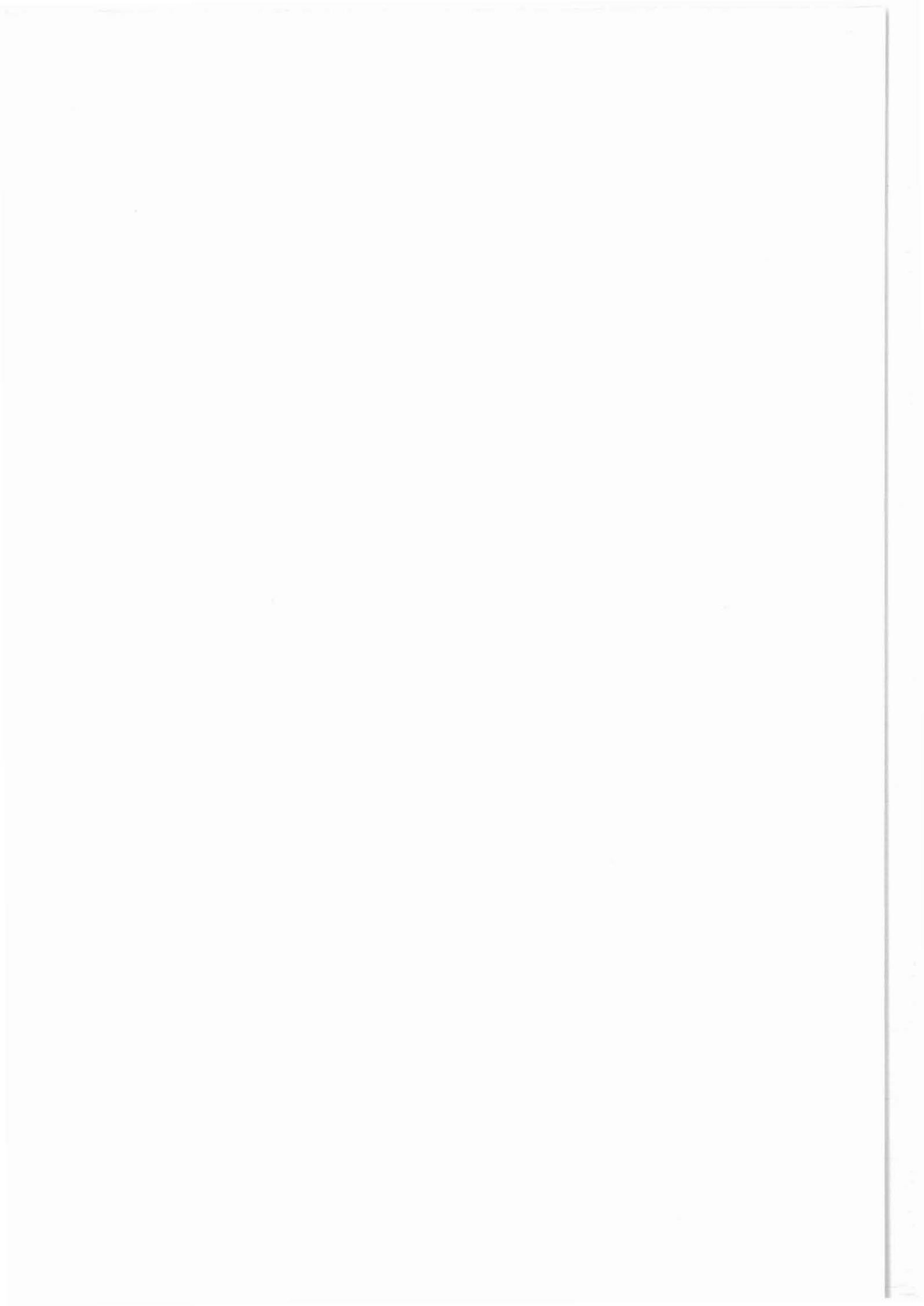
Depth (m)	5800	5850	5900	5950	6000
Lithology	Amphibolite	Cataclastic Amphibolite	Amphibolite	Cataclastic Amphibolite	Amphibolite
Minerali- sation					
Alteration					
Faults					
Core Run Gam Low					
Dip					
Gamma-Ray (cpm/g)					
Cutting - AMF					
AMF	0	20	20	20	20
GNT	0	20	20	20	20
PLH	0	20	20	20	20
EPD	0	20	20	20	20
BIO	0	20	20	20	20
CHL	0	20	20	20	20
SiO <sub>2</sub>	0	80	80	80	80
K <sub>2</sub> O	0	80	80	80	80
MgO	0	12	12	12	12
CH <sub>4</sub>	0	300	300	300	300
Ni	0	250	250	250	250





## C. Geochemistry/Mineralogy

J. Erzinger  
Ch. Figgemeier  
N. Gleiß  
J. Hansmann  
H. Kamm  
L. Machon  
T. Umsonst  
M. Zimmer



KTB REPORT	92-2	C1-C45	21 Figures	Hannover 1992
------------	------	--------	------------	---------------

**KTB Hauptbohrung, Geoscientific Investigations in the KTB-Field-Laboratory,  
Depth interval 0-6000m**

**C. Geochemistry/Mineralogy**

**Figgemeier, Ch., Machon, L., Kamm, H., Hansmann, J., Gleiß, N., Umsonst, T. \*) and  
Zimmer, M. \*\*)  
with a contribution by Erzinger, J. et al. \*\*)**

Summary.....	C3
C.1 Drill mud analysis.....	C4
C.1.1 Introduction.....	C4
C.1.2 Analytical methods.....	C4
C.1.3 KTB drill mud parameters and properties.....	C5
C.1.4 Results of "quasi-on-line analysis".....	C7
C.1.5 Results of fluids collected by fluid samplers.....	C10
C.1.6 Conclusions.....	C11
C.2 Gas analysis.....	C12
C.2.1 Introduction.....	C12
C.2.2 Experimental methods.....	C12
C.2.3 Results.....	C13
C.2.3.1 Contamination of the drill mud and artificially generated gases.....	C13
C.2.3.2 Gas inflows.....	C17
C.2.3.3 Quantification of gases dissolved in drill mud.....	C23
C.2.4 Conclusions.....	C25

C.3	Geochemical investigations of solids.....	C26
C.3.1	Sample preparation.....	C26
C.3.2	Methods.....	C26
C.3.2.1	Mineralogical phase analysis.....	C26
C.3.2.2	Determination of major and trace elements.....	C26
C.3.3	Results.....	C27
C.4	Acknowledgements.....	C27
C.5	References.....	C28
C.6	Appendix.....	C29
C.6.1	Results of cation and anion analysis.....	C29
C.6.2	Results of solid analysis.....	C33
C.7	On-line determination of <sup>222</sup> Radon in the drilling fluid.....	C39

\*) Authors address: KTB Feldlabor  
W-8486 Windischeschenbach

\*\*\*) Authors address: Institut für Geowissenschaften und Lithosphärenforschung  
W-6300 Gießen



## Summary

Extensive geochemical investigations of cores, cuttings, drilling fluid, formation waters and dissolved gases form an essential part of the geoscientific work in the KTB field laboratory.

During drilling of the Hauptbohrung the same drilling fluid system is being used as in the pilot hole. This drilling fluid is a mixture of water with 1.5% Dehydril-HT, an inorganic viscosifier with high temperature stability, giving fluid with thixotropic properties. In addition a polymer was used below 2091m with the name "Hostadrill 3118" in order to reduce corrosion of the drill pipe.

The drill mud analysis show enrichments of specific elements like K, Al, Ca, Sr,  $\text{SO}_4^{2-}$  and  $\text{Cl}^-$  produced by fluid/rock interactions (leaching- or oxidation processes) and fluid inflows.

In the pilot hole chloride was found to be a very sensitive fluid-inflow indicator. Such fluid inflows were observed below 3000 at the Hauptbohrung. In all zones the gases helium and methane were detected. These zones correlate with cataclastic horizons, fractures and open pores.

Samples obtained by a fluid sampler from a depth of 3184m showed enrichments of Na, Ca, Sr and  $\text{Cl}^-$ , which are interpreted as due to inflows of  $\text{NaCl}$ - and  $\text{CaCl}_2$ - and containing formation waters.

The gas phase dissolved from the drill mud in a gas trap has been determined by on-line-analysis using mass spectrometry, gas chromatography and a radon logging device. The major portion of this gas phase is due to contamination in the open mud tanks.

A hydrogen content up to 1 % is artificially generated by corrosion reactions at the iron casing. On the other hand, oxygen is used up during these reactions.

Gas inflows from rocks are recognized by enrichments of radon, helium and hydrocarbons. The amount of deliberated helium and methane was determined by comparison with well-defined gas injection tests.

Complete degassing of the drill mud results in strong enrichments of nitrogen, methane and helium.

Cuttings and rock flour produced by drilling were analysed at intervals of 2m, in areas of lithological changes of 1m.

The mineral content (in wt.%) was determined by X-ray diffraction using a software-product with a fully automatic qualitative and quantitative program for phase analysis. By X-ray fluorescence analysis 11 main constituents ( $\text{SiO}_2$ ,  $\text{TiO}_2$ ,  $\text{Al}_2\text{O}_3$ ,  $\text{Fe}_2\text{O}_3$ , MnO, MgO, CaO,  $\text{Na}_2\text{O}$ ,  $\text{K}_2\text{O}$ ,  $\text{P}_2\text{O}_5$ ) and 12 trace elements (Sr, Rb, Y, Zr, Nb, Cr, Ni, Zn, V, Cu, Th, U) were measured.

## C.1 DRILL MUD ANALYSIS

### C.1.1 Introduction

The chemistry of the drill mud is determined by "quasi-on-line" analysis. The main objective of this analysis is the detection of inflow-horizons of formation waters in order to allow direct sampling of uncontaminated fluid. Furthermore, drill mud analysis is necessary for controlling changes of mud properties such as pH value, conductivity and concentration of mud additives.

### C.1.2 Analytical methods

The contents of Na, K, Li, Mg, Ca, Sr, Ba, Fe, Al, Cl<sup>-</sup> and SO<sub>4</sub><sup>2-</sup> in the drill mud were continuously measured during drilling. Anions were measured using a chromatography system (IC), cations using an atomic emission spectrometer (ICP-AES). Technical details are described in the KTB report 88-2 (HEINSCHILD et al., 1988) and KTB report 88-6 (STROH et al., 1988).

Sample preparation generally follows the scheme shown in figure C.1.1.

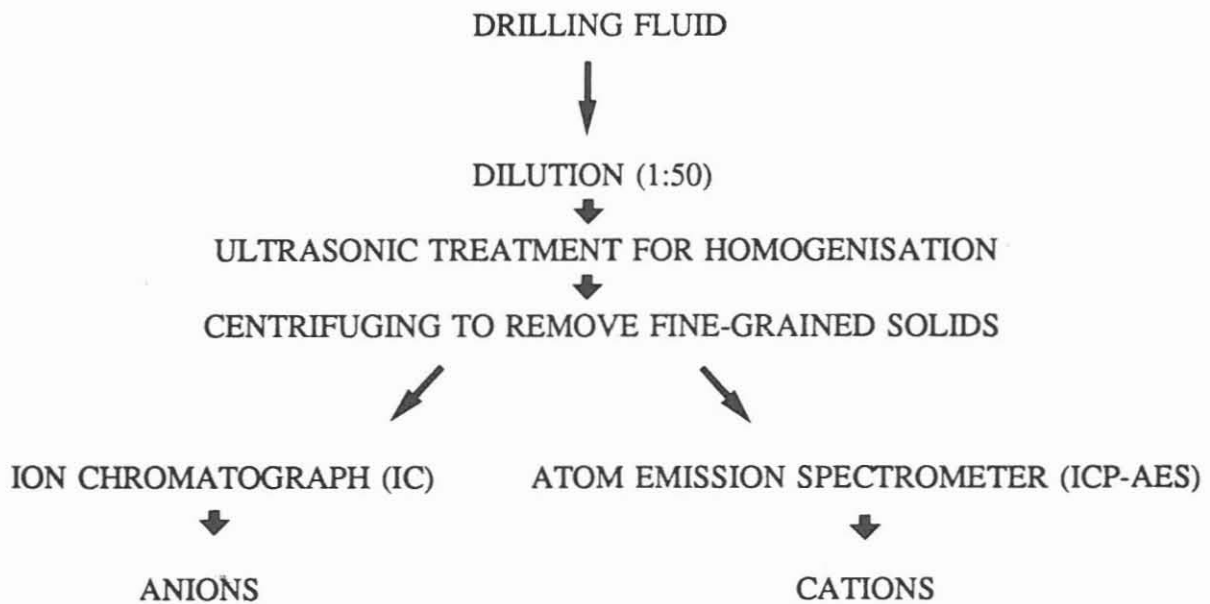


Fig.C.1.1: Preparation for anion and cation determination

### C.1.3 KTB drill mud parameters and properties

During drilling of the Hauptbohrung the same drill mud system was used as in the pilot hole. This mud is a mixture of water with Dehydril-HT (synthetic hectorite consisting of Si, Mg, Na, Li and H<sub>2</sub>O), NaOH and Na<sub>2</sub>CO<sub>3</sub> giving a mud with thixotropy properties. Thixotropy and viscosity of the drill mud depend on the concentration of the additive, the pH value and the electrolyte content (see HEROLD et al.,1987). The chemistry of the initial drill mud is shown in table C.1.1.

Tab.C.1.1: Chemical composition of initial drill mud (1.9 wt.% Dehydril-HT)

elements	content in ppm
Na	350
K	10
Ca	42
Sr	0.2
Li	58
Mg	2640
Si	4560
SO <sub>4</sub> <sup>2-</sup>	60
Cl <sup>-</sup>	10

D-HT has an excellent carrying capacity for cuttings and rock flour and does not affect chemical analysis of solids and dissolved gases and allows for detection of even small amounts of inflowing saline formation waters.

Below a depth of 2091m a polymer ("Hostadrill 3118") was added to the drill mud in order to reduce corrosion of the drill pipe. This polymer has the following structure:

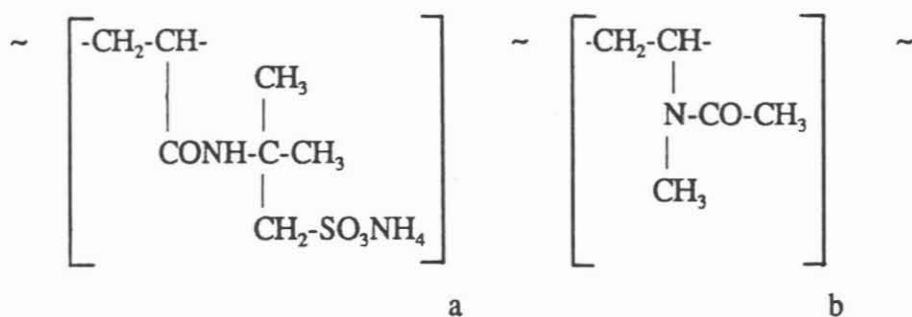


Table C.1.2 demonstrates the influence of drill mud additives (D-HT, NaOH, etc.) on the chemical properties of drill mud, which is important for interpretation of anion and cation data.

Tab.C.1.2: Drill mud composition

depth (m)	composition of drill mud	reason for changes	effects on the chemistry (see appendix C.6.1)
0	1.9% D-HT + NaOH		pH 9.9-10.1; increased Na and conductivity (see Fig.C.1.2)
304	+ NaHCO <sub>3</sub>	cementation of casing	increased Na, Ca, Sr, Cl <sup>-</sup>
305	drill mud exchange 1.5% D-HT + NaOH	unstable drill mud properties	pH 9.9-10.1
750-1450	+ Na <sub>2</sub> CO <sub>3</sub>	pipe corrosion	increased Na content; decreased D-HT content; strong cation variation
1500	+ NaOH	pipe corrosion	pH 11
2092	+ polymer "Hostadrill 3118"	pipe corrosion	no effects
2876-3003	+ BaSO <sub>4</sub>	mud weighting	increased Ba, Sr
3003	no drill mud exchange	cementation of casing	increased Ca, Sr, Cl <sup>-</sup>
5595.5		back cementation	increased Ca, Sr, Cl <sup>-</sup>

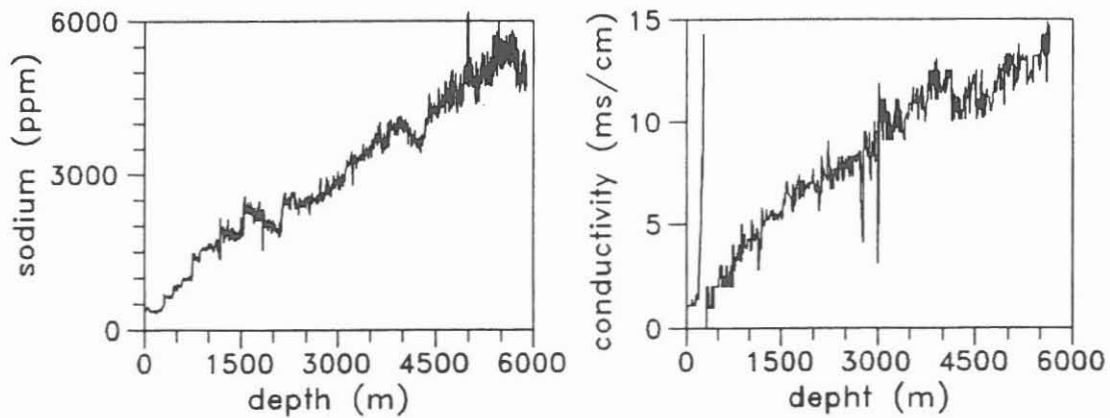


Fig.C.1.2: Sodium content versus conductivity

### C.1.4 Results of "quasi-on-line analysis"

Analysis of drill mud shows enrichments of K, Al, Ca, Sr,  $\text{SO}_4^{2-}$  and  $\text{Cl}^-$  produced by drill mud/rock interactions and fluid inflows. The observed K/Al ratio is about 0.4. Muscovite is the only major rock-forming mineral with a similar K/Al-ratio (0.48). According to leaching experiments (see HOMANN and MÜLLER, 1989), the reaction of the drill mud with sheet silicates (muscovite) in the drilled material leads to an increase of the potassium and aluminium concentrations (Fig. C.1.3).

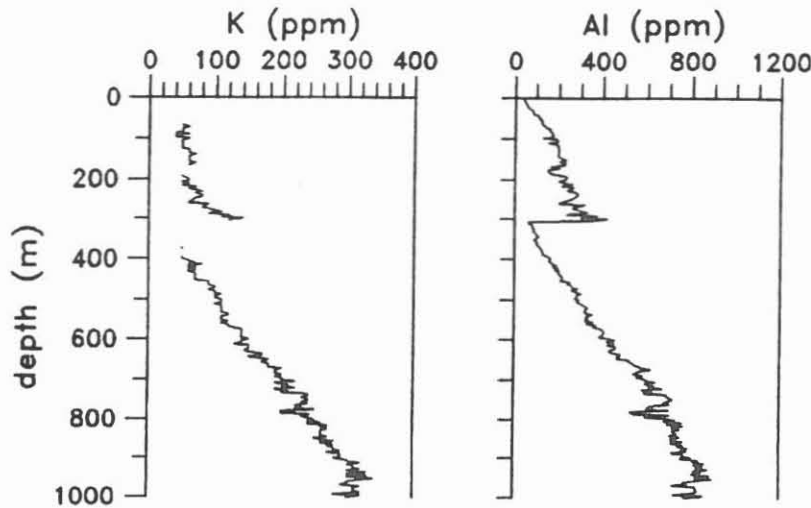


Fig.C.1.3: Enrichments of K and Al in the drill mud. The sudden decrease at 305m results from a drill mud exchange.

Ca and Sr are enriched due to a reaction of the drill mud with the minerals hornblende, plagioclase and calcite. The distinct Ca and Sr increase at 200m (Fig.C.1.4) can be explained by carbonate bearing cataclastic gneisses and calcsilicates.

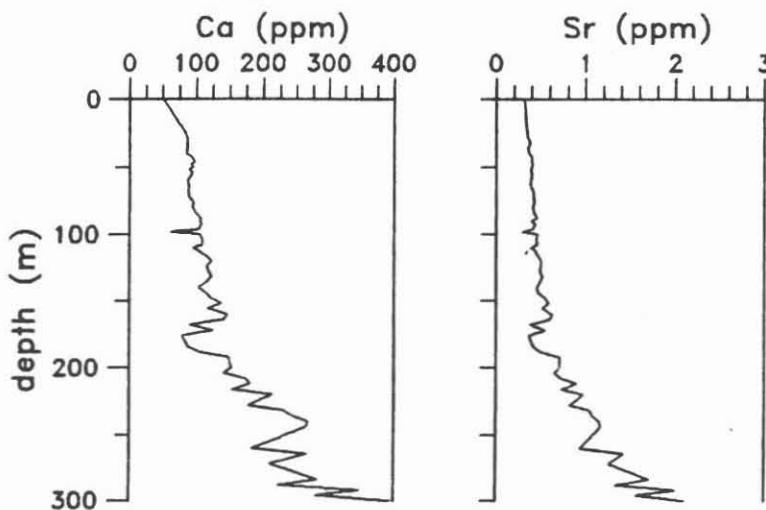


Fig. C.1.4: Enrichments of Ca and Sr in the drill mud

The interaction of drill mud with pyrite and pyrrhotite leads to sulfate formation at 260m-300m and 400m-550m. Oxidation of these minerals can be described by the following reactions:



or in alkaline environment:



The sulfuric acid produced from these reactions leads to a decrease of the pH value of the drill mud system especially when drilling shear zones with sulfide mineralization. Fig.C.1.5 presents the sulfate content of the drill mud and the sulfur content of the cuttings (RFA-analysis). The first significant increase of sulfate at 260m correlates directly with sulfur enrichments caused by pyrite-bearing biotite-hornblende gneisses. The sudden decrease at 305m is due to drill mud exchange. Sulfate enrichments of the drill mud (up 150ppm) at 400m-550m can be related to pyrite- and pyrrhotite rich garnet-sillimanite-biotite gneisses.

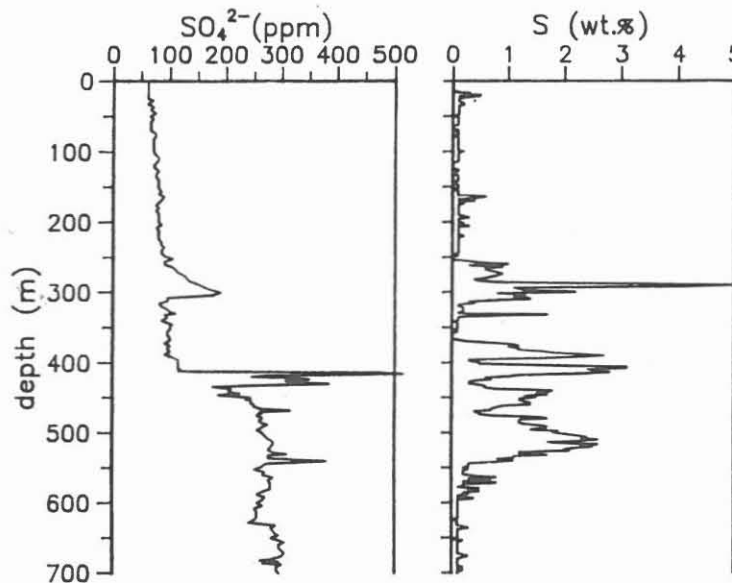


Fig.C.1.5: Sulfate content of drill mud and sulfur content of cuttings

The result of the pilot hole show that chloride is a very sensitive indicator for inflow-horizons (STROH et al., 1990). Several significant chloride enrichments were detected below 3000m at the Hauptbohrung. They generally go together with enrichments of helium and methane. Table C.1.3 shows the depth intervals where these significant enrichments were observed. The element concentrations correspond with the maximal values within the depth intervals. Figure C.1.6 shows the concentration distribution of chloride, methane and helium in the depth interval from 4100m-4130m.

Tab.C.3.3: Chloride, methane and helium correlations

depth interval (m)	chloride (ppm)	methane (ppm)	helium (ppm)
3442-3446	140 [110]	no values	no values
3474-3478	145 [110]	no values	no values
3534-3548	160 [110]	255 [50]	13 [7]
4117-4125	175 [155]	490 [125]	17 [9]
4144-4146	190 [165]	40 [30]	7 [6]
4715-4716	130 [115]	770 [50]	25 [7]
4806-4824	150 [115]	900 [70]	32 [10]
4985-4995	135 [115]	405 [100]	20 [9]
5364-5368	180 [160]	2700 [100]	76 [7]
5390-5393	200 [175]	2300 [300]	59 [10]
5500	230 [185]	250 [150]	9 [8]
5532-5536	250 [200]	500 [200]	17 [9]
5822-5826	260 [220]	280 [100]	11 [9]

[ ]: Background concentration

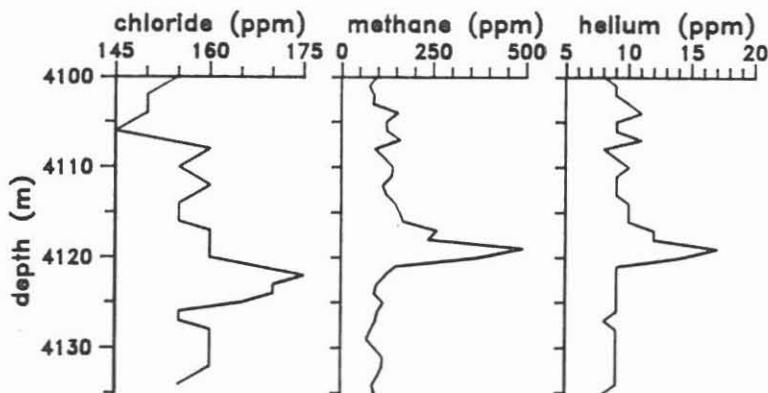


Fig.C.1.6: Concentration distribution of Cl<sup>-</sup>, CH<sub>4</sub> and He from 4100m-4130m

The fluid inflows correlate with cataclastic zones, fractures and open pores (see part B Geology). Sodium- and calciumchloride rich formation waters and gases were already collected during the pump test at the pilot hole (4000m).

**C.1.5 Results of fluids collected by fluid samplers**

During the logging phases fluid samples were taken according to fluid-, gas-, conductivity- and temperature measurements.

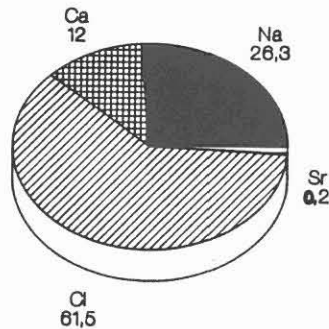
Tab. C.1.4: Fluid- and gas composition of fluidsamplers

depth (m)	Ca (ppm)	Sr (ppm)	Cl (ppm)	p (mbar)	N <sub>2</sub> /Ar	CH <sub>4</sub> (ppm)	He (ppm)
1530	145	3	80	37	84	1	5
1960	140	3	60	12	213	42	8
2975	155	3	60	10	107	1	4
3001	150	3	55	6	168	1	2
B.C.	130	3	55				
3184	1060	18	4900	0	-	-	-
B.C.	130	3	120				
3950.5	210	3	135	56	98	180	14
B.C.	175	3	120				
4115	175	2	200	175	90	100	9
B.C.	150	2	200				
5388	120	1	230	0	-	-	-
B.C.	105	1	225				

B.C.: Background concentration

The sample of the depth 3184m showed significant Ca, Sr and Cl<sup>-</sup> enrichments. Sodium content caused by fluid inflows is not detectable because of the high background concentration ( $\phi$  5200ppm) of this element, but it can be calculated according to the amount of Ca and Cl<sup>-</sup> present. The relationship between elements (Fig.C.1.7) characterise the fluid.

Fig. C.1.7: Composition of "3184m fluid" (data in %)





After using the fluidsampler at depth 3184m drill mud was circulated out. Figure C.1.8 demonstrates the chloride content of the drill mud during circulation at about 3184m. A significant Cl<sup>-</sup> enrichment was observed. The mixing of drill mud (550m<sup>3</sup>) with this formation water resulted in increasing the Cl<sup>-</sup> background from 120ppm to 160ppm.

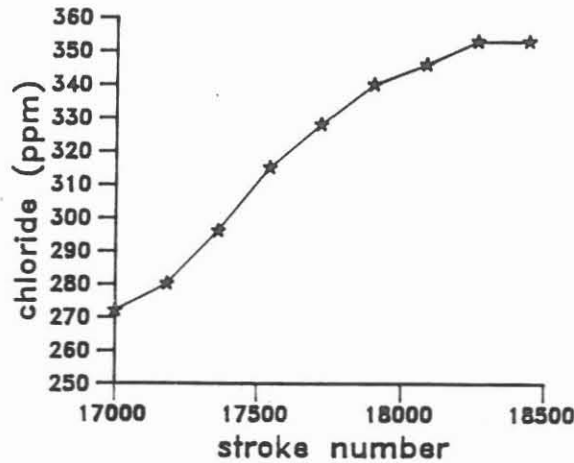


Fig.C.1.8: Chloride content of the drilling fluid during circulation

Except of the fluid samples taken from 3184 m and 5388 m , a resolved gas phase was found after expanding the fluids into an evacuated volume of 1 litre. The composition of this gas phase generally agrees with the composition measured by on-line-analysis. The high N<sub>2</sub>/Ar-ratio of the resolved gas phase indicates gas inflows. However significant contents of helium and methane were only found at 1960 m , 3950,5 m and 4115 m. Even these values are much lower than the values measured before by on-line-analysis from the same inflows.

### C.1.6 Conclusions

The results of drill mud analysis show enrichments of certain elements (K, Al, Ca, Sr, SO<sub>4</sub><sup>2-</sup> and Cl<sup>-</sup>) produced by drill mud/rock interactions (leaching or oxidation processes) and fluid infows.

Chloride was found to be a very sensitive indicator for fluid inflows. Such fluid inflows were observed below 3000m. All fluid bearing zones were accompanied by enrichments of helium and methane and correlate with cataclastic areas, fractures and open pores.

Samples obtained by a fluid sampler from a depth of 3184m showed enrichments of Na, Ca, Sr and Cl<sup>-</sup>, which are interpreted as due to inflows of NaCl- and CaCl<sub>2</sub>- containing formation waters.

## C.2 GAS ANALYSIS

### C.2.1 Introduction

Gas inflows into the borehole are detected already during drilling by on-line-analysis of the gas phase released from the circulated out drill mud. Subsequent sampling (i.e. apply of fluid samplers) is done in a very few well chosen cases depending on results of the on-line-analysis. On-line-analysis may be the method to gain information on the gas composition at greater depth as high temperature and pressure may prevent use of logging tools and fluid samplers. Furthermore, the on-line-analysis gives immediate information on the quantity of gases entering the borehole and the vertical extension of gas-bearing zones.

### C.2.2 Experimental methods

Down to a depth of 3003 m the gas phase was released and collected by two swirl degassers attached in front of the mud shakers. This open system led to gas losses as well as air contamination. Therefore results obtained down to this depth have only qualitative character.

At 3003 m the borehole was cased and a bypass system was installed 50 cm below the drill mud outlet. A constant part (about 100 l/min) of gas-bearing drill mud is pumped through the bypass and then directly led to a swirl degasser which is isolated against atmosphere. The released gas phase is completely sucked off and led through a hose to the logging unit as shown in Fig.C.2.1. To prevent air contamination or sucking off drill mud the pressure in the gas trap is balanced by charging argon.

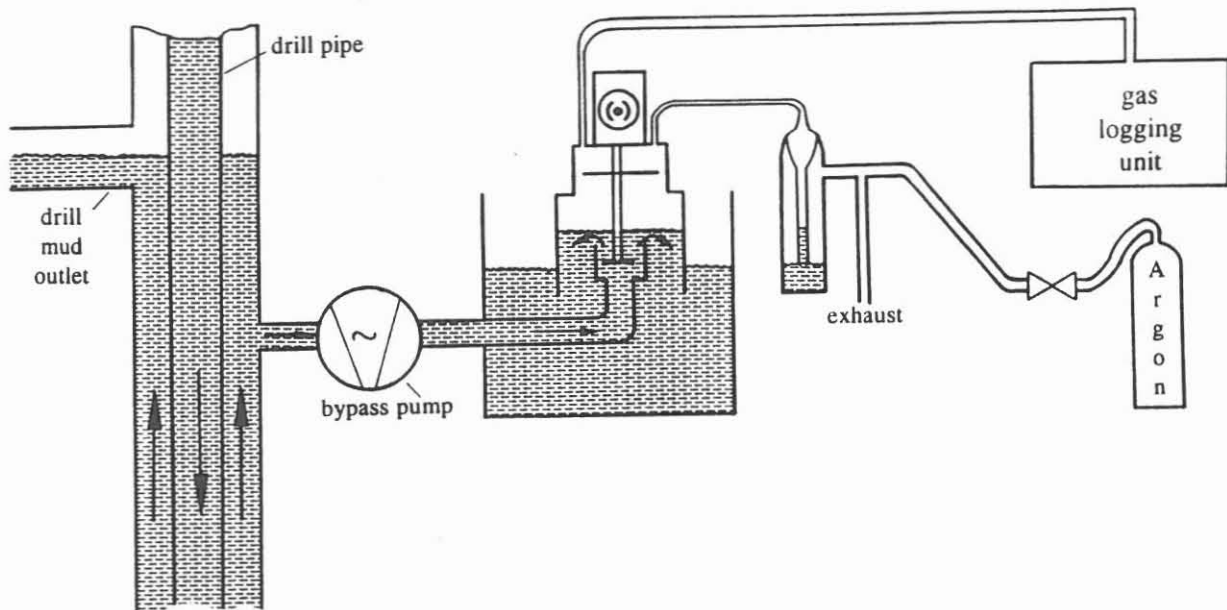
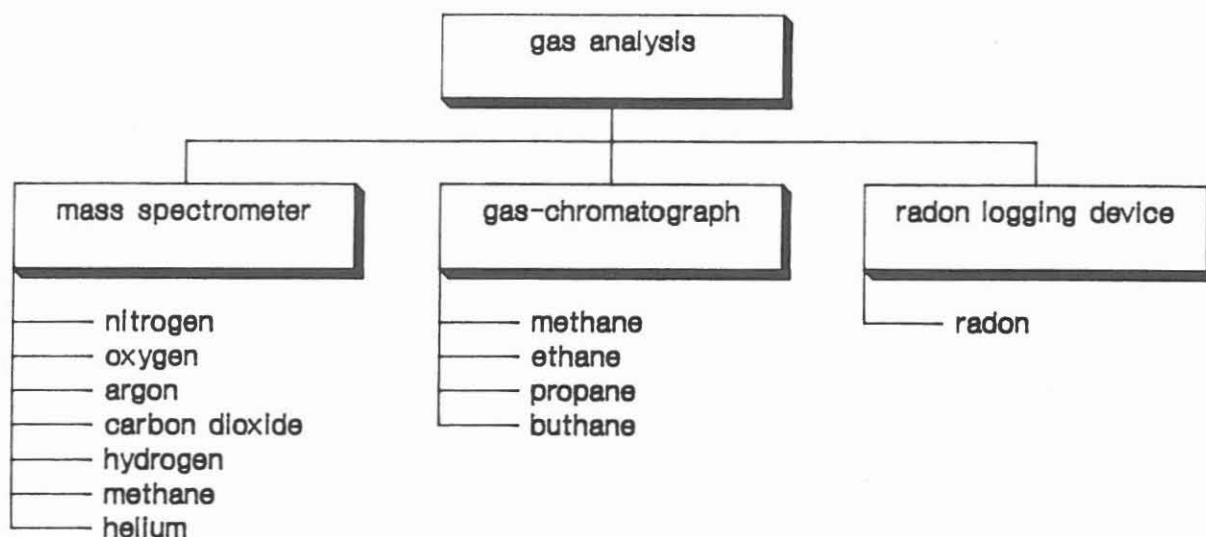


Fig.C.2.1: Bypass gas sampling system

The logging unit consists of a single focussing magnetic sector mass spectrometer (Vacuum Generators LTD, MM8-80), a gaschromatograph (Geodata, F-30D) and a radon logging device which is explained in a special contribution to this report (chapter C.7). The operation principles of the mass spectrometer and the gaschromatograph have been explained by STROH et al. (1988) and FIGGEMEIER et al. (1991). From the hose line the gas phase is distributed parallel to the logging devices.

The following gases are measured:



## C.2.3 Results

### C.2.3.1 Contamination of the drill mud and artificially generated gases

The gas phase from the drill mud is composed mainly of nitrogen, oxygen and argon, i. e. the main constituents of air. CO<sub>2</sub> is usually not detected because of reaction with NaOH, which is added to the mud in order to stabilize the pH. Since 1535 m, when the pH had been fixed to about 10.5 the CO<sub>2</sub>-content of the gas phase is always lower than 50 ppm. Before this depth the CO<sub>2</sub>-values represented air values.

The O<sub>2</sub>-content of the drill mud depends on the persistence inside the borehole and the duration of the contact with the drill string and the iron-casing above 3000 m. Therefore the average O<sub>2</sub>-content of the released gas phase decreases with increasing depth, i. e. increasing turn-round time (Fig.C.2.2). Furthermore, the O<sub>2</sub>-content correlates with the drill mud flow rate (Fig.C.2.3).

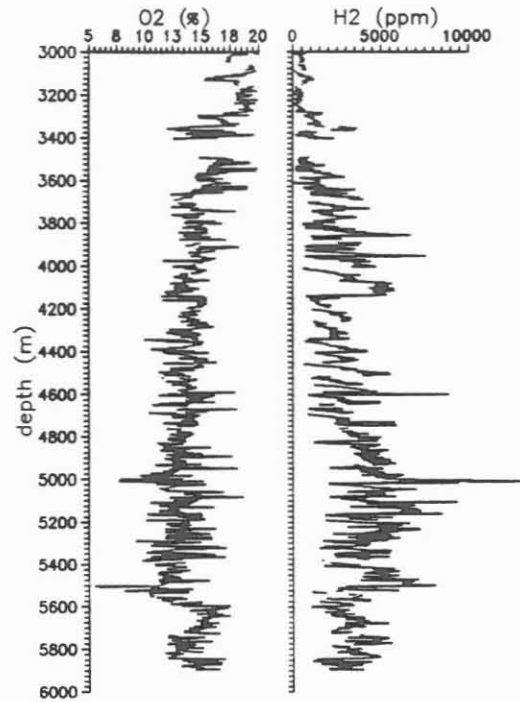


Fig.C.2.2: Variation of oxygen and hydrogen in the dissolved gas phase with depth

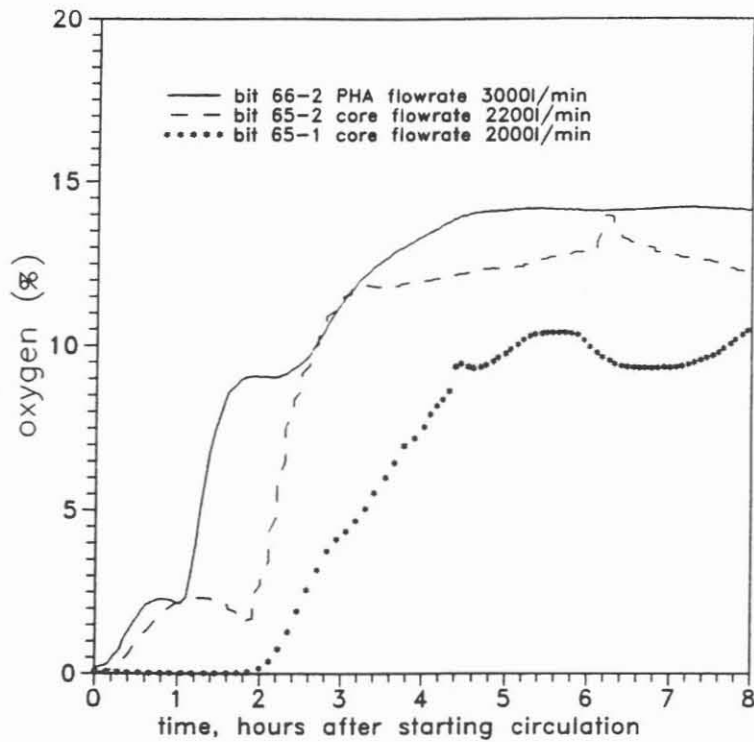


Fig.C.2.3: Oxygen concentration in the dissolved gas phase at different drill mud flow rates.

An extended contact with the iron-casing leads to an almost complete consumption of oxygen in the drill mud by corrosion reactions. Consequently the O<sub>2</sub>-content of the released gas phase is very low after resumption to drill mud circulation after an interruption (for example, bit change). The O<sub>2</sub>-content increases when drill mud which remained below the casing during the drill break is circulated out (Fig.C.2.4). The oxygen minimum is accompanied by a maximum of hydrogen, set free by dissociation of water in the course of corrosion reactions.

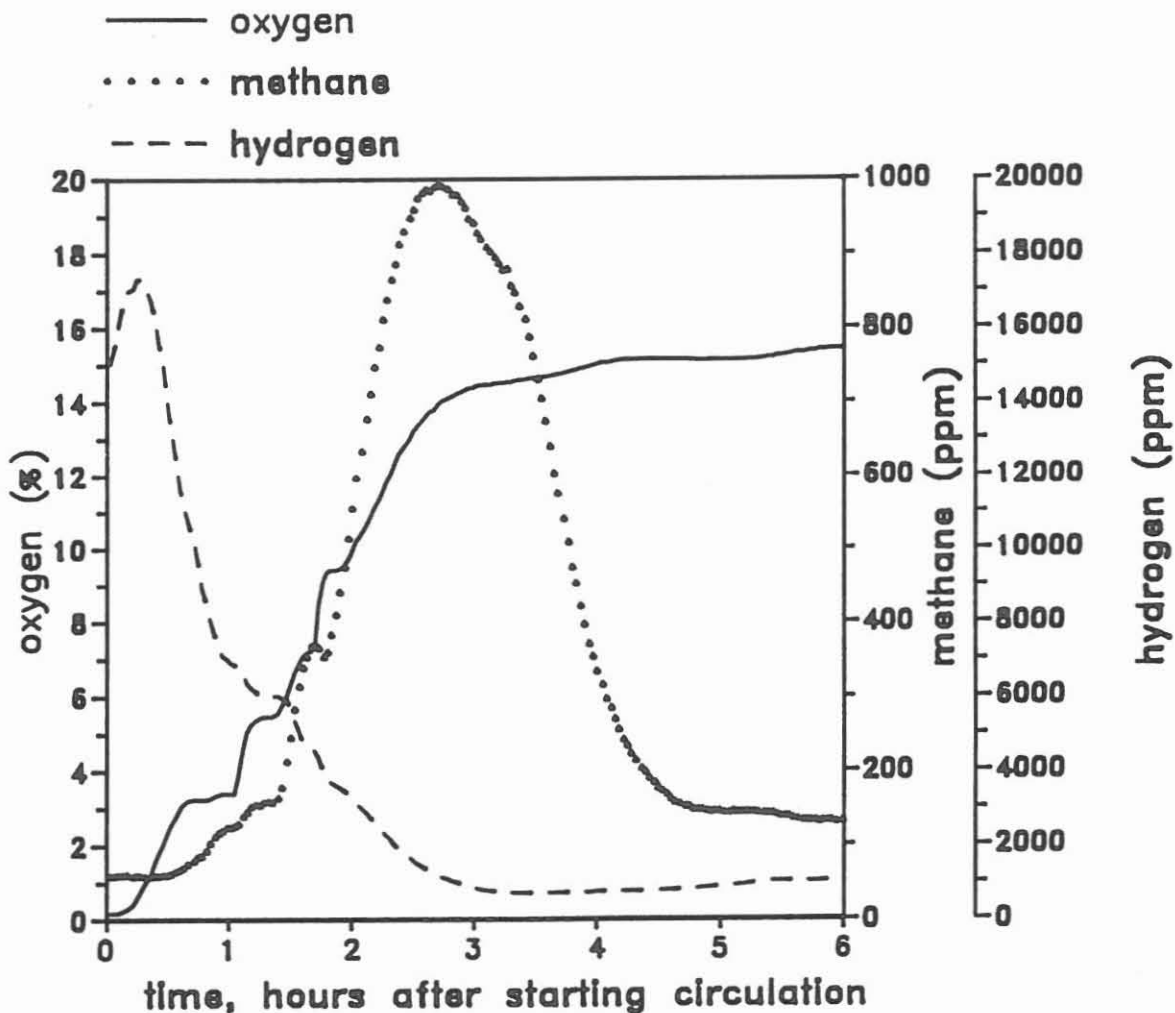


Fig.C.2.4: Concentrations of oxygen, hydrogen and methane in the dissolved gas phase after restarting the mud circulation from a drill break (bit change)

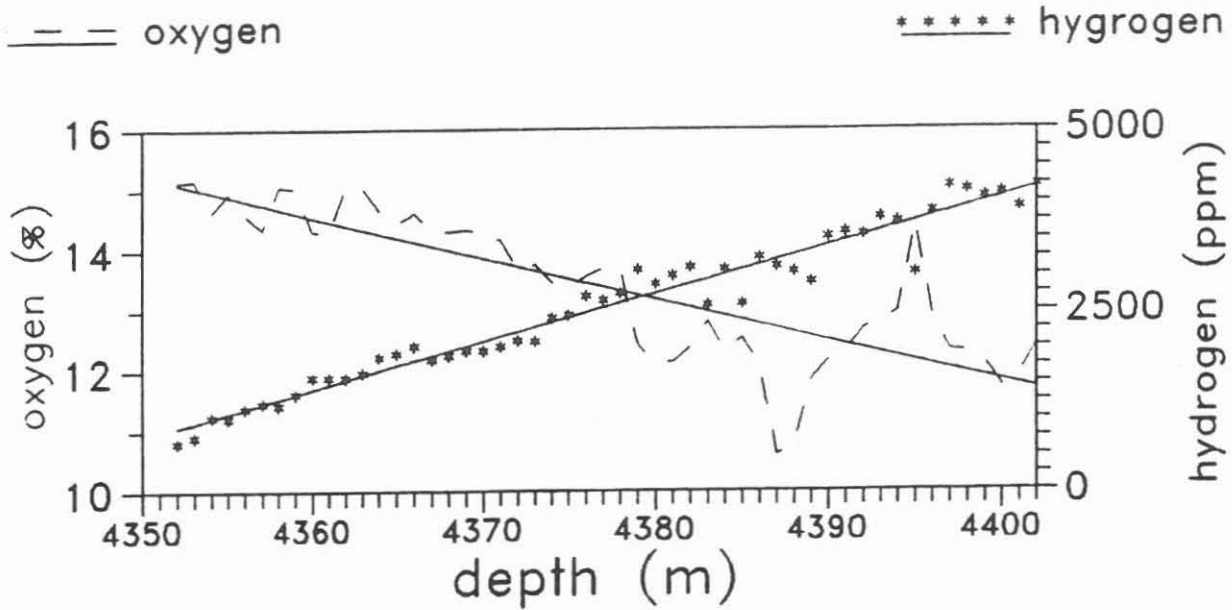
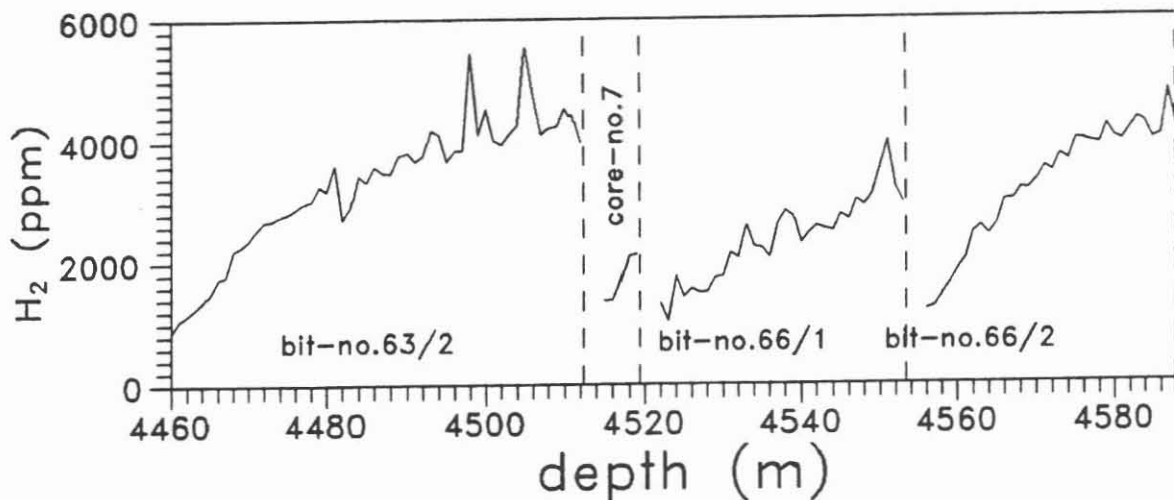


Fig.C.2.5: Variation of oxygen and hydrogen during continuous drill progress

Generally, because of its formation by corrosion reactions, the average H<sub>2</sub>-content is inversely connected to the O<sub>2</sub>-content as already shown in Fig.C.2.5. It drops when the mud circulation is interrupted (drill break) because hydrogen recombines with oxygen beyond the iron-casing, and increases after the mud circulation is restarted (drilling). Fig.C.2.6 shows the distribution of the H<sub>2</sub>-content in the course of some bit trips.



C.2.6: Variation of hydrogen content between depth area 4460m-4590m

Compared to air there is a relative increase of nitrogen and argon in the gas phase, according to the lack of oxygen. That is, the drill mud is highly contaminated by air. This contamination occurs at the open mud tanks, enforced by two agitators, before the drill mud is pumped into the borehole.

### C.2.3.2 Gas inflows

Gas inflows occur during rock-penetration and during drill breaks ('Tripgas'). These trip-gases are regularly produced by accumulation at bottomhole (methane-maximum in Fig.C.2.4).

Gas inflows are characterised by their contents of radon, helium and low-boiling hydrocarbons (methane, ethane, propane, butane) (Fig.C.2.10). Nitrogen content cannot be taken into account because of intense air contamination.

These inflows, even minor ones, often accompany cataclastic zones and/or open pores. Microscopical investigations of cuttings from these zones frequently show secondary mineralization of quartz, prehnite or epidote. This is observed more frequently in amphibolites than in gneisses, corresponding with the background accumulation of very small inflows increases with lithological changes from gneiss to amphibolite.

A special event occurred at 3184 m where an inflow was activated, for the first time, by lowering the drill mud level during a drill break at 4500 m. Later a second activation of this inflow resulted in production of gas over several days, after the hole had been refilled with drill mud. The gas phase released from this inflow was analysed after circulation out of the borehole.

Two different types of gas-bearing horizons can generally be distinguished. The first type includes dry inflows (i.e. without fluid) from graphite-bearing cataclastic shear zones down to a depth of about 3000 m, the second fluid-inflows frequently related to open pores and a prehnite-mineralisation appearing below 3000 m.

The dry inflows are characterized by their high radon-content. Significant values appear only here at 1445 m, 1530 m, 1960 m and 2416 m, as shown in Fig.C.2.7. The background decrease is caused by closing small inflows after the installation of the casing at 3003 m. The dry inflows are relatively hydrocarbon rich, whereas fluid-bearing inflows are helium rich (Fig.C.2.8). In addition the ratio between methane and ethane is much smaller at dry inflows (Fig.C.2.9). Between 1936 m and 1990 m the content of propane and butane exceeds normal background during the penetration of such a wide, graphite-bearing zone in a cataclastic gneiss (Fig.C.2.10).

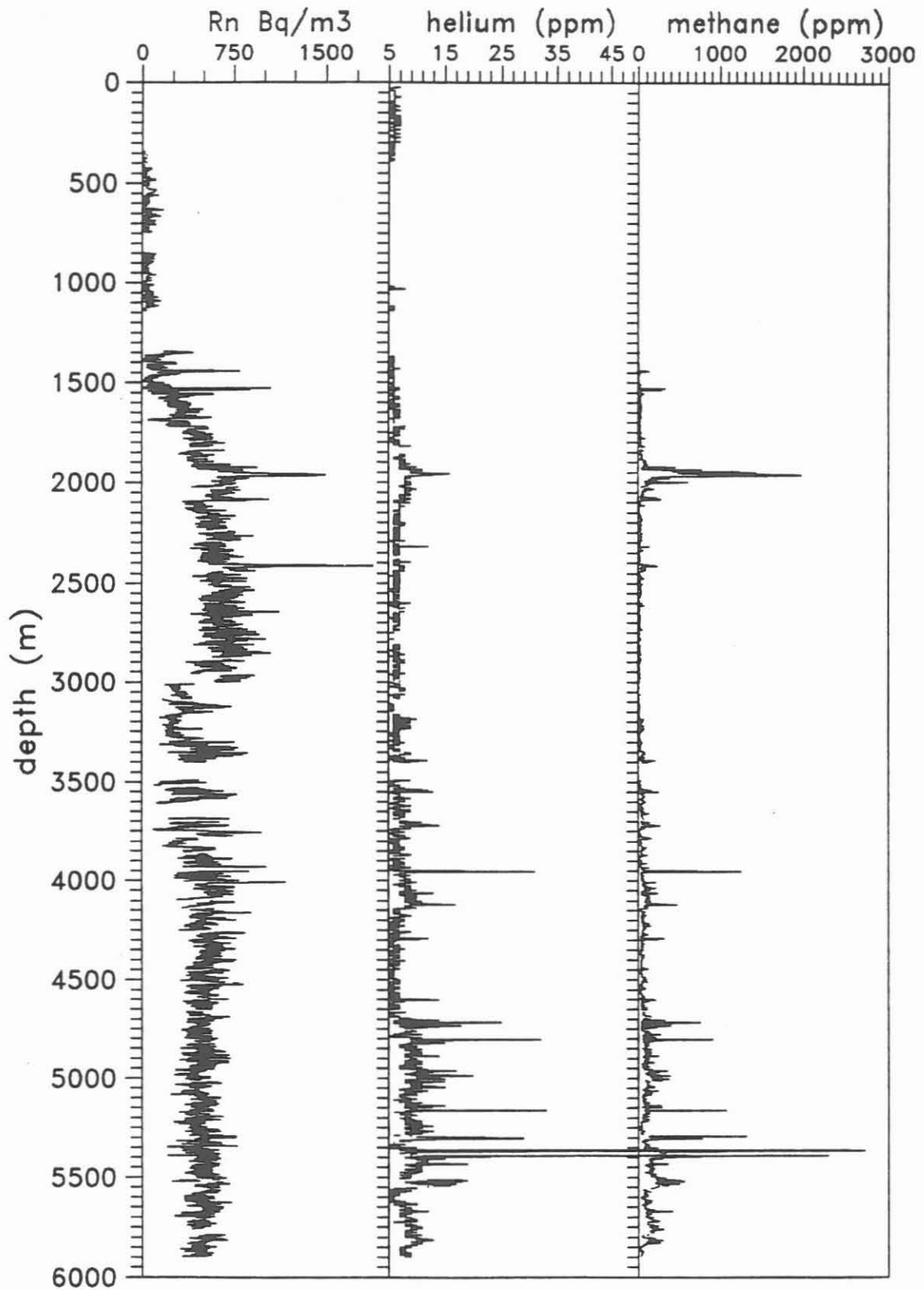


Fig.C.2.7: Variation of radon, helium and methane with depth



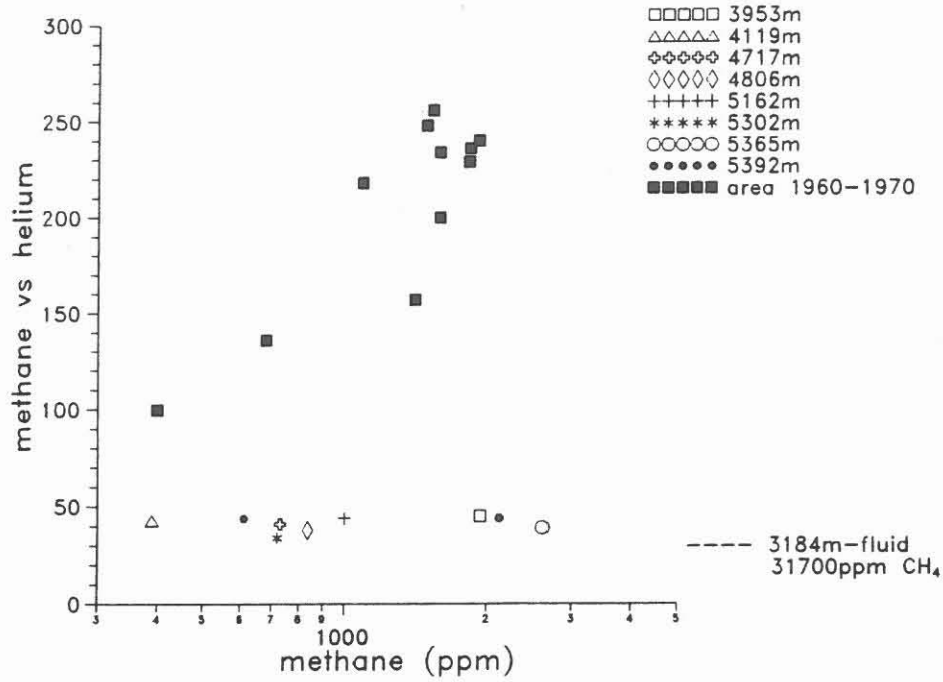


Fig.C.2.8: Characterization of distinct gas-bearing zones

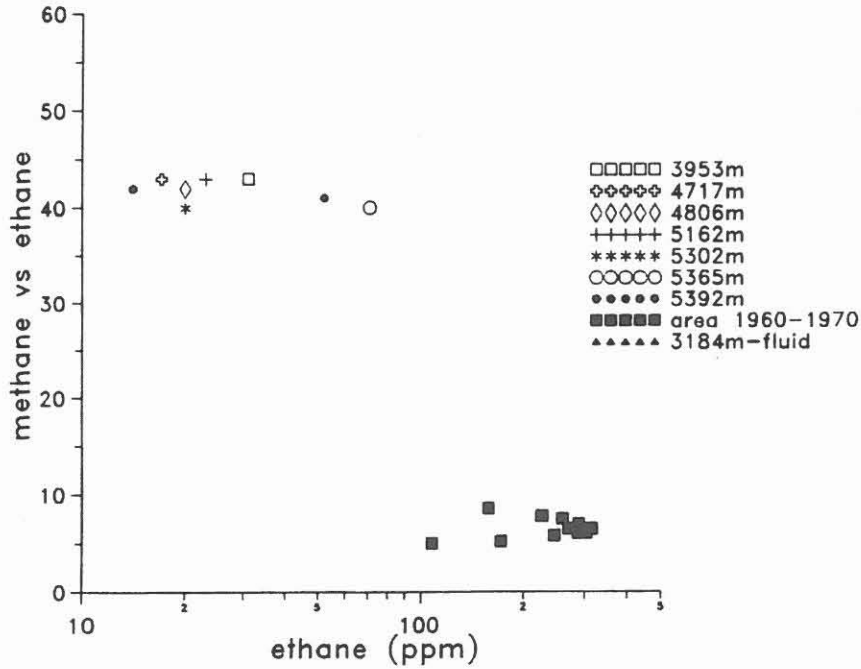


Fig.C.2.9: Distribution of different hydrocarbons in the gas-bearing zones

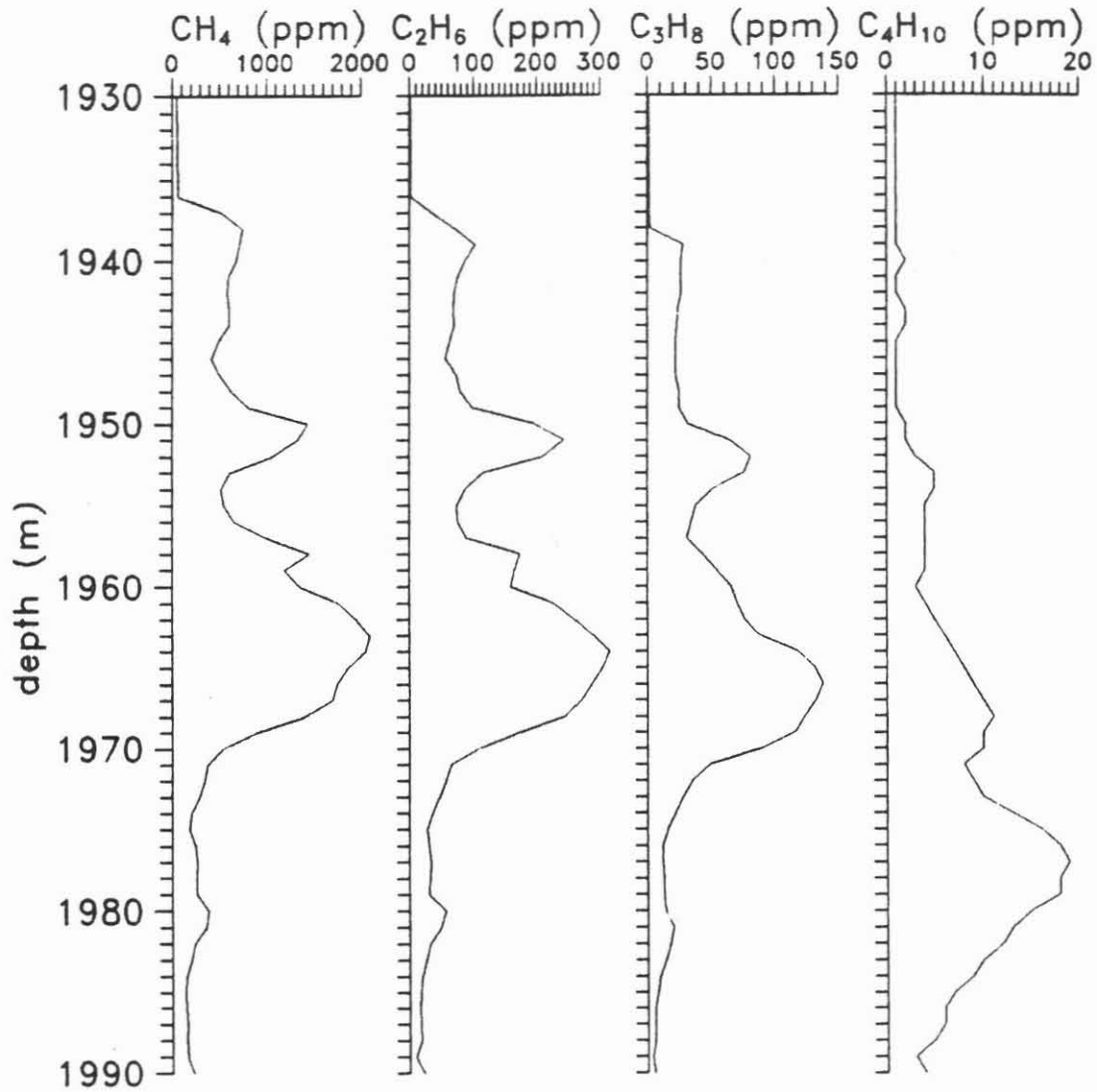


Fig.C.2.10: Content of hydrocarbones in the dissolved gas phase from an gas access in the graphite-bearing zone in a cataclastic gneiss between 1936 m and 1990 m.

In order to quantify the amount of accessed helium and methane injection test were carried out with defined quantities of both gases. Fig.C.2.11 shows the concentration distribution of helium released from the drill mud after several distinct injections, each injection lasting 5 minutes.

gas injection HB

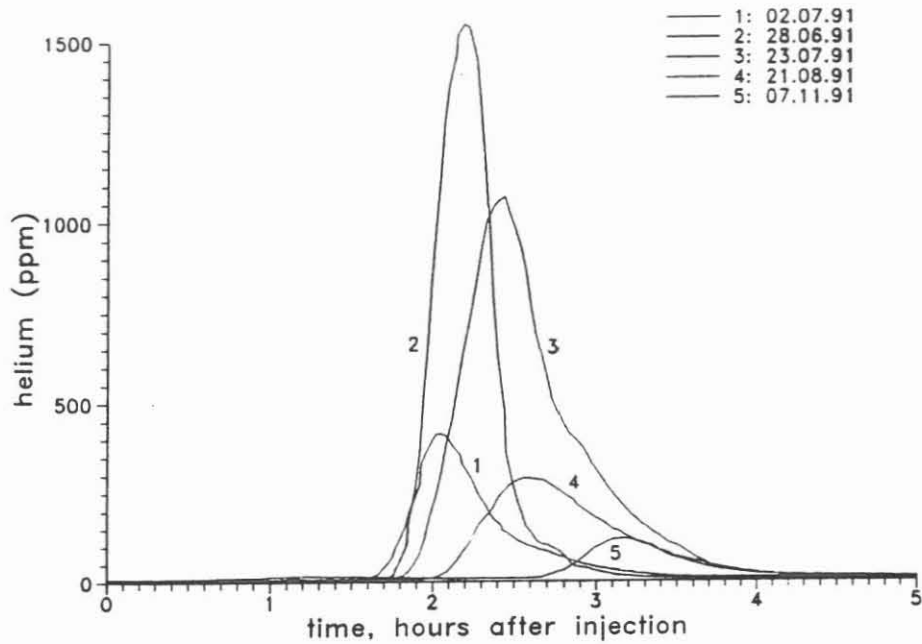


Fig.C.2.11: Concentration of dissolved helium conditioned by time after several distinct helium injections

The concentration distribution (i.e. peak form) and the maximum concentration depend on the fluid volume inside the gas trap. The peak area is proportional to the injected gas amount. Hence, on the basis of test injections, calibration curves could be established for helium and methane (Fig.C.2.12). Therefore its possible to quantify gas inflows detected by on-line-analysis. Detection limits for a fluid inflow of 5 minutes are 10ml helium and 100ml methane.

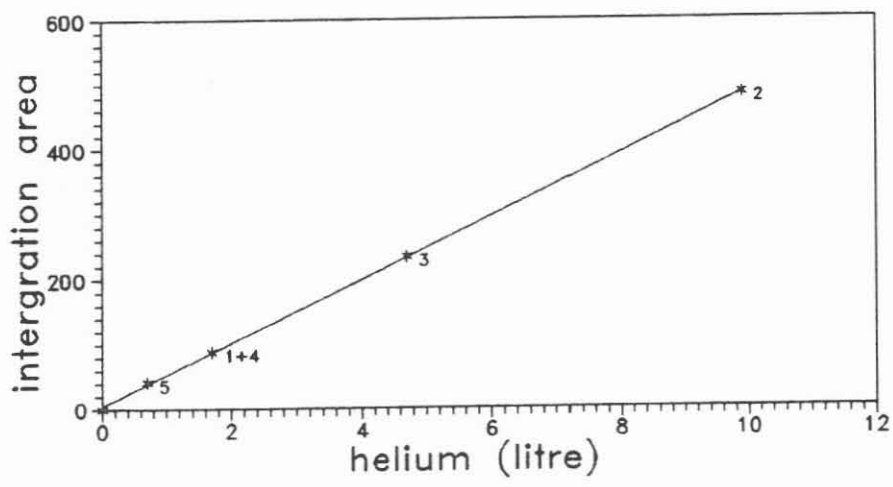


Fig.C.2.12: Helium calibration curve on the basis of injection tests

Table C.2.1 shows characteristics of the most important inflows determined by the just explained method. Quantities of the '3184 m fluid', activated on several occasions were also measured. A quantification of the inflows above 3000 m is not possible because of the late installation of the bypass system.

Table C.2.1: Quantities of helium and methane of the main accesses from below 3000 m.

Depth	CH <sub>4</sub> [ml]	He [ml]	CH <sub>4</sub> /He	Lithology ; fissure mineralization
3911 m	5160	120	43	Gnt-amphibolite ; prehnite, quartz
4119 m	16070	400	40	mixed layer amphibolite/Hbl-gneiss; prehnite
4717 m	12240	340	36	cataclastic amphibolite; epidote, quartz
4806 m	8690	215	40.4	cataclastic amphibolite; prehnite, epidote
5162 m	11540	295	39	Gnt-amphibolite ; prehnite
5302 m	16900	650	26	Mus-Bio-Chl-gneiss ; prehnite
5365 m	43320	1165	37	amphibolite ; prehnite
5392 m	20290	530	38	cataclastic amphibolite ; prehnite, calcite
5398 m	5190	125	41.5	
3184m fluid	300 litre	8 litre	38	amphibolite; epidote,prehnite,quartz

The amount of gases entering the borehole tend to increase with increasing depth. The two inflows at 5392 m and 5398 m have to be taken as one because they are two maxima of a permanent inflow in this zone.

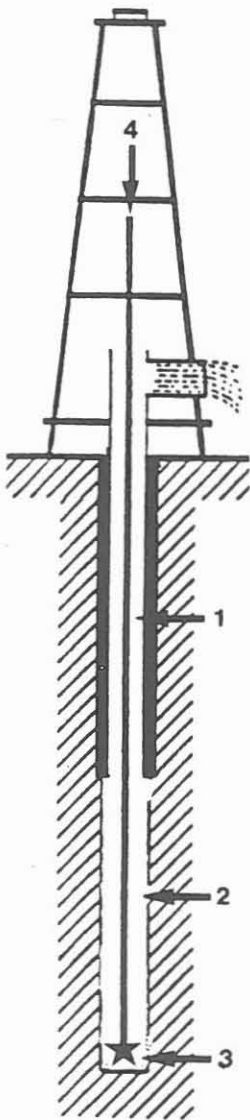
The methane/helium-ratio of all quantified inflows varies between 36 and 43. This corresponds to the methane/helium-ratio of the '4000 m fluid' produced during the pump-test at the pilot hole. Only the inflow detected at 5302 m shows a significantly lower methane/helium-ratio.

Quantification of the '3184 m fluid'(the only tripgas analysis in table C.2.1) shows good agreement to the '4000 m fluid'. Accordingly there is an almost equal methane/helium-ratio. The ratio of the determined quantity of helium (8 litre) to the quantity of the accessed fluid (about 2000 litre) also agrees with the relations at the '4000 m fluid'(KTB Report 90-8).

### C.2.3.3 Quantification of gases dissolved in drill mud

With the on-line device in operation at the KTB-Hauptbohrung it is difficult, due to "air contamination" of the drill mud, to quantify nitrogen and oxygen as well as smaller amounts of gases entering the borehole. However, by completely degassing drill mud samples drawn before being pumped into the borehole and after one circulation at the outflow line quantification of these gases is possible. Figure C.2.13 shows borehole sections where gases are produced artificially or enter the borehole from the wall-rock.

Table C.2.2 presents gas amounts (Gas ml [STP]/1000 ml drill mud) dissolved in samples taken during roundtrips and during drilling. During roundtrips gases entering the borehole from surrounding rocks are collected in the drill mud. After restarting fluid circulation, drill mud from different depth sections could be sampled.



In trip gases from section 1 the oxygen content and relatively high hydrogen content is due to a reaction with the iron-casing. In the open drillhole (section 2), the oxygen amount detected in the drill mud is, in comparison to section 1, higher as a result of minor ox. - red. processes.

Trip gases from freshly drilled bottomhole (section 3) show higher contents of nitrogen, methane and helium.

The gas content in the drill mud, before being pumped into the borehole (section 4), shows that the drilling fluid is nearly equilibrated with air. However the oxygen concentration at this stage is lower, due to the reactions in the borehole with graphite, sulfides and ferrous iron as well as the iron casing and drill pipe. The time in the mud tanks, i.e. under atmospheric conditions, is too short to allow for complete reequilibration. Gas contents in drill mud samples, taken during drilling, show, in addition to higher nitrogen, methane and helium, enhanced hydrogen amounts pointing to an artificial generation during the drilling process.

A few samples were taken during drilling at 45 minute intervals. Sample 1 (11:00) and 3 (12:30) from 23.7.91 show only a weak enrichment in nitrogen, methane and helium. However, concentrations of these gases were higher in sample 2 (11:45), thus indicating that this sample originated from a gas-enriched borehole section. This section must be a relatively small zone, as penetration took, at the most, 1 hour.

Sample 4 (16.11.91, 14:00) also shows a stronger enrichment of nitrogen, methane and helium, compared to sample 5 (14:45) and 6 (15:30). This observation also refers to penetration of the small inflow zone at 14:00.

The gas ratios of the gasphase entering from wall-rock correspond with those observed during high temperature vacuum extraction from rocks of the KTB pilot hole (ERZINGER et al., 1991).

Fig. C.2.13

Tab.C.2.2: Dissolved gas amounts (Gas ml [STP]/1000ml drill mud)

1. Roundtrip gases from 03.10.91 depth 4447m (Amphibolite)

gases	section 1 in the casing	section 2 open borehole	section 3 bottom- hole	section 4 before being pumped down
N <sub>2</sub>	10.85	11.32	14.26	10.98
O <sub>2</sub>	0.16	0.93	1.58	3.35
Ar	0.17	0.17	0.17	0.17
CH <sub>4</sub>	1.74*10 <sup>-3</sup>	4.21*10 <sup>-3</sup>	28.31*10 <sup>-3</sup>	1.01*10 <sup>-3</sup>
H <sub>2</sub>	0.038	0.022	0.027	0.016
He	3.40*10 <sup>-5</sup>	1.67*10 <sup>-4</sup>	12.55*10 <sup>-4</sup>	1.50*10 <sup>-5</sup>

2. Drill gas from 23.07.91 depth 3600m (Aplite with 10% Gnt-amphibolite, cataclastic)

gases	sample 1 (11:00h)	sample 2 (11:45h)	sample 3 (12:30h)	before being pumped down
N <sub>2</sub>	10.81	13.50	10.76	10.66
O <sub>2</sub>	2.87	2.93	3.01	3.19
Ar	0.17	0.17	0.17	0.17
CH <sub>4</sub>	2.18*10 <sup>-3</sup>	19.1*10 <sup>-3</sup>	5.7*10 <sup>-4</sup>	0.2*10 <sup>-3</sup>
H <sub>2</sub>	0.048	0.047	0.036	0.01
He	1.57*10 <sup>-4</sup>	9.37*10 <sup>-3</sup>	8.33*10 <sup>-5</sup>	3.7*10 <sup>-5</sup>

3. Drill gas from 16.11.91 depth 4925m (Gnt-amphibolite/Bio-Hbl-gneisses)

gases	sample 4 (14:00h)	sample 5 (14:45h)	sample 6 (15:30h)	before being pumped down
N <sub>2</sub>	14.26	11.21	11.42	11.14
O <sub>2</sub>	2.87	3.02	2.32	3.19
Ar	0.17	0.17	0.17	0.17
CH <sub>4</sub>	13.81*10 <sup>-3</sup>	0.63*10 <sup>-3</sup>	1.55*10 <sup>-3</sup>	0.31*10 <sup>-3</sup>
H <sub>2</sub>	0.077	0.058		0.028
He	9.18*10 <sup>-4</sup>	4.10*10 <sup>-5</sup>	1.29*10 <sup>-4</sup>	1.40*10 <sup>-5</sup>

#### C.2.4 Conclusions

The drill mud is highly contaminated by air and artificially generated hydrogen.

The detection limit of on-line-analysis is about 10 ml helium and 100 ml methane for a fluid inflow of 5 minutes.

Two different types of gas accesses could be detected,

- dry accesses with comparatively high hydrocarbon- and radon-contents from graphite-bearing cataclastic shear zones reaching down to a depth of about 3000 m.
- nitrogen-, methane- and helium-rich fluids related to open pores and hydrothermal mineralizations below 3000 m, corresponding to the 4000 m - fluid collected during the pump test out of the pilot hole.

The average volume of fluid inclusions in the ground basement rocks is not sufficient to explain the amount of inflows entering the borehole, thus, open fissures must be responsible.

Activation of inflows is possible by lowering the drill mud level, i. e. the hydrostatic pressure inside the borehole.

Drill mud which is pressed into fissures during drilling pours back into the borehole when the drill mud level is decreased, as demonstrated by the fluid sample taken from 5388 m where an increased temperature had been measured.

Therefore these inflows are thought to be produced by open fissure systems under hydrostatic pressure.

## **C.3 GEOCHEMICAL INVESTIGATIONS OF SOLIDS**

### **C.3.1 Sample preparation**

Cuttings and rock flour samples (50-100g) were taken at intervals of 1m and analyzed for every second meter. The samples were dried at 105 C and powdered in a tungsten carbide ball mill for 30 minutes. The powder was then pressed into standardized pellets which were used for both XRD and XRF measurements.

For core material investigations (below 4150m) core pieces or plugs were available. The core material was crushed in a tungsten carbide jaw breaker and then handled in the same way as the cuttings and the rock flour.

Cuttings and rock flour make up the main parts of samples available. Because within these samples contamination, dispersion, delay and mixing can occur, there might be some systematic changes in the composition of the actually drilled rocks and the sample material. A proper investigation of the mineralogical and geochemical data becomes sometimes difficult. (See also chapter D in this issue)

### **C.3.2 Methods**

#### **C.3.2.1 Mineralogical phase analysis**

The mineralogical qualitative and quantitative phase analysis is performed by X-ray diffraction using a SIEMENS D500 diffractometer. The routine procedure was developed in the primary stages of the KTB-Pilot-Hole and used during pilot drilling. The main parts of the procedure are a special mineral-database, including approximately 250 mineral phases separated from various kinds of igneous and metamorphic rock types, and a software-program with full automatic qualitative and quantitative phase analysis. As a rule the detection limit of this method lies somewhat between 1 and 3 wt.-%. A detailed description of the whole procedure is given by Emmermann and Lauterjung (1990).

#### **C.3.2.2 Determination of major and trace elements**

For analysis of major and trace elements a fullautomatic and computersupported SIEMENS 303 AS X-ray-fluorescence-spectrometer is used. The routine measurements includes 11 main constituents ( $\text{SiO}_2$ ,  $\text{TiO}_2$ ,  $\text{Al}_2\text{O}_3$ ,  $\text{Fe}_2\text{O}_3$  total, MnO, MgO, CaO,  $\text{Na}_2\text{O}$ ,  $\text{K}_2\text{O}$ ,  $\text{P}_2\text{O}_5$ , S) and 12 trace elements (Sr, Rb, Y, Zr, Nb, Cr, Ni, Zn, V, Cu, Th, U). The total measurement time takes about 40 minutes for each sample. Measurements of international reference rock as unknowns yield relative standard derivations smaller than 1%.



### C.3.3 Results

Selected minerals (amphibole, biotite, chlorite, garnet, epidote and prehnite) and different geochemical parameters have been plotted in detail together with the geological cutting profile (see chapter B.4 in this issue). These parameters have been chosen, because their concentration is very sensitive to changes in lithology.

High concentrations of amphibole, MgO and Ni are characteristic for the metabasites. Furthermore increased Ni contents (up to 305 ppm) may indicate some ultramafic intercalations within the amphibolite sequences.

In general the paragneisses possess higher SiO<sub>2</sub> and K<sub>2</sub>O contents than the amphibolites. The highest K<sub>2</sub>O concentrations were observed within the muscovite-biotite gneisses.

A comparison of biotite and chlorite contents allows the estimation of alteration.

Finally the methane contents is shown in detail, because it is the most sensitive parameter for gas in flow into the borehole (for detailed explanation see chapter C.2 in this issue).

In the depth range from about 2000-3100m the high Zn concentrations in the cutting material are mainly caused by fine abrasion of the Zn-silicate coated drill-stem.

The Ca- and Sr-peak at 3000m depth cohere with drill out of the cementing shoe.

A plot which shows all geochemical parameters is given in the table C.6.2.1 - 6 of this chapter. For further information on single geochemical data see also the KTBASE (KTB-Database).

The mineralogical composition of the paragneisses measured by XRD partly differ from the nomenclature used for the rock. This can be explained by the methodological difference between the cutting-determination under the binocular and XRD-analysis.

With the binocular the still visible original paragenesis will be defined while XRD-analysis gives the actual mineral composition. Typical are transformations of biotite to chlorite and plagioclase or sillimanite to sericite.

Therefore minerals which are part of the name of the rock like sillimanite, kyanite, biotite or garnet are below detection limit (1 to 3 wt.-%).

### C.4 Acknowledgements

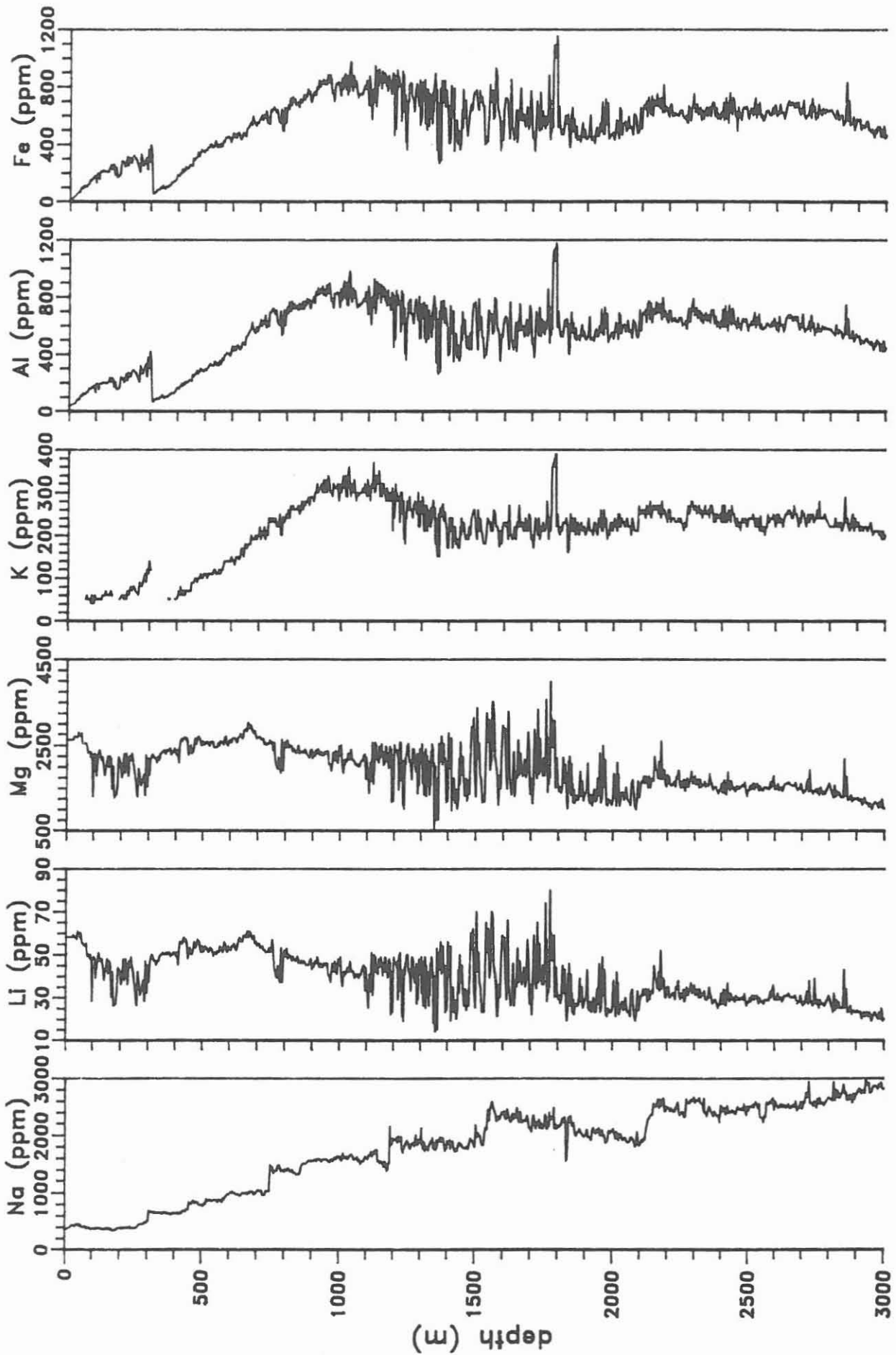
We gratefully acknowledge our technical employees Miss. S. Donner, Miss. I. Hermann, Miss. S. Giersch, Mr. M. Brückner and Mr. S. Lang for their support and dedication. We would like to thank Prof. Dr. R. Emmermann, Dr. J. Lauterjung and Miss. M. Lavin for their constructive comments and reviewing of this paper.

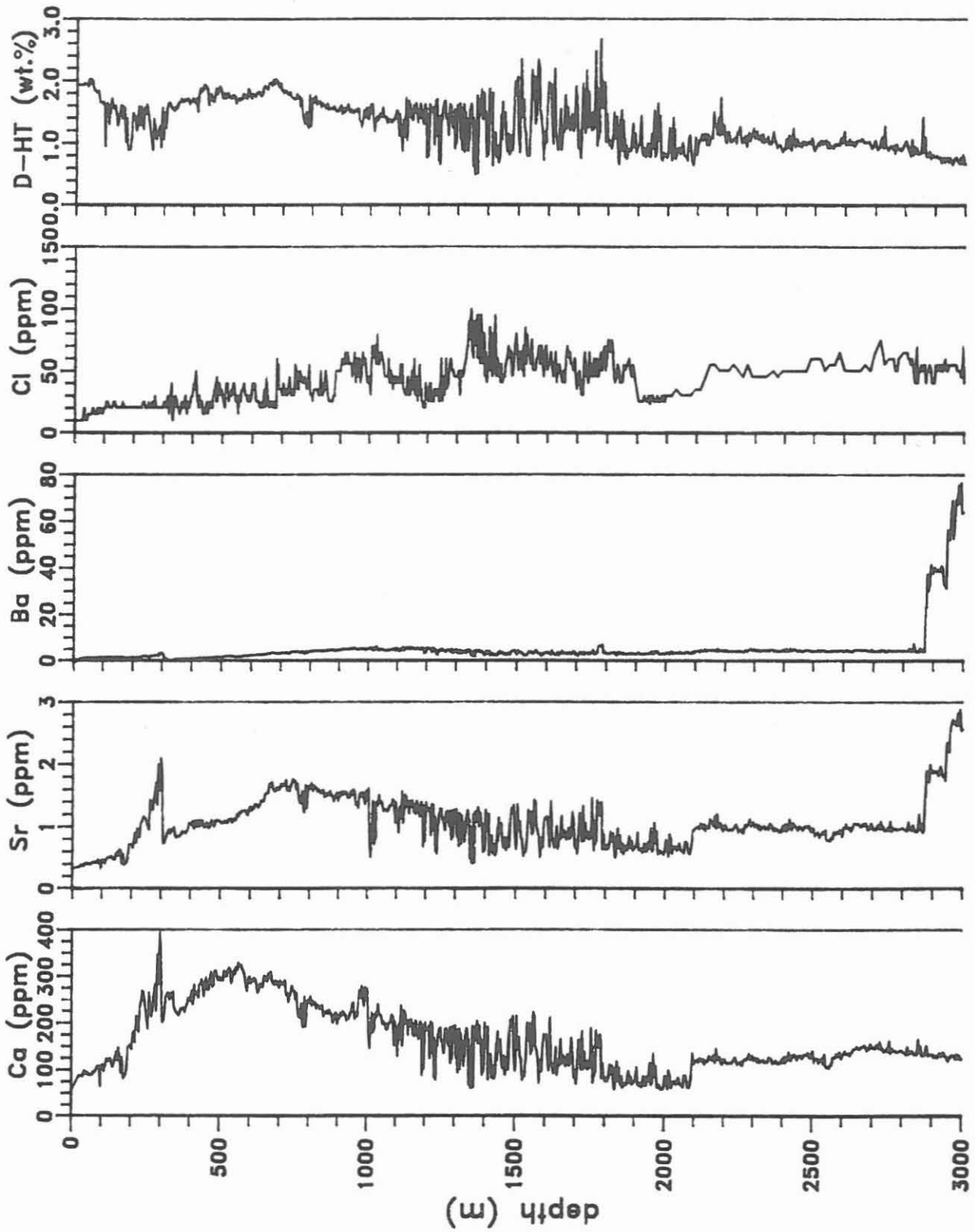
## C.5 REFERENCES

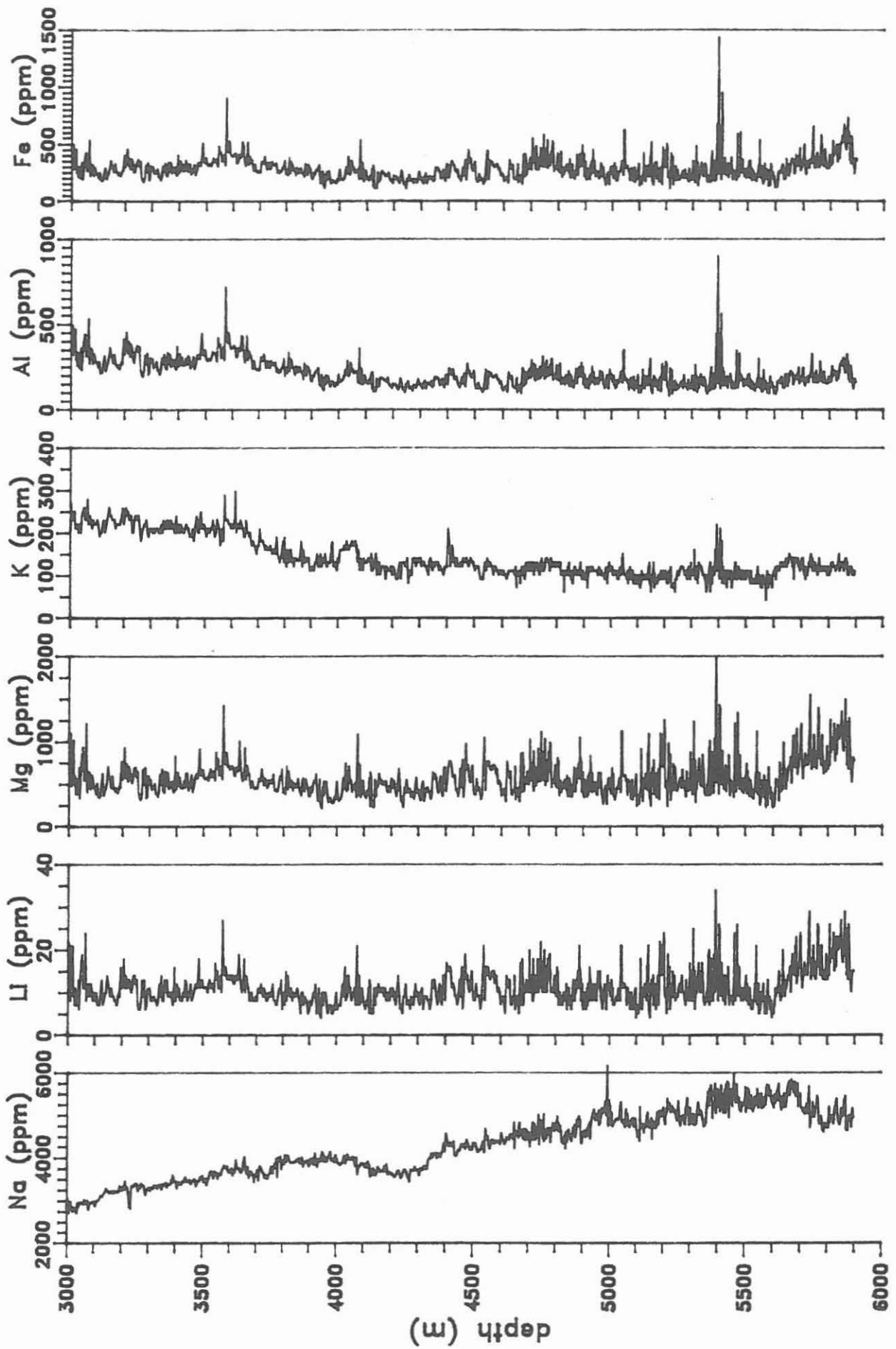
- ERZINGER, J., ZIMMER, M., FIGGEMEIER, CH., SAMEL, M. & HEINSCHILD, H.J. (1991):** Zur Geochemie von Gasen in Krustengesteinen, Formationsfluiden und Bohrspülung - Ergebnisse aus der KTB-Vorbohrung. - In: EMMERMANN, R., LAUTERJUNG, J. (Hrsg.): KTB-Report, 91-1:393-422, Hannover.
- FIGGEMEIER, CH., HANSMANN, J., HEINSCHILD, H.J. & KAMM, H.:** Tiefbohrung KTB-Oberpfalz HB, Ergebnisse der geowissenschaftlichen Bohrungsbearbeitung im KTB-Feldlabor (Windischeschenbach), Teufenbereich von 0m-1720m.- In: EMMERMANN, R., DIETRICH, H.-G., LAUTERJUNG, J., WÖHRL, T. (Hrsg.): KTB-Report 91-3: C1-C41, Hannover.
- HEINSCHILD, H.J., HOMANN, K.D., STROH, A. & TAPFER, M. (1988):** Tiefbohrung KTB-Oberpfalz VB, Ergebnisse der geowissenschaftlichen Bohrungsbearbeitung im KTB-Feldlabor (Windischeschenbach), Teufenbereich von 480m bis 992m. - In: EMMERMANN, R., DIETRICH, H.-G., HEINISCH, M., WÖHRL, T. (Hrsg.): KTB-Report, 88-2: C1-C107, Hannover.
- HEROLD, C.-P., MÜLLER, H., von TAPAVICZA, S. (1987):** A New High Temperature Stable Mud Additiv for Geological and Deep Drilling Operations. Third International Symposium on Deep Drilling in Crystalline Bedrock. Mora, Sweden 1987.
- HOMANN, K.D. & MÜLLER, H. (1989):** Wechselwirkung zwischen Dehydrit-HT Bohrspülung und Gesteinsmehl. Tiefbohrung KTB-Oberpfalz VB, Ergebnisse der geowissenschaftlichen Bohrungsbearbeitung im KTB-Feldlabor (Windischeschenbach), Teufenbereich von 1709m bis 25000m. - In: EMMERMANN, R., DIETRICH, H.-G., HEINISCH, M., WÖHRL, T. (Hrsg.): KTB-Report, 89-1: F1-F45, Hannover.
- STROH, A., HEINSCHILD, H.J., HOMANN, K.D. & TAPFER, M. (1988):** Tiefbohrung KTB-Oberpfalz VB, Ergebnisse der geowissenschaftlichen Bohrungsbearbeitung im KTB-Feldlabor (Windischeschenbach), Teufenbereich von 992m bis 1530m. - In: EMMERMANN, R., DIETRICH, H.-G., HEINISCH, M., WÖHRL, T. (Hrsg.): KTB-Report, 88-6: C1-C109, Hannover.
- STROH, A., HANSMANN, J., HEINSCHILD, H.J., HOMANN, K.D., TAPFER, M., WITTENBECHER, M., ZIMMER, M.:** Drill hole KTB Oberpfalz VB, Geoscientific Investigations in the KTB-Field-Laboratory, Depth interval 0-4000.1m. - In: EMMERMANN, R., DIETRICH, H.-G., LAUTERJUNG, J., WÖHRL, TH. (Hrsg.): KTB-Report, 90-8: C1-C37, Hannover.
- ZIMMER, M., ERZINGER, J. & HEINSCHILD, H.J. (1990):** Ergebnisse der gasanalytischen Untersuchungen an der KTB-Bohrspülung. - In: EMMERMANN, R. & GIESE P. (Hrsg.), KTB-Report, 90-4: 57-64, Hannover.

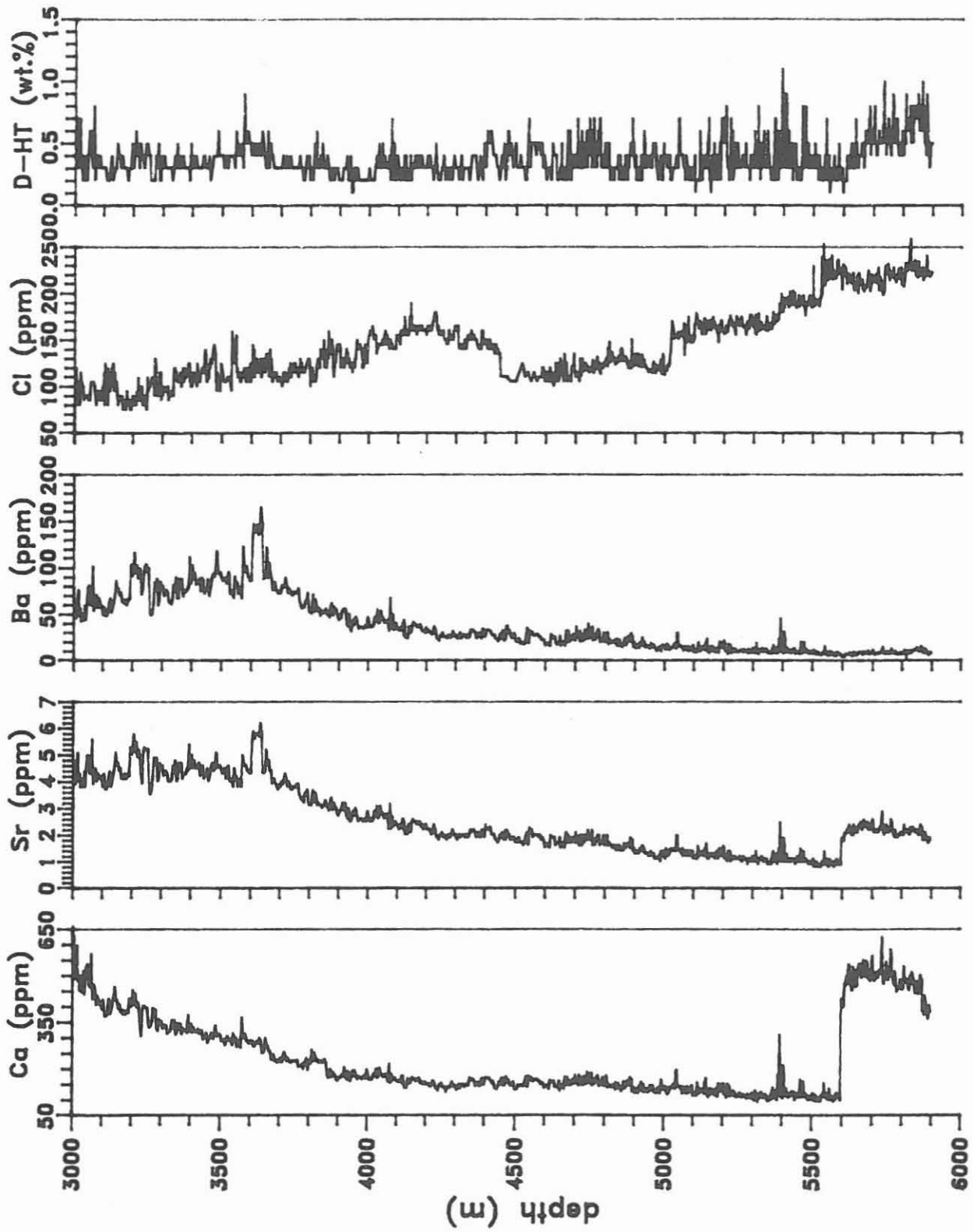
C.6 Appendix

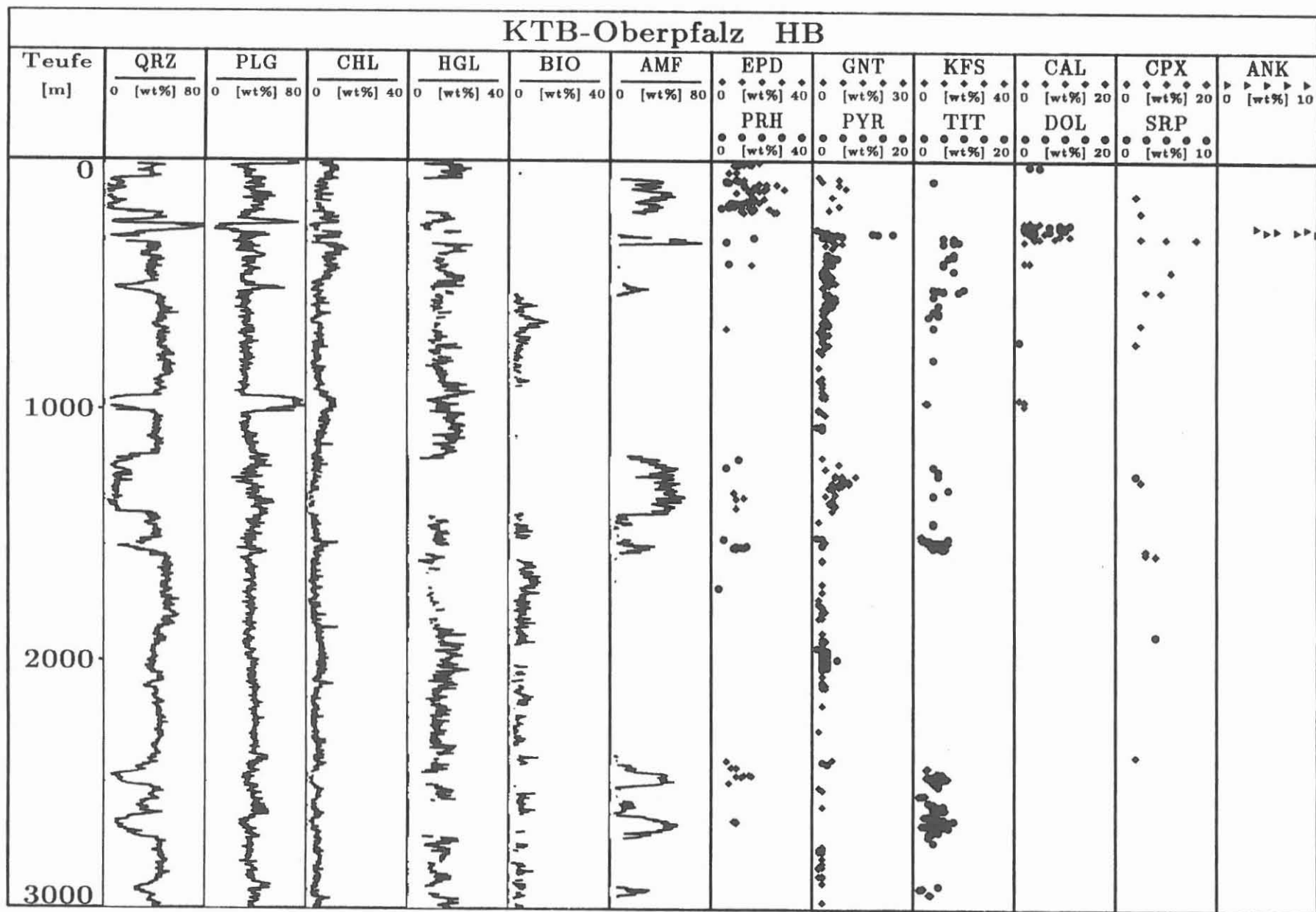
C.6.1 Results of cation and anion analysis



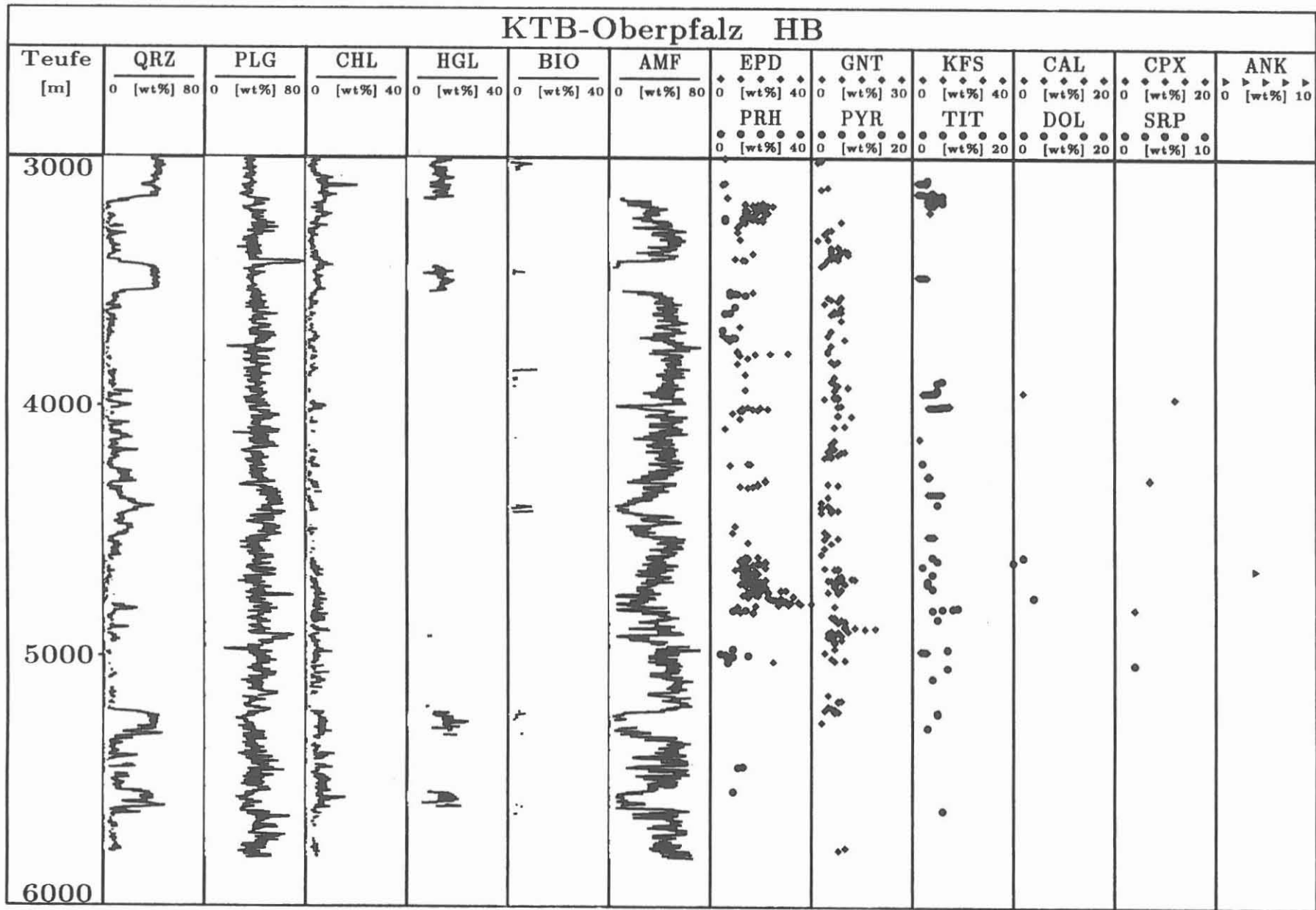






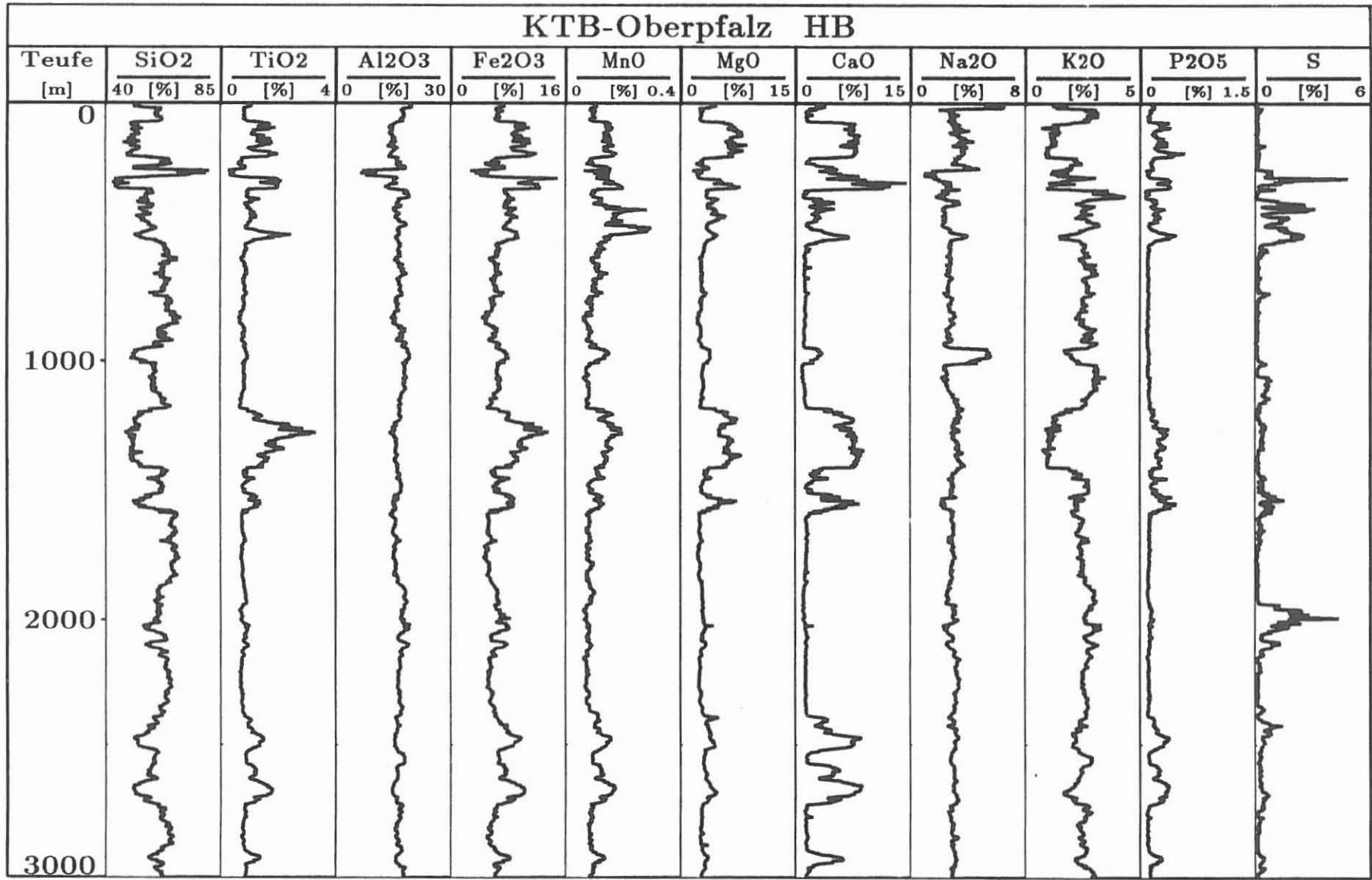


C.6.2.1 Overview of the mineralogical composition of the cutting analyses in the depth range 0m-3000m.

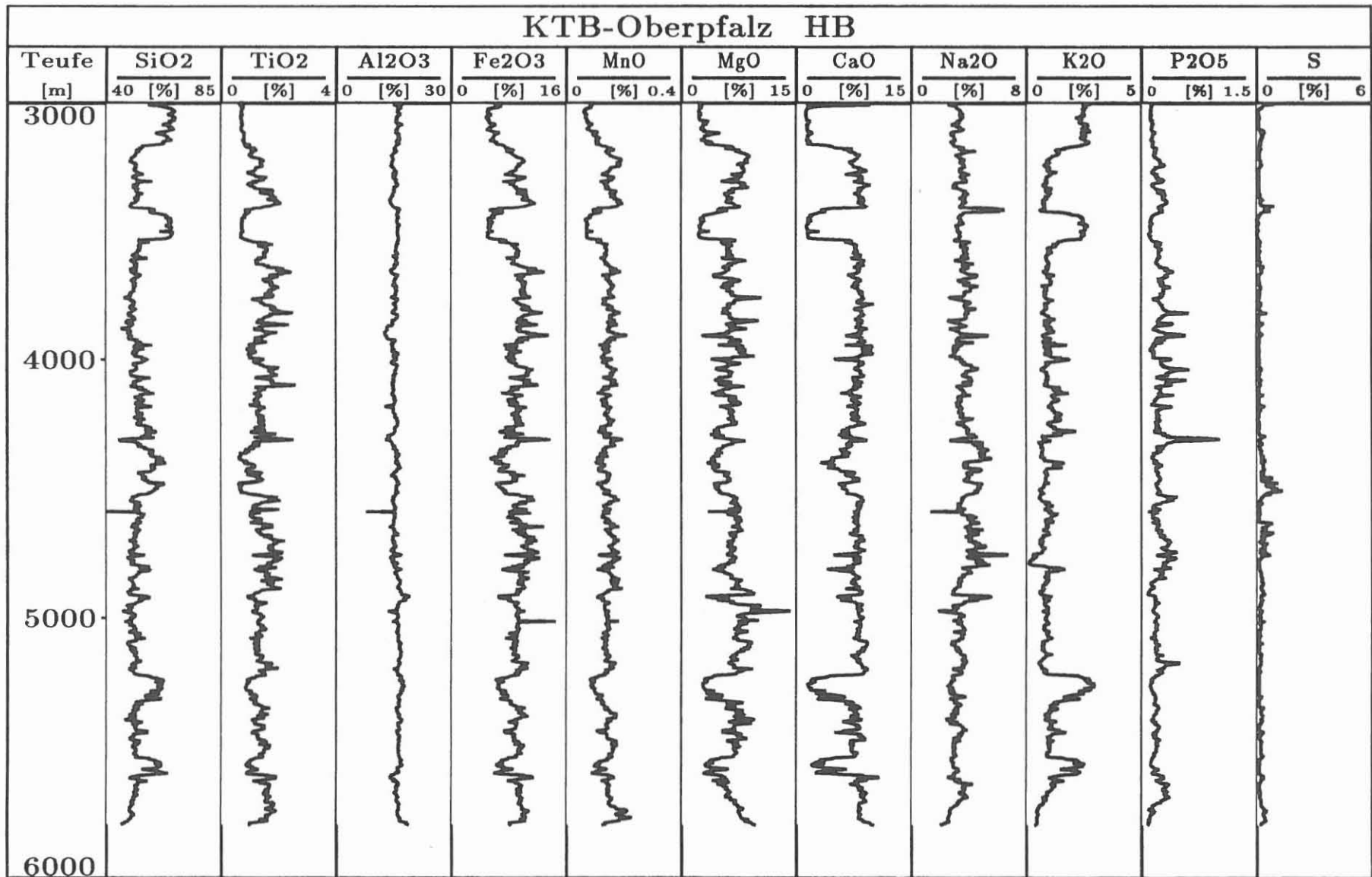


C.6.2.2 Overview of the mineralogical composition of the cutting analyses in the depth range 3000m-6000m.

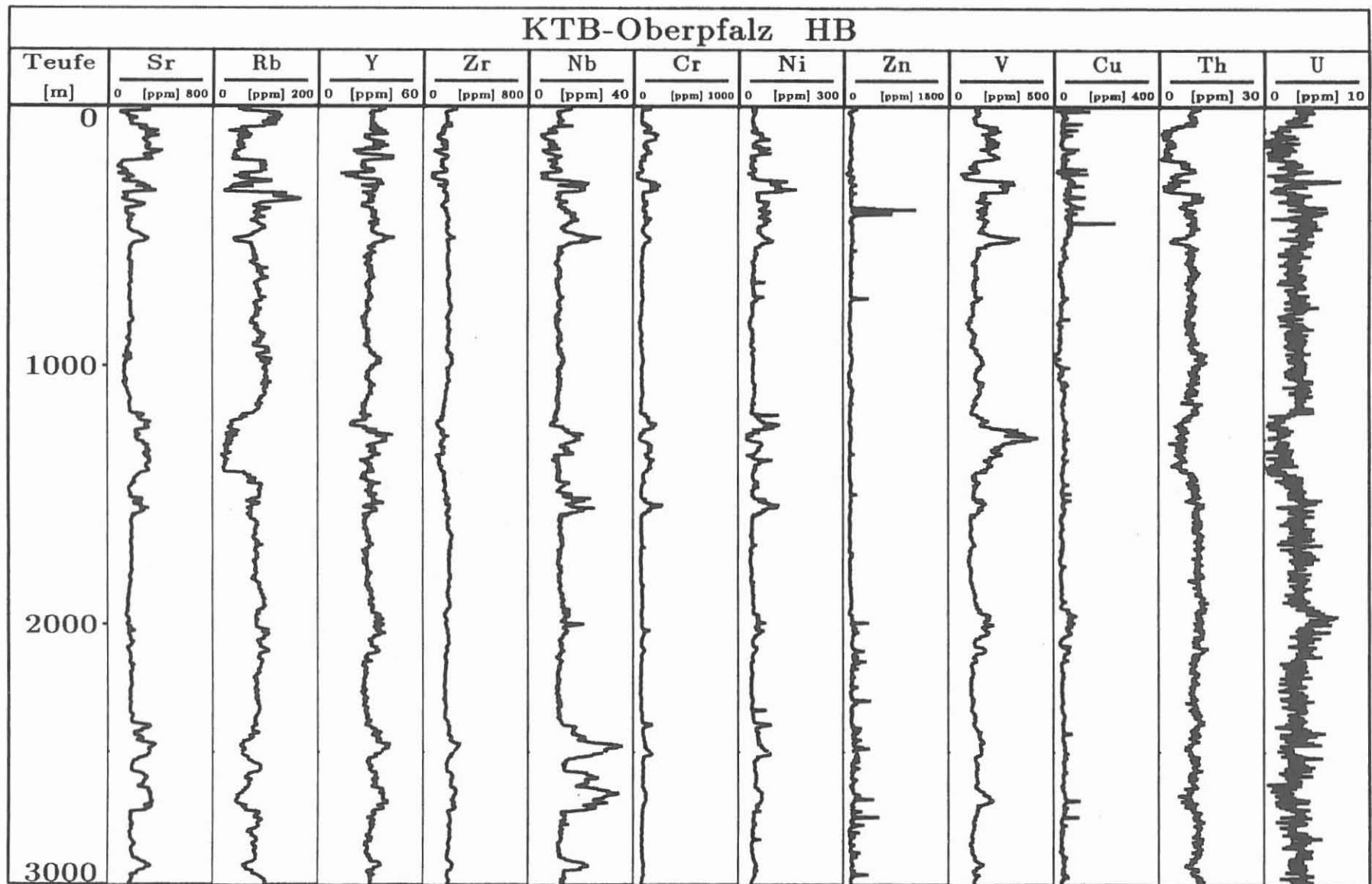




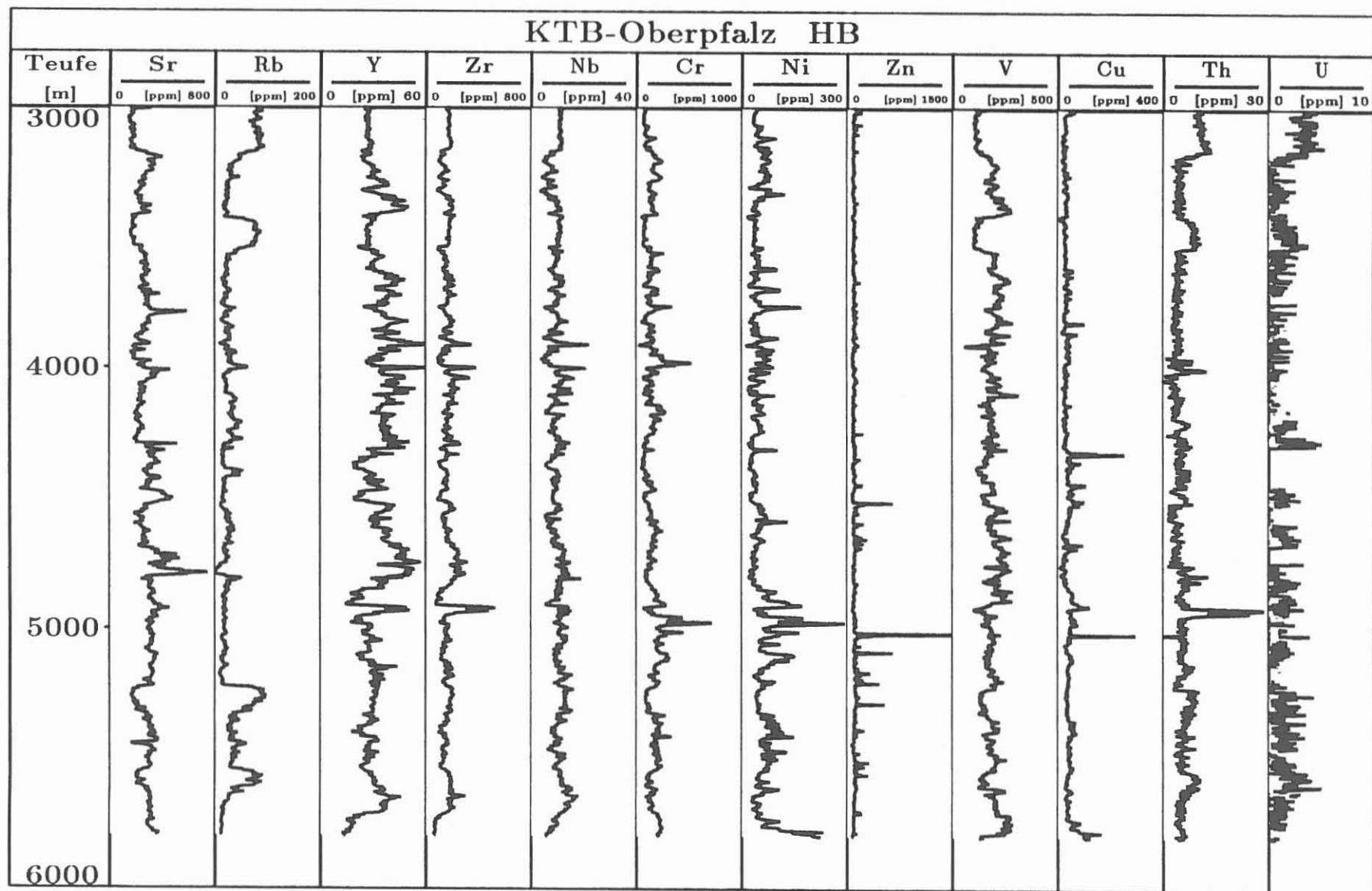
C.6.2.3 The chemical main constituents of cuttings in the depth range 0m-3000m



C.6.2.4 The chemical main constituents of cuttings in the depth range 3000m-6000m



C.6.2.5 Trace element composition of cuttings in the depth range 0m-3000m



C.6.2.6 Trace element composition of cuttings in the depth range 3000m-6000m

KTB REPORT	92-2	6 Pages	3 Figures	Hannover 1992
------------	------	---------	-----------	---------------

## C.7 On-line Determination of <sup>222</sup>Radon in Drilling Fluids of the KTB Hauptbohrung

Erzinger, J.\*), Hansmann, J., Kamm, H. and Heinschild H.J.\*\*)

C.7.1 Introduction.....	C40
C.7.2 Radon in the KTB drilling fluid.....	C41
C.7.3 Radon-measuring assembly.....	C42
C.7.4 Results from the KTB Hauptbohrung.....	C43
C.7.5 References.....	C45

Authors address:

\*) Institut für Geowissenschaften und Lithosphärenforschung  
Justus-Liebig Universität  
Senckenbergstr. 3  
W-6300 Gießen

\*\*\*) KTB Feldlabor  
W-8486 Windischeschenbach

### C.7.1 Introduction

Radon is a radioactive noble gas, occurring naturally in three important isotopes, as  $^{222}\text{Rn}$  (half-life 3.84 d) from the  $^{238}\text{U}$  decay series, as  $^{220}\text{Rn}$  ( $t_{1/2}=55$  sec) from the  $^{232}\text{Th}$  decay series and as  $^{219}\text{Rn}$  ( $t_{1/2} = 3.9$  sec) from the  $^{235}\text{U}$ -decay series. These isotopes are generated continuously in rocks and minerals as a result of the decay of  $^{226}\text{Ra}$ ,  $^{224}\text{Ra}$  and  $^{223}\text{Ra}$ . Because of its considerable long lifetime only the isotope  $^{222}\text{Rn}$  (radon) can travel over long distances in rocks and ground waters and has any geochemical significance. Therefore this paper deals only with  $^{222}\text{Rn}$ . Finally radon decays via  $^{218}\text{Po}$  ( $\alpha$ ) to  $^{214}\text{Po}$  ( $\beta$ ) (Fig.C.7.1). Part of this radon escapes from rocks and minerals into the surrounding fluid phase, i.e. formation water or the atmosphere (emanation).

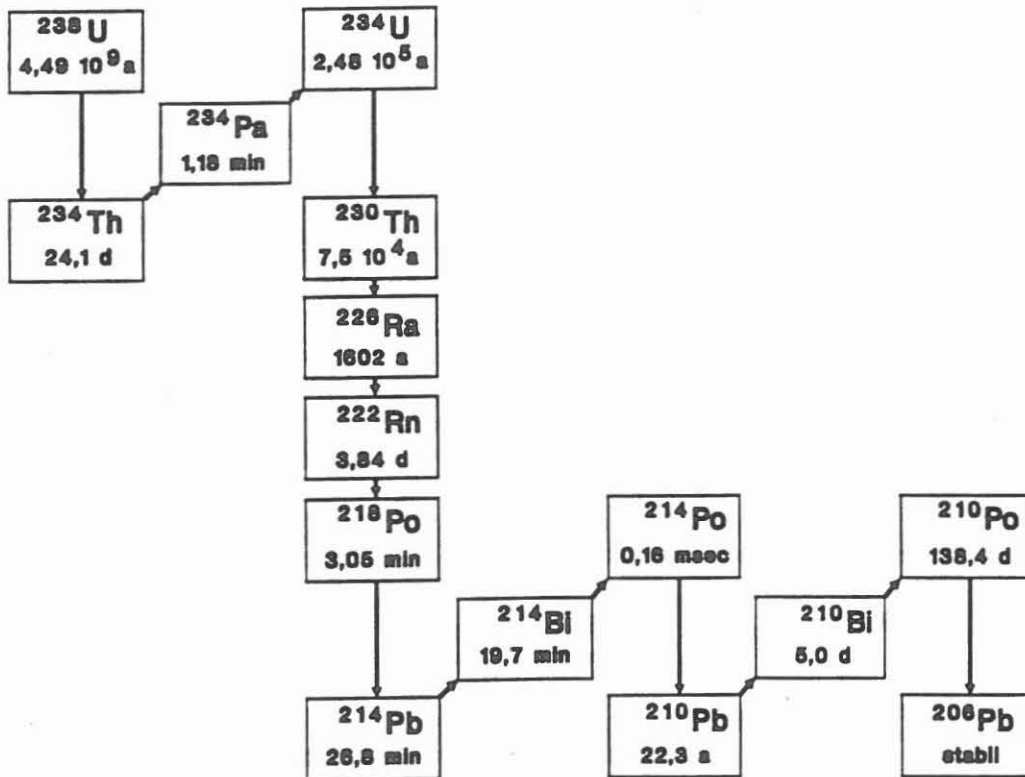


Fig.C.7.1: Scheme of  $^{238}\text{U}$  decay

Mobility and rate of diffusion of radon is relatively high in comparison to all other gases and noble gases. Although only very few detailed investigations on the mechanism of this increased mobility of radon are available, it has, in the meantime, been proven that the radon mobility depends on 1) the recoiling effect, i.e. an energy-rich impulse which the radon obtains "at birth" from  $^{226}\text{Ra}$  and 2) the fact that the mother nuclides  $^{238}\text{U}$  and  $^{226}\text{Ra}$  are especially enriched on grain boundaries.

In order to explain the increased mobility of radon, some authors are of the opinion that a nanopore network inside rock-forming minerals cuts through the mineral surface thus producing pathways for the gases. Because this net-like surface covers many square meters per cubic centimeter the radon mobility could perhaps herewith be explained (Rama & Moore 1984).

More recent investigations have shown that especially the inhomogeneous distribution of radium in minerals, i.e. enrichments on the grain boundaries could be responsible for the high emanation rates of radon (Krishnaswami & Seidemann, 1988). In addition the radiation damage of crystal lattices caused by the mother nuclides are most probably of great importance.

The occurrence of gaseous decay products with high mobility within the  $^{238}\text{U}$  and  $^{232}\text{Th}$ -decay series and the relatively good solubility of radon in fluids, could play an important role in the occurrence of secular unequillibriums within these decay series. This could perhaps explain the discordant U/Pb distribution and the difference between U/Pb and K/Ar age values in the zircon/biotite-system (Suzuki, 1987).

Natural  $^{222}\text{Rn}$  concentrations in the atmosphere vary between 2 - 20 Bq/m<sup>3</sup>, in river water they average 0.05 Bq/l and in sea water the concentration of radon is very low with only 0.03 mBq/l. Formation and spring water which have been in contact with radon releasing rocks, can however, contain high quantities of radon up to 40 Bq/l or even as much as 2kBq/l in radon spas.

During or shortly before earthquake activities, significantly increased radon concentrations have been found worldwide in ground waters and natural gases. An increase in the radon emanation rate has also been observed with tectonic stress changes. Nowadays worldwide radon measurements can help with the better prediction of earthquakes (Fleischer & Mogro-Campero, 1985).

### **C.7.2 Radon in the KTB Drilling Fluid**

In order to obtain a better understanding of the mobility and geochemistry of radon, samples of drilling mud were collected during the pilot phase of the KTB and examined for radon. In cooperation with Prof. Brandt's working group (Marburg), a simple  $\alpha$ -track method for the quantitative determination of  $^{222}\text{Rn}$  in water was adapted for analysis of the drilling mud in the KTB (Haase et al., 1988, Zhao et al., in print).

Increased radon concentrations in the drilling mud of the KTB pilot hole (KTB VB) could clearly be correlated to fluid inflow zones or trip gas enrichments. Most of the radon concentration maxima correlate excellently with increasing helium and methane contents in the drilling mud. In addition the cataclastic fracture zone at 2000 m was seen to have degased over a longer time period so that radon concentrations below 1800 m were 5 - 10 times higher than in the upper 1800 m of the KTB pilot hole (Erzinger et al., 1991).

Herewith radon has proved to be, along with helium and methane, a further sensitive and clear indicator of fluid inflow zones. Because of this an alpha spectroscopical on-line device for routine operation was developed for the KTB HB (Erzinger & Keller, 1990). However the sampling frequency of the the KTB VB of one sample per day was by no means sufficient for successful detection of fluid inflow zones, therefore, the automatized radon-measuring assembly described here was installed in the KTB field laboratory.

### C.7.3 Radon-Measuring Assembly

The KTB drilling fluids taken from the KTB borehole is partly degased using a gas trap. The gas is then lead through a pipe to a magnetic sector mass spectrometer, a gas chromatograph and finally to the radon-measuring device. The gas stream is transferred through a needle valve (NV), passes through a flow-meter (FM) into a stainless steel sphere of one liter volume (Fig.C.7.2) which had first been evacuated with a vacuum pump (VP) and closed by an electromagnetic valve (EV). The rate at which the gas enters the sphere is determined by the rate of degasing of the drilling fluid at the drill rig and is approximately 2 - 3 litres per hour. This means that the sphere is under atmospheric pressure again after 15 - 30 minutes.

Dust particles and moisture in the inflowing gas are extracted by means of a dry and aerosol filter (DF). The detector device is electrically isolated against the sphere and solely constructed for this apparatus. All high voltage components are enclosed in a isolating covering.

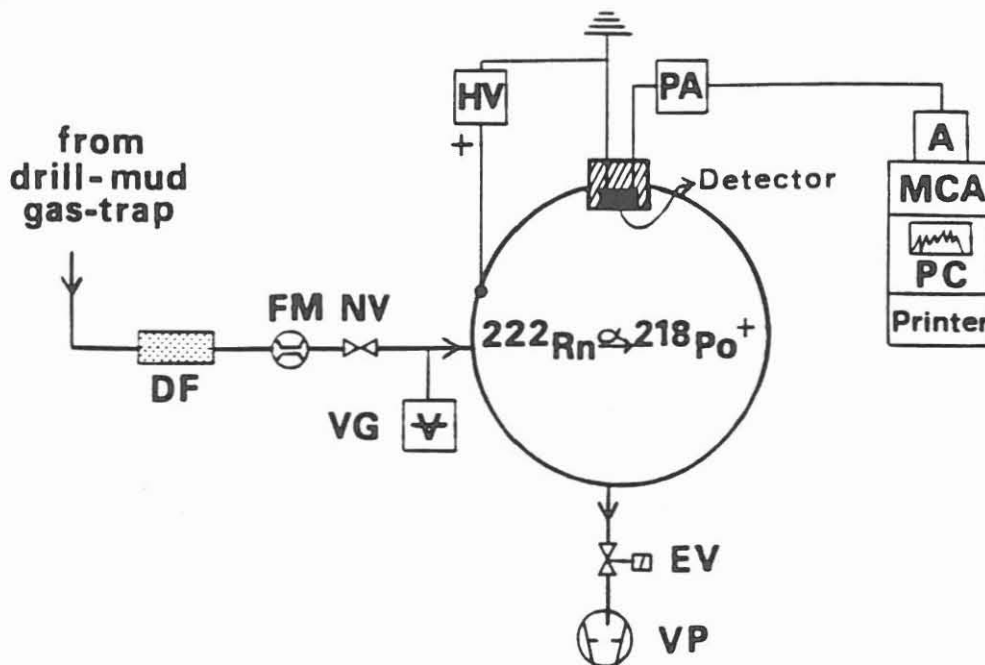


Fig.C.7.2: Radon-measuring assembly

<sup>222</sup>Radon decays in the sphere by emission of alpha particles to <sup>218</sup>Po (Fig.C.7.1). Caused by the emission of the  $\alpha$ -particle electrons are entrained resulting in a short-life positively charged <sup>218</sup>Po-Ion. The high electric field within the sphere (3000 Volts) "shoots" the polonium ions directly onto the semiconductor surface detector, connected to earth potential. The electrostatic deposition of polonium ions directly on to the detector surface produces ideal conditions for subsequent alpha spectroscopy. The following alpha decay of <sup>218</sup>Po to <sup>214</sup>Pb (particle energy 6.0 MeV) as well as the decay of <sup>214</sup>Po to <sup>210</sup>Pb (particle energy 7.69 MeV) are spectroscopically detected.



Small detector signals are amplified using a preamplifier (PA) and an amplifier (A) (Fig. C.7.2). The energy spectrum is recorded using a multi-channel-analyser (MCA) and then evaluated, printed and stored by a computer. For use in the KTB field laboratory special input and output software has been developed.

Depending on the radon concentration 15 - 20 minutes analysing time is needed. Calibration of the equipment is done with the help of known concentrations of  $^{222}\text{Rn}$  emanated from  $^{226}\text{Ra}$  chloride solutions.

In order to increase the sampling frequency two detector devices were installed which are controlled by one analysing system. We are now in the position, in spite of very low gas amounts, to carry out automatically 2 - 3 radon measurements per hour. The detection limit reaches the average background values in the atmosphere of 5 - 15 Bq/m<sup>3</sup>.

#### C.7.4 Results from the KTB HB

Fig.C.7.3 shows the logs for radon, helium and methane below 1300 m. It is obvious, that down to 3000 m, methane, helium and radon occur simultaneously with maximum concentration values. During this depth interval radon is just as sensitive indicator of fluid inflow zones as methane and helium. Fluid inflow zones at 1445 m, 1530 m-1540 m and at 2410 m are clearest indicated by radon, as the analytical sensitivity of radon is much higher than, for example, helium. Below 3000 m it is difficult to establish a correlation of radon with helium and methane. Unfortunately, for this depth interval, due to technical difficulties, gaps occurred in the radon data set where methane and helium clearly indicated fluid inflow zones. This change in the composition of the gas phase mirrors the difference between fluids from cataclastic zones and fluids leaking out of open fractures.

Most of the fluid inflow zones down to 3000 m and very few below this depth are connected to graphite-rich cataclastic shear zones. Uran is strongly enriched here and pathways allowing for mobility of gases are present. Herewith the graphite-filled cataclastic zones provide an ideal system for emanation of radon. Below 3290 m open fractures, clearly indicated by methane and helium enrichments in the borehole, occur.

Furthermore, it can be clearly seen from the gas logs that radon is being continuously introduced into the drilling mud as a result of open cracks so that background radon concentration increases rapidly with depth. This however, is not visible for methane and helium proving the much greater mobility of radon, although it must be taken into account that cuttings in the borehole are continuously releasing radon, something which does not happen with methane and which cannot be proven for helium.

The continuous degasing of the open formation is however the main factor for recognizing that after casing of the Hauptbohrung at 3000 m the background concentrations of radon decreased drastically and increased again slowly. Below 3300 m higher radon amounts are emanated and background concentrations for all three gases are considerably increased. This points to either an average higher occurrence of permeability or the appearance of open faults, as was seen from investigations of cuttings and in the KTB pilot hole.

Below 4500 m fluids entering the borehole are not enriched in radon, a completely different fluid system seems to be present which may be due to the occurrence of almost 100 % amphibolites between 4500 m and 6000 m.

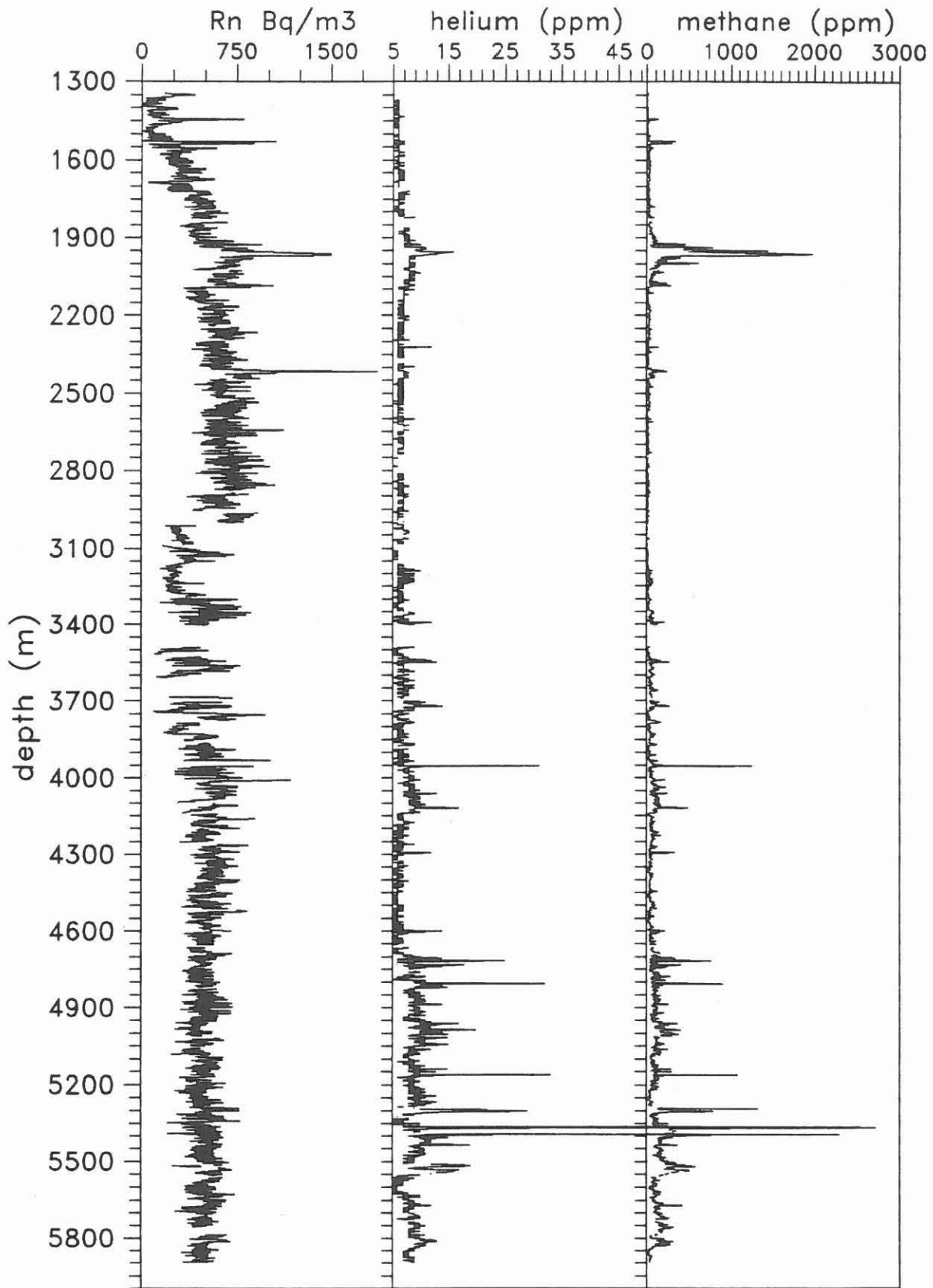


Fig.C.7.3: Variations of methane, helium and radon with depth

### C.7.5 References

ERZINGER, J. & KELLER, G. (1990): Technische Realisierung einer Meßeinrichtung zur on-line Bestimmung von Radon in Bohrspülungsgasen im KTB-Feldlabor.- Schlußbericht zum BMFT F&E-Projekt RG 86040, NlfB Hannover.

ERZINGER, J., ZIMMER, M., FIGGEMEIER, CHR., SAMEL, M. & HEINSCHILD, H.-J. (1991): Zur Geochemie von Gasen in Krustengesteinen, Formationfluiden und Bohrspülungen - Ergebnisse aus der KTB-Vorbohrung -- In: KTB-Report 91-1 des NlfB, R.Emmermann & J. Lauterjung (eds.), Schweizerbart-Verlag, Stuttgart, 393-422

FLEISCHER, R.L. & MOGRO-CAMPERO, A. (1985): Association of subsurface radon changes in Alaska and the northeastern United States with earthquakes.- Geochim. Cosmochim. Acta, 49, 1061-1071.

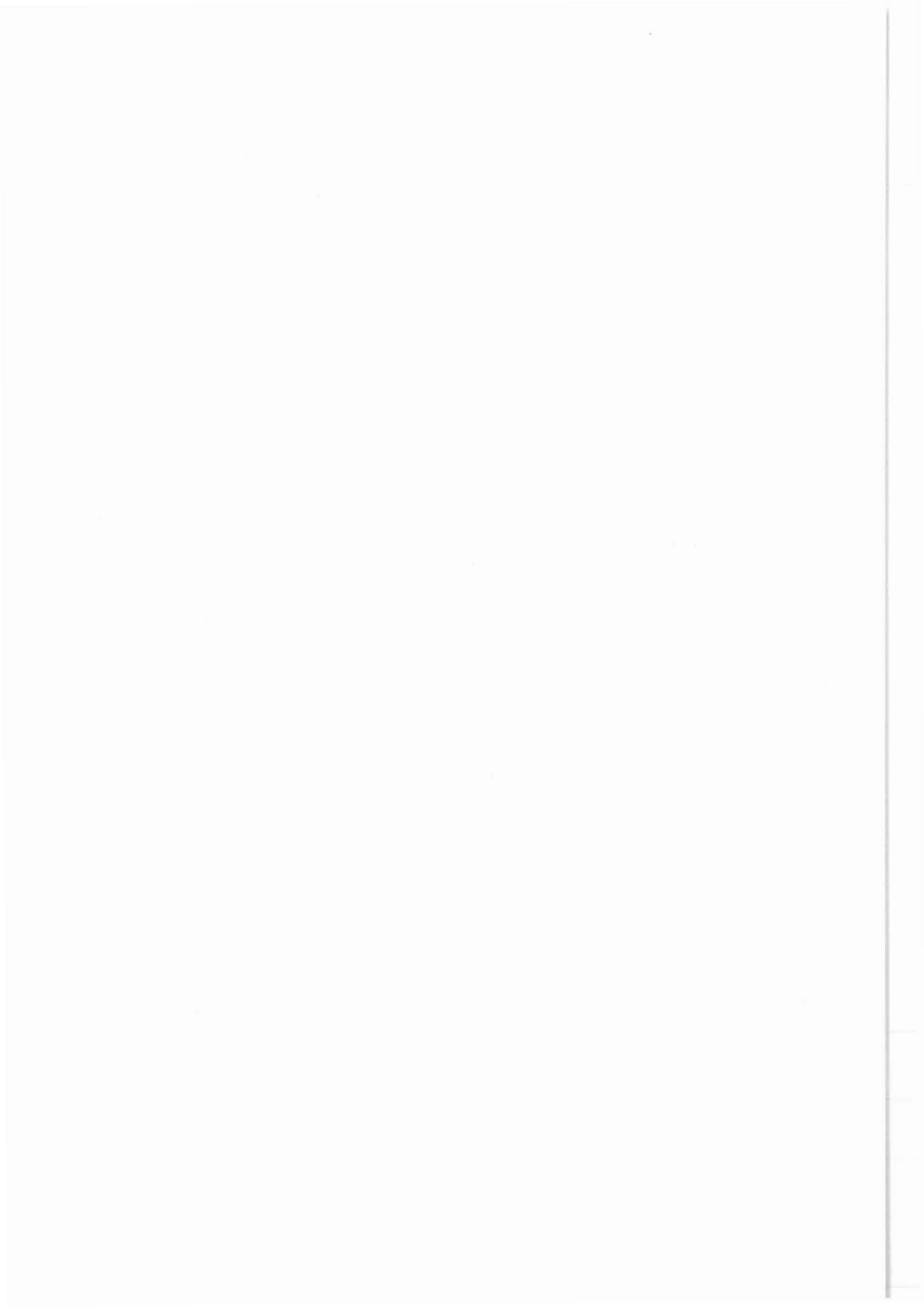
HAASE, G., ERZINGER, J., MOLZAHN, D., TUFAIL, M., KHAN, H.A., VATER, P. & BRANDT, R. (1988): Entwicklung einer Methode zur quantitativen Bestimmung von  $^{222}\text{Rn}$  in Bohrspülungen.- In: EMMERMANN, R., DIETRICH, H.-G., HEINISCH, M., WÖHRL, T. (Hrsg.), KTB-Report 88-10, 456, NlfB Hannover.

KRISHNASWAMI, S. & SEIDEMANN, D.E. (1988): Comparative study of  $^{222}\text{Rn}$ ,  $^{40}\text{Ar}$ ,  $^{39}\text{Ar}$ , and  $^{37}\text{Ar}$  leakage from rocks and minerals: Implications for the role of nanopores in gas transport through natural silicates.- Geochim.Cosmochim. Acta, 52, 655-658.

SUZUKI, K. (1987): Discordant distribution of U and Pb in zircon of Naegi granite: A possible indication of Rn migration through radiation damage.- Geochim. J., 21, 173-183.

RAMA & MOORE, W.S. (1984): Mechanism of transport of U-Th series radioisotopes from solids into groundwater.- Geochim.Cosmochim.Acta, 48, 395-399.

ZHAO, C.-D., HAASE, G., HECK, M., TUFAIL, M., VATER, P., KHAN, H.A., BRANDT, R. & ERZINGER, J.: The determination of  $^{222}\text{Rn}$  in drilling fluids of the KTB pilot borehole using SSNTD techniques.- Im Druck.



## D. Geophysics

Ch. Bucker  
D. Pribnow  
A. Rauen  
H. C. Soffel  
E. Spangenberg  
J. Wienand



KTB-Report	92-2	42 pages	24 Fig.	Hannover 1992
------------	------	----------	---------	---------------

KTB Hauptbohrung, Geoscientific Investigations in the KTB-  
Field-Laboratory,

Depth Interval 0-6000m

### D. Geophysics

Pribnow, D., Bücker, Ch., Rauen, A., Spangenberg, E.,  
Wienand, J. & Soffel, H.C.\*

#### Contents

D.1	Introduction .....	D 02
D.2	Density .....	D 03
D.3	Natural Gamma Ray Activity .....	D 06
D.4	Magnetic Susceptibility .....	D 14
D.5	Thermal Conductivity .....	D 21
D.6	Electrical Resistivity .....	D 26
D.7	Ultrasonic Seismics .....	D 29
D.8	Depth Corrections Based On Petrophysical Data .....	D 32
D.9	Summary and Discussion .....	D 35
D.10	References .....	D 41

Author's adresses: KTB-Feldlabor P.O. Box 67  
D-8486 Windischeschenbach, FRG  
\* Inst. F. Allg. u. Angew. Geophysik  
Universität München  
Theresienstr. 41/IV  
D-8000 München 2, FRG

## D.1 Introduction

In contrast to the almost completely cored Vorbohrung (KTB pilot hole), coring in the Hauptbohrung (KTB main hole) started below 4000 m and continued at irregular intervals. In order to get continuous and detailed logs despite of lacking cores the density, natural gamma ray activity, magnetic susceptibility and thermal conductivity are measured on cuttings in the field laboratory.

Table D.1.1: Physical properties measured on cuttings

	density	nat. gamma ray activity	suscepti- bility	thermal conductivity
measuring interval (m)	2	5	2	10
amount of cuttings (g)	30-130	≈ 300	5 samples of 10-15	≈ 250

In addition, these properties are also measured on available cores together with other properties like natural remanent magnetization, compressional and shear wave velocities, electrical resistivity, permeability, internal surface and porosity. In order to compare the methods, also the cuttings from the cored sections are investigated. Borehole measurements are also taken into account.

Chapters (D.2-D.5) describe the measurements on cuttings in detail. Measurements on cores, if available, are also presented. First results of seismic velocity and electrical resistivity measurements are discussed in chapters D.6 and D.7. Chapter D.8 shows the relevance of petrophysical properties for the determination of the coherence between drilling depth, logging depth and cutting depth as well as for the identification of the lithology.



## D.2 Density

### D.2.1 Method

The density is necessary for the discrimination between lithological units and for the determination of several other properties in the KTB field laboratory like heat production rate from potassium, uranium and thorium contents, volume susceptibility, thermal conductivity, etc. For the determination of density of cuttings and cores the 'Archimedian method' is used. The sample is weighted dry and in water. Knowing the density of water and the volume, the density of the sample can be calculated. Air absorbed by the large surface of cuttings causes errors in the calculated volume. Therefore, the specific surface of the cuttings has to be minimized by using only cuttings greater than 2 mm in diameter. Generally, the measuring interval is 2 m.

### D.2.2 Results

Fig. D.2.1 shows cuttings densities measured with the 'Archimedian method'. The results are well correlated with the lithological units. Metabasites often contain quartz and feldspar from mobilisates. Quartz can cause a high scatter in the metabasite sections due to its low density ( $2.65 \text{ g/cm}^3$ ) with respect to amphibole ( $3.3 \text{ g/cm}^3$ ). In a histogram (Fig. D.2.2) gneisses and metabasites can be clearly distinguished. Due to the influence of the mobilisates, metabasites show a higher standard deviation than gneisses. The average density values for the two main lithological units are in good agreement with the results of measurements on cores from the pilot hole (Tab. D.2.1).

### D.2.3 Summary and Conclusions

Besides its importance for the discrimination of the lithologies, the density is an important property for other petrophysical investigations. Using the simple and fast 'Archimedian method' it was possible to measure the density of cuttings every 2 m. In average, the densities of the two main lithological units are in good agreement with the results measured on cores from the pilot hole. Due to the averaging character of cuttings, small scale variations of the formation density - seen in core measurements - are not detectable. By comparing core and borehole measurements it was possible to determine the exact depth of the core pieces and to identify areas of no core recovery (see chapt. D8).

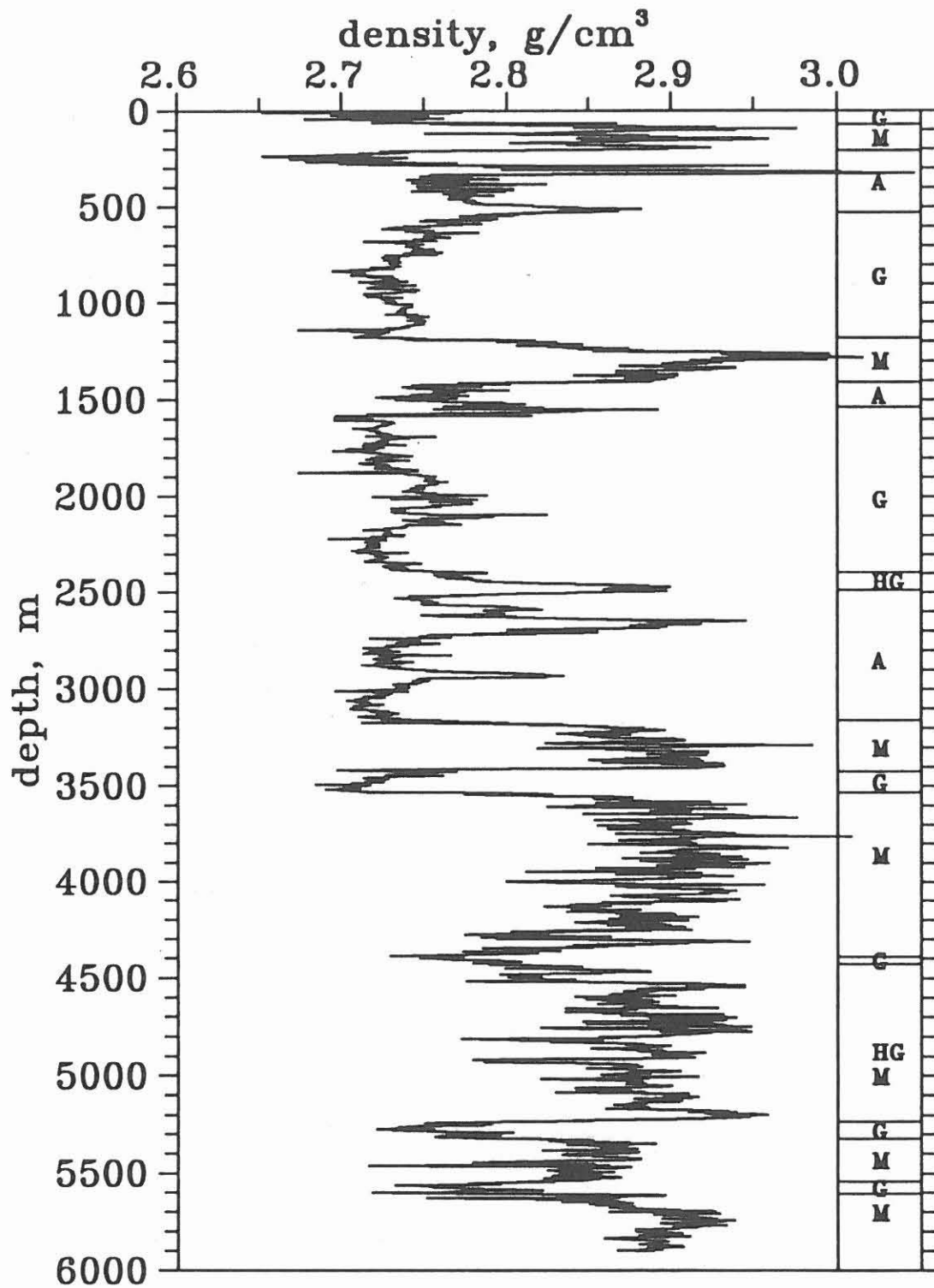


Fig. D.2.1: Cuttings density log from 0-6000m together with a simplified lithological profile. G: gneiss; HG: hornblende gneiss; M: metabasite; A: alternating sequence of gneisses and metabasites.

The average density of 2.81 g/cm<sup>3</sup> indicates that the drill hole is still within the nappe structure of the Zone of Erbendorf-Vohenstrauß (ZEV). From surface gravity measurements a thickness of the ZEV of about 6 km and an average density of 2.8 g/cm<sup>3</sup> within and 2.7 g/cm<sup>3</sup> beneath the ZEV (SOFFEL et al., 1989) has been postulated.

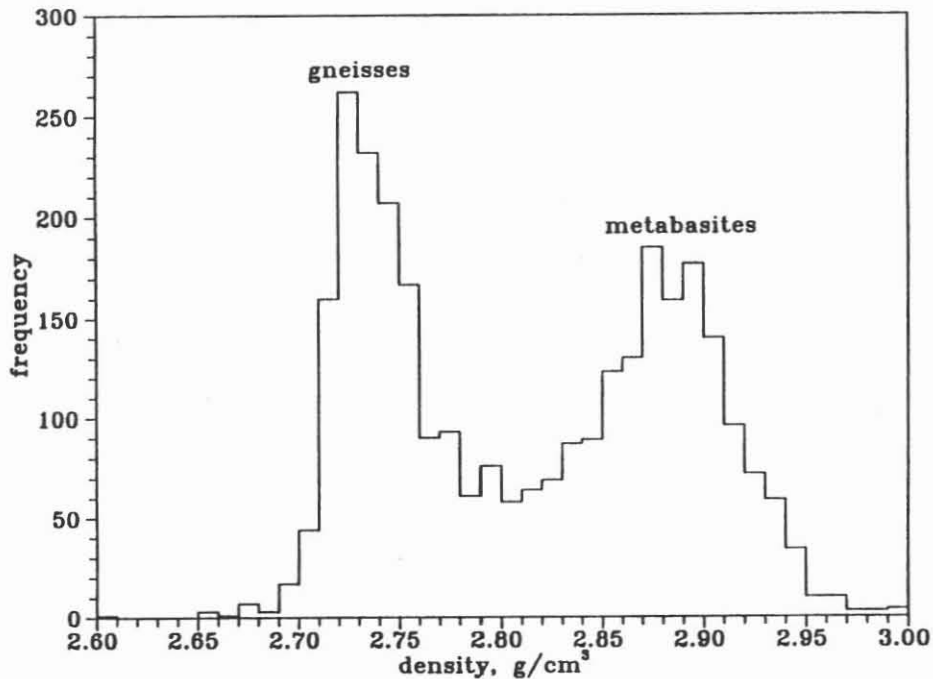


Fig. D.2.2: Frequency distribution of the cuttings density.

Table D.2.1: Average values of measurements on cores from the Vorbohrung (VB) and on cuttings from the Hauptbohrung (HB). Numbers in parentheses indicate the number of measurements.

	density (g/ccm)	
	VB (cores) 0-4000m	HB (cuttings) 0-6000m
metabasites	2.93 ± 0.09 (733)	2.87 ± 0.05 (1314)
gneisses	2.74 ± 0.04 (2501)	2.74 ± 0.03 (1275)
total	2.80 ± 0.10 (4131)	2.81 ± 0.08 (2853)

### D.3 Natural Gamma Ray Activity

#### D.3.1 Method

The analysis of the natural gamma radiation allows to identify various gamma ray emitters. In the KTB field laboratory, the natural gamma ray activity is measured for several reasons:

- quick production of a first gamma ray log on cuttings for the analysis of the lithology
- quantitative determination of potassium, uranium and thorium contents for example for the detection of cataclastic and fractured zones in the borehole
- calculation of the heat production rate due to the decay of radionuclides using the formula after RYBACH (1976) for a temperature forecast
- as the natural gamma radiation is measured as part of the logging programme and on cores, cuttings and mud in the laboratory, a depth correlation between borehole measurements and data from cores and cuttings is possible. This depth correlation is very important for a calibration of all measurements in the borehole and in the laboratory with regard to their depth (see BÜCKER & ZIMMERMANN, 1989)
- correction and calibration of the borehole measurements

In the laboratory, gamma radiation is measured with a germanium semiconductor detector and with NaI detectors, each 3" in length and 3" in diameter. Cuttings and mud samples are measured in air tight Marinelli-beakers with a volume of 250 cm<sup>3</sup>. For the core measurements a special, automatically operating equipment with three NaI detectors is used. The principle of this equipment was described by BÜCKER et al. (1991). The results of the KTB pilot hole are published by SOFFEL et al. (1991). For the quantitative evaluation of the K-, U- and Th-contents, the following peaks in the gamma ray spectra are used and calibrated against standards:

NaI-detector:

K-40(1460.8keV), Bi-214(1764.5 keV), Tl-208(2614.5keV)

Ge-detector:

Pb-214(351.92 keV), Bi-214(609.31 keV), Tl-208(860.56 keV), Bi-214(1120.29 keV), K-40(1460.83 keV)

The influence of the background radiation has been taken into account.



In general, a measuring time of 12 h for the NaI detector and of 2 h for the germanium detector was chosen. However, the evaluation of the germanium detector spectra is more accurate due to the high resolution of 1.7 keV at 1.33 MeV (Co-60 peak).

Due to problems with the germanium detector, only few measurements with the NaI detector are available from the first 1400 m. Below 1400 m potassium, uranium and thorium were measured with the germanium detector.

On average, samples were taken every 2-4 m yielding more than 1700 gamma spectra measurements. For further investigations all spectra are stored digitally.

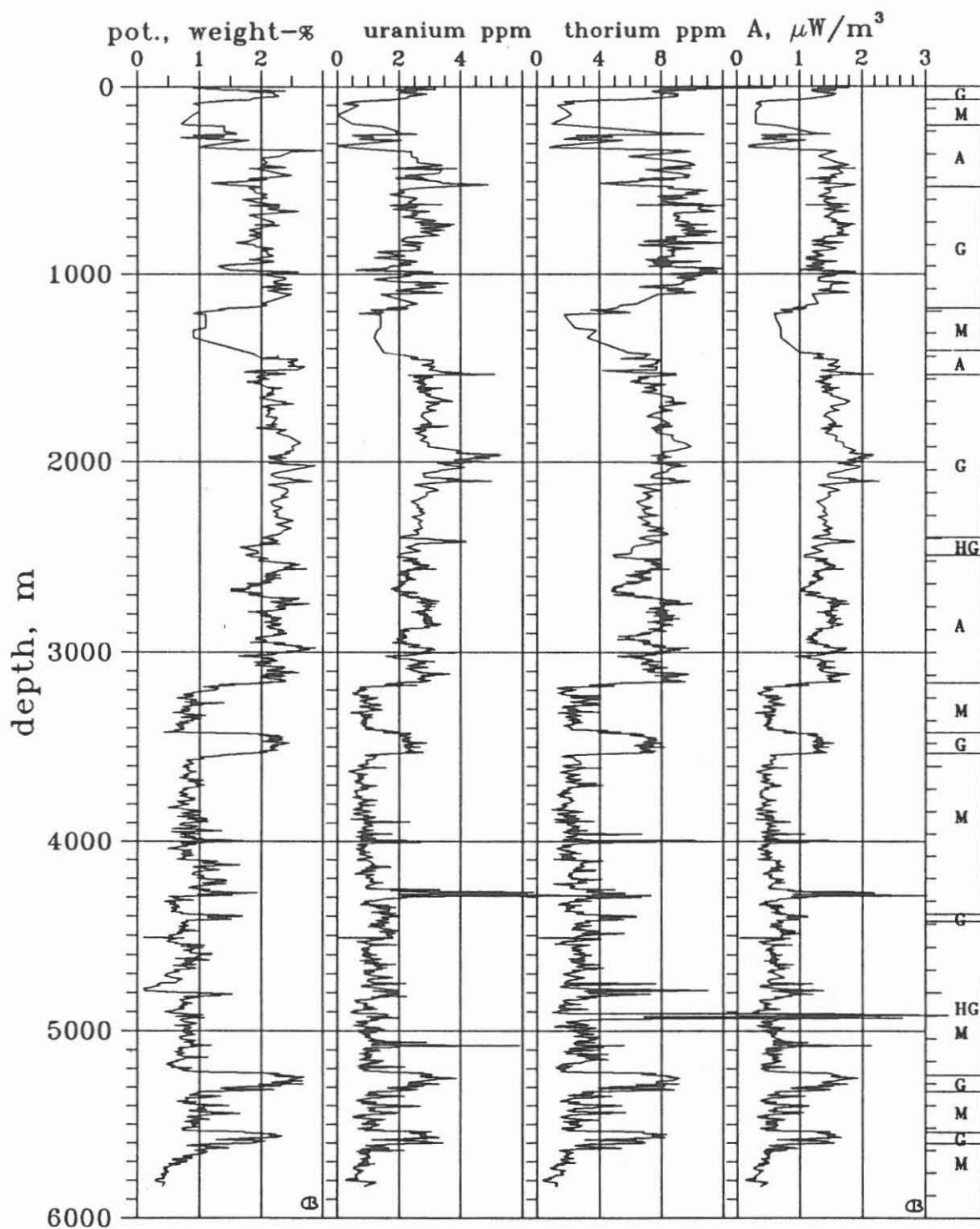
### D.3.2 Results

The log of the specific gamma ray count rate measured on cuttings is shown in Fig. D.3.1 together with the borehole gamma ray log (KTB-Referat Bohrlochmessungen) and a simplified lithological profile. A detailed geological profile (scale 1:1.000) is given in chapter B of this report.

A clear lithological differentiation can be seen in the data from cuttings as well as in the borehole measurements. The metabasites are characterized by low values of about 20 counts/sec\*kg (c/sec\*kg) with low variance, the gneisses show values of about 50 c/sec\*kg with higher variance. The hornblende gneisses display intermediate values around 40 c/sec\*kg. There are several sharp peaks in the gamma ray log which can be correlated with uranium and thorium enrichments for example at 1980m and 4000m. However, it is remarkable to note that in the Vorbohrung comparable peaks have been seen in the same depth ranges (see BÜCKER et al., 1990). There is good correlation between the borehole and the laboratory gamma ray measurements. Differences are in most cases related to breakouts or cavings.

In the detailed lithology-log (see chapter B) depth shifts up to 9 m between cuttings and borehole measurements can be detected. For the cuttings, there is no systematic increase of this depth shift with depth.

The results of the potassium-, uranium- and thorium-evaluation together with the calculated heat production are shown in Fig. D.3.2. There is a good correlation between lithology and the content of radionuclides. As a general trend, there are higher contents of K, U and Th in the gneiss sections and lower contents in the metabasite sections. Table D.3.1 summarizes the mean values and their standard variations of potassium, uranium, thorium and heat production values for the three main lithological units. In Fig. D.3.3 the frequency distributions reflect the lithological units.



sampling rate: 2-10m

Fig. D.3.2: Depth log of potassium, uranium and thorium and the production rate calculated with the formula after RYBACH (1976).

Remarkable sections with extreme high and extreme low values, respectively, can be detected in the depth log (Fig. D.3.2). Uranium contents increase at 1980m, at 4270m and at 5080m. Thorium enrichments could be detected at 4000m and at 4940m with more than 25 ppm. In these cases high epidote

	K %	U ppm	Th ppm	A $\mu\text{W}/\text{m}^3$
gneiss	$2.2\pm 0.3$	$2.8\pm 0.6$	$7.6\pm 1.1$	$1.5\pm 0.2$
metabasite	$0.9\pm 0.4$	$1.3\pm 0.8$	$2.9\pm 1.6$	$0.6\pm 0.3$
hbl.-gneiss	$1.5\pm 0.6$	$1.7\pm 0.7$	$4.5\pm 2.1$	$0.9\pm 0.4$

Table D.3.1: Arithmetic mean values for potassium, uranium and thorium and the heat production rate for the three main lithological units. hbl: Hornblende.

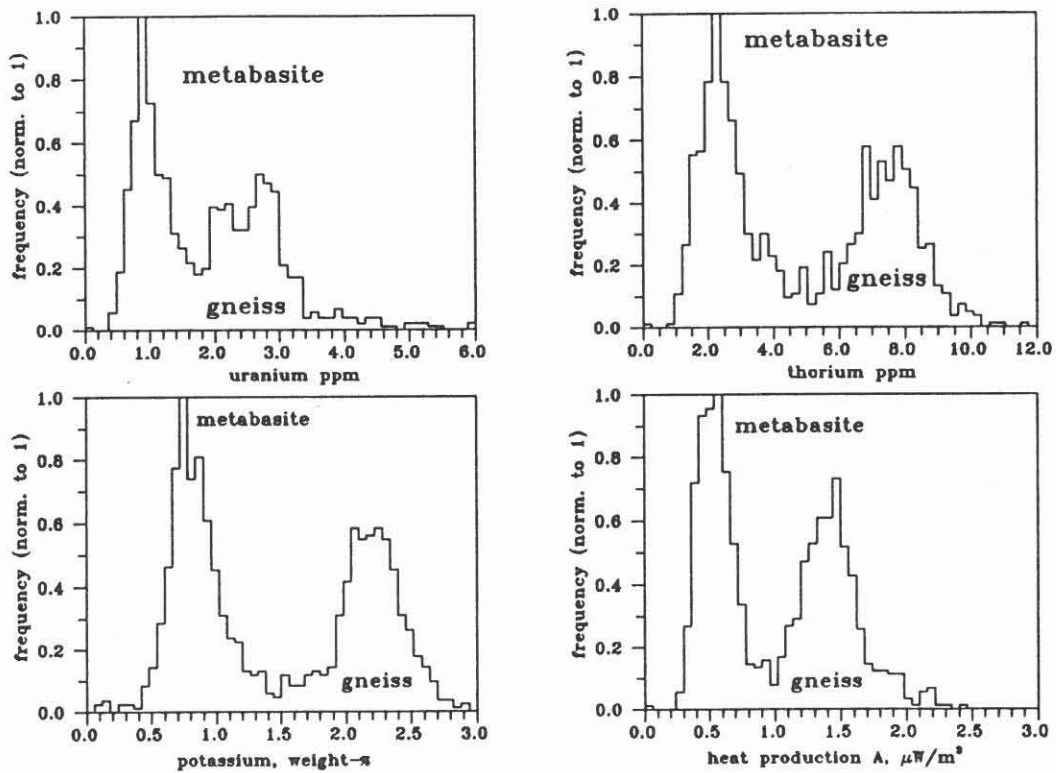


Fig. D.3.3: Frequency distributions of the radionuclides potassium, uranium and thorium and the heat production rate. The maxima are related to the main lithological units metabasites and gneisses.



contents have been seen by XRD-measurements (see chapter C). The decrease in potassium down to 0.1-0.2 weight-% at 4770m can be related to an epidote-rich plagioclase. In this depth range also open pores have been detected in the cuttings material (see chapter B), which may explain the escape of potassium from this permeable zone.

In Fig D.3.4 thorium to uranium ratios for all samples are plotted. On average, a relation of  $\text{Th}/\text{U} \approx 3$  can be seen. The mean value of  $\text{Th}/\text{U} \approx 3$  is little lower than the mean value of  $\text{Th}/\text{U} = 3.9$  for rocks from the continental upper crust (see HAACK, 1982). Already the measurements on cores from the Vorbohrung (see SOFFEL et al., 1991) as well as measurements from GOHN et al. (1991) also showed  $\text{Th}/\text{U}$  ratios of about 3. GOHN et al. (1991) pointed out, that the rocks from the KTB Vorbohrung have decreased contents of radionuclides, especially Th and K.

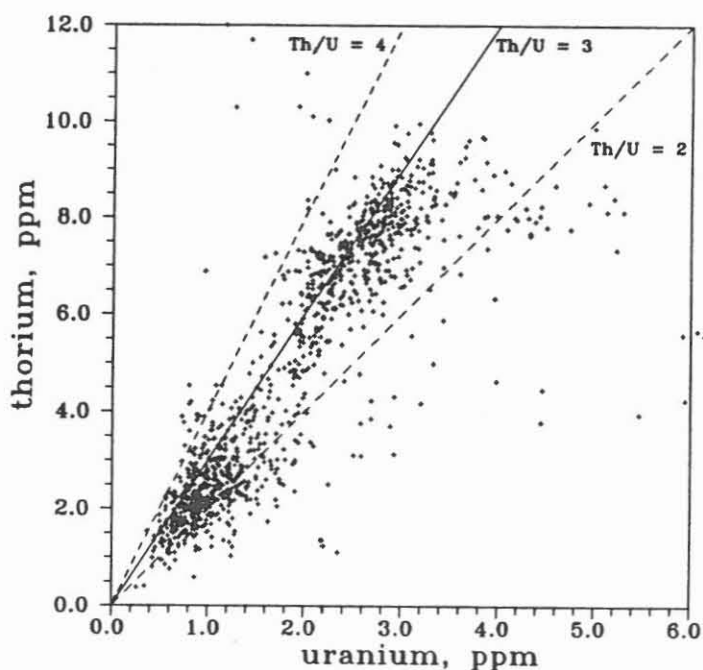


Fig. D.3.4: Thorium versus uranium for cuttings samples. The solid and broken lines indicate the noted ratios.

The correlation between density and gamma ray count rate, both measured on the same sample, is shown in Fig. D.3.5. Three clusters can clearly be distinguished: biotite-gneisses with a count rate of about 50 c/sec\*kg and a density of about  $2.73 \text{ gcm}^{-3}$  (see also chapter D.2), secondly metabasites with a count rate of 20 c/sec\*kg and a density around  $2.90 \text{ gcm}^{-3}$  and a third group with densities higher than  $2.75 \text{ gcm}^{-3}$  and a count rate between 30 c/sec\*kg and 50 c/sec\*kg. This third group represents hornblende-gneisses and mobilisate-rich amphibolites.

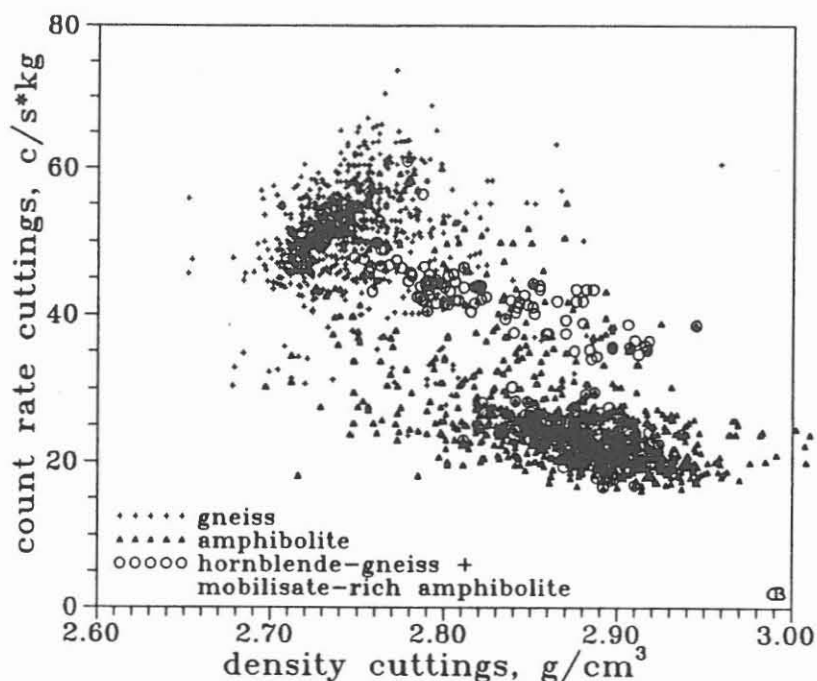


Fig. D.3.5: Correlation between density and gamma ray count rate. Low density and high count rate values can be related to gneisses whereas high densities and low count rates correlate with amphibolites. The intermediate group represents hornblende gneisses and mobilisate-rich amphibolites.

### D.3.3 Summary and Conclusion

The gamma ray log can be consulted for quick lithological differentiations. By comparing the borehole gamma ray log with the corresponding data from cuttings, the depth shift between both measurements can be detected and estimated (see BÜCKER & ZIMMERMANN, 1989).

The quantitative interpretation of the spectra measured with the germanium detector yields the contents of the radionuclides potassium, uranium and thorium with high accuracy. The heat production rate can be calculated. For mean values see table D.3.1. Fractured or cataclastic zones can also be detected.

The correlation between density and count rate (see Fig. D.3.5) helps to differentiate between metabasites and the group of rocks consisting of hornblende-gneisses and mobilisate rich amphibolites.

The agreement between natural gamma spectroscopy from borehole measurements (NGS, for potassium, uranium and thorium) and from the laboratory measurements is good.

## D.4 Magnetic Susceptibility

### D.4.1 Methods and Introduction

The volume susceptibility is determined on cuttings as well as on core samples by an inductive device (BARTINGTON). Measurements on core pieces are made every centimeter by a computerized equipment. For each core sample a mean value of susceptibility is computed.

Measurements on cuttings are performed on 5 random samples of the same depth (mass  $\approx 10$  g, fraction 2-5 mm). The sampling interval is 2 m. The mean value of susceptibility at each depth and its maximum variation is stored on a computer file.

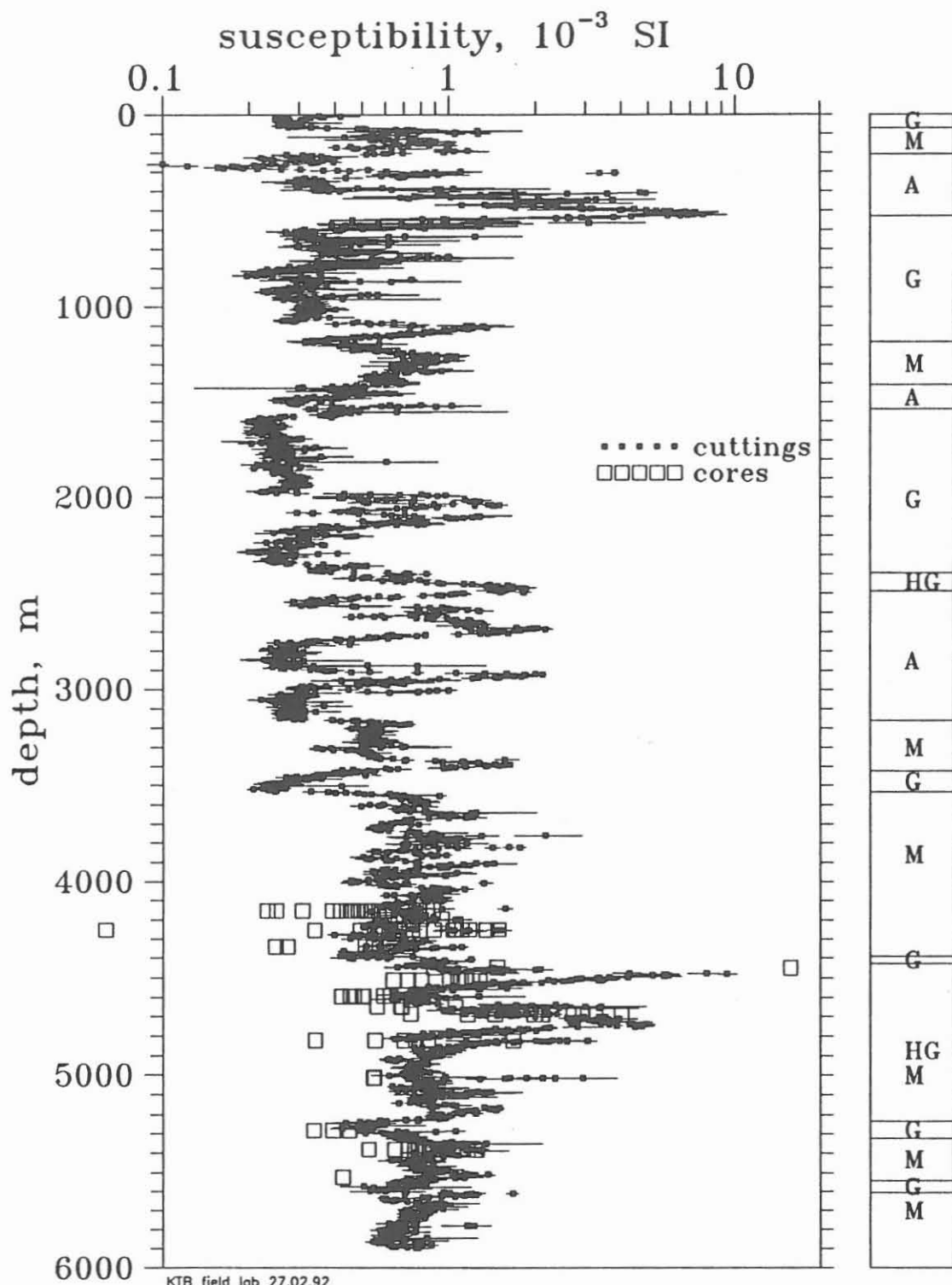
Cutting samples with abnormally high readings are controlled. Metallic material (iron, scrap) is removed and the measurement is repeated. As shown in chapter D.4.3, the remaining content of ferromagnetic metallic abraded material leads to an artificial increase of susceptibility, even if the visible metallic particles are removed before measurement.

### D.4.2 Results

Fig. D.4.1 shows the susceptibility log together with a simplified lithology. High susceptibilities (up to  $9.4 \cdot 10^{-3}$  SI) occur in amphibolites as well as in gneisses (up to  $7.3 \cdot 10^{-3}$  SI). Magnetite (e.g. at 4480 m) and pyrrhotite (e.g. at 510 m) are responsible for these high values (see section on 'ore mineralization' in chapter B of this issue). Cores have lower as well as higher values of susceptibility than cuttings of equal depths. This is caused by the sampling of the cuttings, which averages over a certain depth interval (see chapter A).

The histogram (Fig. D.4.2) shows the superposition of two lognormal distributions. The lower values correspond to the gneisses, with a calculated geometric mean of  $0.40 \cdot 10^{-3}$  SI units by considering all values in gneiss sections. The high susceptibilities can be explained by the occurrence of metabasites (mainly amphibolites and hornblende-gneisses). The geometric mean of all amphibolite sections is  $0.87 \cdot 10^{-3}$  SI, that of all hornblende-gneisses is  $0.88 \cdot 10^{-3}$  SI.

The susceptibility as a function of density (Fig. D.4.3) shows two main clusters, which represent gneisses and metabasic rocks. Hornblende-gneiss and mobilisate rich amphibolite plot in an intermediate area and overlap the two main clusters. Their susceptibilities are comparable to those of the amphibolites, while their densities tend to be lower.



**Fig. D.4.1:** Log of susceptibility. For cuttings, mean values of 5 samples and the maximum variation are plotted. Core measurements are shown as mean values per core. Right column: a simplified lithological profile (G = gneiss, M = metabasite, A = alternating layer and HG = hornblende gneiss and mobilisate-rich amphibolite).

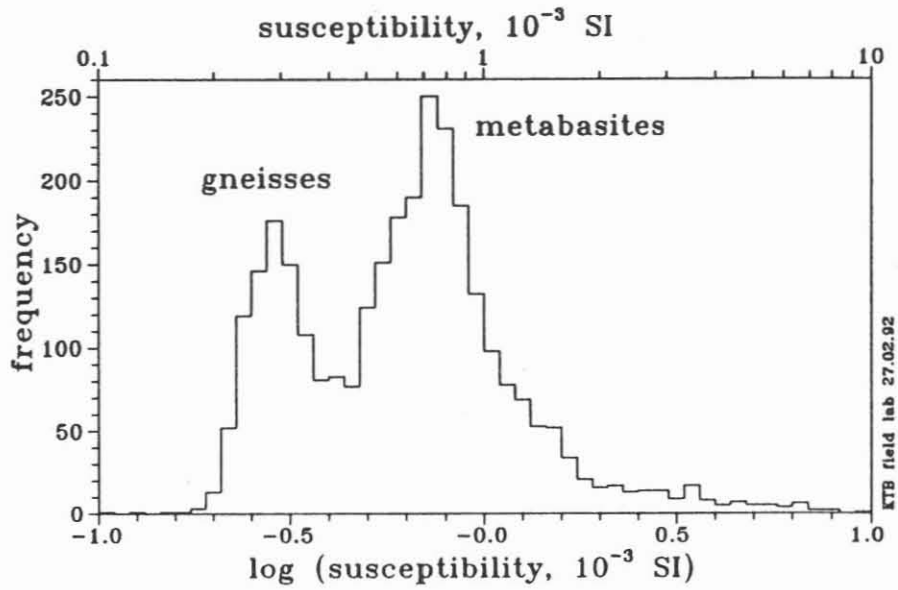


Fig. D.4.2: Frequency distribution of cuttings susceptibilities. The susceptibility interval from 10<sup>-4</sup> SI to 10<sup>-2</sup> SI is logarithmically divided into 50 intervals.

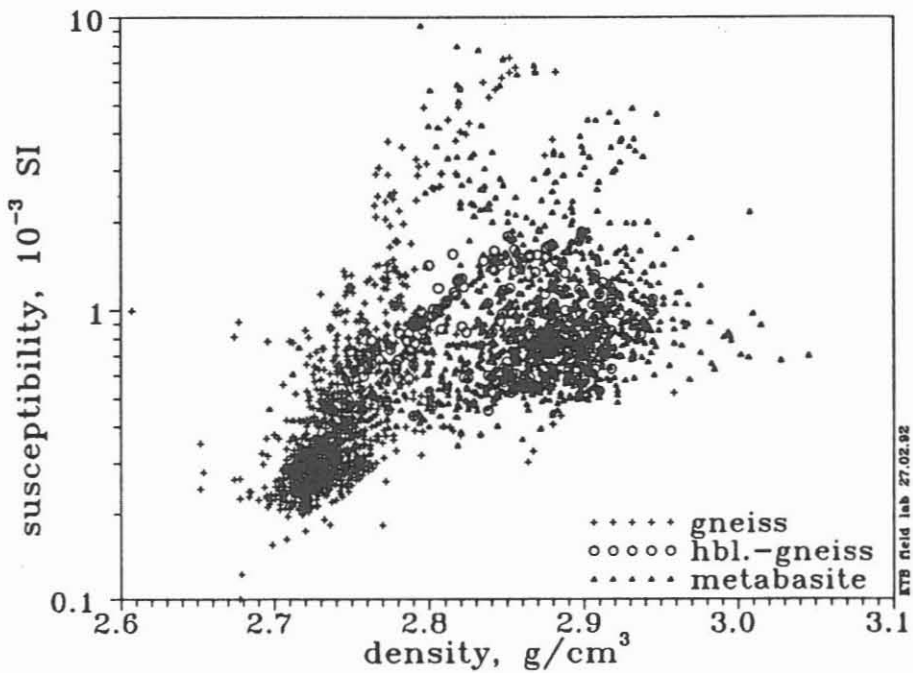


Fig. D.4.3: Cross plot of susceptibility versus density (see chapter D.1), measured on cuttings from the same depth interval. Gneisses, hornblende-gneisses and amphibolite sections form different, but partly overlapping clusters.

#### D.4.3 An Example for the Influence of Abraded Metallic Artefacts on the Susceptibility Values

In some cases macroscopically visible metallic particles (often rusty scrap) within the cutting samples cause high susceptibility values. Removing these artefacts by picking or using a hand magnet, results in susceptibilities approaching normal values. The susceptibility data reported here, as well as the XRF data (see chapter 'C' in this issue) are cleaned by magnetic means from the scrap before measuring.

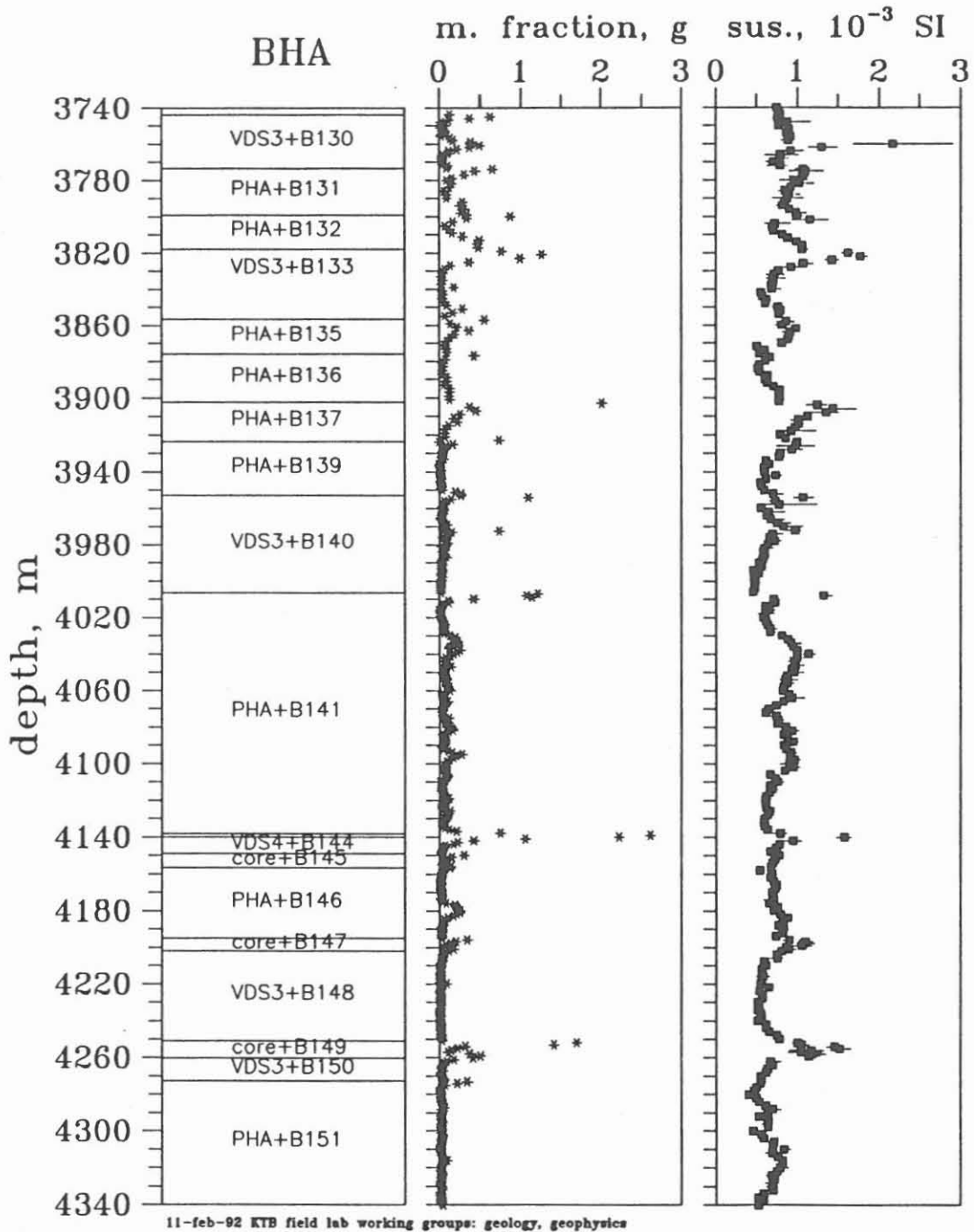
The content of abraded metallic material was quantified by the geology group in the depth interval 3744 - 4340 m (see 'drilling artefacts in cutting samples' in chapter 'B' in this issue).

Original cutting samples of a defined volume were separated into magnetic and non magnetic fractions by using a hand magnet. In general, the magnetic fraction consists of abraded material as well as of strongly magnetic ore particles.

It was found, that the exchange of the bottom hole assembly BHA (so called trip in and trip out of the drill string) and sticking of the drill string correlate with higher contents of abraded material in the cuttings (see Fig. B.2.3). High amounts of strongly magnetic material correlate with susceptibility peaks (e.g. at 4006, 4140 and 4251 m), even though the visible scrap was removed before measuring the susceptibility (see Fig. D.4.4).

To distinguish between metallic particles and magnetic ore content, the magnetic fraction and susceptibility are plotted together with density and some element concentrations from XRF measurements. High concentrations of iron and sulfur can indicate pyrrhotite as magnetic ore, while high copper, zinc and also iron contents point to artefacts (abraded material from the drill string [Fe] or its zinc silicate coating [Zn] or the drill string grease [Cu]). Fig. D.4.5 shows the results in the interval 3780 - 3830 m, where two characteristic susceptibility peaks could be observed.

There are arguments for the first peak (3802 m) to be an artefact due to abraded material and for the second one (3824 m) to be a real effect of rock susceptibility.



11-feb-92 KTB field lab working groups: geology, geophysics

Fig. D.4.4: Left: The bottom hole assembly (BHA) phases are shown as horizontal lines (VDS3/4 = vertical drilling system 3/4, PHA = packed hole assembly, core = coring tool, B# = bit with number). Centre: semi-quantitative amount of the strongly magnetic material (sum of scrap and ore) in the original cutting samples (total mass  $\approx$  15 g). Right: depth log of magnetic susceptibility (maximum, minimum and mean value of 5 measurements, see Fig. D.4.1. Scrap and abraded particles have been removed before).



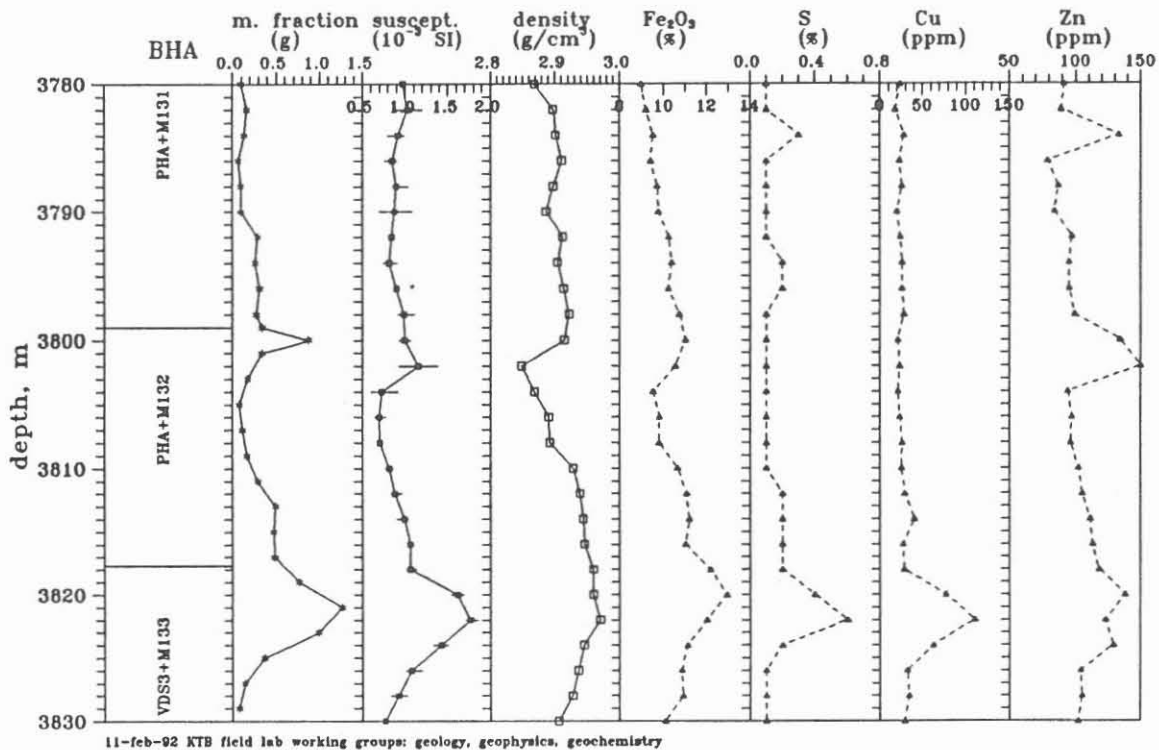


Fig. D.4.5: From the left to the right: Bottom hole assembly (BHA, phases as horizontal lines); magnetic fraction, susceptibility (see Fig. D.4.4); density (see chapter D.2); content of iron ( $Fe_2O_3$ ), sulfur, copper and zinc from XRF measurements (scrap and abraded particles are removed, see chemistry, chapter 'C', in this issue).

The 3824 m peak correlates with density, the 3802 m peak does not (see Fig. D.4.3). Both peaks correlate with an iron increase, but only at 3824 m the sulfur values are increased. Here pyrrhotite seems to be the magnetic component, whereas the increased iron content at 3802 m is due to a rest of abraded iron from the drill stem. Also the increased zinc values at 3802 m are caused by the drill string, especially its zinc silicate coating. Finally the analysis of polished sections shows much pyrrhotite in two sections (3817 m & 3820 m), but no indication for magnetic ores at 3800 m (see 'ore mineralization' in chapter 'B' in this issue). The increased copper concentration at 3822 m is (at least partly) produced by chalcopyrite, which is recognized in the polished section at 3820 m.

#### D.4.4 Conclusions

High susceptibilities up to  $\approx 10^{-2}$  SI units are obtained in gneisses as well as in metabasite sections. The values are not as high as those measured on core samples of the pilot hole (up to  $\approx 0.2$  SI). This may be due to a smoothing effect of cutting samples and loss of ferrimagnetic components during drilling (see chapter A in this issue).

In some cases, abraded metallic and ferromagnetic material affects the measured susceptibility. It follows, that the replacement of drill tools can cause higher amounts of abraded particles (scrap) in the cuttings. Although these artefacts are removed from the samples before measuring the susceptibility, a rest of it remains and spoils the results. By comparing the susceptibility values with other data, which are less affected (density; sulfur from XRF), artefacts and ore mineralization can be distinguished. This will be the future strategy for all susceptibility data from cuttings.

## D.5 Thermal Conductivity

### D.5.1 Method

For the measurement of thermal conductivity (k) a transient heat flow method (half space line source) is used in the KTB field laboratory. A needle probe is embedded in the surface of an isolating plexiglass block ( $k = 0.16 \text{ W/m/K}$ ). While heating with constant power, the temperature increase of the line source is measured. This heating curve is used to evaluate k (HUENGES et al., 1990).

In order to measure k, the cuttings are mixed with water and then pressed together by the plexiglass block (Fig. D.5.1). This measurement yields the geometric mean of the thermal conductivities in a two-phase mixture model:

$$k_{\text{meas}} = k_{\text{cutt}}^{1-\Phi} * k_{\text{wat}}^{\Phi}$$

$k_{\text{meas}}$  - measured thermal conductivity  
 $k_{\text{cutt}}$  - thermal conductivity of the cuttings  
 $k_{\text{wat}}$  - thermal conductivity of water  
 $\Phi$  - volume fraction of water in the model

By measuring the weight of the dry cuttings and the mixture of cuttings and water, the parameter  $\Phi$  can be determined knowing the density of the cuttings and water. As  $k_{\text{wat}} = 0.6 \text{ W/m/K}$  is known,  $k_{\text{cutt}}$  can be evaluated. The geometric mean model has been introduced by SASS et al. (1971) using a steady state method for thermal conductivity measurements.

Table D.5.1: Specification of measurements

length of line source .....	70 mm
diameter of line source .....	2 mm
heating power .....	$\approx 10 \text{ W/m}$
heating duration .....	100 sec
temperature increase of the source ....	6-8 K
amount of cuttings .....	$\approx 250 \text{ g}$
.....	$\approx 90 \text{ cm}^3$
size of cuttings .....	< 2 mm
average amount of water .....	32 vol%
measuring interval .....	10 m

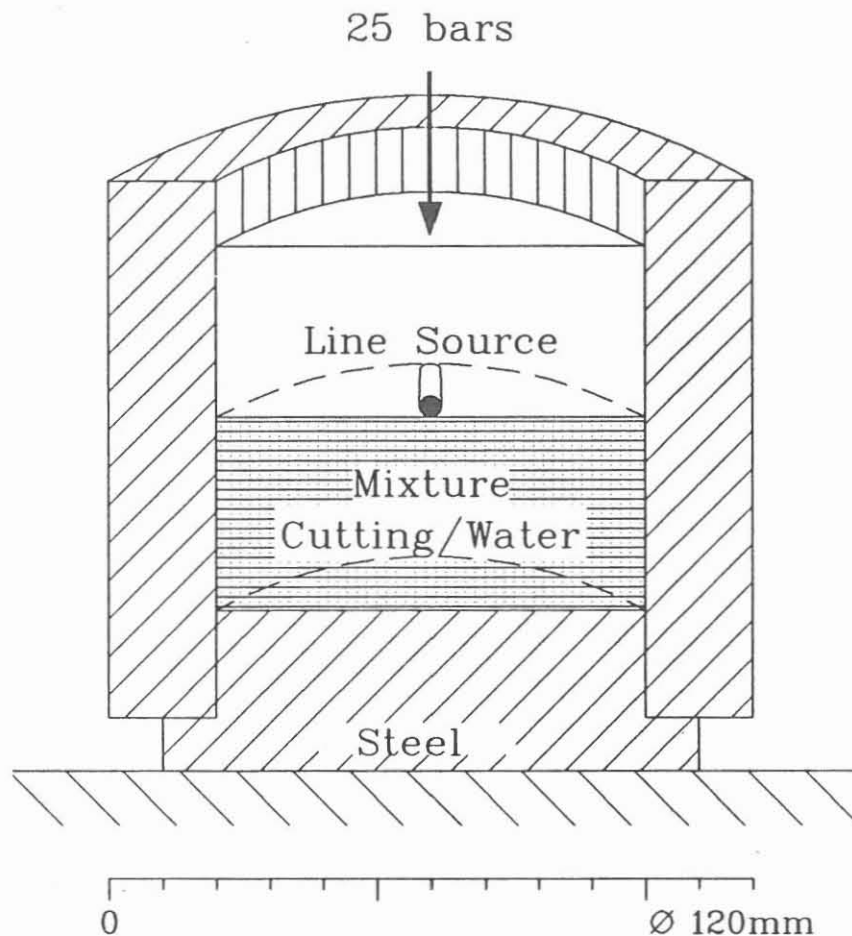


Fig. D.5.1: Half space line source measurements of a mixture of water and cuttings

To test this method, cores from the KTB Vorbohrung with known thermal conductivity and a standard (glass ceramic) were ground to cutting size (smaller than 5 mm) and  $k$  was determined in the described way. Additionally,  $k$  was measured by J. Sass (USGS, Flagstaff) with a steady state method on these artificial cuttings. Fig. D.5.2 shows good agreement of these measurements. Differences to core measurements may be due to the anisotropy of the gneisses (up to 30%). The transient heat flow method is suitable to measure the thermal conductivity on cuttings using the geometric mean model to eliminate the influence of the water.

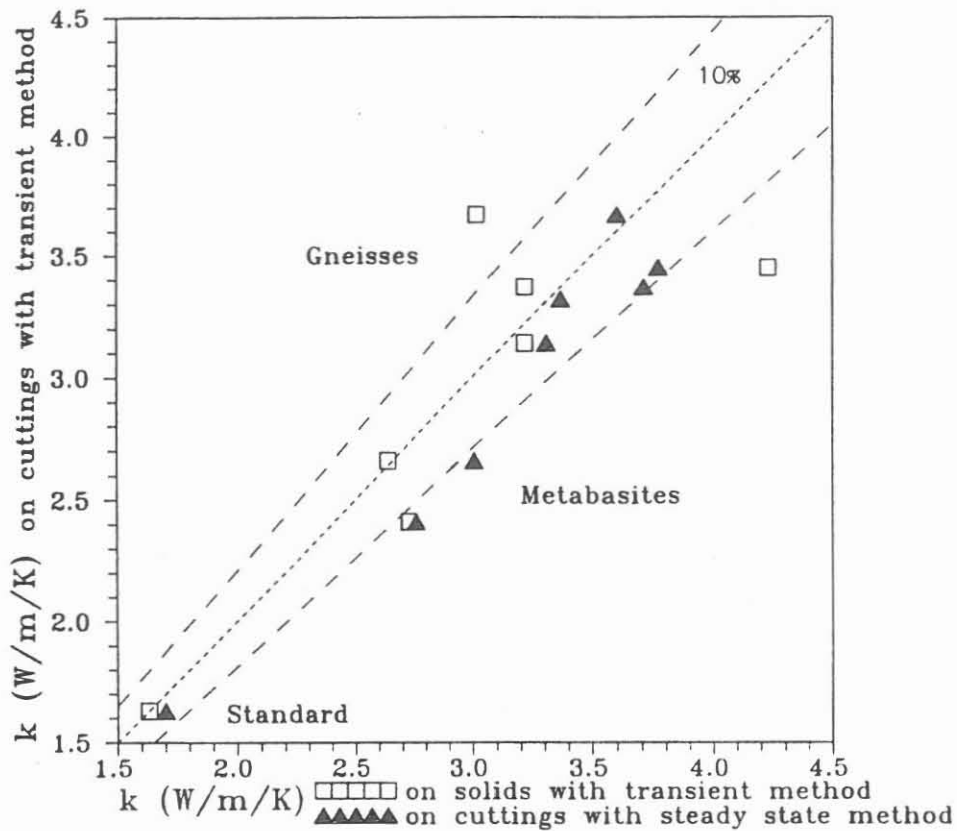


Fig. D.5.2: Comparison of measurements with the half space line source (transient method) on cores and cuttings as well as measurements on cuttings with the transient and the steady state method. The standard is a glass-ceramic ( $k=1.609$  W/m/K).

### D.5.2 Results

Fig. D.5.3 shows the thermal conductivity log measured with the transient heat flow method on cuttings from the KTB Hauptbohrung. The  $k$ -values show good correlation with the lithological units. Quartz is a good heat conductor ( $k = 6-12$  W/m/K). Thus, the quartz content in a sample strongly influences the thermal conductivity. The high  $k$ -values at 260 m and 270 m are due to quartz veins in that area. Another example is the gneiss with low quartz and high plagioclase contents between 950 and 990 m causing lower thermal conductivities.

In the frequency distribution of all measurements (Fig. D.5.4) gneisses and metabasites can be recognized clearly in both, the measurements on the water-cutting mixture and the calculated  $k$ -values according to the geometric mean model. Gneisses generally have higher quartz contents than metabasites. The quartz in the metabasite samples results from mobilisates. The average thermal conductivity values for the main lithological units are in good agreement with the results of measurements on cores from the Vorbohrung.

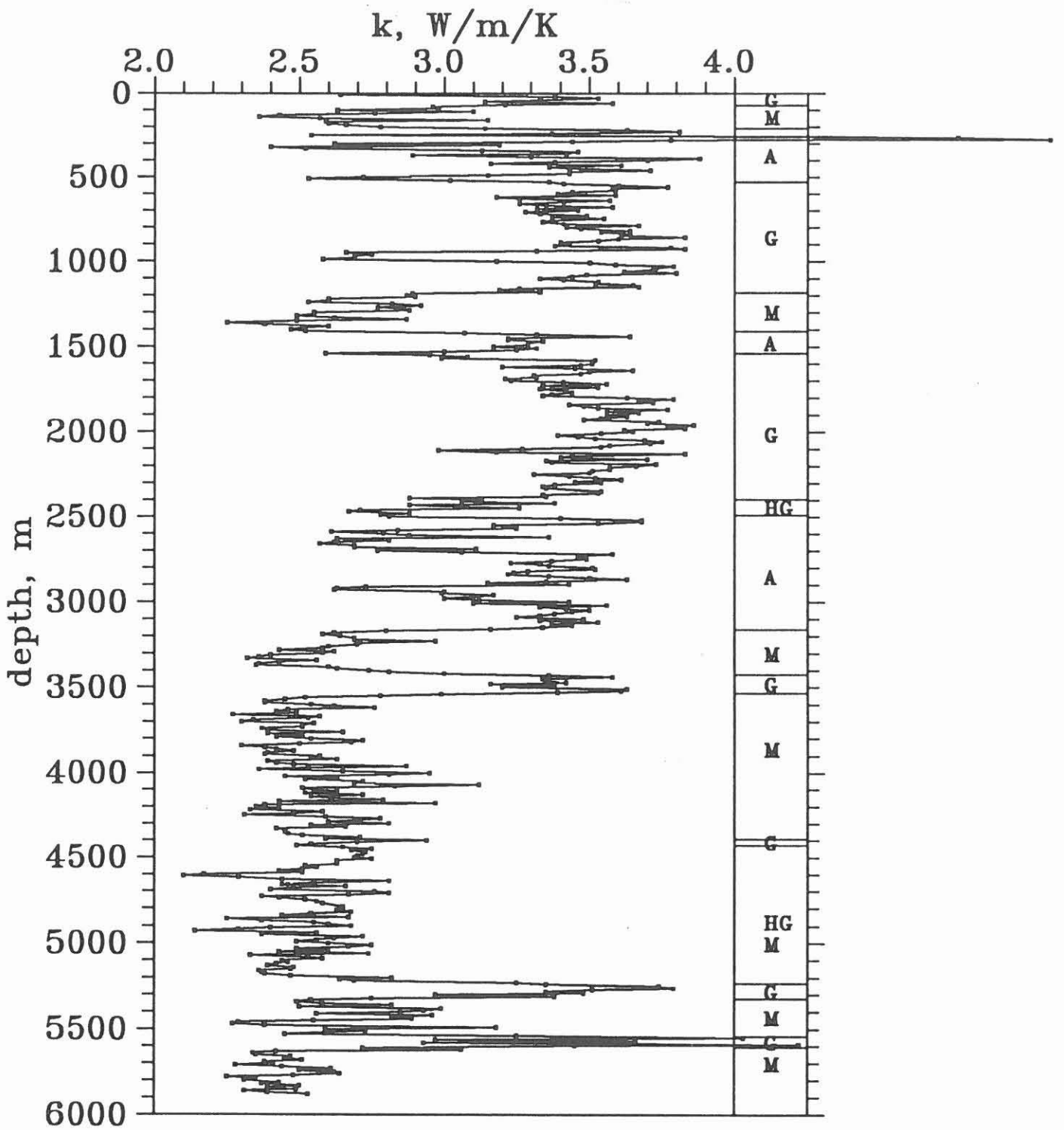


Fig. D.5.3: Thermal conductivity log measured with the transient method on cuttings together with a simplified lithological profile. G: gneiss; HG: hornblende gneiss; M: metabasite; A: alternating sequence of gneisses and metabasites.

Table D.5.2: Average values of measurements on cores from the Vorbohrung (VB) and on cuttings from the Hauptbohrung (HB). Numbers in parentheses indicate the number of measurements.

	thermal conductivity (W/m/K)	
	VB (cores) 0-4000m	HB (cuttings) 0-6000m
metabasites	2.6 ± 0.4 (132)	2.6 ± 0.2 (237)
gneisses	3.3 ± 0.5 (357)	3.4 ± 0.3 (259)
total	3.1 ± 0.5 (543)	3.0 ± 0.5 (560)

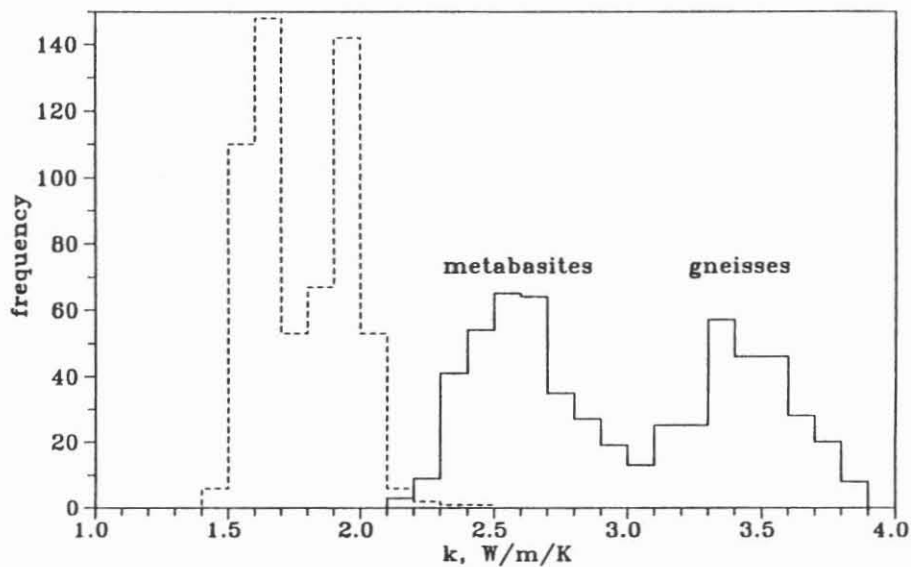


Fig. D.5.4: Frequency distribution of the measurements on the mixture of water and cuttings (---) and the calculated thermal conductivities of the cuttings (—) using the geometric mean model.

### D.5.3 Summary and Conclusions

Using the geometric mean model for a two-phase mixture, a transient heat flow method was tested successfully for the determination of thermal conductivity of cuttings. Average values for the main lithological units are in good agreement with results from measurements on cores from the Vorbohrung. Measurements on cuttings were carried out in 10 m intervals yielding a detailed log of the mean thermal conductivity.

## D.6 Electrical Resistivity

### D.6.1 Introduction and Method

Different conduction mechanisms occur in rocks. The geometry, structure and filling of the pore volume, together with the internal surface contribute to complex electrical parameters as well as bulk properties. In addition, anisotropic and frequency dependent behaviour of resistivity strongly influences results of geoelectric soundings. Thus complex electrical resistivity determined on cores is an important parameter to understand these effects, in addition to other petrophysical properties as permeability, porosity and inner surface.

In the Hauptbohrung, cores were sampled only occasionally below 4000 m. Therefore only few data can be presented. The measurements were performed short time after core recovery. In cases of time delay, the cores are stored in a basin with tap water.

The resistivity is measured by a computer controlled equipment (see Fig. D.6.1 and RAUEN, 1991). A lock-in-amplifier measures current and voltage at a fixed frequency of 120 Hz.

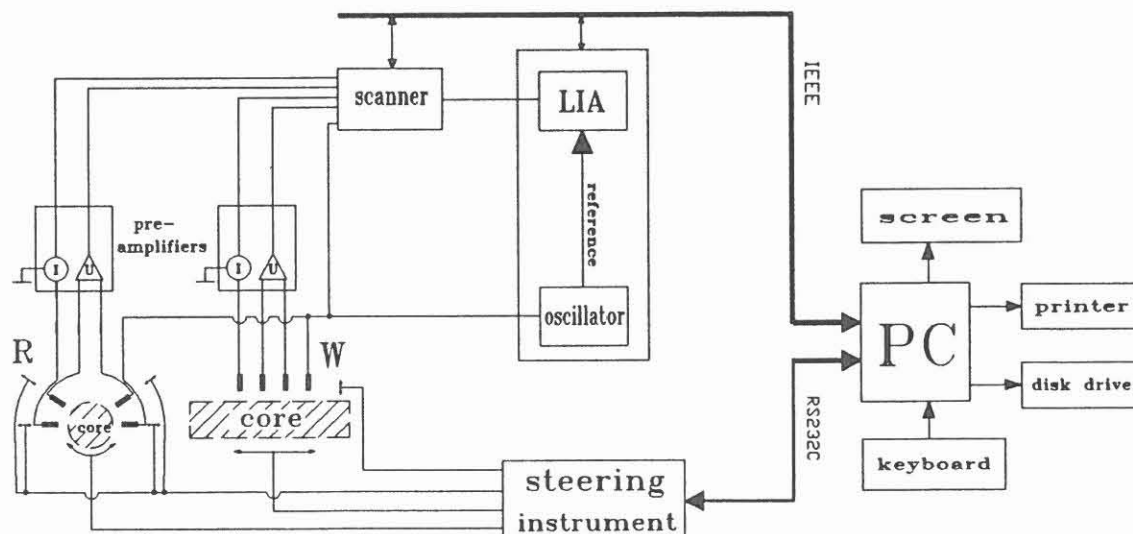


Fig. D.6.1: Schematic arrangement of the computerized equipment to measure the resistivity and its horizontal anisotropy on a drill core (RAUEN, 1991). Two sets of each four electrodes are arranged in radial (R) and in Wenner-type (W) configuration. By rotating the core and moving the electrodes, the magnitude of the complex resistivity (120 Hz) is measured as a function of azimuth and depth.



The nearly point-like electrodes consist of a porous plastic material filled with a NaCl solution. Four electrodes are arranged in radial configuration in a plane normal to the core axis (R), four other electrodes in a Wenner-type configuration (W) parallel to the z axis of the core. By rotating the core and moving the electrodes, the core is scanned at steps of 15° in azimuth and 10-20 mm in depth.

The resistivity values of all depth positions and same azimuth are stacked to one resistivity as an averaged function of azimuth. The maximum ( $R_{max}$ ), minimum ( $R_{min}$ ) and mean value ( $R_{\bar{}}$ ) of resistivity and the factor of horizontal anisotropy (A), which is defined as  $A = \sqrt{R_{max}/R_{min}}$ , are calculated.

### D.6.2 Results

Fig. D.6.2 shows the depth logs of resistivities and factors of horizontal anisotropy (A).

The parameter A varies from 1.13 to 2.20. The higher values of A up to 2.20 are measured in gneisses (cores 1,7 and 13), obviously caused by the foliation. In all cases, the foliation dips relatively steep. Lower values of resistivity are commonly measured in a direction parallel to the foliation. This may be due to microcracks and grain contacts parallel to the planes of foliation. The electrolytic filling and internal surfaces of these cracks cause the reduced resistivity in this direction.

Amphibolites (cores 3,4,8,10,11 and 12) show lower values of A (up to 1.54), which correlate with a weaker foliation. The massive and unfoliated metagabbro sample (core 14) is the most isotropic, with an A of 1.13. Core 16 consists of both, amphibolite and gneiss, with a subvertical boundary and an A of 2.1.

The metagabbro sample (core 14) shows the maximum resistivity of 5300  $\Omega m$ . The lowest values of 430  $\Omega m$  (core 8) and 300  $\Omega m$  (core 10) are obtained in amphibolites, which show small healed fissures.

### D.6.3 Conclusions

The resistivity and its horizontal anisotropy were measured using point electrodes and a measuring frequency of 120 Hz. The samples are unprepared cores. High factors of anisotropy (1.8 up to 2.2) are measured in gneisses, with the lower resistivity in a direction parallel to the foliation. The obtained anisotropies in the metabasites are lower (1.1 to 1.5). Therefore the factor of anisotropy seems to be a proper mean to separate gneisses from amphibolites.

The resistivity ranges from 5300  $\Omega\text{m}$  (massive metagabbro) to 210  $\Omega\text{m}$  (amphibolite with small healed fissures). High resistivities ( $> 1000 \Omega\text{m}$ ) are measured in gneisses as well as in amphibolites. In general, resistivities of cores of the Vorbohrung show higher values (see RAUEN, 1991). The geometric mean of all Vorbohrung metabasite samples is 4120  $\Omega\text{m}$ , that of all Hauptbohrung metabasites is 917  $\Omega\text{m}$ . This may be caused by a higher content of fractures filled with water, because of a higher grade of disintegration (see chapter D.9).

Measurements of the frequency dependent complex resistivity and other petrophysical investigations (permeability, porosity and inner surface) will be carried out in the near future on plugs.

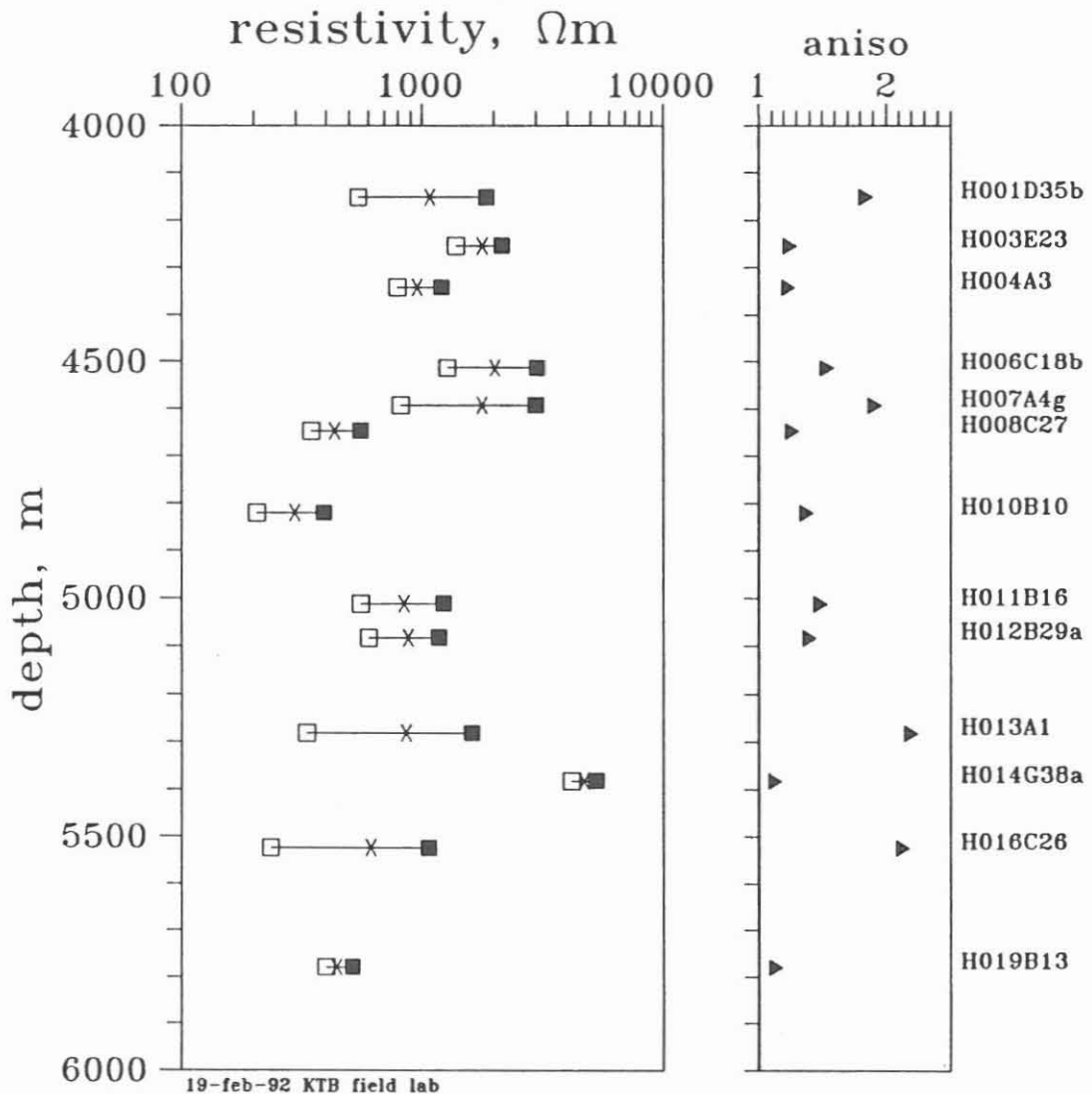


Fig. D.6.2: Depth log of resistivity (minimum, maximum and mean values, depending on measuring azimuth) and factor of anisotropy, as defined in the text. On the right side, the core numbers are plotted for identification of the samples.

## D.7 Ultrasonic Seismics

### D.7.1 Introduction and Methods

The reason for the investigation of ultrasonic velocities on a routine basis at normal temperature and pressure in the KTB field laboratory are the following:

- correlation between seismic velocities and other physical and lithological rock properties,
- improved understanding of seismic velocities and structures derived from seismic field experiments,
- as basis for a purposeful selection of samples for more detailed laboratory investigations,
- for comparison of rock properties at in-situ and at normal conditions,
- for the investigation of time - dependent petrophysical effects after core recovery.

Ultrasonic wave propagation through core samples is studied in a water tank to insure good signal transmission between transducer, rock specimen and receiver and to avoid time-consuming mechanical preparations.

A specifically designed instrumentation was used, which allows to measure the radial p-wave velocity in the plane normal to the core axis and, if the core sample is long enough, also the axial p- and s- wave velocities by common mid-point (CMP) refraction experiments, with water as the upper and the core as the lower layer. By rotating the cores, all measurements are performed for variable azimuths. Computer control of all mechanical and electrical operations, digital 10-bit data acquisition, signal stacking and interactive seismogram evaluation are essential features of the system.

### D.7.2 Results

Data are available only from the few cores taken below 4000 m. The investigations were carried out on the longest core samples of each cored interval ( 16 specimen). Except one gneiss specimen, all samples were metabasites. Compared with the core material from the KTB Vorbohrung, the samples were shorter and the surface roughness was much higher due to drilling with roller core bits.

The radial p-wave velocity was measured in azimuthal steps of 10° and axial steps of 10mm. The results are shown in Fig.D 7.1., including the mean radial p- wave velocity and the anisotropy coefficient  $(v_{p \text{ max}} - v_{p \text{ min}}) / v_{p \text{ mean}}$  as functions of depth. The variations of velocities and anisotropy coefficients in small depth intervals of only a few centimeters are considerable.

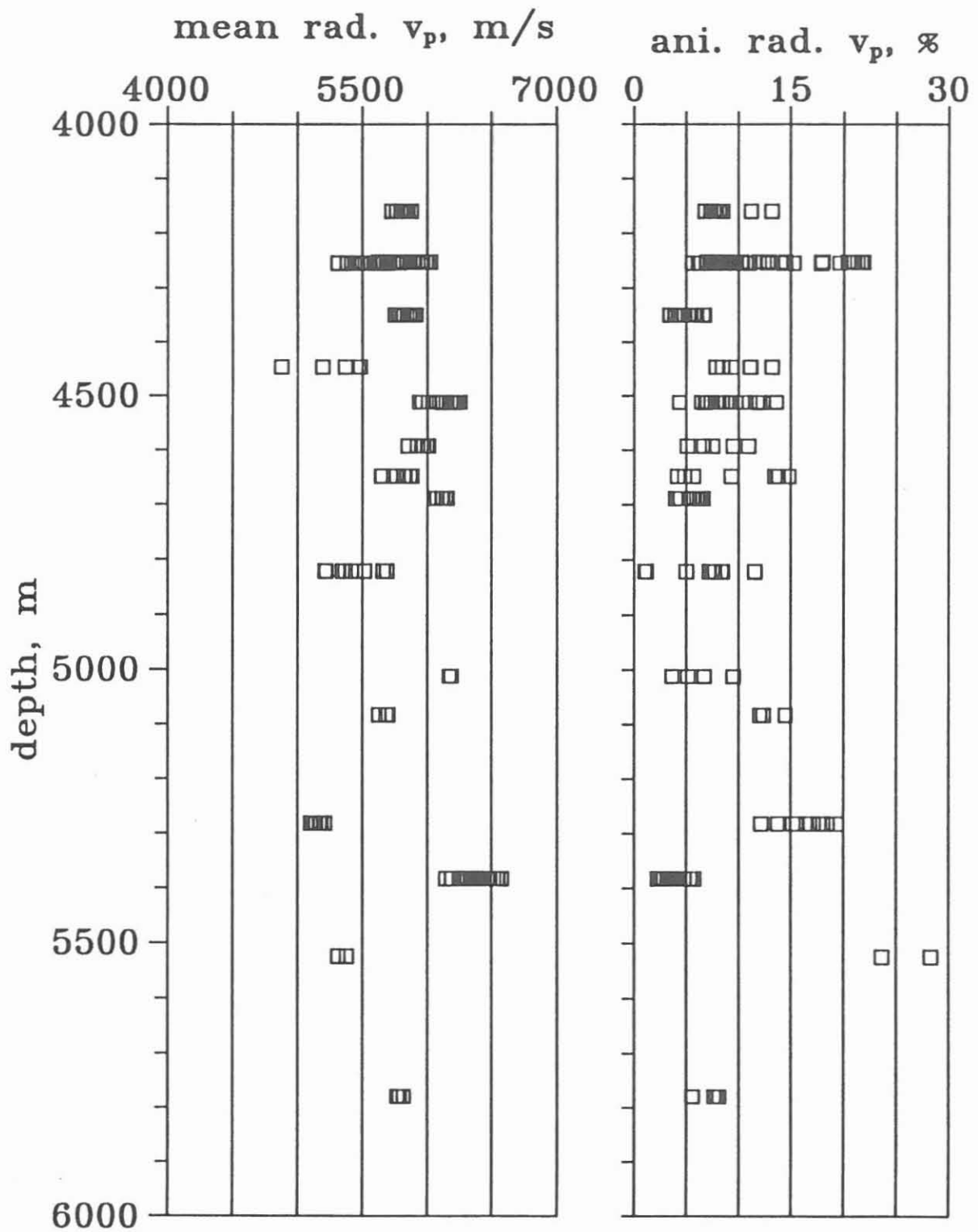


Fig. D.7.1: Mean radial p- wave velocities and anisotropy coefficients of KTB - cores

Reasons for this variations are:

- changes in structural features like frequency, distribution and incident angle of fractures and microcracks
- inhomogeneous distribution of mineralogical components
- variations in the mineralogical composition

Although the cores were measured as soon as possible after core recovery (1 hour) the results may be strongly influenced by the pressure-temperature-relief. It must be assumed, that relaxation is in process for more than 20 hours (drill-time + half round-trip-time) and also the saturation is different from that under in-situ conditions.

Repeatative measurements show variations of velocity up to 10% dependent on the foliation angle and foliation degree. The effect is most pronounced for wave propagation normal to foliation. The main reasons for this variations are:

- time-dependent effects of core relaxation which result in decreasing velocities due to a growing number of microfractures
- increasing velocities because of progressive fluid penetration in new fractures, generated by stress relaxation
- coupling effects on account of surface roughness

The determination of axial p- and s- wave velocities was impossible because the core surfaces were not smooth enough and because the core samples were too short for the CMP refraction experiment.

The mean axial p-wave velocity for metabasites of the KTB Hauptbohrung is about 5% lower than the velocity of equivalent rock samples of the KTB pilot hole. A possible reason for this may be, that the fabric loosening by coring with a roller cone bit is higher than with a diamond core bit.

## D.8 Depth Corrections Based on Petrophysical Data

Differences between core or cuttings depth and logging depth in general are caused by the weight and buoyancy of the probes as well as the lengthening and friction of the drill string. The lengthening of the logging cable will be corrected by the measured tension of the cable. Errors in the bottoms up time for the cuttings may be neglected.

For all comparisons between laboratory and log measurements the knowledge of the quantitative depth offset is important.

Fig D.8.1 shows two examples for differences between logging depth and cuttings depth indicated by the gamma ray. In the left diagram the "mixed samples" character can be seen at the transition zone from gneisses to metabasites. The logging indicates a transition zone of about 4 m whereas the cuttings show a transition zone of more than 8 m. The right diagram shows clear depth differences of about 4 m between cuttings and logger's depth. This depth difference is due to the difference between the logger's and the driller's depth. But for the cuttings, there is no clear systematic increase of depth shift with depth as it has been found for the cores of the Vorbohrung (see BÜCKER & ZIMMERMANN, 89). The detailed lithology log in chapter B shows the depth differences for all depth sections.

In the Vorbohrung the gamma-ray measurements, determined on cores and in the borehole with high sampling rates, had been used to determine the depth offset between driller and logger (see ZIMMERMANN et al. 1992). Due to the poor core recovery and the bad quality of the cores from the Hauptbohrung, the gamma-ray measurements, which need core pieces of more than 30 cm in length, could not be used. Thus the density, measurable on each core piece, was used to determine the depth offset. In depth sections with only little breakouts or cavings, a good correlation between core density and log density has been observed (see GATTO & BÜCKER, 1990).

Fig. D.8.2 shows an example for the depth offset between borehole and laboratory indicated by density measurements. In the left diagram, the laboratory measurements are plotted without any depth corrections. A correlation between borehole and core measurements cannot be detected. The cuttings measurements seem to be like a strong filtered or averaged borehole measurement. But by shifting the core measurements or parts of them until reaching best correlation with the borehole measurements, the depth shifts can be evaluated. In the case of the first core H001, the depth shift increases for the drilled core section of 7.8 m from 3.7 m to 5.3 m as indicated at the right margin of Fig. D.8.2.

The core losses of total 2.5 m are partly at the bottom, at

the top and in the midst of the cored section, resp. (see middle diagram of Fig. D.8.2). The borehole caliper, indicating good reliability of the borehole density measurements, is shown in the right diagram. On average, the logger's depth is 4.5 m deeper than the driller's depth. This result is in good agreement with the average increase of depth shift with depth of 1m/1000m shown by ZIMMERMANN et al. (1992) for the Vorbohrung.

Correlations for the other cores are just in work and will be shown in the next report.

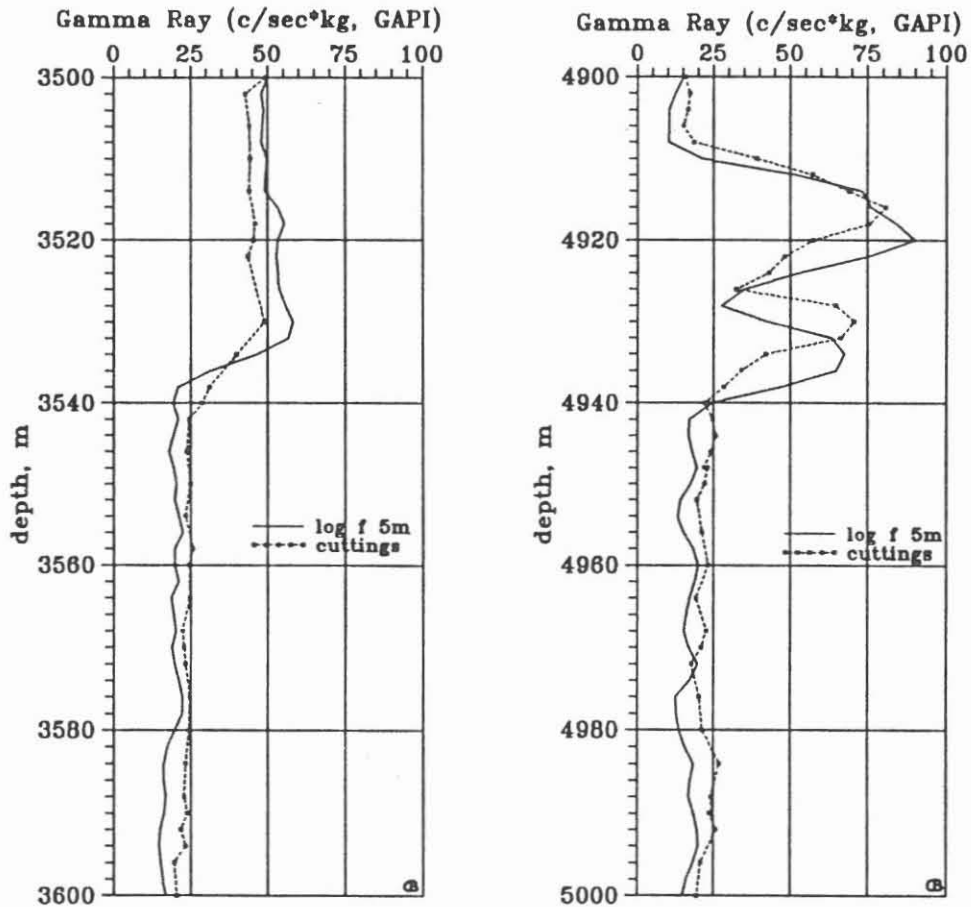


Fig. D.8.1: Two examples for differences between logging depth and cuttings depth indicated by the gamma ray.

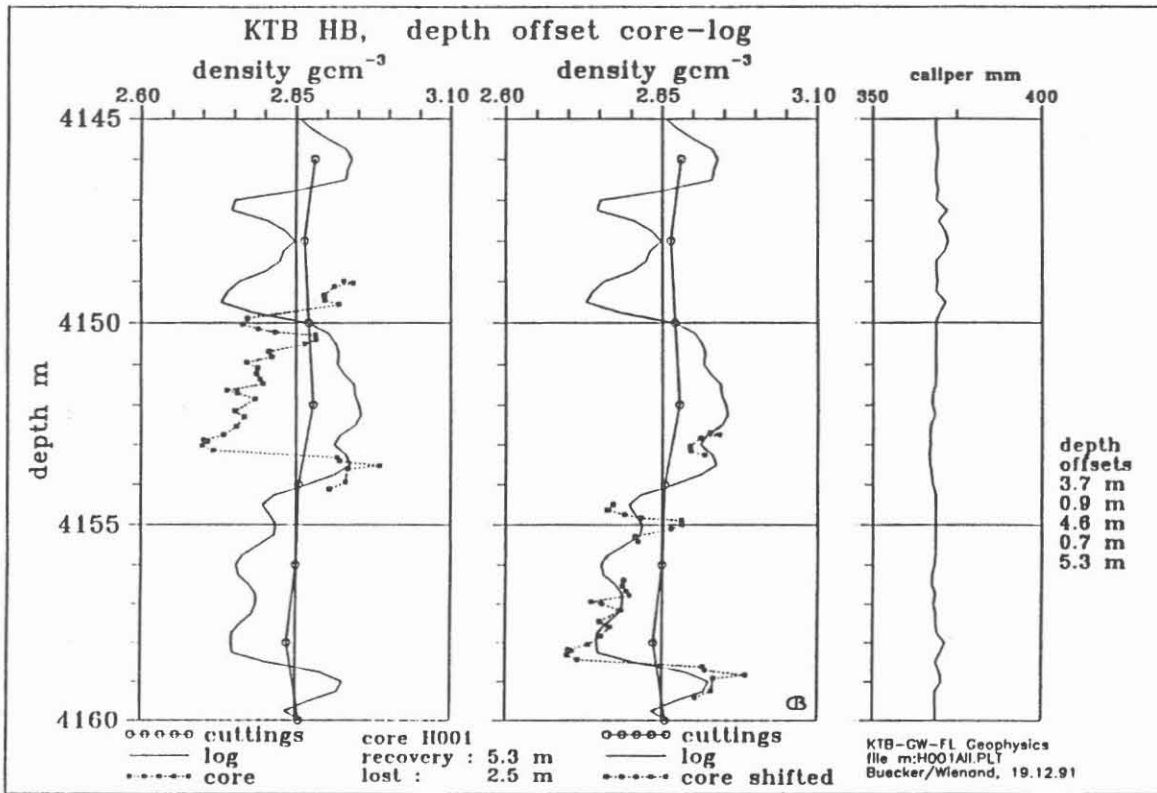


Fig. D.8.2: Example for the difference between logger's depth and driller's depth for core H001. The density measurements indicate a depth shift of up to 5.3 m.



## D.9 Summary and Discussion

For the determination of physical properties cuttings are continuously available from the Hauptbohrung. Coring started below 4000 m and is carried out at irregular intervals. Several petrophysical properties are to be measured for the identification and characterization of lithological units (Fig. D.9.1). Due to the low quartz content in the gneisses between 940 and 980 m, the thermal conductivity, for instance, decreases significantly while all other properties remain at their average levels. Another example of that kind occurs between 3360 and 3430 m. The magnetic susceptibility is enhanced by the presence of small amounts of magnetite and pyrrhotite, however, with negligible effects on cuttings density. The strong increase of natural gamma ray activity around 4280 m is caused by an enrichment of uranium which does not influence the other three properties. Thus, only the combination of these properties allows a detailed discrimination and description of lithological units.

An intensive measuring program of physical properties on cores from below 4000m in the Hauptbohrung is in progress.

Using small interval measurements of density and natural gamma ray activity from cuttings and cores it was possible to determine a coherence between drilling depth, logging depth and cutting depth.

	<u>density</u>	<u>natural gamma ray activity</u>					<u>suscept.</u>	<u>th. c.</u>
	(g/cm <sup>3</sup> )	(cnts s*kg)	potass. (%)	uranium (ppm)	thorium (ppm)	hpr (μW/m <sup>3</sup> )	(10 <sup>-3</sup> SI)	(W/m/K)
gneiss	2.74±0.03 (1275)	51±6 (1025)	2.2±0.3 (367)	2.8±0.6 (367)	7.6±1.1 (367)	1.5±0.2 (365)	0.40 (1277)	3.4±0.3 (259)
amphibolite	2.87±0.05 (1314)	25±7 (1168)	0.9±0.4 (550)	1.3±0.8 (550)	2.9±1.6 (550)	0.6±0.3 (547)	0.87 (1314)	2.6±0.2 (237)
Hornbl.- Gneis	2.85±0.05 (191)	35±10 (179)	1.5±0.6 (115)	1.7±0.7 (115)	4.5±2.1 (115)	0.9±0.4 (115)	0.88 (191)	2.7±0.3 (40)

**Table D.9.1:** Average values of measurements on cuttings from the Hauptbohrung. Numbers in parentheses indicate the number of measurements. hpr: heat production rate; th.c.: thermal conductivity; Susceptibility values are logarithmic averages. Gneisses and metabasites can clearly be distinguished from all properties. Differences between metabasites and hornblende gneisses appear only in the natural gamma ray activity values.

In order to investigate the influence of different sample types, the results obtained from cuttings of the Hauptbohrung (HB) are compared with the results obtained from cores of the Vorbohrung (VB) in Fig. D.9.1 and D.9.2. This comparison is also important for the correlation between the lithological units encountered in both drill holes in addition to the correlation using mineralogical and petrological data alone. Generally, the results from the measurements on cuttings show lower scatter. This is due to the averaging effect of the cutting samples, which represent a certain depth interval and provide only isotropic mean values.

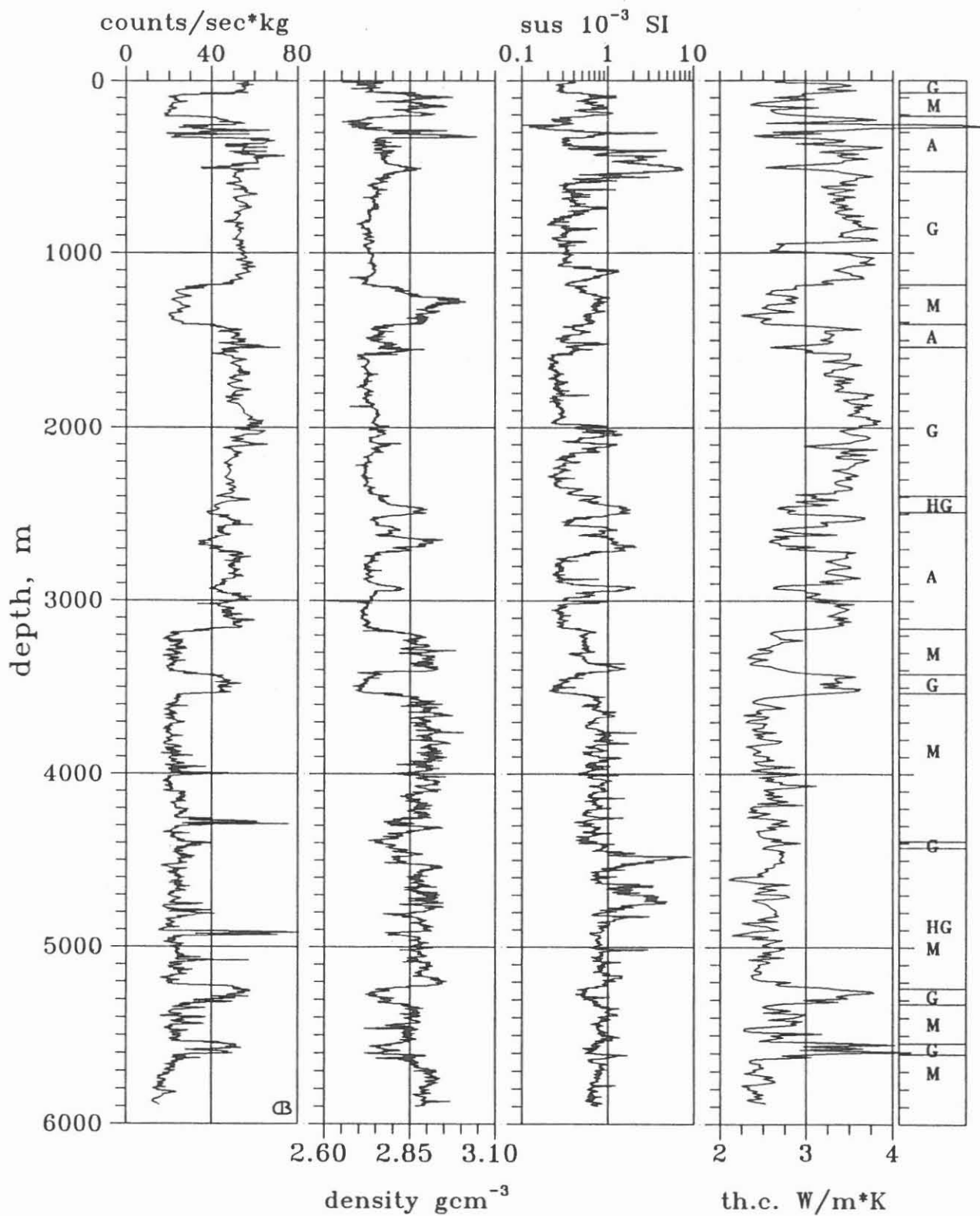
The correlation between both drill holes is discussed in chapter B, mostly based on mineralogical and petrological data. Their interpretation is supported in general by correlating petrophysical properties as well. The simplified lithologies of the VB are shown in the left column. G1, G2 and G3 are gneisses which have been identified to be the same units in both drill holes using mineralogical and petrological arguments. In a similar way, M1 and M2 have been identified as metabasites. The thickness of the M1 metabasite layer seems to differ at both drill locations. As the VB was finished at 4000 m, there is no information about the actual thickness of the M2 layer at this site. Unspecified lithological sections are either intercalations of gneisses, metabasites, lamprophyres, etc. or there is not enough data available.

Corresponding units of gneisses and metabasites have been compared (Fig. D.9.3). Average values of density, susceptibility in logarithmic scale, thermal conductivity and heat production rates were calculated together with the standard deviation of the mean (horizontal bars). So far, only the data of the more or less uniform gneiss (G1, G2, G3) and metabasite (M1, M2) sections have been used for the correlation between both drill holes. Corresponding investigations for the other sections are in progress.

Generally, density measurements on cuttings yield slightly (<1%) lower values due to the effect of the large specific surface (see chapt. D.5.2). In addition to this effect, the metabasite unit M2 has a significantly lower average density in the HB. A higher grade of cataclasis in the HB might be an explanation for that.

Average values of susceptibility are in good agreement. The slightly higher values in M1 from cutting measurements can be caused by a higher degree of bit metamorphism (see chapt. B.2), mainly occurring in metabasites.

Good agreement is also shown for thermal conductivity measurements. The gneiss unit G2 yields an about 10% lower value for the VB. The average quartz contents are 38% (VB) and 44% (HB). Due to the high thermal conductivity of



sampling rates: GR: 2-10m, dens.: 2m, sus.: 2m, th.c.: 10m

Fig. D.9.1: Compilation of physical properties measured on cuttings from the KTB Hauptbohrung.

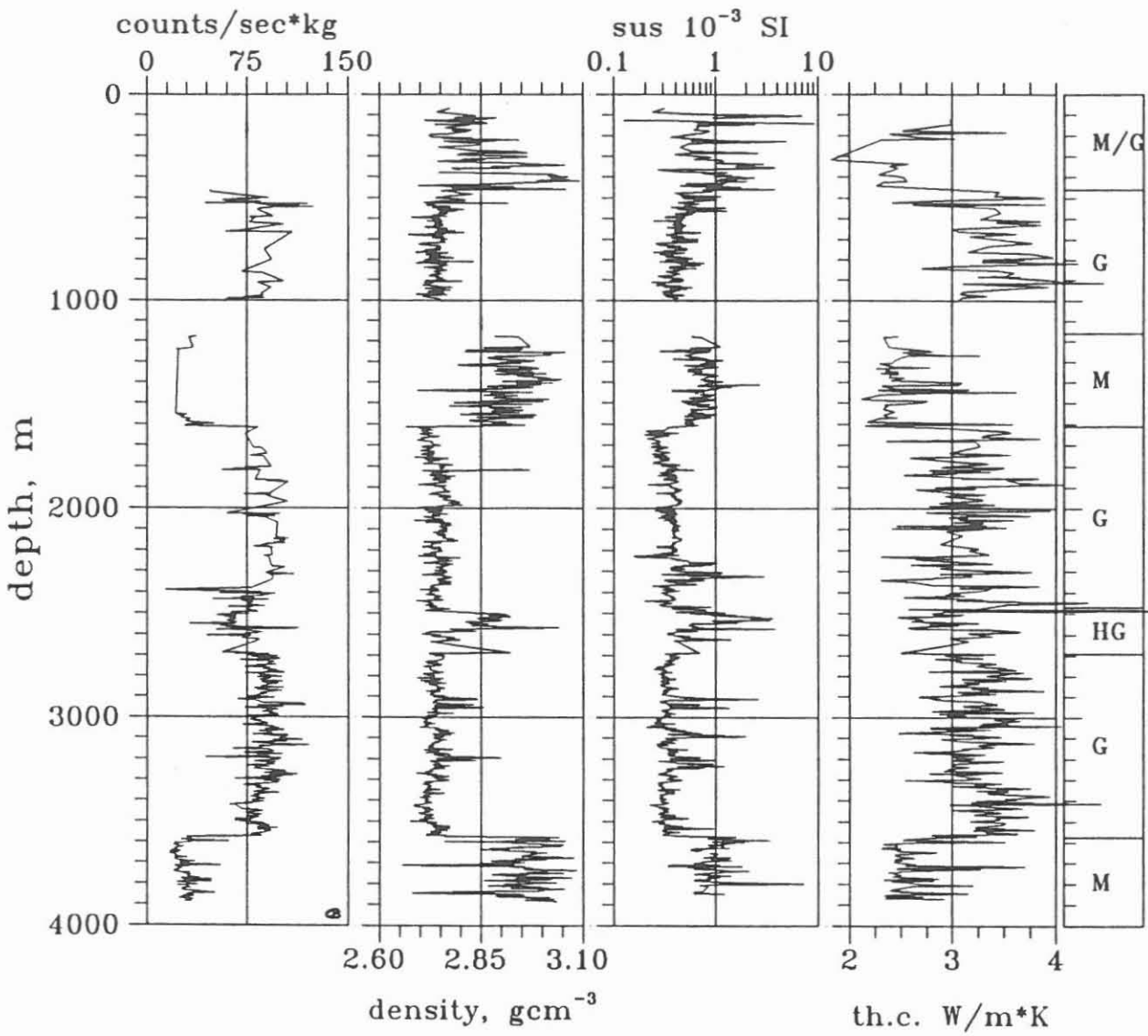


Fig. D.9.2: Compilation of physical properties measured on cores from the KTB Vorbohrung.

quartz, the difference of 6% is sufficient to cause this reduction of thermal conductivity.

Since the number of available data is low the average heat production rate was not yet calculated for the M1 unit. Values for the gneisses are in good agreement. The significant higher value for M2 from the HB is caused by a number of uranium and thorium enrichments, connected to fluid and gas inflow zones especially below 4000 m. This would suggest a higher grade of cataclasis for the M2 unit in the HB.

Measurements on cores from the HB below 4000 m generally show lower seismic velocities and electrical resistivities than comparable metabasite sections of the VB, obviously correlated with a higher crack porosity and inner surface. One reason could be the coring technique using a roller cone bit (VB: diamond bit). Another reason would be a more disintegrated metabasite section in the HB.

Summarizing, average values of density, heat production, seismic velocities and electrical resistivities indicate that the metabasite unit below 3600 m in the HB is more disintegrated than the corresponding unit in the VB. Measurements of density, susceptibility, thermal conductivity and natural gamma ray activity from cuttings and cores are in good agreement. Nevertheless, all information about anisotropy and the influence of texture is lost for cutting measurements. Further, more sophisticated correlations for the petrophysical properties including all other data stored in the database of the field laboratory are in progress in order to quantify the relationship between the two drill holes.

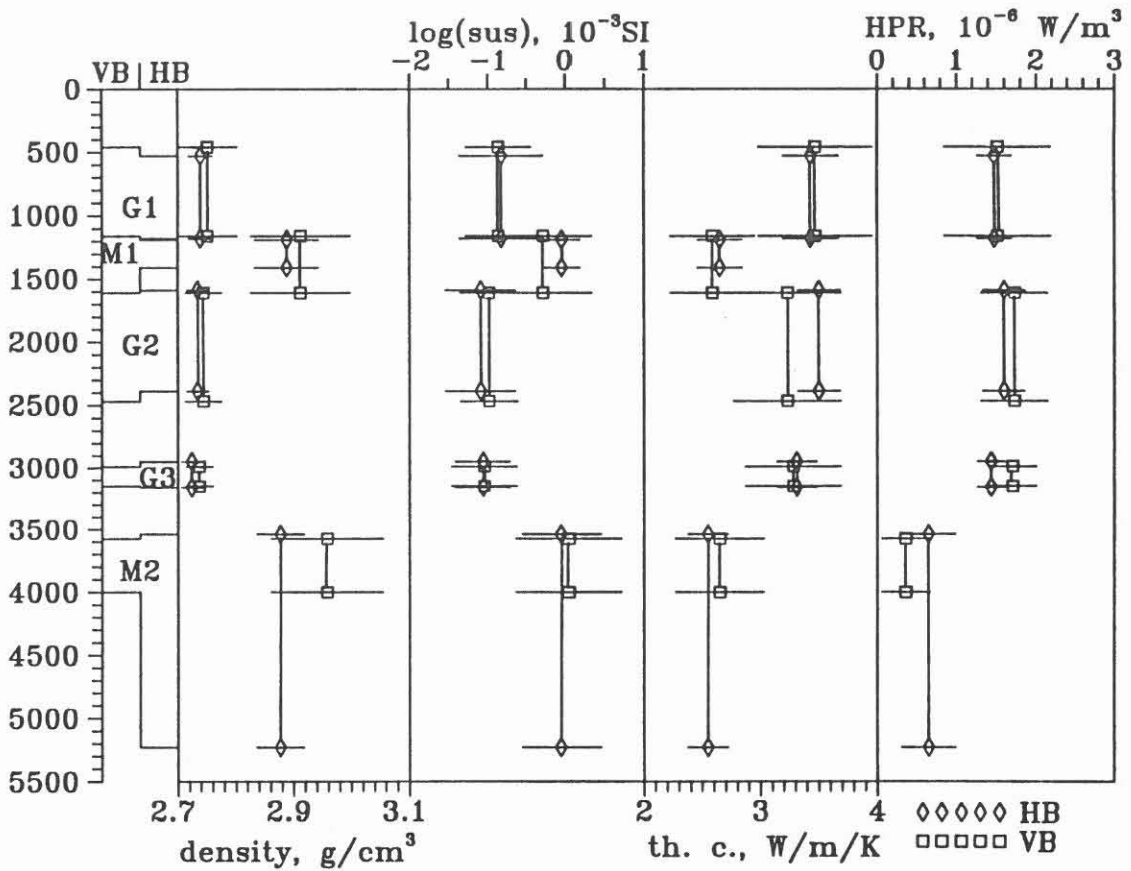


Fig. D.9.3: Comparison of average values for corresponding lithological units from the Vorbohrung (VB) and the Hauptbohrung (HB). G1-G3: gneiss; M1,M2: metabasite; HPR: heat production rate; th.c.: thermal conductivity; sus: susceptibility.

**Acknowledgement.** The authors wish to thank Hubert Köstler and Robert Fürnrohr for performing most of the measurements discussed in this report. We also thank H. Gebrande, J. Lauterjung, J. Pohl and A. Schult for their critical and improving comments. Financial support of the DFG (Deutsche Forschungsgemeinschaft) is gratefully acknowledged.

## D.10 References

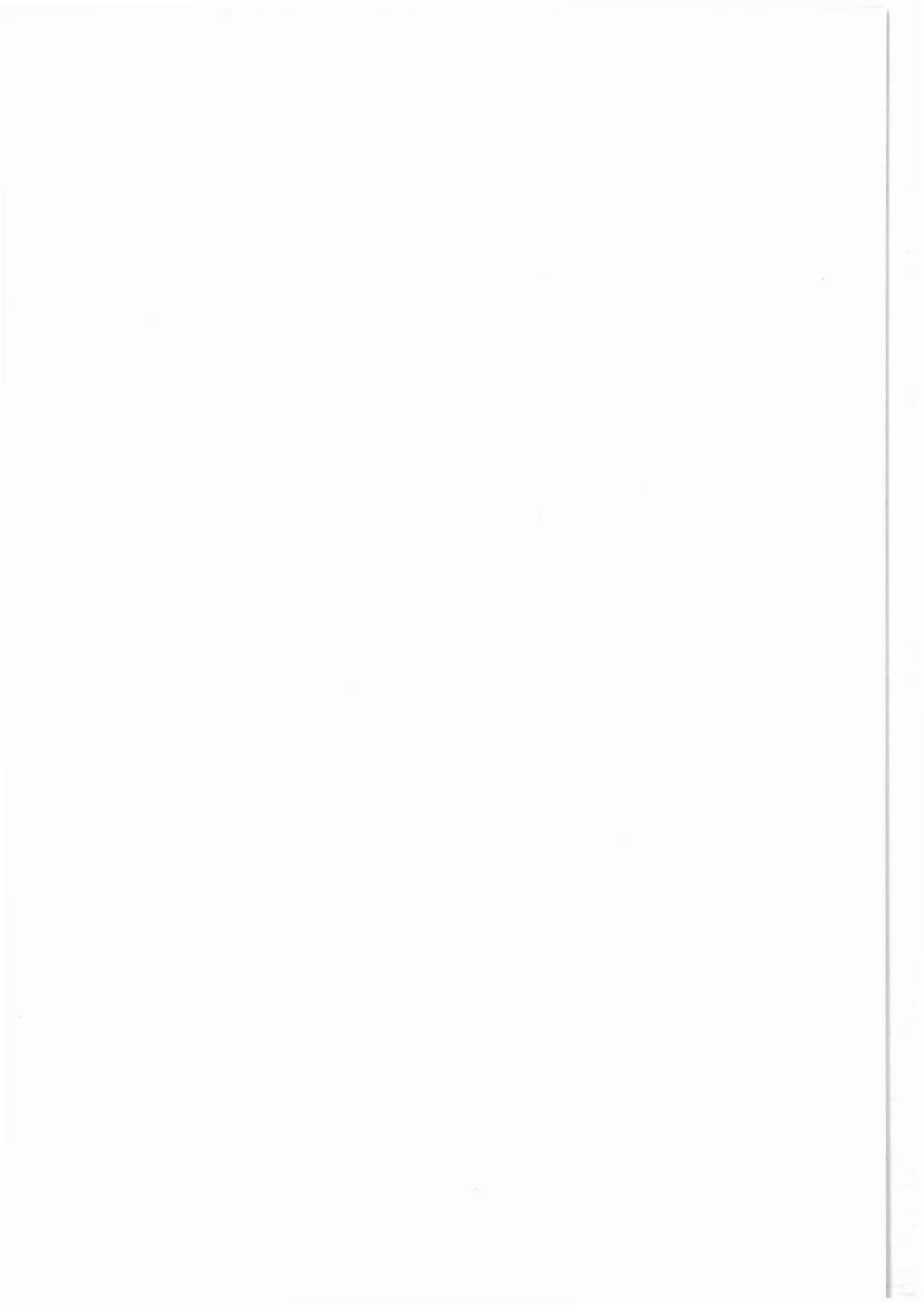
- BÜCKER, Ch., EIGNER, K.-H., RAUCH, E., RAUEN, A., WIENAND, J. & K.E. WOLTER (1988): Tiefbohrung KTB Oberpfalz VB, Ergebnisse der geowissenschaftlichen Bohrungsbearbeitung im KTB-Feldlabor, Teufenbereich 0-480 m.- D. Geophysik. In: Emmermann, Dietrich, Heinisch, Wöhrl (eds.), KTB-Report 88-1: D1-D42, NLFb, Hannover.
- BÜCKER, C., HUENGES, E., LIPPMANN, E., RAUEN, A., STREIT, M., WIENAND, J. and H.C. SOFFEL (1990): KTB pilot hole. Results obtained in the KTB Field Laboratory.- D. Geophysics - In: Emmermann, Dietrich, Lauterjung & Wöhrl (eds.), Result of Geoscientific Investigation in the KTB Field Laboratory, 0-4000, KTB-Report 90-8, NLFb, Hannover.
- BÜCKER, Ch. & G. ZIMMERMANN (1989): Vergleichende Untersuchungen der Gamma-Ray-Messungen (GR) im Bohrloch und an Bohrkernen im Teufenbereich 3000-3500 m.- In: Emmermann, Dietrich, Heinisch, Wöhrl (eds.), KTB-Report 89-5, E1-E9, NLFb, Hannover.
- BÜCKER, Ch., LIPPMANN, E., PRIBNOW, D. RAUEN, A. & WIENAND, J. (1991): Tiefbohrung KTB Oberpfalz HB, Ergebnisse der geowissenschaftlichen Bohrungsbearbeitung im KTB-Feldlabor, Teufenbereich 0-1720 m.- D. Geophysik. In: Emmermann, Dietrich, Lauterjung, Wöhrl (eds.), KTB-Report 91-3: D1-D42, Hannover.
- GATTO, H. & C. BÜCKER (1990): Vergleich der Gesteinsdichte mittels Messungen von Schlumberger (litho-density log) und an Kernen durch das Feldlabor.- In: Draxler (eds.), KTB-Report 90-1, Hannover.
- GOHN, E., HORN, K., LASCHTOWITZ, K., POHLMANN, M., REINEKING, A., SCHMIDT, K.H. (1991): Vergleich von Meßverfahren und Porbenmaterial zur Bestimmung der Wärmeproduktionsraten in der KTB-Vorbohrung. In: R. Emmermann und J. Lauterjung: Forschungsergebnisse im Rahmen des DFG-Schwerpunktprogramms "KTB", KTB-Report 91-1, Hannover.
- HAACK, U. (1982): Radioactivity of Rocks. In: Angenheister, G. (ed), Landolt-Börnstein, New Ser. Bd. V, p.433-481.
- HUENGES, E., BÜCKER, Ch., WOLTER, K.E., WIENAND, J., RAUEN, A. & E. LIPPMANN (1989): Deep Drilling KTB-Oberpfalz VB, Results of the Geoscientific Proceedings in the KTB-Laboratory; Depth Interval: 1709 - 2500 m.- D. Geophysik.- In: Emmermann, Dietrich, Heinisch, Wöhrl (eds.), KTB-Report 89-2, D1-D83, Hannover.

- HUENGES, E., BURKHARDT, H. & ERBAS, K. (1990): Thermal Conductivity Profile of the KTB Pilot Corehole. Scientific Drilling, 1, 224-230.
- HAAK, U., GOHN, E., BÜCKER, Ch. and G. ZOTH (1990): Radiogenic heat production measured by laboratory and bore hole methods, a comparison.- Scientific Drilling, 1, 211-216.
- RAUEN, A., LIPPMANN, E., HUENGES, E., BÜCKER, Ch., WIENAND, J. & K.E. WOLTER (1988): Tiefbohrung KTB Oberpfalz VB, Ergebnisse der geowissenschaftlichen Bohrungsbearbeitung im KTB-Feldlabor (Windischeschenbach), Teufenbereich von 992 bis 1530 m: D. Geophysik.- In: Emmermann, Dietrich, Heinisch, Wöhrl (eds.), KTB-Report 88-6: D1-D60, Hannover.
- RAUEN, A. (1991): Untersuchungen des komplexen elektrischen Widerstands, insbesondere dessen Anisotropie und Frequenzabhängigkeit, von Proben des Kontinentalen Tiefbohrprogramms der Bundesrepublik Deutschland (KTB). Dissertation, Ludwig-Maximilians-Universität München.
- RYBACH, L. (1976): Radiogenic heat production: a physical property determined by the chemistry of rocks. In: Strens, R.G.J. (ed.): The physics and chemistry of rocks. Wiley & Sons, London, pp. 309-318.
- SASS, J., LACHENBRUCH, A. & MUNROE, R. (1971): Thermal Conductivity of Rocks from Measurements on Fragments and its Application to Heat-Flow Determinations. JGR, 76, 3391-3401.
- SOFFEL, H.C., BÜCKER, CH., GEBRANDE, H., HUENGES, E., LIPPMANN, E., POHL, J., RAUEN, A. SCHULT, A., STREIT, K.M. and WIENAND, J. (1992): Physical Properties Measured on Cores and Cuttings from the Pilot Well (0 - 4000.1 m) of the German Continental Deep Drilling Program (KTB) in the Oberpfalz Area, Bavaria, Federal Republic of Germany.- Surveys in Geophysics.
- SOFFEL, H.C., PLAUMANN, S., PUCHER, R., BÜCKER, C., GÖTZE, H.J., WAGENER, M. and HAAK, V. (1989): Gravity and Magnetic Investigations at the KTB Locations Schwarzwald and Oberpfalz.- In: R. Emmermann and J. Wohlenberg (eds.): The German Continental Deep Drilling Program (KTB), Springer Verlag, Berlin Heidelberg, New York.
- ZIMMERMANN, G., BÜCKER, Ch., MELCHERT, M. and Th. WÖHRL (1992): Comparison of Gamma-ray Log and Core Measurements in the KTB Pilot Well - a Method to Estimate the Depth Offset Between Logging and Coring. Scientific Drilling, 92.



## E. Rock Mechanics

Th. Roeckel  
O. Natau



KTB Report	92-2	E1-E7	4 Fig.	Hannover 1992
------------	------	-------	--------	---------------

KTB Main Hole Geoscientific Investigations in the  
KTB-Field Laboratory,

Depth Interval 0 - 6000 m

**E. Rock Mechanics**

ROECKEL, Th.\*., NATAU, O.\*\*)

Contents

E.1	Introduction.....	E. 2
E.2	Test Results.....	E. 3
E.2.1	Uniaxial Compression Tests.....	E. 3
E.2.2	Indirect Tensile Tests.....	E. 6
E.3	Reference.....	E. 7

Authors` Addresses)

\* KTB Field Laboratory P.O. Box 67,  
D-8486 Windischeschenbach  
Federal Republic of Germany

\*\* Head of the Department of Rock Mechanics  
University of Karlsruhe  
7500 Karlsruhe 1  
Federal Republic of Germany

## E.1 Introduction

Rock mechanical parameters are of great scientific as well as technical importance for deep drilling projects. They are an integral part for the determination of the state of stress in the earth's crust and of direct interest to the borehole stability.

At a depth of 4149.0 m the first core in the KTB main hole was drilled. The uniaxial compressive strength and indirect tensile strength were determined on rock samples from nearly every core run. The main lithological components of the rocks of the KTB main hole are metabasites and paragneisses. From 4149,0 m to the actual depth (5600 m) 17 cores were drilled. 15 metabasite cores and one biotitgneiss core were retrieved from the well. One core was lost completely. Fig. E.1 shows a failed sample from the KTB main hole after a uniaxial compression test.

The selection of samples, their geometry, test equipment and methods have been described by ROECKEL&NATAU (1989).

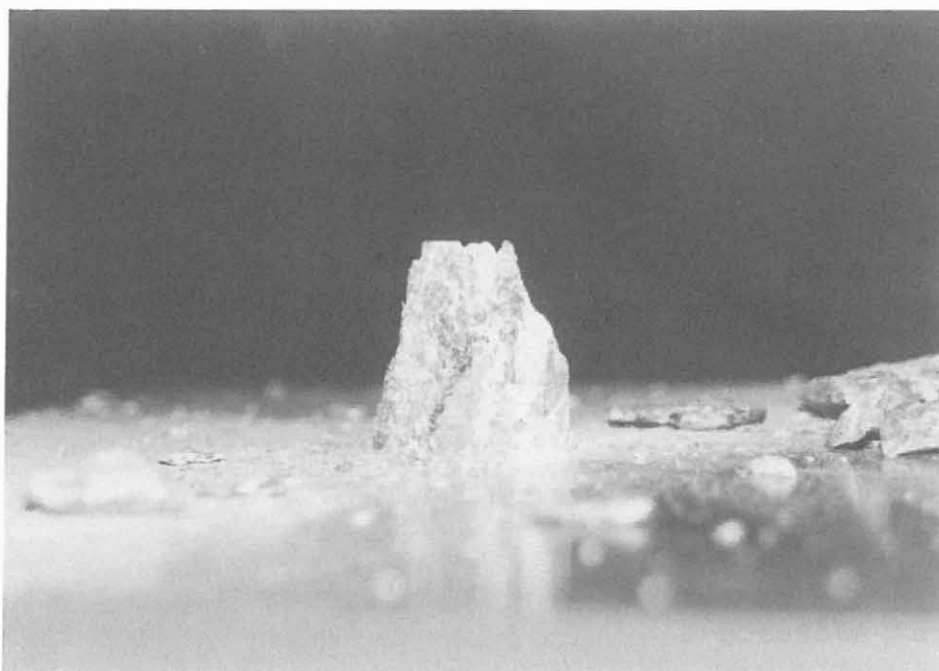


Fig. E.1: Uniaxial compression test on a metabasite sample (H004A4) from a depth of 4341.70m.

## E.2 Test Results

### E. 2.1 Uniaxial Compression Tests

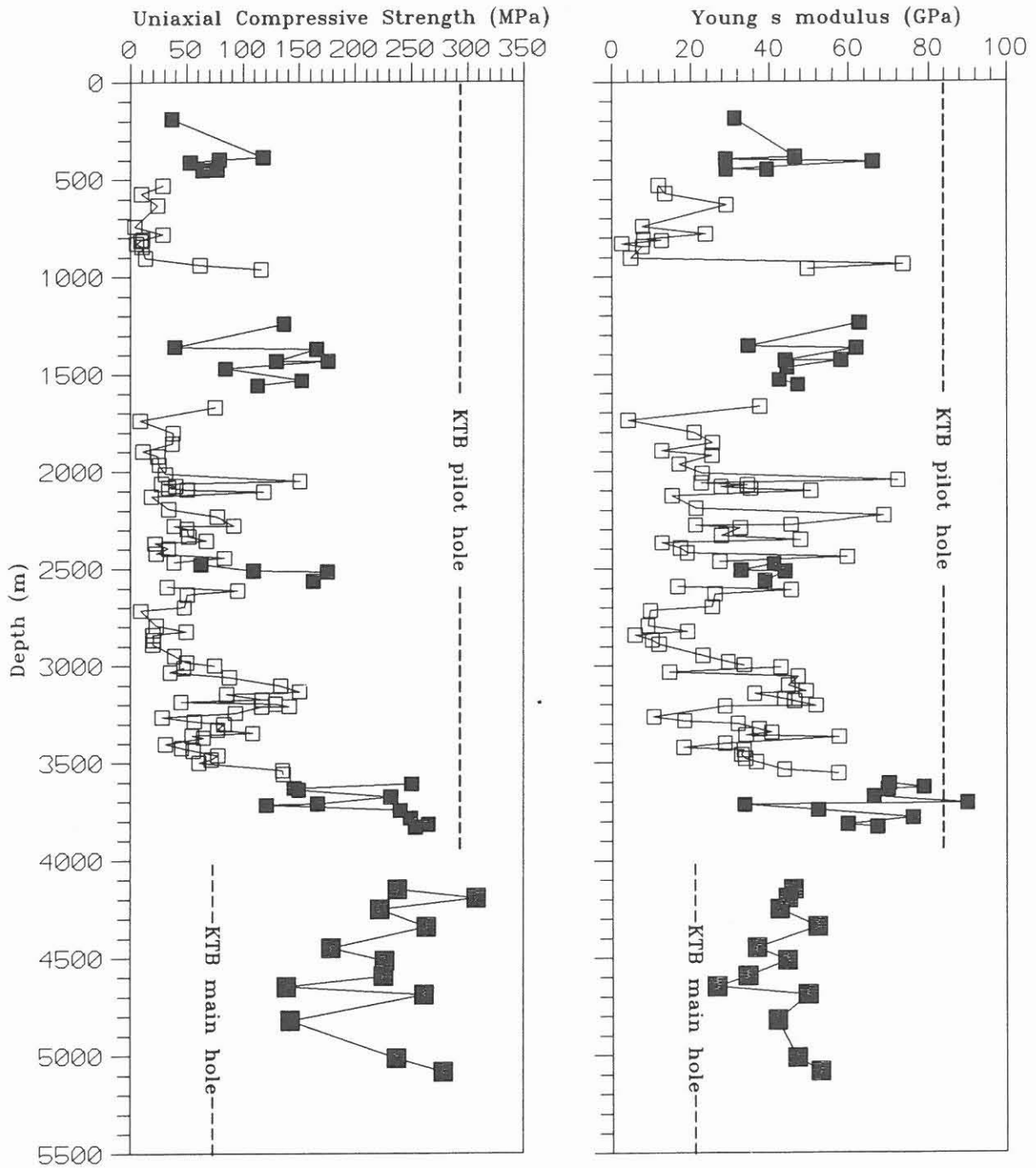
Until now 12 metabasite samples were tested. The maximum depth is 5084.44 m. The only gneiss core (H013) was not available for testing until now.

The uniaxial compression tests on the metabasites of the KTB main hole show high to very high uniaxial compressive strengths. The lowest uniaxial compressive strength (139.1 MPa) was measured on core piece H008C33 from a depth of 4648.1 m. The highest uniaxial compressive strength (307.9 MPa) was measured in the metabasite sample H002B15b from a depth of 4195.9 m. The mean value with 226.9 MPa for all 12 samples is very high. The mean value of the metabasites in the KTB main hole corresponds well with the mean value of the metabasites in the KTB pilot hole (217.2 MPa) in the depth interval from 3570 to 3832 m. The uniaxial compressive strength data of the KTB pilot hole and the KTB main hole are shown in fig. E.2. The results from the uniaxial compressive strength tests are given in tab E.1. The high elasticity is typical for the metabasites. After closing of the micro-cracks, the sample shows a nearly linear-elastic behaviour.

Tab. E.1: Results from the uniaxial compression test ( $\sigma_u$  = uniaxial compressive strength, E = Young's modulus).

Core Piece	Depth (m)	$\sigma_u$ (MPa)	E (GPa)
H001D30	4151.4	238.0	46.0
H002B15b	4195.9	307.9	44.6
H003C14a	4253.0	222.2	42.5
H004A4a	4341.7	263.7	52.1
H005D32	4449.6	179.1	36.7
H006C18b	4513.8	226.7	44.5
H007B7a	4593.2	225.7	34.4
H008C33	4648.1	139.1	26.5
H009F40	4688.7	261.6	49.7
H010B10	4820.8	142.5	42.0
H011A5a	5012.3	237.2	47.0
H012C56	5084.4	278.7	52.8

The mean value for the Young's moduli of the metabasites in the KTB main hole in the depth interval from 4149,0 m - 5084,44 m is 42.3 GPa. The lowest value measured is only 26.5 GPa, the highest is 52.8 GPa. In the metabasites of the KTB pilot hole the mean Young's modulus was 70.0 GPa in the depth interval between 3575 m and 3832 m.



**Fig. E.2a:** Dependence of uniaxial compressive strength on depth. Small black squares = metabasites of the KTB pilot hole, open squares = gneisses of the KTB pilot hole and big black squares = metabasites of the KTB main hole.  
**E.2.b:** Dependence of the Young's modulus on depth.

These data show a significant difference between Young's moduli of the metabasites in the KTB pilot hole and the KTB main hole. In fig. E.2b the Young's moduli from cores of the KTB pilot hole and KTB main hole are shown.

On one side it is remarkable, that the Young's moduli in the metabasites of the KTB main hole are significantly lower than those in the metabasites of KTB pilot hole. On the other side a crossplot of the uniaxial compressive strengths and the Young's modulus shows the relationship between these parameters (fig. E.3).

This difference may be explained by different drilling techniques. In the pilot hole the cores were drilled with a diamond core bit, whereas the cores in the KTB main hole are drilled with roller cone core bits. This leads to low core recovery in the KTB main hole (see chapter A). In addition to high thermal stresses (temperature drop of more than 100°C) strong mechanical stresses were applied on the cores of the KTB main hole which may lead to stronger micro-cracking (see chapter D.9).

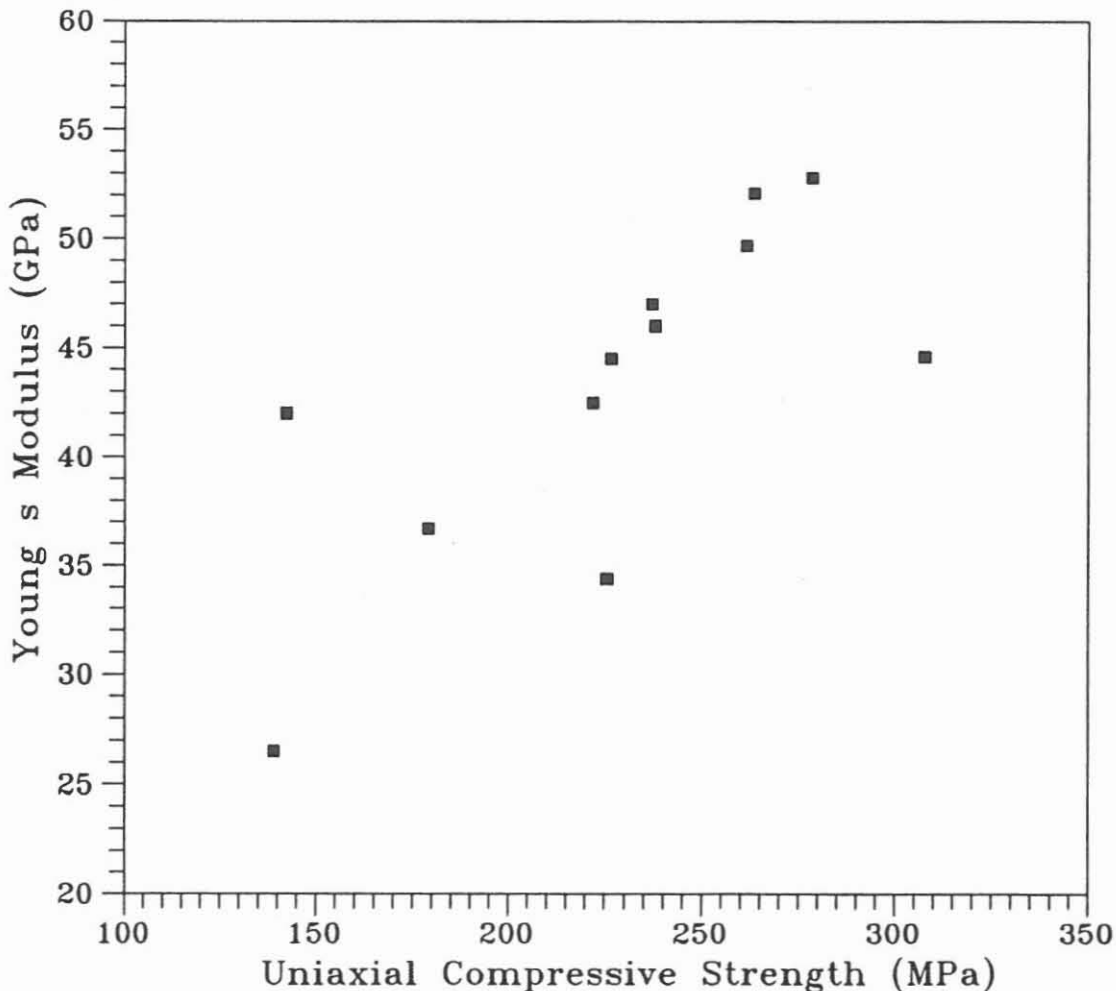


Fig. E.3: Crossplot of the uniaxial compressive strength versus Young's modulus of metabasites of the KTB main hole

### E. 2.2 Indirect Tensile Tests

The tensile strength in the KTB main hole was measured with the Brazilian-test on 50 mm plugs (fig. E.4). Until now 12 test could be carried out with success. These tests were made on metabasit samples in the depth interval from 4153 m to 5082.5 m.

Tab. E.2: Results from Indirect Tensile Tests ( $\sigma_t$  = indirect tensile strength).

Core Piece	Depth (m)	$\sigma_t$ (MPa)
H001G54	4153.6	10,5
H002B23d	4196.6	20.4
H003A5	4251.4	13.1
H004C17	4343.0	20.0
H005C25	4448.8	6.4
H006A3	4512.1	10.9
H007B14	4593.6	10.0
H009B10	4685.5	8.6
H010B10	4820.8	9.3
H011A1	5012.0	11.0
H012A9	5082.5	9.2

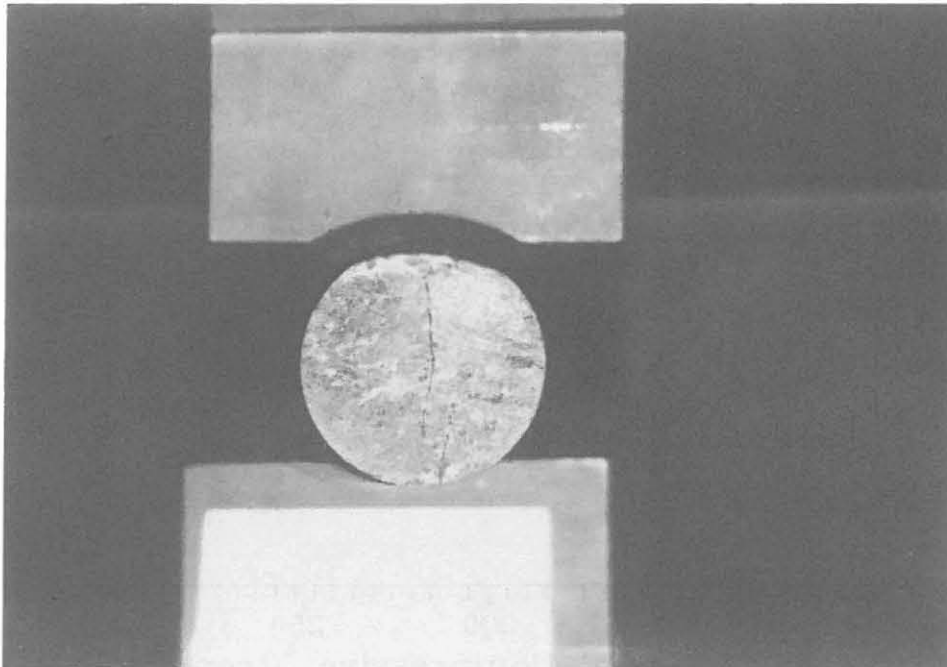


Fig. X.4: Brazilian-test to determine the tensile strength on a metabasite sample (H009B10 from a depth of 4485.5 m).

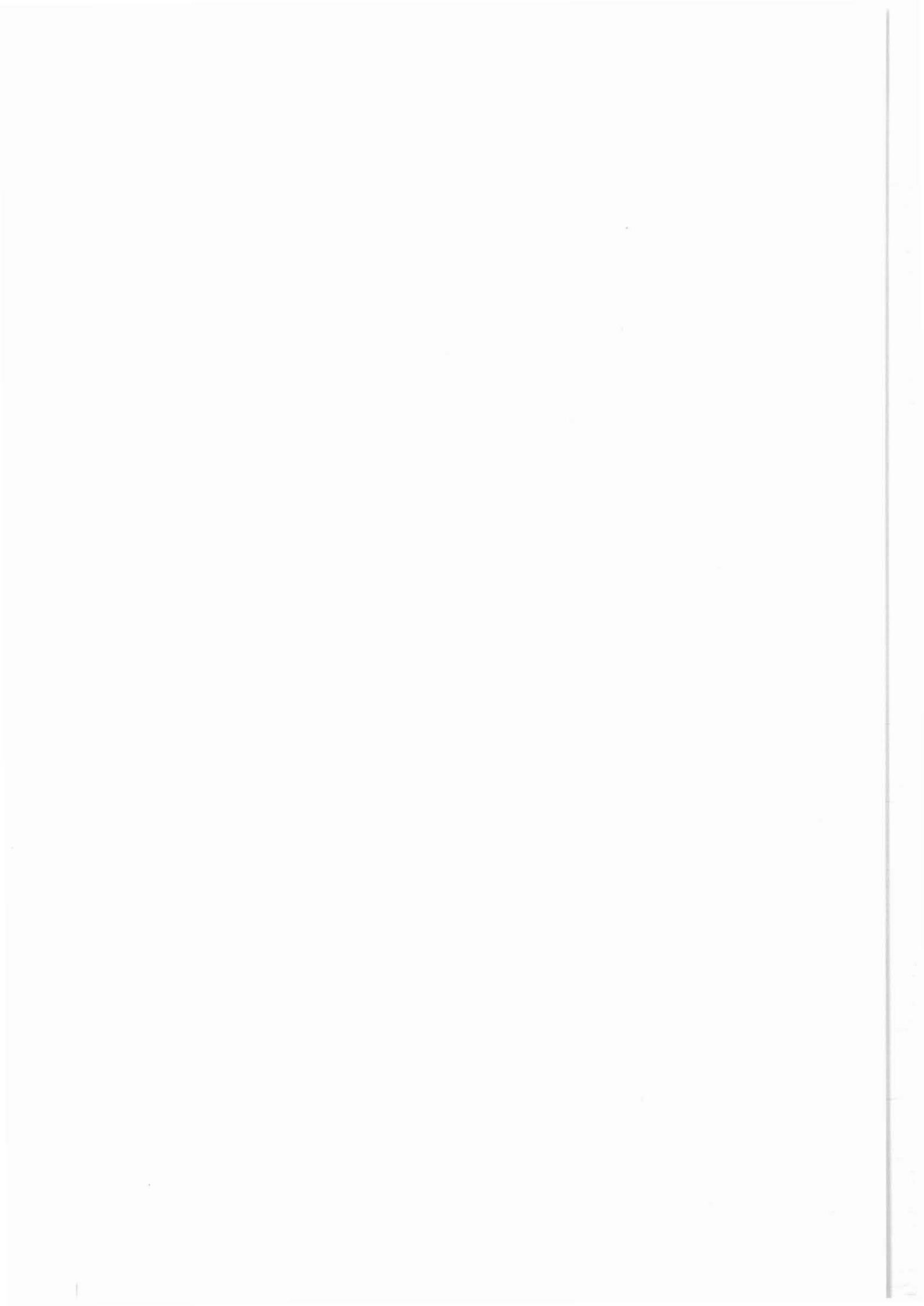


The mean tensile strength for this depth interval was 11.8 MPa. The lowest tensile strength (6.4 MPa) was measured on sample H005C25 from a depth of 4448.8 m. The highest tensile strength (20.4 MPa) was measured on sample H002B23d from a depth of 4196.2 m. On this core section the highest uniaxial compressive strengths and the highest tensile strengths of the KTB pilot hole and main hole were measured. The results of the indirect tensile strength test are given in tab. E.2.

The high strength of the metabasites in the KTB main hole may be explained by low core recovery (see chapter A). The weak rocks probably crush during coring and only the strong rocks "survive" in the core barrel. In this case, the strength data from the KTB main hole give us the upper limit for the rock strength in this borehole.

### E.3 Reference

- ROECKEL, Th., NATAU, O. (1989): Tiefbohrung KTB Oberpfalz VB  
- Erste Ergebnisse felsmechanischer Index-Versuche bis  
1998 m.  
KTB-Report 89-2



# F. Core Reorientation by Comparison of Core Instabilities and Borehole Instabilities

H.-G. Dietrich  
O. Natau  
Th. Roeckel



KTB-Report	92-2	F1-F17	12 Fig.	Hannover 1992
------------	------	--------	---------	---------------

**Core Reorientation by Comparison of Core Instabilities and  
Borehole Instabilities**

ROECKEL, Th.,\* NATAU, O.\*\* and DIETRICH H.-G.\*)

Contents:

	Abstract	
F.1	Introduction.....F.	2
F.2	Core Disking.....F.	4
F.2.1	General.....F.	4
F.2.2	Shape of Core Disks.....F.	5
F.3	Evaluation of the Orientation of Core Disking High Points .....F.	6
F.3.1	In Situ Stress Indicators.....F.	9
F.3.1.1	KTB Pilot Hole VB.....F.	9
F.3.1.2	"Practical use".....F.	13
F.3.1.3	Core Orientation of the KTB Main Hole HB.....F.	15
F.4	References.....F.	16

Authors' Addresses)

\* KTB Field Laboratory,  
D-8486 Windischeschenbach  
Federal Republic of Germany

\*\* Head of the Department of Rock Mechanics  
University of Karlsruhe  
75 Karlsruhe 1  
Federal Republic of Germany

### Abstract

In many deep boreholes instabilities occur in the borehole wall as well as in cores. These instabilities are often related to the in situ stress field and can be used for the reorientation of cores. For all cores in the depth interval between 3570 m and 3800 m the mean value of the core disk high points - which indicates the orientation of the least horizontal stress ( $S_h$ ) - is  $N67^\circ E \pm 17^\circ$  and  $N248^\circ \pm 17^\circ$ . These data are in good agreement with the orientation of drilling induced fracs in the borehole wall of the KTB pilot hole. The drilling induced fracs indicate the orientation of the maximum horizontal stress direction. The mean value of the drilling induced fracs in the depth interval between 3000 m and 3620 m is  $N158^\circ E \pm 10^\circ$ . This means, that the orientation of the core disk high points is perpendicular to the drilling induced fracs.

### F.1 Introduction

For many scientific questions the orientation of the cores is of great interest. The orientation of cores in the KTB pilot hole was mostly carried out by use of an indirect method. This method compares structures on the cores with the same structures on orientated images of the borehole wall gained by geophysical logging tools (fig. F.1) e. g. Formation MicroScanner Tool (FMST) and Borehole Televiewer (BHTV).

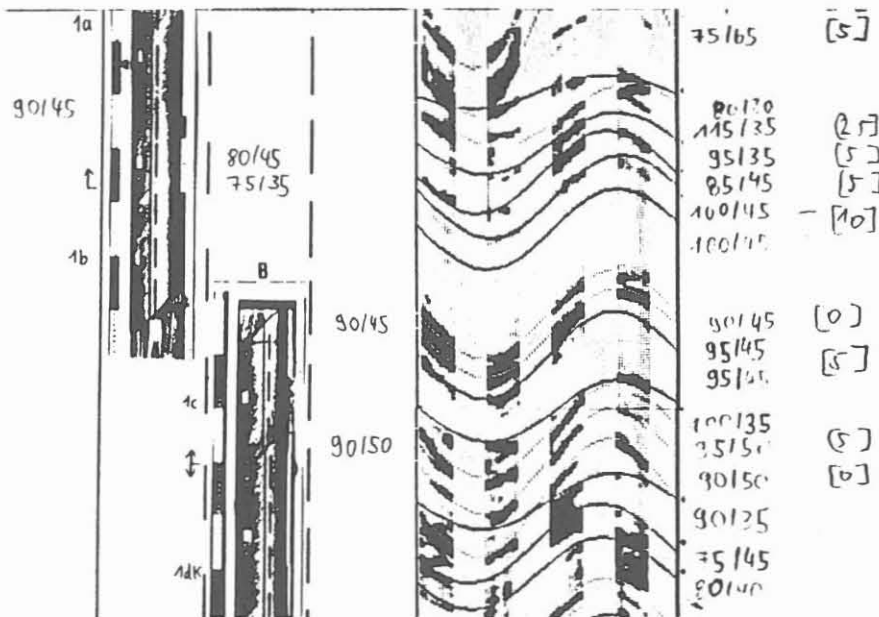


Fig F.1: Example of core reorientation from a depth of about 3385 m from the KTB pilot hole. On the left side about 1 m of core photographs with the orientation of core structures is shown. On the right side about 1 m of FMS log with the orientation of the structures in the borehole is shown.

Since core recovery over large sections of the well amounted to almost 100 per cent and the depth offset between driller's depth and logging depth could be determined very precisely, the majority of the core could be reorientated successfully with this method (KOHL et al. 1991).

The orientation of cores of the KTB main hole is very complicated. The most important reasons for this are:

- discontinuous coring
- poor core recovery by use of roller cone core bits (see chapter A), so the original position of the core pieces in the borehole is not known exactly
- In comparison to the KTB pilot hole the log quality in the KTB main hole is poorer because of smaller coverage. (The ratio between core diameter and borehole diameter decreased strongly. In the pilot hole this ratio was 94 mm/152 mm, the actual ratio is 102 mm/374 mm).

These problems do not allow to reorientate the cores as done in the KTB pilot hole.

In the KTB pilot hole instabilities were observed on both the borehole wall and the cores. There were two kinds of borehole instabilities (a+b) as well as two kinds of core instabilities (c+d):

- a) borehole breakouts and
- b) drilling induced (tensile) fractures,
- c) core diskings and
- d) centerline fractures.

The orientation of borehole instabilities can be detected by geophysical tools e. g. the Formation MicroScanner Tool (resistivity log) and by the Borehole Televiewer (acoustic log). The orientation of core instabilities can be determined after the reorientation of the cores. The directions of the instabilities, which are not related to the rock fabric, are obviously caused by stress concentrations. These stress concentrations caused by the anisotropic stress field are acting on the borehole wall as well as on the core, when the core is being cut at the bottom of the hole.

This leads to the conclusion, that preferred orientations of borehole wall instabilities and core instabilities are strongly influenced by the stress field.

## F.2 Core Disking

### F.2.1 General

The phenomenon, that cores tend to disintegrate to disks while being drilled is called **core disk**ing. The fracture planes of these disks, however, are neither related to natural joints nor to bedding planes. The first complete disk occurred in a massive garnet-amphibolite at a depth of 1468 m. Two disks were also found in an isotropic lamprophyre dyke at a depth of about 2700 m and another disk in hornblende-gneisses at a depth of about 2900 m.



Fig. F.2: Core disking in core 876B2ab (3581.70 m).

In the KTB pilot hole core disking frequently occurred below 3570 m (fig. F.2). There the lithology changed from foliated paragneisses to more massive and isotropic metabasites (NATAU et al. 1989). Above 3570 m core disking in the pilot hole is predominantly related to isotropic and massive rocks. In the uniaxial compressive strength tests these rocks show linear-elastic behaviour (ROECKEL&NATAU 1990).

A major factor leading to core disking is the concentration of radial stresses at great depths. There are various theories explaining the occurrence of core disking (BORM et al. 1989) such as:



- elastic extension: tensile stresses at the base of the core exceed the tensile strength of the rock;
- fracture mechanics: tensile stresses at crack tips of microfractures exceed critical values,
- hydraulic fracturing: pore pressure of penetrating drilling mud exceeds the tensile strength of the rocks;
- eigenstress: rapid unloading of crystalline rocks at great depth may induce excessive microscopic tensile stresses within the rocks.

### F.2.2 Shape of Core Disks

The regularity of core diskling structures is nearly perfect over large intervals. The upper surface of the disks is convex in the direction of the high axis, on the lower side the surface is concave. In the direction perpendicular to the high axis the fracture is plane. This phenomenon is seen on all disks observed in the KTB pilot hole. The high points of the core diskling structures are shown in fig F.3. The high axis is the connecting line between point 1 and 2.

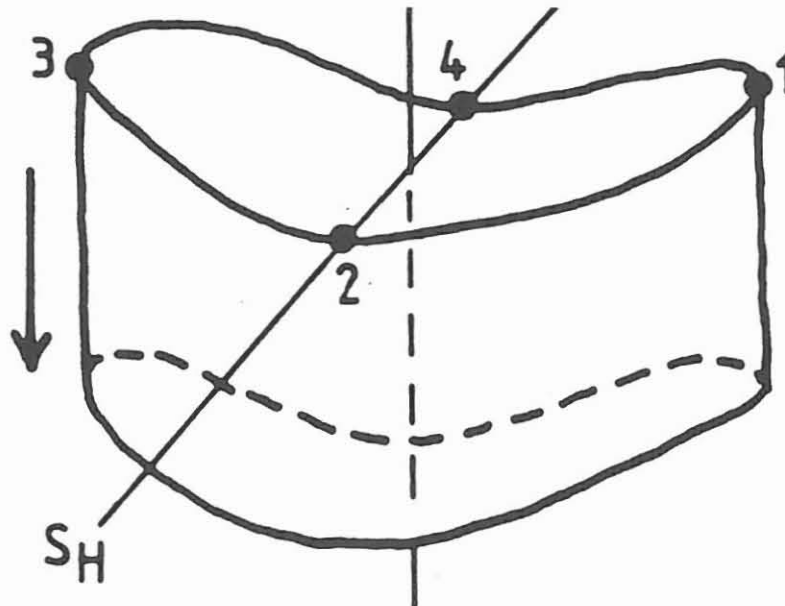


Fig. F.3: Shape of disk (after WOLTER et al. 1990).  
Definition of "high" points (1,3) and "low" points (2,4).

It is particularly remarkable, that the orientation of the high points for each core run is stable over the whole core run (fig. F.4). The thickness of the disks in the KTB pilot hole is mostly 2.5 cm - 3.0 cm. Disks with a thickness of 1,0 cm to 10 cm, however, were also found.

Ideally the azimuth of the high points is  $180^\circ$  from each other (fig. F.4, F.5). Sometimes it is observed, that the orientation of the high points is slightly influenced by the rock fabric. Normally the shape of the disk is symmetric to the core axis.

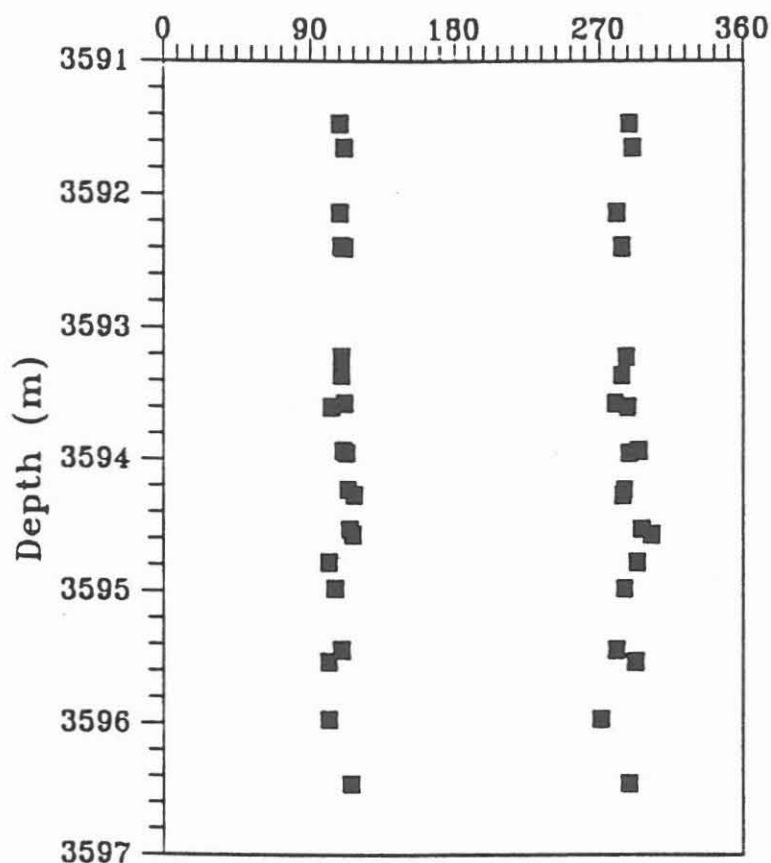


Fig. F.4: Orientation of core disk high points from core run N°878 from a depth interval between 3591 m and 3597 m.

### F.3 Evaluation of the Orientation of Core Disking High Points

The evaluation of the core disking structures was carried out as following:

- for the core discription all core pieces were put together and marked with a common reference line.
- the cores were "unrolled" on a copy machine. A copy of the unrolled core piece 882A4a1 is shown in fig. F.5.
- the core disking high points were determined from the copies.
- after reorientation of the cores the structures were orientated with respect to magnetic north.

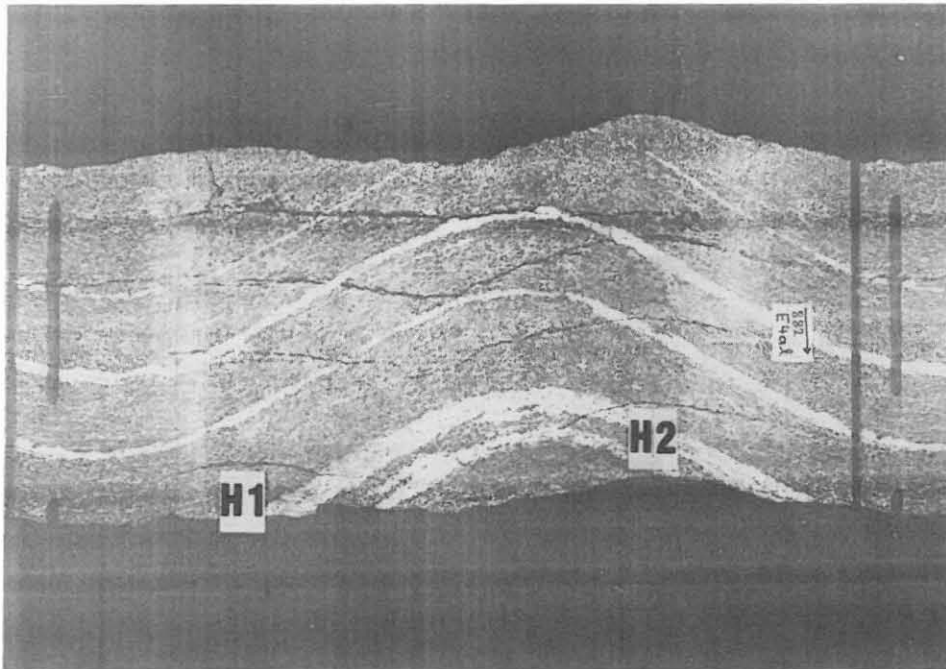


Fig. F.5: Unrolled core piece 882E4a1 with core diskings structures (H1, H2 = high points) from a depth of 3604.74 m

Tab. F.1: Mean values and standard deviations of the core diskings high points in the depth interval between 3571,7 m and 3800 m. E1, E2 = sum of high points, H1, H2 = orientation of core diskings high points (fig F.3);  $\sigma_h$  = mean orientation of least horizontal stress direction.

Depth interval (m)	E1	E2	high point 1	high point 2	$\sigma_h$
3571.70 - 3574.48	9	9	67±11	254± 8	71
3589.86 - 3584.29	37	37	102± 6	282± 6	102*
3585.02 - 3590.58	10	10	79± 7	263± 3	81
3591.47 - 3596.46	21	21	109± 5	287± 7	108*
3601.73 - 3615.60	13	13	89± 4	271± 8	90
3628.15 - 3649.03	36	35	59±20	253±15	66
3653.30 - 3663.40	21	15	68±11	247±11	68
3664.53 - 3669.40	13	9	90±12	260±12	90
3670.10 - 3675.43	22	20	73± 9	247±11	70
3676.80 - 3682.33	8	5	65± 5	252± 6	68
3684.29 - 3696.51	6	5	68± 6	246± 9	67
3699.30 - 3715.70	2	6	60±11	251± 8	65
3721.20 - 3746.10	37	37	56± 9	240±10	58
3758.00 - 3800.00	32	47	58±19	236±14	57
3571.70 - 3800.00	267	269	67±17	248±16	67**

\* core reorientation uncertain

\*\* these values are calculated without the values marked with\*

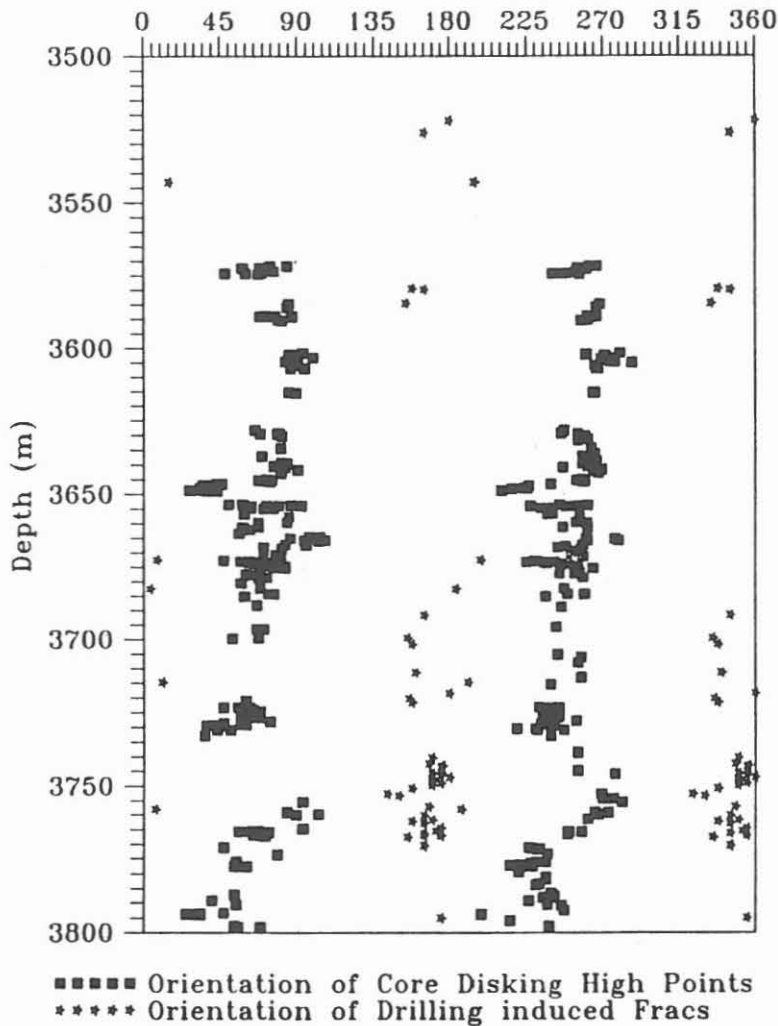


Fig. F.6: Orientation of core diskings high points and drilling induced fracs in the depth interval between 3570 m and 3800 m.

The orientation of core diskings structures versus depth (fig. F.6) shows intervals with homogeneous orientations. For all core runs in the depth interval between 3580 m and 3800 m, which were reorientated successfully, the mean values and the standard deviations are given in tab. F.1.

The mean values for all core diskings high points in the depth interval from 3570 m - 3800 m is  $N67^{\circ}E \pm 17^{\circ}$  and  $N248^{\circ} \pm 16^{\circ}$ . From these data the maximum horizontal stress direction ( $S_{Hmax}$ ) is determined as  $N158^{\circ}E \pm 17^{\circ}$ .

Core diskings especially occurs in isotropic and massive metabasites. Obviously, the preferred orientation of core diskings structures is not strongly influenced by the rock fabric (fig. F.5). Since the deviatoric stresses also increase with depth, the question, whether core diskings structures are related to the in situ stresses, was to solve.

### F.3.1 In Situ Stress Indicators

#### F.3.1.1 KTB Pilot Hole

In the KTB pilot hole there are different indicators for in situ stresses. These are among others, measurement of:

- anelastic strain retardation
- hydraulic fracturing
- borehole breakouts
- drilling induced fracs and
- differential strain analysis.

A comparison of the orientation of core diskings structures and anelastic strain retardation data showed that both methods yielded similar results for the evaluation of stress orientation (WOLTER et al. 1990). It was clearly shown, that the orientation of core diskings high axis corresponds well with the maximum horizontal strain of the anelastic strain retardation measurement. In isotropic rocks the maximum strain is assumed to correspond with the direction of the maximum horizontal stress.

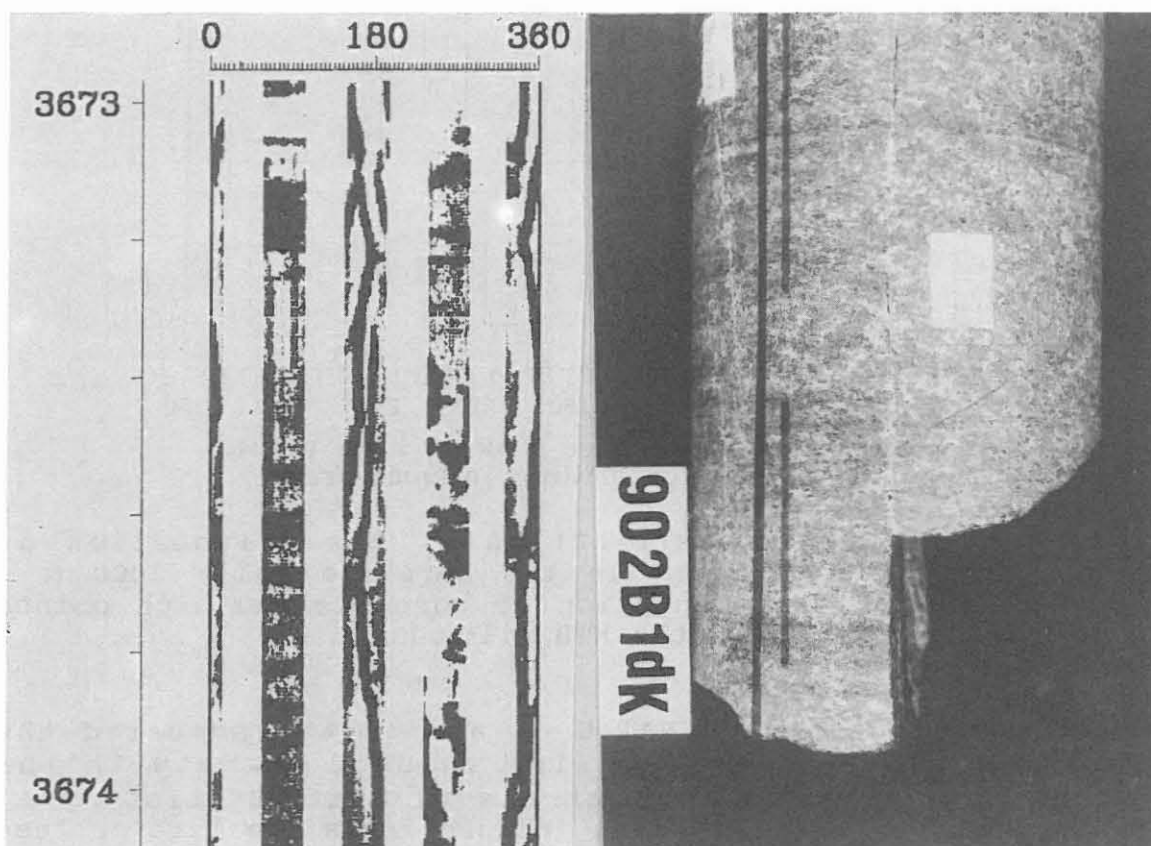


Fig. F.7a: Drilling induced hydraulic frac in the borhole wall at a logging depth of 3673 m. b: Core 902B1dK from about the same depth shows core diskings structures cut from centerline fracture.

Drilling induced fracs were often found in the borehole wall of the KTB pilot hole. These fracs are caused by hydraulic and thermal stresses. The strike of these fracs corresponds well with the orientation of the maximum horizontal stress direction. One example for a drilling induced frac from a depth of 3673 m is given in fig. F.7.a.

Core diskings is frequently found in the depth interval from 3570 m - 3800 m. Drilling induced fracs in the interval from 3500 - 3800 m are also very common. The orientation of both these structures are shown in fig. F.6. A comparison of the strike direction of drilling induced fracs in the borehole wall and core diskings high points on cores indicates, that both directions are nearly perpendicular to each other. This fact is also clearly shown in a frequency distribution of these structures (fig. F.8).

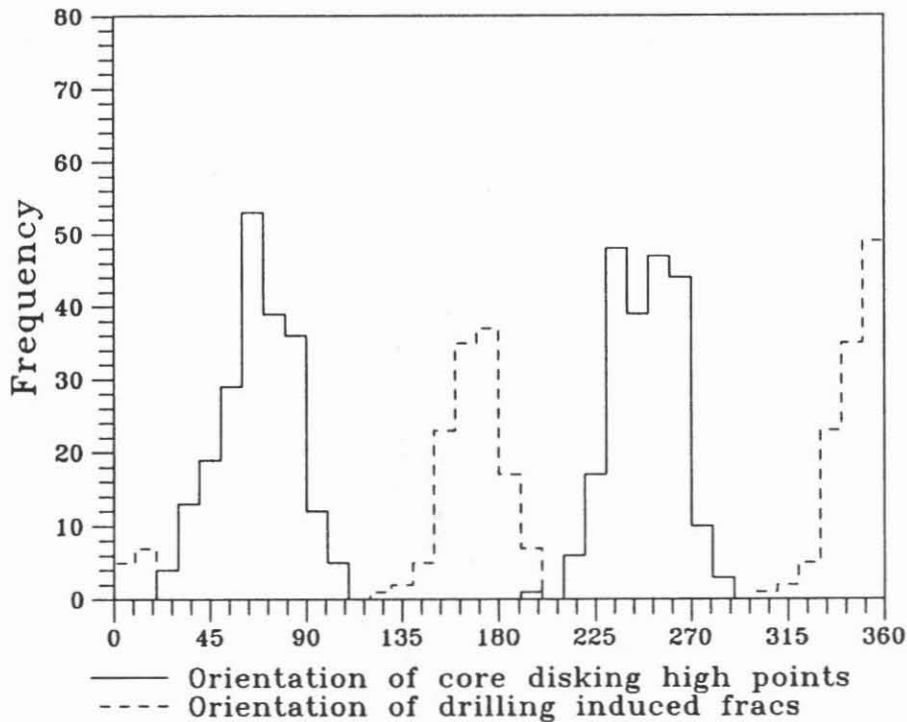


Fig. F.8: Frequency distribution of the orientation of drilling induced fracs in the borehole wall (3000 m - 3800 m) and the orientation of core diskings high points (3570 m - 3800 m) in the KTB pilot hole.

BORM et al. (1989) and NATAU et al. (1989) compared the orientation of these drilling induced fracs with the orientation of borehole breakouts in the KTB pilot hole. They found, that the drilling induced fracs are more or less orthogonal to the direction of the breakouts.

In the core pieces of core run 902 (3670.2 m - 3676.0 m) not only core diskings structures but also centerline fractures were found, for example in core piece 902B1dK (fig. F.7.b).

The strike of the core diskings high axis is perpendicular to the strike of the centerline fracture (fig. F.9). The centerline fracture is fresh and no mineralization could be found on the fracture plane.

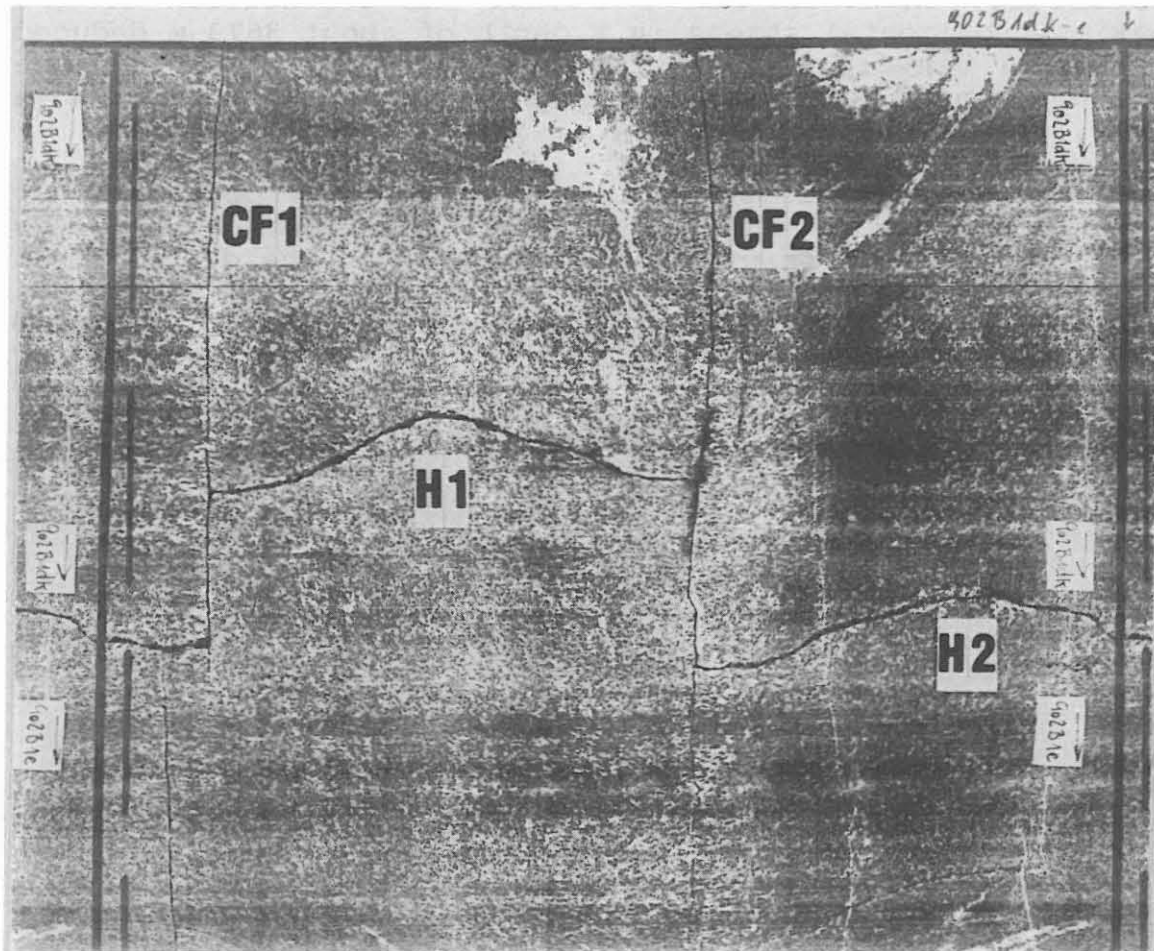


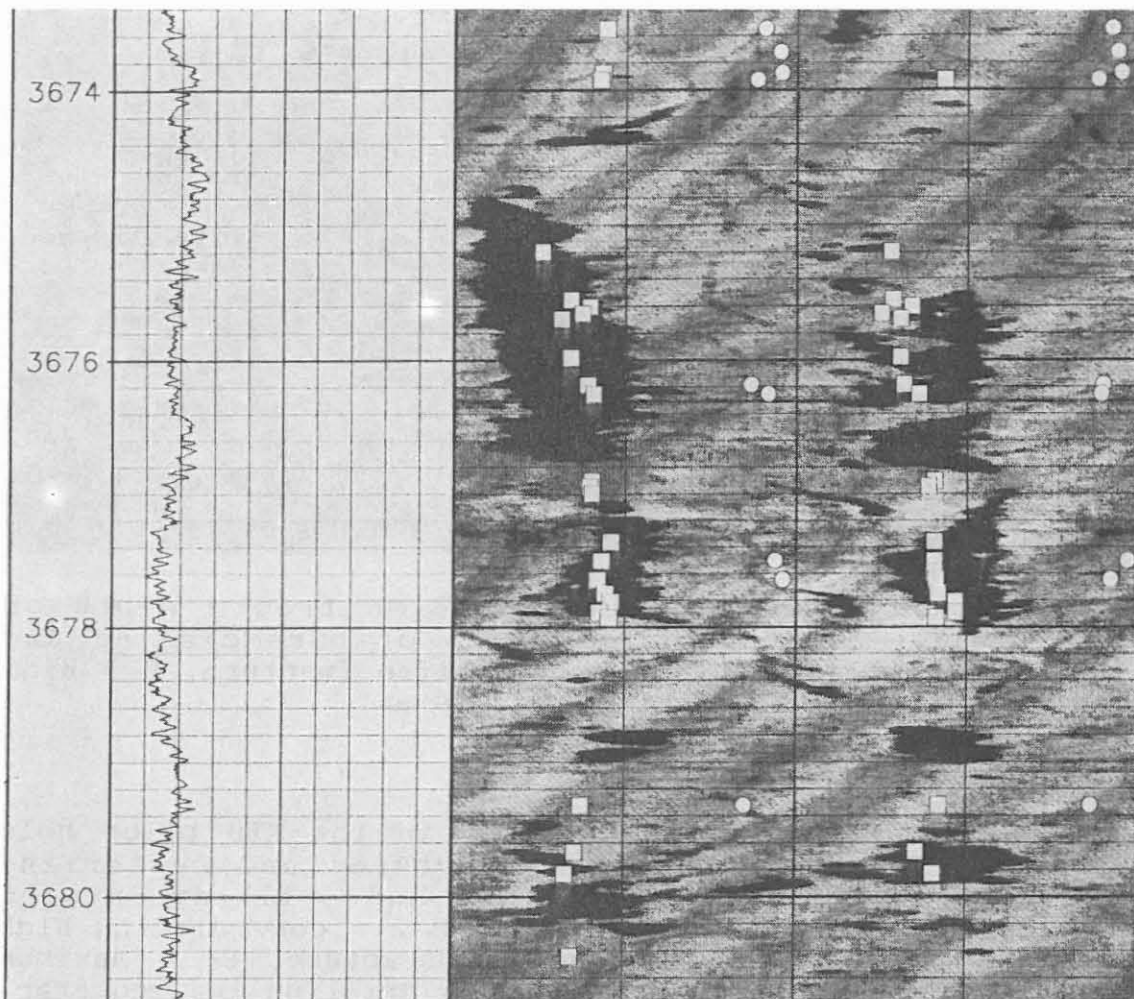
Fig. F.9: Unrolled core piece 902B1dK from a depth of about 3671 m with a combination of core diskings and centerline fractures. CF = centerline fracture, H = high points of the core diskings structures.

Tab. F.2: In situ stress direction in the KTB pilot hole deduced from core diskings structures and centerline fractures in core piece 902B1dK and drilling induced fracs on the borehole wall. H 1, H 2 = core diskings high points, CF 1, CF 2 = centerline fracture,  $S_H$  = maximum horizontal stress direction, DIF = drilling induced frac.

Core Disking		Centerline Fracture		DIF	
H1	( $S_H$ ) H2	CF1	( $S_H$ ) CF2	DIF1	( $S_H$ ) DIF2
N167°E	N164°E	N171°E	N168°E	N170°E	N170°E

For the core piece 902B1dK (from a depth of 3671.05 m) a comparison of the orientation of core diskings high points and centerline fractures combined with drilling induced fracs on the borehole wall (3673 m) is given in tab. 2. It is clearly shown in tab. F.2 that the orientation of the maximum horizontal stress in a depth of about 3673 m deduced from the centerline fractures corresponds well with the orientation of the drilling induced fracs on the borehole wall.

The same interval is shown in fig F.10. It is obvious, that the orientation of the core diskings high points corresponds with the orientation of borehole breakouts. The depth offset between core and the structures on the FMS log is about 2 m. The depth of the borehole televiewer log (3674 m) is about 3 m greater than core piece 902B1dK.



**Fig. F.10:** Borehole televiewer image from the depth interval between 3674 m and 3680 m of the KTB pilot hole. Breakouts appear as paired vertical dark bands. Additionally core diskings high points (open squares) and centerline fracture (open circles) data from this depth range are inserted in this image.



In the depth ranges from 3550 m to 3650 m and from 3700 m to 3800 m evaluation of the orientation of SH from borehole breakouts is given by MASTIN et al. (1989). In these depth intervals the orientation of borehole breakouts and core diskings structures are controlled by the stress field (tab. F.3). Core diskings and breakouts are good indicators for the in situ stress directions if they occur in the same depth interval. The reason for this is, that core diskings occur, when the rock is isotropic and shows a linear elastic behaviour.

If breakouts occur without core diskings structures, they can be caused by the anisotropy of the rock strength. Anisotropic rock strength is especially found in the metamorphic gneisses of the KTB pilot hole (ROECKEL & NATAU 1990).

Tab. F.3: Comparison of the orientation of the maximum horizontal stress direction ( $S_H$ ) in massive metabasites deduced from core diskings structures and borehole breakouts (MASTIN et al. 1989).

Depth (m)	Breakout ( $S_H$ )	Core Disking ( $S_H$ )	
		High 1	High 2
3550-3650	166°±12°	159°±19°	168°±13°
3700-3750	142°±11°	146°± 9°	151°±10°
3750-3800	150°±13°	149°±19°	148°±17°

### 3.1.2 "Practical Use"

Core reorientation is possible, if the orientation of joints and foliation of the cores can be identified on geophysical borehole logs (fig. F.1). Thus, core reorientation is also possible, if the orientation of core diskings structures is compared with the orientation of borehole breakouts or if the strike of centerline fractures is compared with the strike of drilling induced fracs.

If the centerline frac in the core and the drilling induced frac on the borehole wall are not vertical and if they have a preferred dip direction, it is even possible to determine the dip of the core structures.

Even if no structures can be found on the core and borehole log, it is possible to reorientate the core completely, if there are oblique core diskings structures and the borehole is deviated from the vertical.

The boreholes of Gravberg and Urach 3 are examples for the interplay of rock stresses, borehole azimuth and core diskings. The analysis of the caliper data of the Gravberg well shows a preferred NNE/SSW elongation trend of the borehole, which is mirrored by the drift direction of the well. It is reasonable to assume that the drilling direction is influenced by the stress orientation identified by the breakouts (CULL R. 1988).

A 1983 Schlumberger log from the Urach 3 borehole at a depth of 3440 m shows an azimuth of  $75^\circ$  and a deviation of  $13^\circ$ . For the complete deepening section of the Urach 3 borehole DIETRICH et al. (1987) gave azimuth variations between  $N64^\circ E$  and  $N76^\circ E$ . These values correspond quite well with the orientation of the borehole breakouts estimated by BLUEMLING (1986). He found a preferred breakout orientation of  $N83^\circ E$ .

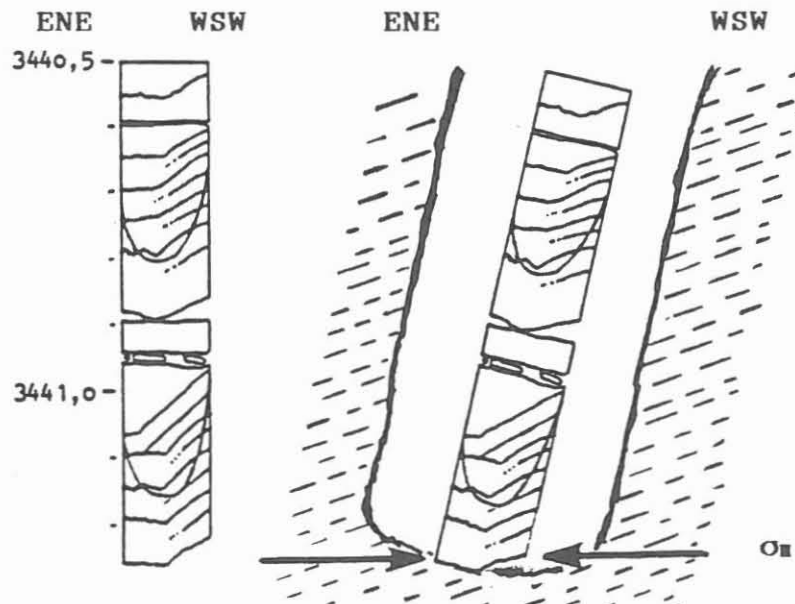


Fig. F.11.a: Oblique core diskings in core N°54 from the borehole Urach 3 (after DIETRICH & NETH 1987).

11.b: Schematic cross section through the bottom of the borehole, when coring core N°54. The borehole is inclined towards ENE and the inclination is  $13^\circ$ . The schematic horizontal arrows indicate high horizontal stresses ( $\sigma_H$ ).

Oblique core diskings, for example in core run N° 54 from a depth of about 3440 m (fig. F.11a) was found in the borehole Urach 3. In this case it seems possible to reorientate the core by use of the core diskings method. One of the core diskings high points is orientated in the direction of  $S_h$ , which is known from borehole breakouts. Core diskings is caused by high radial stresses (BORM et al. 1989). Therefore the core diskings high points should be symmetric to the core axis in a vertical borehole, if the horizontal stresses are principle stresses. In an inclined borehole, the high axis should also be inclined (fig. F.11.b).

principle stresses. In an inclined borehole, the high axis should also be inclined (fig. F.11.b).

In case the borehole exhibits an ENE drift, and core diking occurs in a horizontal plane, the core diking high point which is orientated WSW should have the higher position than the ENE orientated high point in the core (fig. F.11.a and F.11.b). For core N°54 from the Urach borehole this means that the higher core diking high point on the right side of fig. F.11.a should be orientated in WSW direction.

### F.3.1.3 Core Orientation in the KTB Main Hole

In the KTB main hole it was planned to start coring below 4000 m. Between 4169 m and the actual depth of 5600 m 17 cores were drilled with varying recovery (see chapter A).

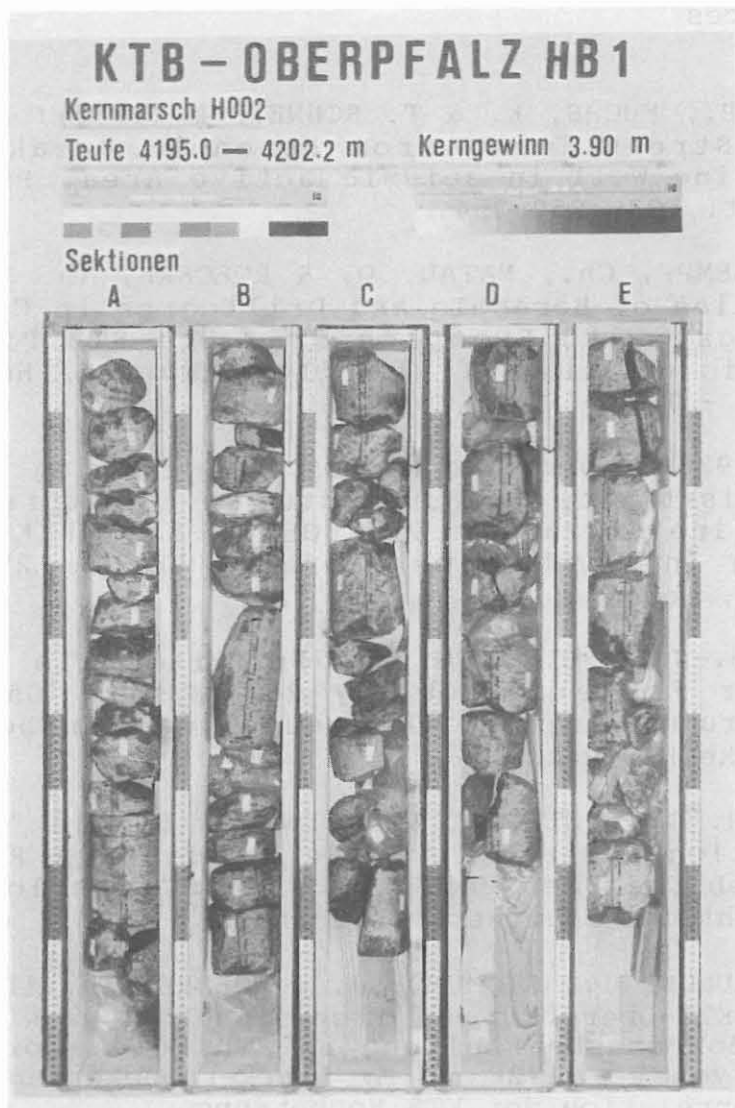


Fig. F.12: Photograph of the core pieces of core run H002.

The method of core reorientation successfully applied in the KTB pilot hole could not be used until now in the KTB main hole, however. Cores of different runs are heavily disked and disturbed (fig. F.12). The use of rotary drilling technique in combination with roller cone core bits often produces rolled and polished disks. Strong mechanical stresses applied to the core material make it difficult to determine the exact orientation of the core disk high points in the core. In some core runs, however, (e.g. H004, H007) it is possible to determine the core disk high points. In these cases, the strike of the core structure can be determined, when the orientation of the stress field is known (e. g. from borehole breakouts and drilling induced fracs). The complete reorientation of cores is possible if structures of the core can be correlated with structures from borehole logs.

#### F.4 References

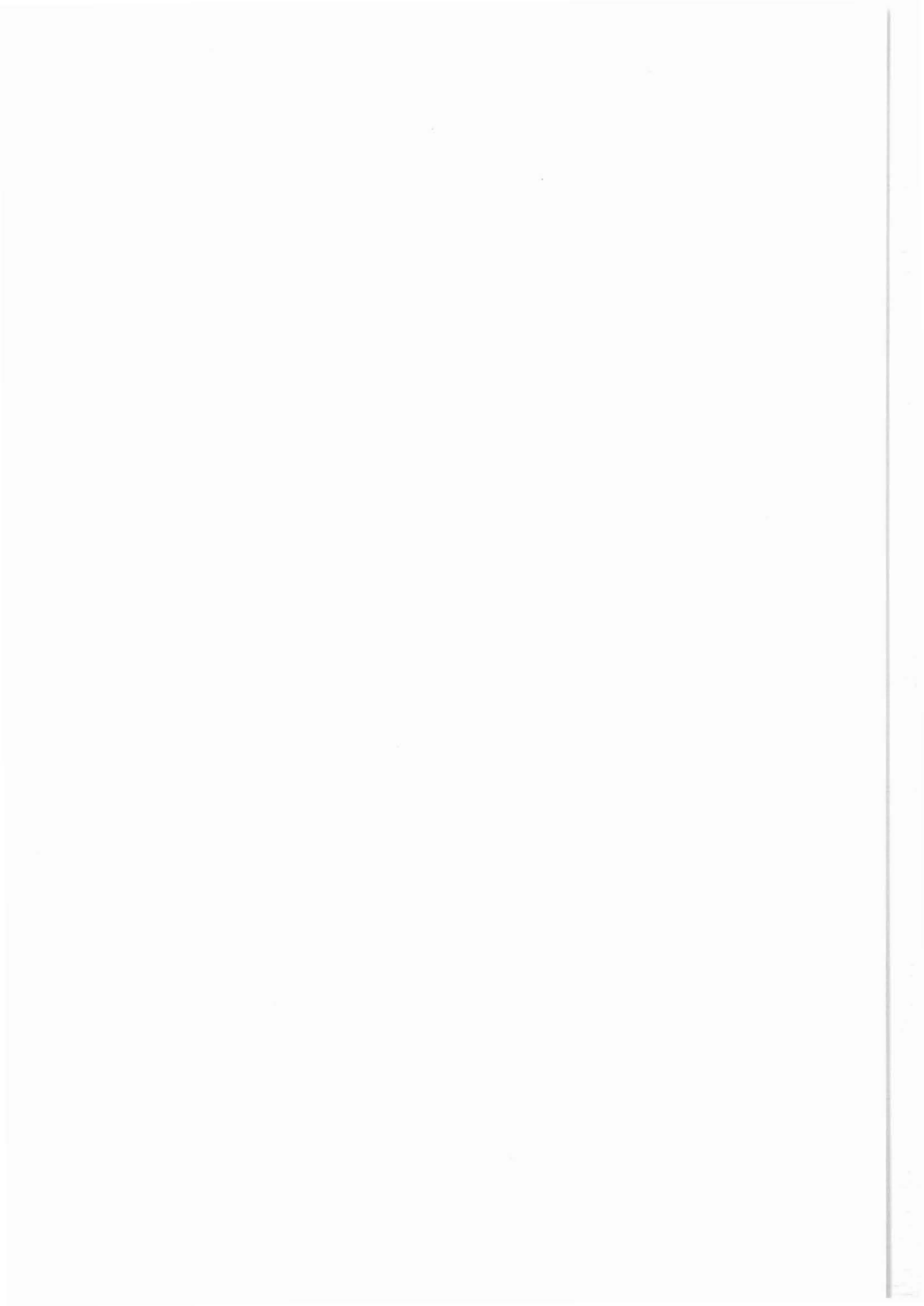
- BLUEMLING, P., FUCHS, K. & T. SCHNEIDER (1983): Orientation of the Stress Field from Borehole Breakouts in a Crystalline Well in seismic active Area, *Phys. Earth Plan. Int.*, 33, 250-254.
- BORM, G., LEMPP, Ch., NATAU, O. & ROECKRL, Th. (1989): Instabilities of Borehole and Drillcores in Crystalline Drillings, With Examples from the KTB Pilot Hole. *Scientific drilling*, 1; 105-114, Springer, Heidelberg - New York - Tokyo.
- CULL, R. (1988): Formation Microscanner Imaging and Laterolog Resistivity Measurements in Interpretation of Crystalline Terrains. In: BOEDEN and ERIKSSON. *Deep Drilling in Crystalline Bedrock*, Volume 2; 315-326, Springer, Berlin.
- DIETRICH, H.-G. & G. NETH (1987): "Erweiterte Zirkulation wässriger Fluide im Hot Dry Rock-System (Gneisgebirge) der Bohrung Urach 3" Gefügeanalyse. Endbericht der Stadtwerke Bad Urach
- DIETRICH, H.-G., NETH, G. & H.TENZER (1987): "Erweiterte Zirkulation wässriger Fluide im Hot Dry Rock-System (Gneisgebirge) der Bohrung Urach 3" Bohrlochverlauf. Endbericht der Stadtwerke Bad Urach.
- KOHL, J., KUECK, J., SIGMUND, J. & WOEHL, Th. (1991): Tiefbohrung KTB-Oberpfalz HB, Ergebnisse der geowissenschaftlichen Bohrungsbearbeitung im KTB Feldlabor - Teufenbereich von 0 - 1720 m: F: Bohrkernrückorientierung und Teufenkorrelation der KTB Vorbohrung. KTB Report 91-3 F1-22.

NATAU, O., BORM, G. & ROECKEL Th. (1989): Influence of Lithology and Geological Structure on the Stability of the KTB Pilot Hole.

In MAURY, V. and FORMAINTRAUX, D. (Eds) Rock at Great Depth, Proc. INT. Symp. ISRM, Vol. 3, 1487-1490, Pau, France.

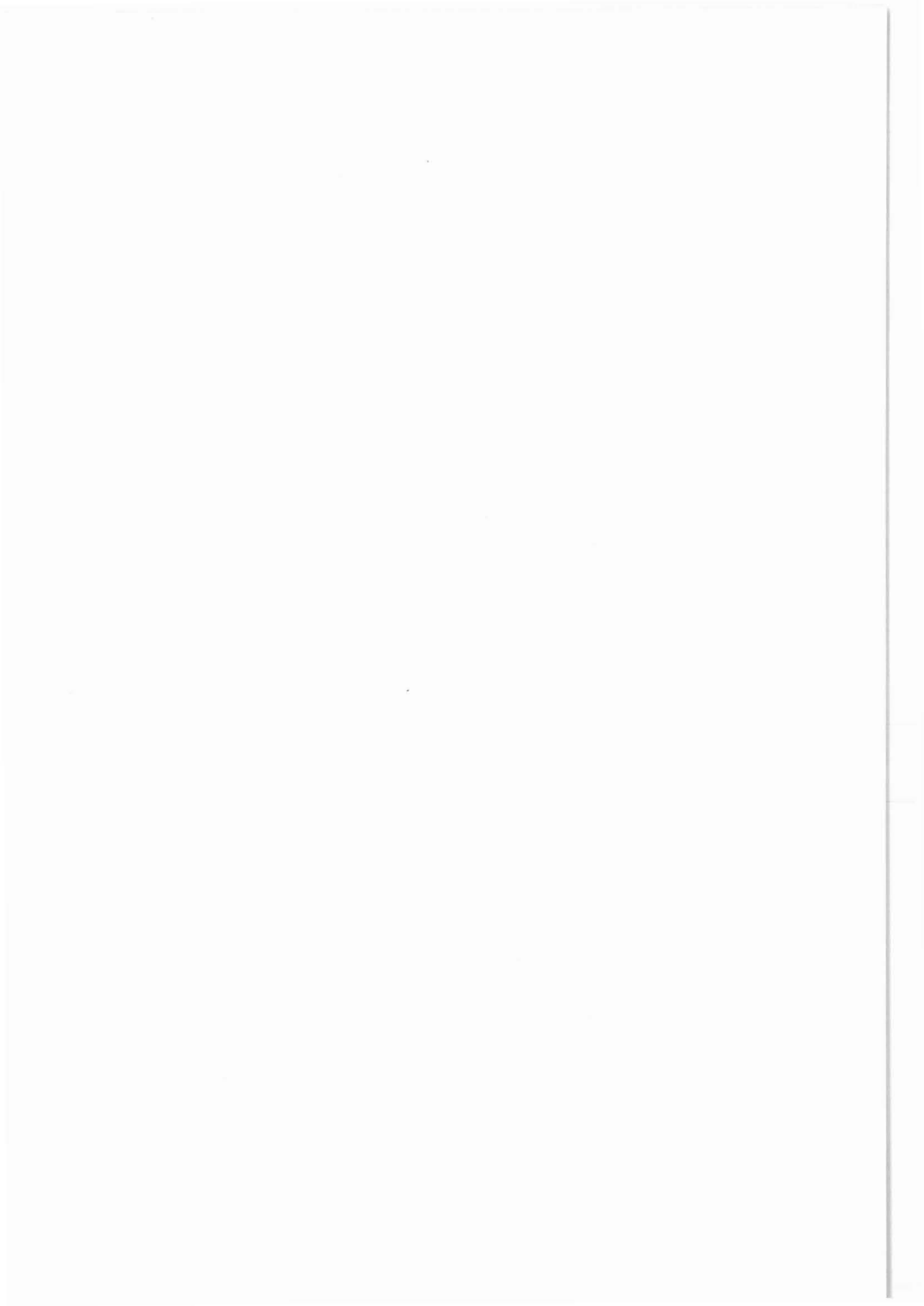
ROECKEL, Th.&NATAU, O. (1990): Results from Rock Mechanical Index Tests of the Pilot Hole "KTB Oberpfalz VB".  
KTB Report 90-8.

WOLTER, K.E., ROECKEL, Th., BUECKER, Ch., DIETRICH, H.-G. & H. BERGHEMER (1990): Core Disking in KTB Drill Cores and the determination of in situ Stress Orientation.  
KTB Report 90-8



G. Advanced Drilling Technology for the Continental  
Deep Drilling Program (KTB): Part of International  
Lithosphere Research

C. Chur  
B. Engeser  
B. Hoffers  
H. Rischmüller  
A. Sperber  
T. Tran Viet  
L. Wohlgemuth





**G. Advanced Drilling Technology for the Continental Deep Drilling Program (KTB): Part of International Lithosphere Research**

H. Rischmüller, C. Chur, B. Engeser, B. Hoffers,  
A. Sperber, T. Tran Viet, L. Wohlgemuth

Abstract	G 1
G 1. Introduction	G 2
G 2. The pilot hole	G 2
G 3. The ultradeep well	G 4
G 4. The coring concept	G 5
G 5. The vertical drilling strategy	G 5
G 6. New heavy deep drilling rig	G 6
G 7. State of work in the ultradeep hole	G 7
G 8. Conclusions	G 9
G 9. References	G 10

**Abstract**

In scientific research drilling, the borehole may be reviewed as an endoscope into the Earth, as it happens to be the case, for example, in the international Ocean Drilling Program (ODP) and the Continental Deep Drilling Program of Germany (KTB). Development of the drilling technology in the last 15 years took place mainly in the two areas of deep and ultradeep drilling, and of horizontal drilling. The impact of big geoscientific research programs on deep drilling technology is remarkable. Scientific drilling projects need intensive and expansive R&D efforts on the one hand and produce an outstanding spin-off on the other hand.

The German Continental Deep Drilling Project (KTB) is part of the international lithosphere research. The two boreholes of the project penetrate crystalline rock from the beginning. The 4,000 m deep pilot hole was drilled from September, 1987 to April, 1989. The ultradeep hole, planned for at least 10,000 m depth, started being drilled in October, 1990. The pilot hole was drilled by applying a large diameter thin kerf wire line coring technology, which was improved to a high extent during drilling. A newly developed synthetic clay based mud has been used successfully. For ultradeep drilling, a straight vertical wellbore trajectory is a must, to minimize drag, torque, and wear. To obtain a vertical wellbore course, active vertical drilling systems were developed and for the first time successfully utilized at the KTB. A new heavy, technologically advanced drilling rig has been constructed and is working satisfactorily.

## G 1. Introduction

The German Continental Deep Drilling Program is a non-commercial project of basic geoscientific research. The deep and the superdeep borehole are an integral part of the program as well as the accompanying comprehensive geoscientific work. Only a borehole can provide information dealing with the composition and the physical state of rocks and fluids at great depths which is necessary for a reliable interpretation of surface and well logging data, and which allows for a higher level of accuracy of geophysical evaluation - making the borehole a telescope into the earth's crust.

In Germany, the first ideas concerning a Continental Deep Drilling Program were discussed as early as in 1977.

The geoscientific targets, the results of the geophysical, the geological and the geochemical site exploration, and the available experience were the basis for the technical concept, the drilling strategy, and the main topics of research and development of the KTB.

The drilling concept may be viewed as a synergism of the pilot hole, the ultra-deep hole and the research and development program.

## G 2. The pilot hole

With its important objectives, the pilot hole is an essential part of the KTB. It serves the following purposes

- Acquisition of a maximum of geoscientific information at lower costs and risk, as compared to the expensive heavy rig of the ultradeep hole.
- Minimization of core runs and logging in the large diameter straight vertical upper section of the ultradeep hole.
- Analysis of the temperature profile for planning the ultradeep hole.
- Obtaining data about problem sections with inflow or lost circulation, well-bore instabilities and/or breakouts.
- Test of drilling and logging tools with regard to the ultradeep hole.

To accomplish these objectives, the pilot hole had to meet the following requirements:

- maximum depth of 5,000 m,
- 6" hole size,
- continuous coring with maximum core recovery.

A new drilling concept was developed, combining the rotary drilling and the wireline coring techniques.

A high speed top drive (Fig. 1), a 5 1/2" external flush mining drillstring (Fig. 2), a double tube wireline core barrel system, combined with memory tool recording of temperature and inclination, and high performance diamond core bits were developed, improved and tested successfully in the pilot hole. The availability of a newly developed geoscientifically compatible drilling fluid system on a synthetic clay base is another reason for the successful drilling operation in the pilot hole.

Drilling of the pilot hole started on September 22, 1987, and was finished on April 4, 1989, after 560 days of drilling and logging. Total depth is 4,000.10 m of which 3,594 m = 90 % have been cored (Fig. 3).

451 m were cored with 10 5/8" rollercone core bits, and 3,143 m with 6" thin kerf diamond core bits. A total of 9 surface set and 60 impregnated diamond core bits (Fig. 4) were used, the average bit life of the diamond bits being 48 m and the rate of penetration (ROP) being 1.66 m/h. The bits purchased from 3 major manufacturers have been improved continually, 5 diamond bits had a bit life of more than 118 m, and a ROP of 2.3 m/h.

Due to core breaking and jamming, the average length of a core run was 3.5 m, corresponding to the worldwide empirical average. Caused by lost bottom hole assemblies after unsuccessful fishing jobs, 2 side tracks had to be performed, the first in 1,998 m depth, and the second in 3,767 m depth. The mining drillstring had to be taken out of operation in February 1989 due to oxygen-pitting-corrosion on the internal pipe wall between the couplings. Because of this, a Moineau downhole-motor with hard rock roller cone bits and a 3 1/2" rotary string were used after the successful second side track. The performance was much poorer compared to the diamond coring system, ROP being only 0.84 m/h and bit life 12.31 m, respectively.

The evaluation of the rig time break down and the overall performance (Fig. 5) shows that, despite the good results of bit life, ROP, and the excellent core recovery of 98 %, there is potential and need for further improvement of this type of drilling technology, firstly, to avoid directional drilling and fishing by using straight hole drilling technology, and secondly, to bring down the time for tripping the drillstring and the core barrel.

The pilot hole penetrated into a succession of highly metamorphic paragneisses and metabasites, most probably Precambrian in age. The rocks are folded, and, prevailingly, rather steeply inclined. They are disrupted by a great number of faults and by - often graphite-bearing - cataclastic zones. These zones caused reduced borehole stability and led to breakouts, and, eventually, to the first sidetrack due to stuck drillstring.

The trajectory of the pilot hole (Fig. 6) is mainly determined by the steep Southern falling of the formations. Total deviation is 190 m.

Coring had to be interrupted three times for directional drilling to bring the hole back to nearly vertical direction. Two sidetracks were necessary. The upper one, caused by stuck pipe and a massive influx of cataclastic fine rock material into the borehole, was performed by conventional technique with benthousing and downhole motor. For the sidetrack in the deep section, an open hole packer was placed above the fish and then connected with an oriented wedging device normally used in cased holes (window cutting device).

Temperature at 4,000 m depth is 118 °C, quite higher than predicted.

### G 3. The ultradeep well

Based on the results of the pilot well (rock instabilities in fault zones, steep dip and tendency of inclination build up, water sensitivity of rock, breakouts, and core discing), the planning for the ultra-deep well, which is located at 200 m distance from the pilot well, had to be revised. The critical temperature range with respect to drilling and logging technology of 250 to 300 °C, whose investigation is a major geoscientific objective on the other hand, will be reached at 10,000 m depth or less.

This is the reason to base the technical planning and the funding on 10,000 m total depth, including an option to continue drilling down to 12,000 m if the temperature is lower than expected.

Due to the wellbore instabilities encountered in the pilot hole, the drilling and casing program for the ultradeep well had been based on open hole sections not longer than 3,000 m. Due to the experience with the borehole stability gained in the ultra deep hole down to a depth of 5,000 m together with the availability of a special designed high strength drillpipe and field proven heavy liner technology, it was decided to extend the 12 1/4" drilling phase to 10,000 m (Fig. 7). Expected benefits are the increased efficiency of 12 1/4"

roller cone bits as well as the improved conditions for verticality and continuity for specially developed tools like active vertical drilling systems and coring systems.

To make use of bits and downhole equipment of international standard and proven dimensions, proven bit sizes have been selected, and the final diameter at total depth is planned to be 8 1/2". In the top sections, where the availability and efficiency of vertical drilling systems was assumed to be successful, reduced clearances were planned, while in the lower sections due to high temperature and expected poorer performance of vertical drilling systems, larger clearances have been chosen.

#### **G 4. The coring concept**

Due to the extensive coring and logging program in the pilot well, coring in the upper section of the ultradeep well (corresponding to the total depth of the pilot well) can be avoided, and logging can be minimized. Below the depth of the pilot well, coring a total of about 1,500 m and comprehensive logging programs before running the casing strings are planned. Sampling and evaluation of cuttings will be performed continuously.

Since cores in good quality and sufficient numbers are of vital importance for the scientific success of the project, major R & D efforts are dedicated to coring strategies and systems.

#### **G 5. The vertical drilling strategy**

Theoretical investigations as well as drilling experiences from the KTB pilot hole, the Russian Kola Well, and other drilling operations in crystalline rock, have identified the need for a straight wellbore trajectory in the KTB superdeep borehole (KTB-HB). At least the upper section down to about 6,000 m should be drilled with a minimum of directional changes, in order to attain low values of torque and drag between drillstring and borehole wall and good conditions for running the narrow clearance 16" and 13 3/8" casing. To achieve a straight trajectory, it should be drilled preferably following the vertical direction (Fig. 8).

The Russian strategy to drill a vertical hole is to use a special passive system which performed well in seven boreholes (Fig. 9). A twin turbine set, approximately 12 m in length with two roller cone bits, sized for borehole diameters from 394-640 mm, is rotated from the surface with 11 - 15 RPM.

KTB engineers worked out a computer program for calculating the equilibrium angle based on the analytical approach of Lubinski. Data on dip of foliation and rock anisotropy factor combined with BHA-dimensions and drilling parameters are taken into consideration.

Provided with the data on wellbore trajectory, drillstring, weight, and friction coefficients of the drilling fluid, another program calculates the total frictional forces causing torque and drag.

The friction coefficients have been calibrated from the evaluation of data from the pilot hole.

The frictional forces have to be taken into consideration when designing the drillstring for an ultradeep hole. The calculations carried out with the KTB computer program showed clearly that, despite of a substantial reduction of drag forces when using a light metal alloy drillstring, there is no other way to reach a target depth of 10,000 m than to drill a straight and vertical hole.

This is a very ambitious goal especially in crooked hole areas characterized by steeply inclined formations and anisotropic rock properties.

The KTB approach is the so-called active system. Intensive R&D efforts and sufficient funding are allocated to this strategy. Self adjusting steerable systems seem to be a promising approach.

Within joint development projects funded by KTB, different concepts for vertical drilling tools using active compensation of deviations through a radial force generation (Fig. 10), were followed.

Such a selfcontained vertical drilling tool, positioned just above the bit, follows a vertical borehole course. Upon any force acting on the system which causes a deviation from the vertical, a radial counterforce is generated within the tool. The resulting steering forces push the corresponding stabilizer against the borehole wall. Data on performance and orientation is transmitted to the surface by mud pulsing technology (MWD).

## **G 6. New heavy deep drilling rig**

To meet the requirements imposed by the target depth and by scientific crystalline rock drilling, several contracts were awarded for studies of rig layout and construction. The result has been the decision to build a new rig with a hook retractor system, and an automated pipehandling system and a load

capacity for at least 12,000 m depth (Fig. 11).

It is considered to be the world's highest and strongest and one of the technologically most advanced rigs:

- Height: 83 m
- Capacity: 12,000 m
- Max. hook load: 8,000 kN
- Remote controlled gear driven drawworks
- Advanced drilling instrumentation and data processing.
- Central rig controls from the drillers cabin.

To meet strong environmental demands, the rig is large-scale noise insulated, and the impact on the environment is controlled by a disposal water conditioning plant.

#### **G 7. State of work in the ultradeep borehole**

Drilling started October 6th, 1990. The 24 1/2"-casing was set and cemented down to 292 m depth. Opening the 17 1/2"-borehole to 28", using for the first time roller cone equipped hole openers in this type of hard crystalline rock, proceeded quite satisfactorily.

The strategy for drilling the 3,000 m section with 17 1/2" bit size had been based mainly on application of tools and techniques as listed:

1. Use of low RPM, high flow and high torque Moineau downhole-motors for smoother running conditions, and to reduce wear, and to enhance borehole wall stability.
2. Continous MWD to control the performance of the vertical drilling systems and the deviation.
3. Use of active vertical drilling systems.
4. Packed hole assembly with continous MWD act as back up for the active systems.
5. Navigational (Motor steering-) systems add further redundancy.

When drilling started, only one prototype each of the two active systems ZBE 5000 and VDS 3 were available. Due to positive experiences with respect to verticality, the number of the systems was increased to 5. Nevertheless, the productivity has not been satisfactory, when held against proven comparable downhole equipment. Long dead time for repair and reconstruction had to be bridged by using packed hole assemblies and motor steering systems (Fig. 12). Out of a total of 50 runs of vertical drilling systems, 23 were not

productive, resulting in a waste of rig time. But the progress in stepping up the learning curve continues in a remarkable way. Despite severe conditions - a large borehole in hard crystalline steeply folded rock with oversize sections due to break outs -, the requirements of very limited borehole curvatures were met, average deviation being less than  $0,5^\circ$ , and the offset in 3,000 m depth amounting to about 12 m.

End of May, 1991, the 17 1/2"-borehole was cased with a 16"/84 lb/ft-casing string down to 3,000.5 m. Due to the strict verticality, the 3,600 kN heavy string could be lowered down to bottom without any difficulties, the clearance between the Hydril-couplings and the borehole wall being only 14 mm. The string was cemented to the surface with a complete displacement of the mud behind the casing, including the oversize sections.

The 14 3/4" section, from 3,000 to 6,000 m depth, was planned to be drilled following to the same strategy as applied in the 17 1/2" section. At the time of the writing of this (January 1992), the well has reached a depth of more than 5,500 m. Drilling was done using the active self steering systems (VDS) together with PHAs, and, below 4,000 m, coring with a 14 3/4" x 4" core barrel was begun. Fig. 13 shows the operational performance of the active vertical drilling systems in the 14 3/4" section drilled so far. Average rate of penetration is 1,1 m/h. Average bit life was 60 m, with a maximum of 131 m. Core recovery ranges from more than 50 % to nearly total loss.

Productivity and technical reliability of the active vertical drilling system could be increased substantially (Fig. 13). The average inclination of the wellbore is still  $0,5^\circ$  with the horizontal distance at 4,000 m not more than 12 m (Fig. 6). No temperature related problems occurred with the downhole electronics (rated for  $125^\circ\text{C}$ ) used for measuring inclination in both PHAs and VDS, and for steering the VDS. This is due to the cooling effect of the mud circulation during each run, and, in addition, due to the cumulative or long-term cooling of the borehole wall and the adjacent rock.

Borehole stability, so far, is not affecting the operation. Wellbore breakouts and washouts are found at irregular intervals all along the 14 3/4" section. The hole enlargements occur mainly at lithologic boundaries (e.g. gneiss and amphibolite) and at tectonically altered zones. Due to the successful improvements of the active vertical drilling systems attained in the 14 3/4" drilling phase and the favorable dynamical temperature curve, with operational temperatures in the downhole electronics not more than  $100^\circ\text{C}$  at a depth of 5,500 m, further application of the vertical drilling strategy down to 8,000 m is decided to be the best way for reaching the target depth of 10 km safely and



economically and to hold the way free for further deepening the hole to 12 km.

To meet the ambitious temperature and pressure requirements for the various downhole components like electronics or hydraulic elements extensive R&D efforts are currently under way.

## G 8. Conclusions

In conclusion, the experiences and results from ultradeep scientific drilling in Germany are summarized:

1. The certainty of scientific and economic success of the 'two-borehole-concept', allocating clearly defined and optimal feasible programs to each well and its specific technology, is higher than the one of a 'single-borehole-concept'.
2. The drilling technology of the pilot well, using the hoisting capability of a rotary rig, a high speed top drive and a new 5 1/2" variable thread mining drillstring, and the so-called intelligent core barrel with wireline technology, and last not least the novel mud, was a breakthrough. Implementing a straight vertical hole technology, a potential depth range of 5,000 to 6,000 m with 6" diameter totally cored seems to be realistic for this drilling concept.
3. Since 1985, it has been recognized that in the upper section of an ultradeep hole, its trajectory should be straight vertical. Passive vertical drilling systems have the disadvantage that side forces, generated from formation inhomogeneities, are overcome by a reaction force depending directly on the inclination angle. Small angles will only generate small compensation forces. Active systems will use the inclination angle only as a signal to activate pistons, ribs, or other devices which are pressed radially against the borehole wall.
4. The international, and the KTB experience in deep and ultradeep crystalline drilling led KTB to a bit-and-casing-program for the ultradeep hole with open hole sections not longer than 4,000 m. The advantages are
  - zones of fluid inflow or mud loss and of rock instability (especially in the upper large diameter sections) are cased earlier,

- with no effect of swab and surge to the open borehole wall in the cased sections, the pulling and lowering velocities during tripping can be optimized, making full use of the pipe handler.
- 5. Related to an amount of coring of less than 25 %, discontinuous full bore coring with thin kerf diamond core bits should be preferred because of economic and geostatistical reasons.
- 6. For the depth range of max. 12,000 m, a special heavy rig had to be constructed, using, wherever possible, proven moduls, and was equipped with a pipe handler, and a hook retractor system.

## G 9. References

- Behr, H.-J., Kehrer, P., Rischmüller, H.: "The German Continental Deep Drilling Program, Objectives and State of Work" In: Boden, A., Erikson, K.G. (eds) Deep Drilling in Crystalline Bedrock, Vol. 2. Springer, Berlin Heidelberg New York London Paris Tokyo, 1988, 64-81
- Chur, C., Engeser, B., Oppelt, J.: "Vertical Drilling Concept for the Main Well", European Magazine of Oil and Gas 16/4, 1990, 26-29
- Eickelberg, H.D., Wehling, B., Steckhan, H., Bosse, D.: "The Heavy Deep Drilling Rig UTB 1 for the Continental Deep Drilling Programme", SPE/IADC Preprint 21977, presented at the 1991 Drilling Conference, Amsterdam, 11-14 March
- Ellins, M., Tran Viet, T.: "Drilling Fluid Concept and Data Acquisition System", European Magazine of Oil and Gas 16/4, 1990, 30-34
- Engeser, B.: "The Coring Strategy for the Main Well", European Magazine of Oil and Gas 16/4, 1990, 36-41
- Marx, C., Rischmüller, H.: "Drilling and Coring Techniques for Hard Rock" In: Behr, H.-J., Stehli, F.G., Vidal, H. (eds): Observation of the Continental Crust through Drilling II. Springer, Berlin Heidelberg New York London Paris Tokyo, 1987, 149-160
- Oppelt, J., Chur, C., Feld, D., Jürgens, R.: "New Concepts for Vertical Drilling of Boreholes", SPE/IADC-Preprint 21905, presented at the 1991 Drilling Conference, Amsterdam 11-14 March

Rischmüller, H.: "Example for Advanced Drilling Technology", European Magazine of Oil and Gas 16/4, 1990, 16-20

Rischmüller, H., Chur, C.: "Technical Concept and Status of Planning for the Wells of the Continental Deep Drilling Program (KTB)". In: Behr, H.-J., Stehli, F.G., Vidal, H. (eds): Observation of the Continental Crust through Drilling II. Springer, Berlin Heidelberg New York London Paris Tokyo, 1987, 136-149

Sperber, A.: "The Casing Concept for the Main Well", European Magazine of Oil and Gas 16/4, 1990, 21-23

Spoerker, HF.: "Thoughts on Problems and Possible Solutions in Ultradeep Drilling". In: Behr, H.-J., Stehli, F.G., Vidal, H. (eds): Observation of the Continental Crust through Drilling II. Springer, Berlin Heidelberg New York London Paris Tokyo, 1987, 170-184

Sumbatov, R.A., Khakhaev, B.N., Gramolin, V.N.: "Drilling Rigs and Technical Facilities for Superdeep Well Drilling", Paper presented at the IGC, Washington, July, 1989

Wohlgemuth, L., Chur, C.: "The KTB Drilling Rig", European Magazine of Oil and Gas 16/4, 1990, 42-46

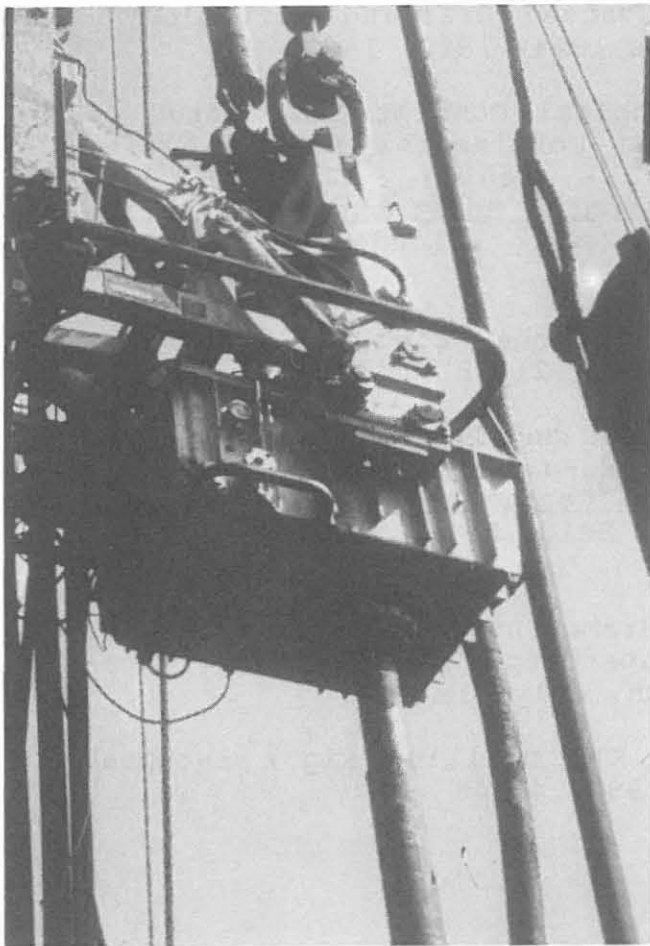


Fig. 1 SMAG-430-kW topdrive

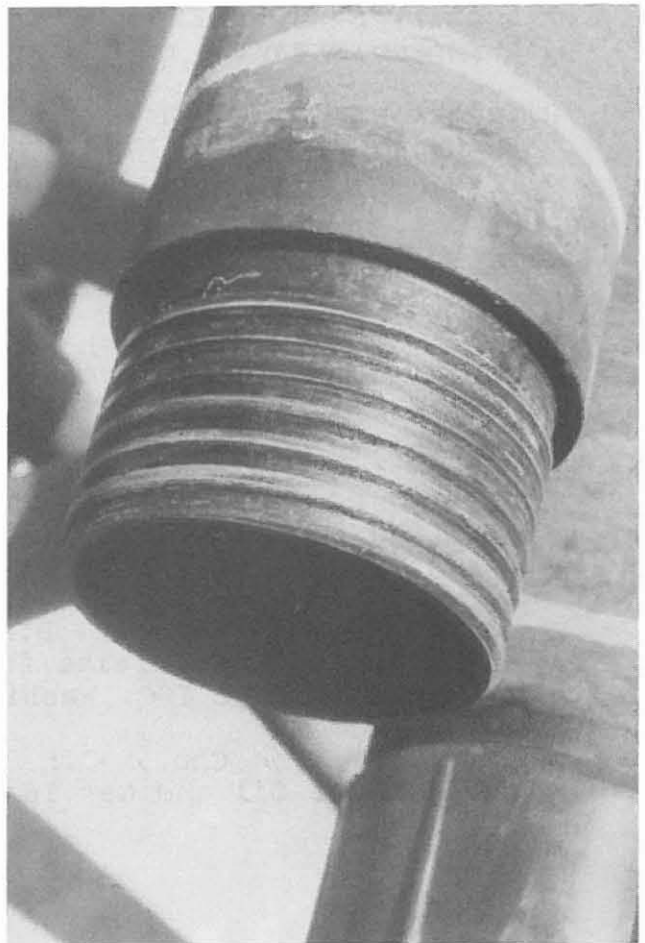


Fig. 2 Coupling of the 5 1/2"-mining drillstring

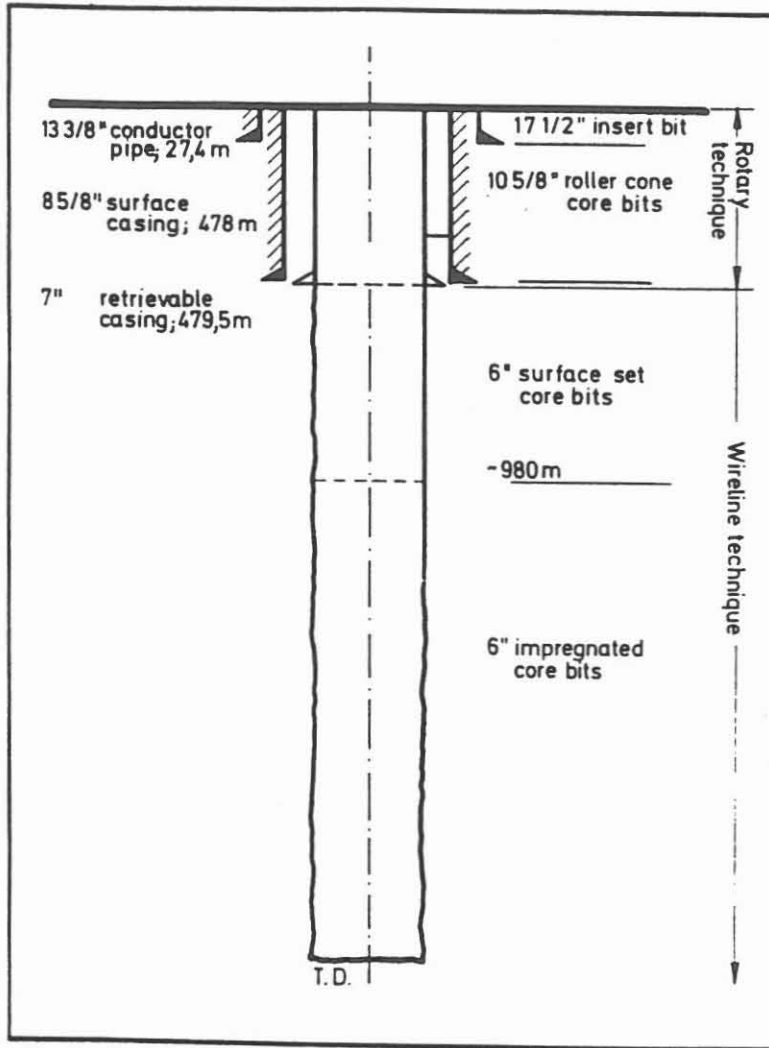


Fig. 3 Bit and casing program of the pilot hole

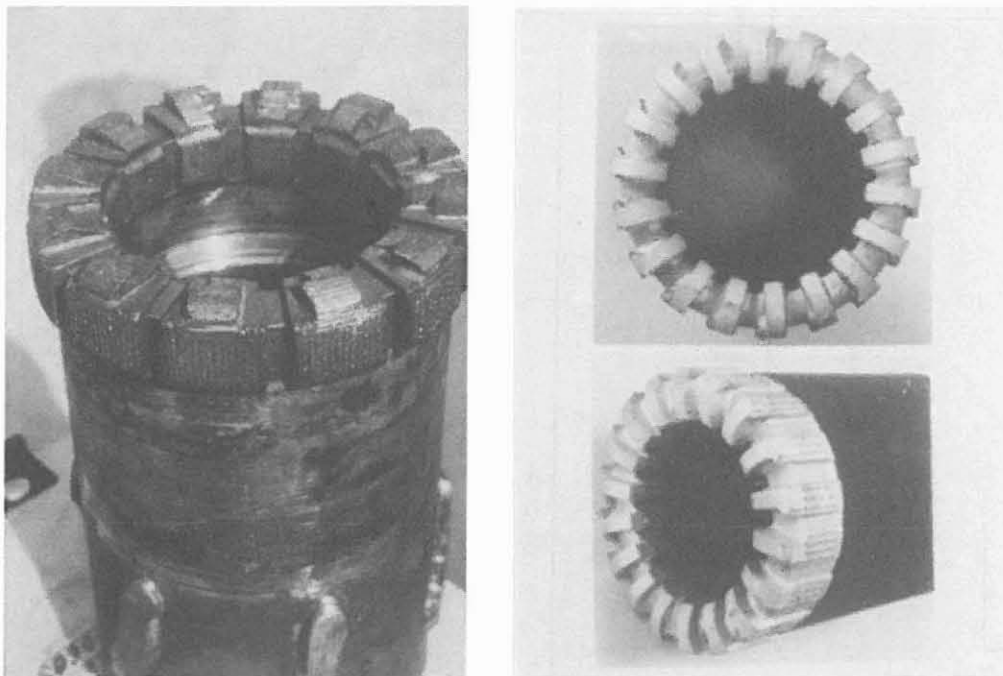


Fig. 4 High-performance impregnated diamond core bit (new, and after drilling 140 m)

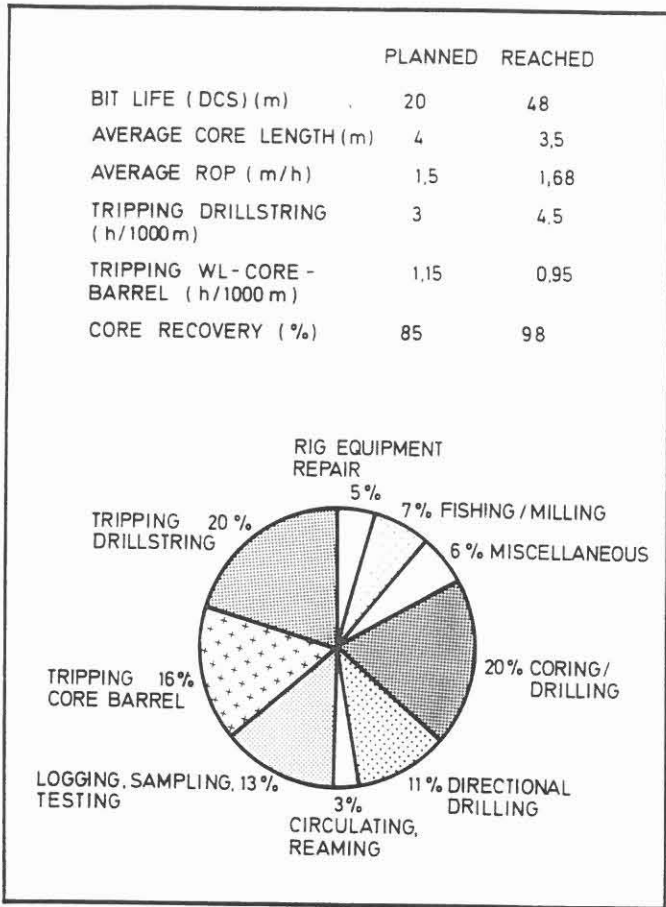


Fig. 5 Rig time break down and performance data of the KTB pilot well

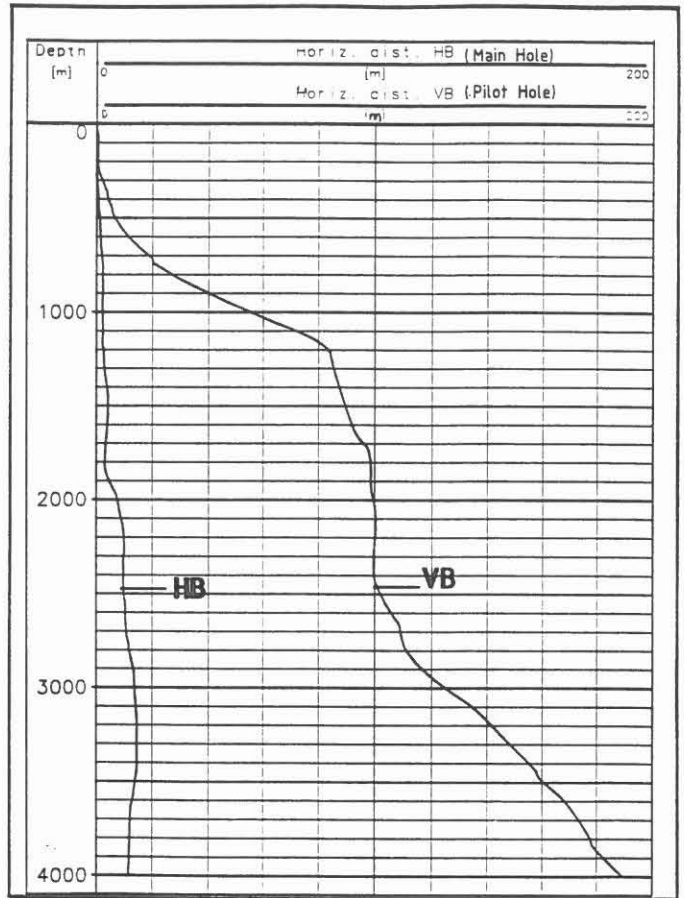


Fig. 6 Effect of the vertical drilling strategy Comparison of wellbore trajectory pilot hole vs main hole

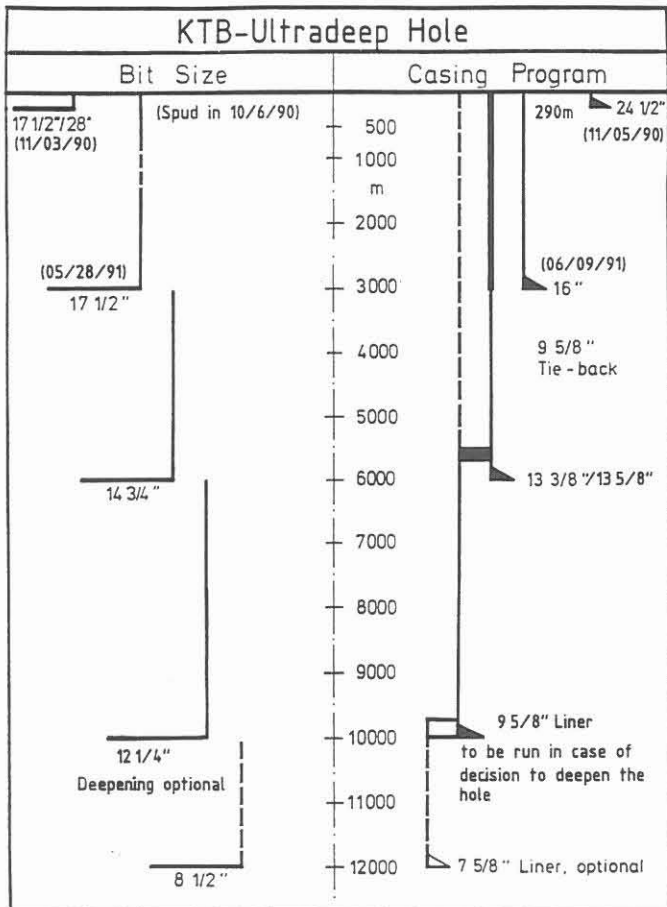


Fig. 7 KTB-Oberpfalz-HB Casing and bit size concept, revised Dec. 1991

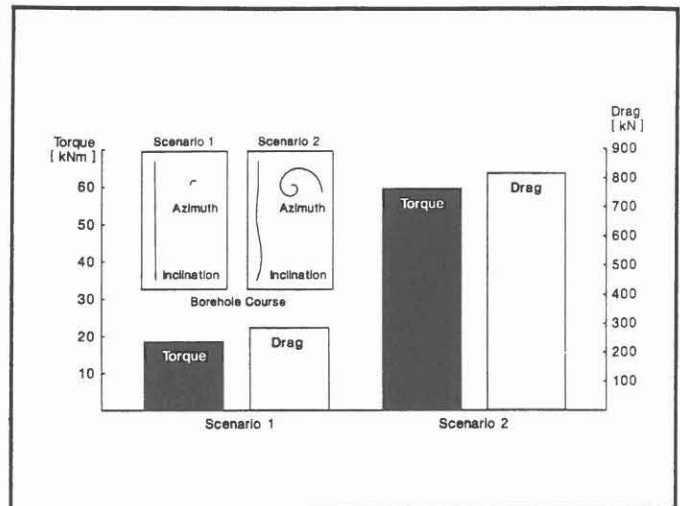


Fig. 8 Torque, drag, and borehole course

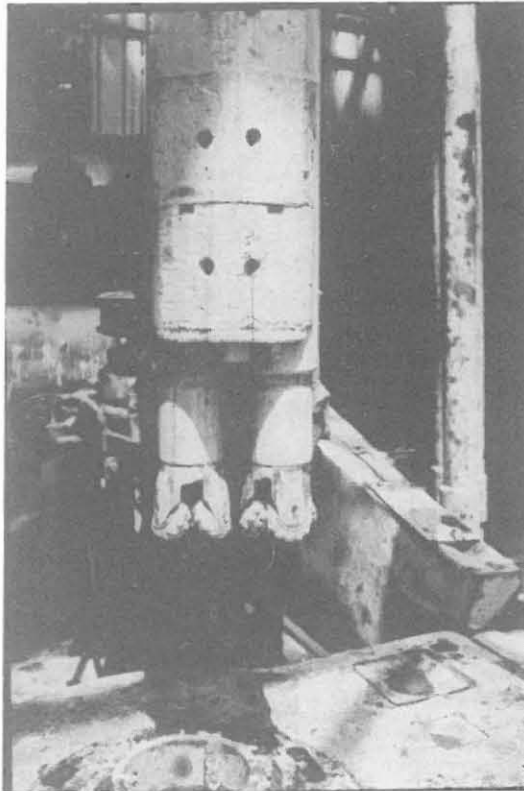


Fig. 9 RTB-Systems - two turbines in a special housing

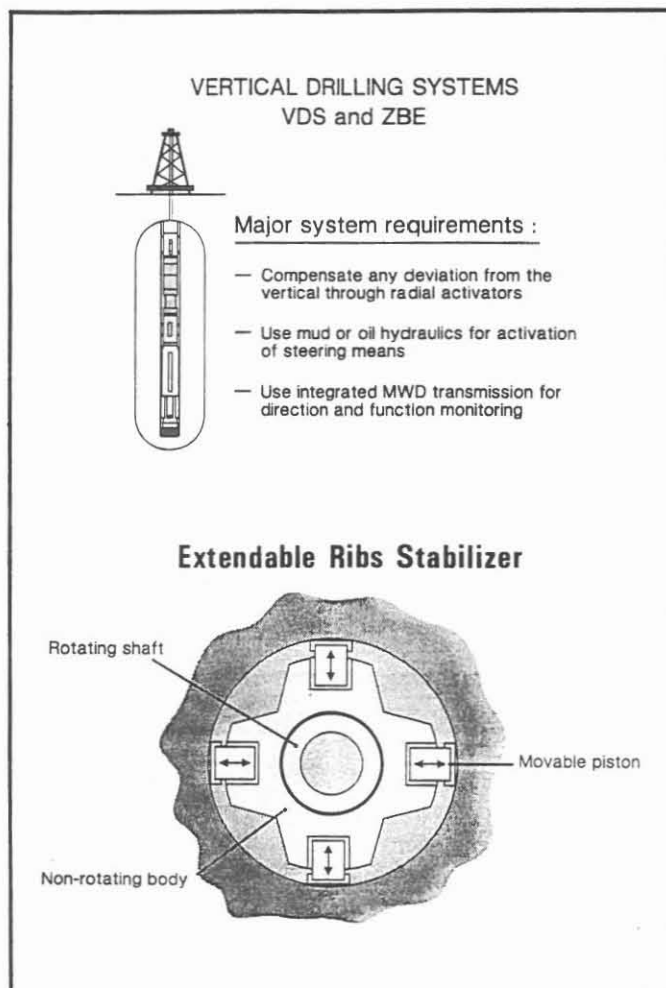


Fig. 10 Vertical drilling systems VDS and ZBE

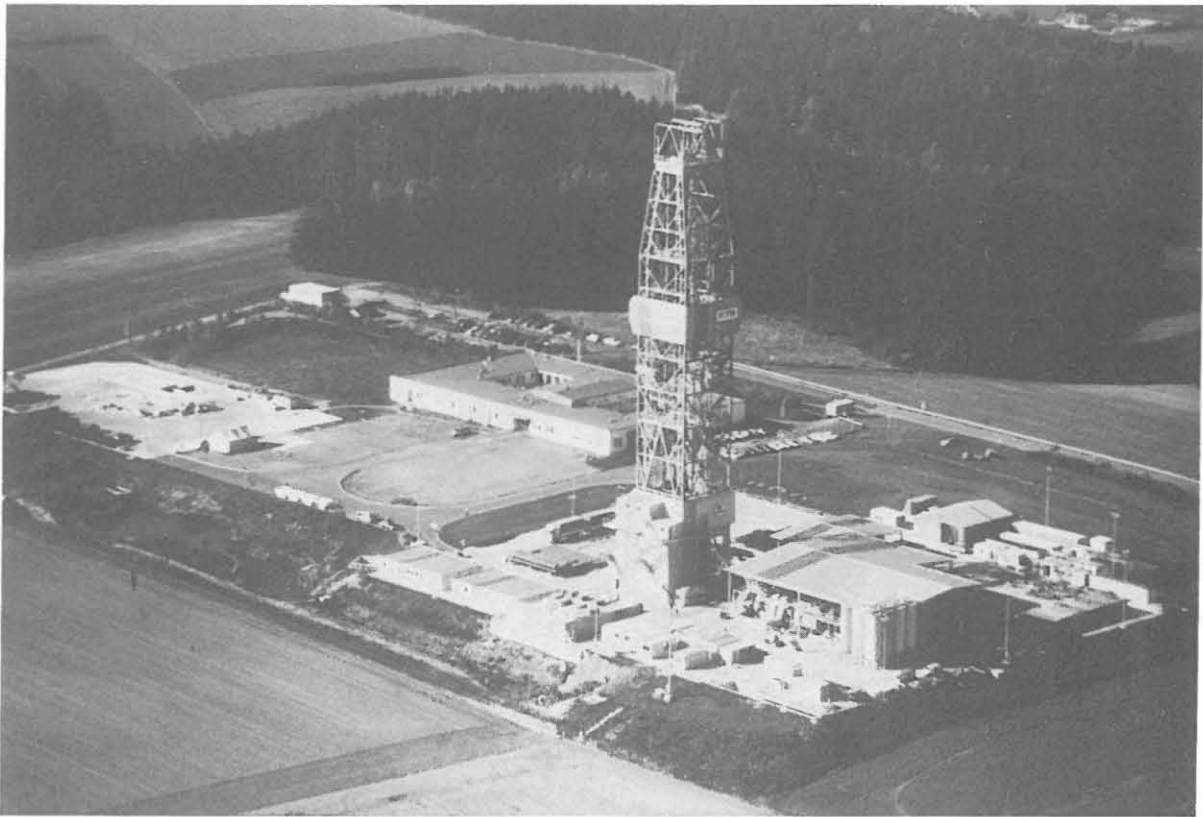
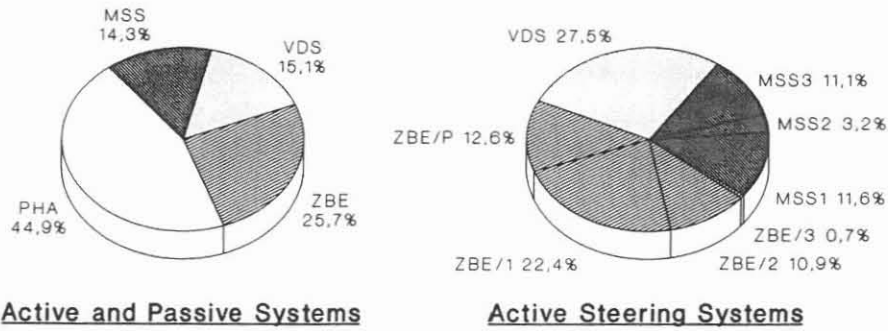


Fig. 11 Air view of the KTB heavy rig



### Performance of Vertical Drilling Systems (Active and Passive Systems) KTB-HB

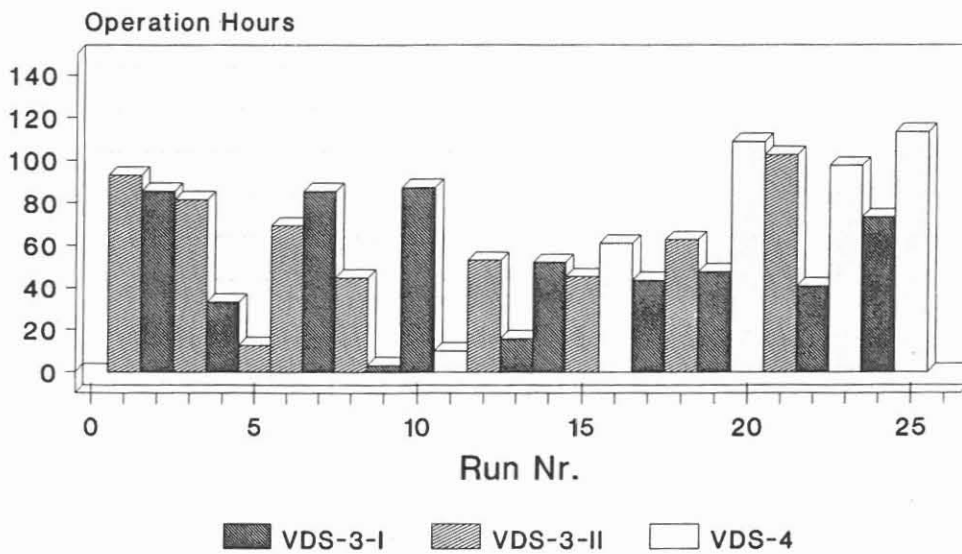


17 1/2" Drilling Phase 0-3003m

TV 10/91

Fig. 12 Performance of 17 1/2"-vertical drilling systems

### Performance of Vertical Drilling Systems KTB-HB



14 3/4" Drilling Phase 3003-5503 m

TV/PI 01/92

Fig. 13 Performance of 14 3/4"-vertical drilling systems



Anlagen



ISSN 0939-8732  
ISBN 3-928559-05-2